NON-THERMAL GALACTIC BACKGROUND RADIATION

by

H.V. Cane, B.Sc. (Hons.)

submitted in fulfilment of the
requirements for the degree of
Doctor of Philosophy

UNIVERSITY OF TASMANIA
HOBART

OCTOBER 1977

Thesis

This thesis contains no material which has been submitted or accepted for the award of any other degree or diploma in any university.

To the best of my knowledge and belief, the thesis contains no copy or paraphrase of material previously published or written by another person, except where due acknowledgement is made in the text.

Hilary. V. Cane.

ABSTRACT

This thesis presents the results and analysis of data obtained using the Llanherne low-frequency array. Surveys of the Galaxy at five frequencies in the range 2 to 20 MHz have been made and the data have been assembled into maps covering the area $320° \lesssim \ell \lesssim 30°$ and $-25° \lesssim b \lesssim 22°$. The data from these maps are combined with data from seven earlier continuum surveys to produce galactic radio spectra in various directions.

A summary is made of most of the measurements, at frequencies less than approximately 400 MHz, of the galactic background radiation and their interpretation. Two new composite maps, at 10 and 30 MHz, are presented. These, combined with the 85 MHz all-sky map, are used to illustrate the variation of the galactic non-thermal radiation across the sky, and with frequency.

The galactic spectra are interpreted in terms of a model of the Galaxy in which synchrotron emission, and absorption in HII regions predominate in spiral arms. However, it is proposed that the synchrotron emission arms and the arms defined by HII regions are not coincident. In addition to the HII absorbing gas the model incorporates a much broader uniform absorbing HI gas which is responsible for high latitude absorption, pulsar signal dispersion and Faraday rotation.

For the HI gas it is found that

$$\int n_e^2 \, T_e^{-1.35} \, dl \simeq 1.1 \times 10^{-7} \text{ cm}^{-6} \text{ K}^{-1.35} \text{ pc}$$

For the HII gas the above quantity varies for different arms. An average value is

$$\int n_e^2 \, T_e^{-1.35} \, dl \simeq 2.7 \times 10^{-6} \text{ cm}^{-6} \text{ K}^{-1.35} \text{ pc}$$

CONTENTS

CHAPTER I

INTRODUCTION

Preface

This thesis is a description of the features of the galactic background radiation at frequencies below about 400 MHz.

The first four chapters present review material. In Chapter 2 we discuss the emission and absorption processes relevant to the work. Chapter 3 covers the problems peculiar to low frequency astronomy. In Chapter 4 we review the observations of the interstellar medium. In this the major objective is to determine the properties and distribution of free electrons in the Galaxy.

Chapter 5, which contains some original work, is relatively long and has been divided into four parts. In Part I we present a catalogue of sky surveys at frequencies less than about 400 MHz and two new composite maps at 10 and 30 MHz. These data are used to discuss the properties of the background radiation. In Part II all the polar spectral points of both polar regions are presented and new polar spectra defined. In addition, spectra for the anti-centre and northern minimum directions are defined. In Part III spectral index variations are discussed. This includes a review of previous investigations and some new work using three composite maps. Part IV is a discussion of the results from emissivity estimates. Measurements are tabled, and plotted in several forms.

Chapters 6 and 7 present the major original contribution of this thesis. Chapter 6 comprises the experimental part and presents the data obtained using the Llanherne array in the form of declination scans and maps. Spectra are then compiled using seven earlier continuum surveys. These spectra exhibit unusual features. In Chapter 7 we present a model of the Galaxy to explain

these spectra which is also compatible with the conclusions of Chapter 5.

In Chapter 8 the uncertain areas in galactic background radiation studies are discussed and measurements suggested to clarify some of the uncertainties.

The thesis concludes with two appendices. The first is a brief summary of the recent work on the Gum Nebula and includes some comments on an early publication by the author.

The second appendix deals with the instrumentation used to obtain the sky surveys. This is included as an appendix because the author was not connected with the majority of the design of the array or receiving equipment. The description of the phasing is included in some detail as the author was responsible for part of the design and because it has not been documented elsewhere.

Acknowledgements

This project was initiated by Professor G.R.A. Ellis and his assistance as supervisor is acknowledged.

During the first four years financial support was provided by a Commonwealth Postgraduate Scholarship. Afterwards support was provided by the A.F.U.W. and Zonta International.

Technical assistance was provided by a number of people but in particular by Mr. G. Gowland and Mr. P. Button.

The project would not have been as successful without the introduction and utilization of the PDP-8 computer. The interfacing and installation was performed by Mr. G. Gowland and the software written by Mr. P.S.Whitham. Mr. P.S. Whitham also wrote the software for the sky observing program and willingly provided assistance with its implementation.

The contour plotting program used to draw the maps was an adaption of a program written by Dr. P.A. Hamilton. Assistance with programming problems was readily supplied by Mr. R.K. Allen and Mr. L.C. Botten. Computer operaters Mrs. D. Fleury and Mrs. S. McQuaid were very helpful in running the long programs required to extract the raw data off the magnetic tapes.

In the final stages of this work the enthusiasm of Professor W.R. Webber during his stay at the University of Tasmania provided the impetus to complete this thesis. His interest and guidance were invaluable.

The assistance provided by Dr. P.A. Hamilton in the final stages of the thesis is acknowledged. His comments and interest were very helpful.

The typing of this thesis was performed by a number of people. The assistance of Mrs. A. Williams and Mrs S. McQuaid is acknowledged.

Finally, the moral support of Attila Vrana is acknowledged. His guidance and help in solving electronics difficulties and in preparing diagrammatic material is also appreciated.

CHAPTER 2

EMISSION AND ABSORPTION MECHANISMS

Introduction

The Galaxy emits both continuum and line radio emissions. Line emissions are emitted during a change in energy state of an atom or molecule and are monochromatic. Radial velocity measurements give information on the distance of the emitting gas and thus line emissions may be used to investigate radial and spiral features. The most important line emission is the $\lambda 21$ cm line from neutral hydrogen and maps obtained from this emission provided the first insight into the spiral structure of the Galaxy. Information on the large scale distribution of ionized hydrogen may be obtained from hydrogen radio recombination lines. These, and other line emissions provide information on properties of the interstellar gas.

In recent years many molecular lines have been found with a new field in astronomy resulting - molecular astronomy. However, line emissions are important only at frequencies greater than a few hundred megahertz so that we will not discuss these mechanisms but will discuss the results of such observations in Chapter 4.

The background radiation from the Galaxy consists of thermal emission from ionized hydrogen and synchrotron emission from cosmic ray electrons. These are continuum emissions which extend over essentially all frequencies with varying intensity. In Chapter 4 we assess how much of the background is thermal but let it suffice at this stage to say that at frequencies of interest to this work ($\lesssim$ 400 MHz) the background is predominately non-thermal.

At low frequencies ($\lesssim$30 MHz) it is found that the galactic background spectra turn over and this is attributed to free-free absorption in ionized hydrogen. However, it is important to discuss the other processes which can contribute to this low frequency cut-off, namely a low energy electron cut-off and the Razin effect.

Synchrotron Emission

Synchrotron radiation is emitted by relativistic electrons accelerated in a magnetic field, and was first observed in synchrotrons from which visible radiation was emitted. In 1950 Kiepenheuer suggested that this mechanism could account for galactic radio emission and that the electrons responsible were the electron component of cosmic rays which radiated as they moved in the interstellar magnetic field.

The theory of the synchrotron emission process is complex; for details see, for example, Westfold (1958). The basic principles are not and most text books on radio astronomy deal with the topic (e.g. Kraus, 1966; Shklovsky, 1960). It is included here to provide completeness and because the results will be applied in Chapter 5.

The energy radiated by a non-relativistic electron gyrating in a magnetic field has a wide angular distribution. For a relativistic electron most of the energy is emitted in the direction of the instantaneous velocity of the electron so that an observer in the plane of the orbit will receive pulses. The frequency spectrum of the radiation is a series of spikes at all harmonics of the fundamental or gyro frequency. The harmonics are so closely spaced that the spectrum is essentially a continuum.

The frequency of the maximum intensity is about a third the characteristic frequency ν_c where

$$\nu_c = 16.1\ B_\perp E^2 \text{ MHz} \qquad (2.1)$$

where $B_\perp$ is the component of the magnetic field B, perpendicular to the particle velocity (in μ Gauss) and E is the electron energy (in Gev).

The spectral distribution of power radiated by a single electron is given by

$$P(\nu) = 2.34 \times 10^{-29}\ B_\perp\ F(\nu/\nu_c) \text{ watts MHz}^{-1}$$

where F(x) is a function which varies approximately as $x^{0.3}$ for small x and $x^{0.5}\ e^{-x}$ for large x. Thus the function has a long low frequency tail. It is tabulated and graphed by Westfold (1959).

In astrophysical applications of synchrotron theory assemblages of electrons need to be considered. In this case the total power radiated is given by

$$P_a(\nu) = \int n(E)\ P(\nu)\ dE$$

where n(E)dE is the particle density for electrons within the energy range E to E + dE. To obtain the emissivity this quantity should be divided by 4π , assuming the radiation field is isotropic.

It is observed that the cosmic ray electron spectrum has a power law distribution so that

$$n(E)dE = n_o E^{-\gamma} dE$$

where $E_1 < E < E_2$.

In equation (2.1) a change of variables can be made from E to ν/ν_c and then the emissivity is given by

$$\varepsilon(\nu) = 9.3 \times 10^{-37}\ n_o\ B_\perp^{(\gamma+1)/2} (6.26 \times 10^{-20}/\nu)^{(\gamma-1)/2}$$

$$\times\ G(\nu/\nu_1,\ \nu/\nu_2, \gamma)\ \text{watts m}^{-3}\ \text{Hz}^{-1}\ \text{ster}^{-1} \qquad (2.2)$$

with ν in MHz, $B_\perp$ in μ Gauss and n_o in electrons m^{-3} $Gev^{\gamma-1}$. ν_1 and ν_2 are the critical frequencies corresponding to E_1 and E_2 and

$$G(\nu/\nu_1,\ \nu/\nu_2,\ \gamma) = \int_{\nu/\nu_2}^{\nu/\nu_1} x^{(\gamma-3)/2}\ F(x)\ dx.$$

The behaviour of G is discussed in Westfold (1959).

Now provided $\nu_1 \lesssim \nu \lesssim \nu_2$, G will be independent of frequency and thus

$$E(\nu) \propto \nu^{-(\gamma-1)/2}$$

$$\propto \nu^{-\alpha}$$

where α is the emission spectral index. Observations of the galactic background radiation indicate that α varies across the sky and with frequency but lies in the range 0.4 - 0.9. The corresponding variation for γ is 1.8 - 2.8.

Although G cannot be evaluated except by numerical integration the limiting case of $G(\infty, 0, \gamma) = g(\gamma)$ can be epxressed as a product of gamma functions. The difference between $G(\nu/\nu_1, \nu/\nu_2, \gamma)$ and $g(\gamma)$ is a measure of how much the emission is reduced because of the 'missing' electrons having energies above or below the cut-off energies E_1 and E_2. If the frequency of observation is the same as one of the critical frequencies then the value of G will be 10% less than the value of g.

The emission described by equation (2.2) is highly polarized and to remove the polarization this emissivity should be averaged over all values of the inclination of the magnetic field. The resulting expression for the mean emissivity is

$$\varepsilon(\nu) = 9.3 \times 10^{-37} n_o B^{(\gamma+1)/2} (6.26 \times 10^{20}/\nu)^{(\gamma-1)/2} \times g'(\gamma) \text{ watts m}^{-3} \text{ Hz}^{-1} \text{ ster}^{-1} \quad (2.3)$$

where the values of $g'(\gamma)$ (obtained from Moffet, 1969) are given in Table 2.1.

Thermal Absorption

Ionized hydrogen in the interstellar medium absorbs low frequency radio waves as the result of acceleration of electrons by the Coulomb field of the ions. The same mechanism is responsible for the thermal emission at high frequencies.

A derivation of the absorption co-efficient K is given in Shklovsky (1960) and another in Ginzburg (1961).

From Ginzburg,

$$K = 10^{-2} n_e^{\,2} / T_e^{\,3/2} \nu^2 [17.7 + \ln (T_e^{\,3/2}/\nu)] \text{ neper cm}^{-1}$$

where

n_e = free electron number density, el. cm^{-3}

T_e = electron kinetic temperature, K

ν = wave frequency, Hz.

TABLE 2.1

γ	0.5	1.0	1.5	2.0	2.5	3.0	3.5
$g'(\gamma)$	19.8	9.12	2.16	1.50	1.21	1.07	1.03

The term in brackets is a slowly varying function of frequency and temperature, as may be seen in Table 2.2, taken from Hamilton (1969).

If the path length through a region of ionized hydrogen is L, the optical depth is given by,

$$\tau = \int_0^L K \, dl \text{ neper}$$

A useful approximation has been given by Mezger and Henderson (1967)

$$\tau = 8.235 \times 10^{-2} T_e^{-1.35} \nu^{-2.1} E \qquad (2.4)$$

where T_e is in K, ν in GHz, and emission measure

$$E = \int_o^L n_e^2 \, dl$$

has dimensions cm^{-6} pc.

For ν in MHz the equation becomes

$$\tau = 1.64 \times 10^5 T_e^{-1.35} \nu^{-2.1} E \qquad (2.5)$$

If radiation passes through a region of ionized hydrogen the intensity is reduced by a factor of $e^{-\tau}$ due to absorption and the spectrum takes the form $\nu^{-\alpha} e^{-\tau}$.

If emission and absorption takes place uniformly in the same region then Hamilton shows that the intensity is reduced by a factor of $(1 - e^{-\tau})/\tau$.

In figure 2.1 we illustrate the difference in spectral shape for these two types of low frequency turn-over where in both cases $\tau = 40/\nu^2$ and the synchrotron emission has a spectral index of 0.6.

TABLE 2.2

VALUES OF $\zeta = 10^{-2} [17.7 + \ln(T_e^{3/2}/\nu)]$

T_e(K)	ν (MHz)						
	1	3	5	10	20	50	100
500	0.13	0.13	0.12	0.11	0.1	0.09	0.09
1000	0.14	0.15	0.13	0.12	0.11	0.10	0.10
2000	0.15	0.15	0.14	0.13	0.12	0.11	0.11
5000	0.17	0.16	0.15	0.14	0.14	0.13	0.13
10000	0.18	0.17	0.16	0.15	0.15	0.14	0.13

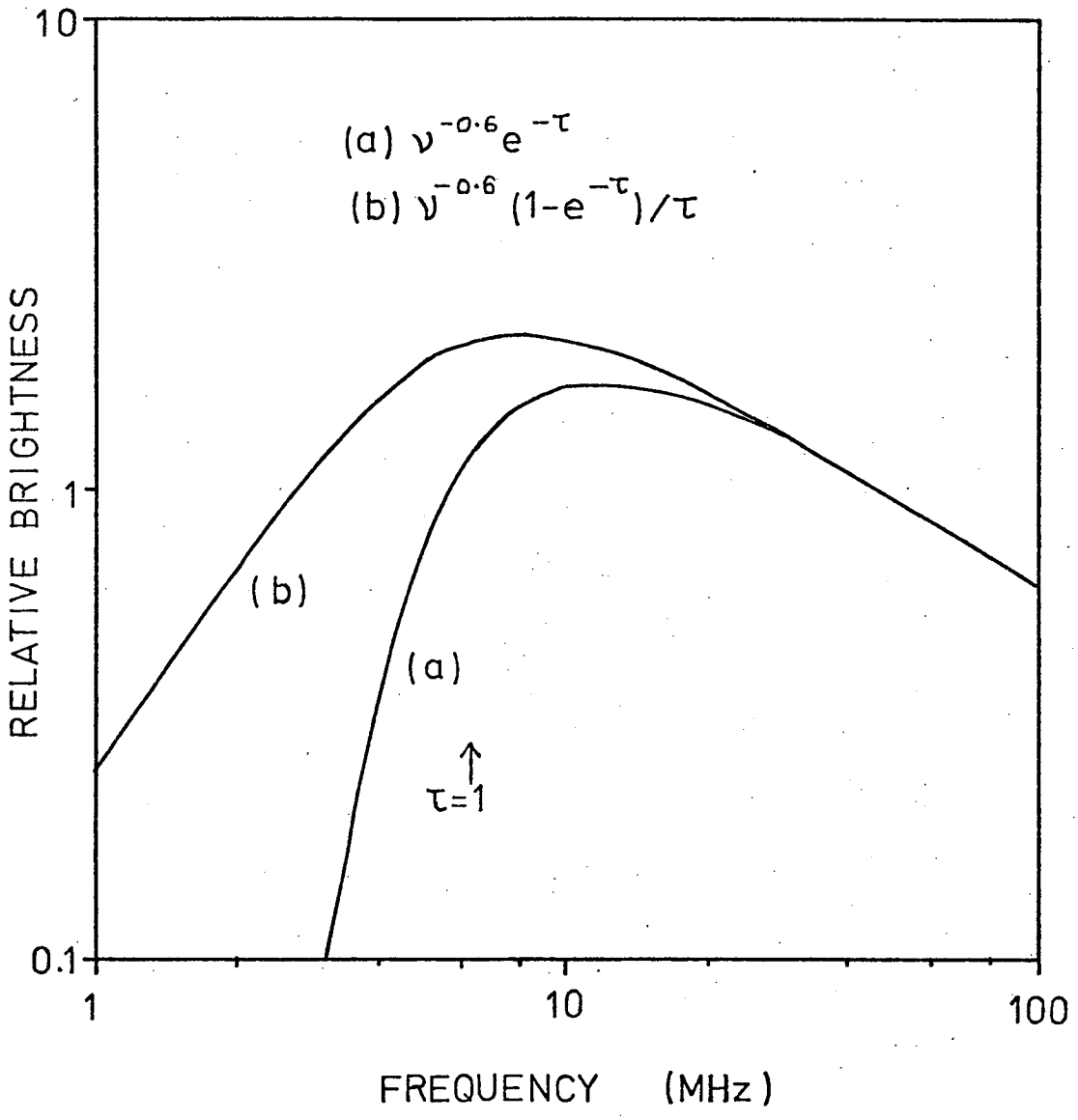
10
1
0.1
1
10
100
RELATIVE BRIGHTNESS
FREQUENCY (MHz)
(a) $\nu^{-0.6}e^{-\tau}$
(b) $\nu^{-0.6}(1-e^{-\tau})/\tau$
(b)
(a)
$\tau=1$

FIGURE 2.1

The effect of the combination of an emitting region A behind a region B of emission and absorption is such that the resulting spectrum is narrower than the spectrum of region B alone when they are normalized at the high frequency end. This is illustrated in figure 2.2. The height of the spectrum of B alone above the spectrum of A+B at the low frequency end is a measure of the magnitude of the brightness of A relative to that of B.

Low Energy Electron Cut-off

If a low energy cut-off exists at some energy E_1 then for observing frequencies much less than ν_1 the intensity of emission is proportional to $\nu^{0.3}$ independent of the value of γ. This is the sharpest low frequency cut-off that can be obtained in a 'pure' synchrotron spectrum not affected by absorption or other processes.

Early interpretations of the galactic background spectral turn over as being due solely to an electron spectral change (Turtle, 1962) were invalidated by lower frequency observations which showed that at frequencies near 1 MHz the north pole spectrum falls off as $\nu^{1.6}$. Nevertheless, an electron cut-off might well exist in addition to absorption by ionized hydrogen. If this was the case then derived optical depths would be over estimates. Figure 2.3 illustrates this. Consider a region of emission and absorption where the emission has a spectral index of 0.4. For spectrum (a) $\tau = 7/\nu^2$ whereas for spectrum (b) $\tau = 4/\nu^2$ and the electron spectrum has a cut-off at an energy such that the synchrotron spectrum turns over at ~3 MHz (spectrum (c)). Only at low frequencies is there any significant difference between spectrum (a) and spectrum (b).

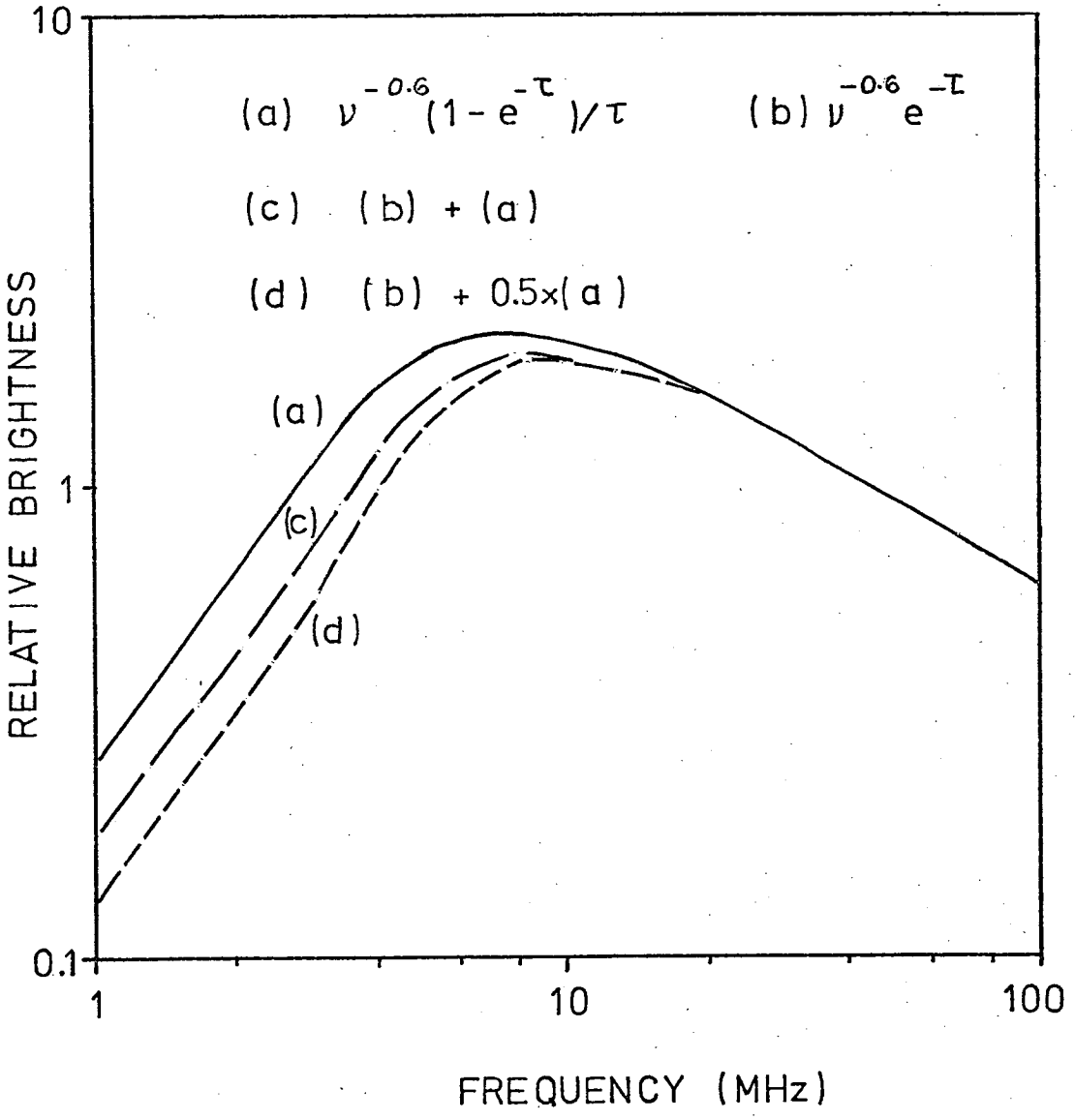
10
1
0.1
1
10
100
RELATIVE BRIGHTNESS
FREQUENCY (MHz)
(a) $\nu^{-0.6}(1-e^{-\tau})/\tau$
(b) $\nu^{-0.6}e^{-\tau}$
(c) (b) + (a)
(d) (b) + 0.5×(a)
(a)
(c)
(d)

FIGURE 2.2

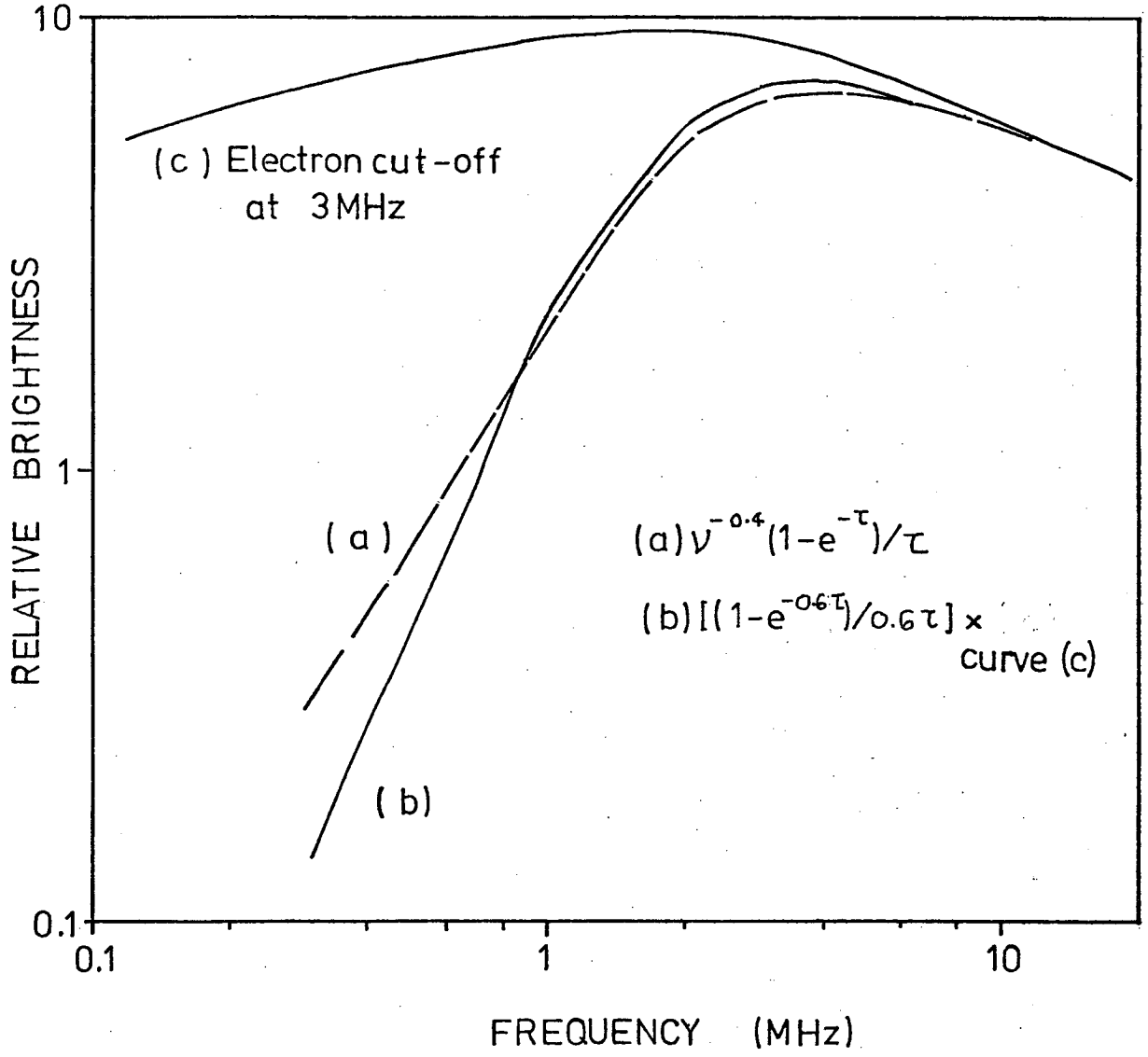
10
1
0.1
0.1
1
10
RELATIVE BRIGHTNESS
FREQUENCY (MHz)
(c) Electron cut-off
at 3MHz
(a)
(b)
(a) $\nu^{-0.4}(1-e^{-\tau})/\tau$
(b) $[(1-e^{-0.6\tau})/0.6\tau]\times$
curve (c)

FIGURE 2.3

The Razin Effect

The Razin (or Razin-Tsytovitch) effect was first investigated in 1951 by Tsytovitch and later by Ginzburg (1953) and Razin (1960). These papers are not readily available but more recently the topic has been dealt with by Ginzburg and Syrovatskii (1964, 1965) and Ramaty (1972). The latter paper is specifically concerned with low frequency background radiation.

The Razin Effect is the suppression of low frequency synchrotron radiation in an ionized medium. It is the result of electromagnetic radiation having a phase velocity in the plasma greater than the speed of light when the plasma has a refractive index less than one. The synchrotron radiation is reduced because the electrons can not keep in phase with the radiation they generate. This is in contrast to the production of synchrotron radiation in a vacuum where the relativistic electrons moving with a velocity near the velocity of light almost keep up with, and strongly reinforce, radiation moving parallel to their path.

One can define a Razin cut-off frequency ν_R which determines the frequency at which the effect of the medium becomes important. For frequencies greater than ν_R the refractive index of the medium is sufficiently close to unity that the emission can be considered to take place in a vacuum.

With this definition of ν_R we have

$$\nu_R = 30 n_e / B \sin\theta \quad \text{MHz}$$

n_e = density of electrons, el. m^{-3}

B = magnetic field, μGauss

θ = observation angle with respect to B

From this equation it is seen that for low frequencies where the emission is suppressed, the strength of the emission will depend on the observation angle with respect to the magnetic field. Thus, except if the component perpendicular to the line of sight of the interstellar magnetic field is small synchrotron emission is only moderately reduced.

Figure 2.4 illustrates that if the Razin effect does cccur and is not accounted for then derived optical depths would be over estimates. Consider a region of emission and absorption where the emission has a spectral index of 0.4. For spectrum (a)$\tau = 7/\nu^2$ whereas for spectrum (b)$\tau = 4/\nu^2$ but the Razin effect is occurring, under the conditions B = 2μG, $n_e = 0.03$ cm^{-3} and $\theta = 90^{o}$. Curve (c) is taken from Ramaty (1972).

It can be seen that the emission spectra illustrated in figures 2.3(b) and 2.4 (b) are almost the same down to ~1 MHz. However, below this frequency the spectrum affected by the interstellar medium falls off more steeply than that from an electron spectrum with a low energy cut-off.

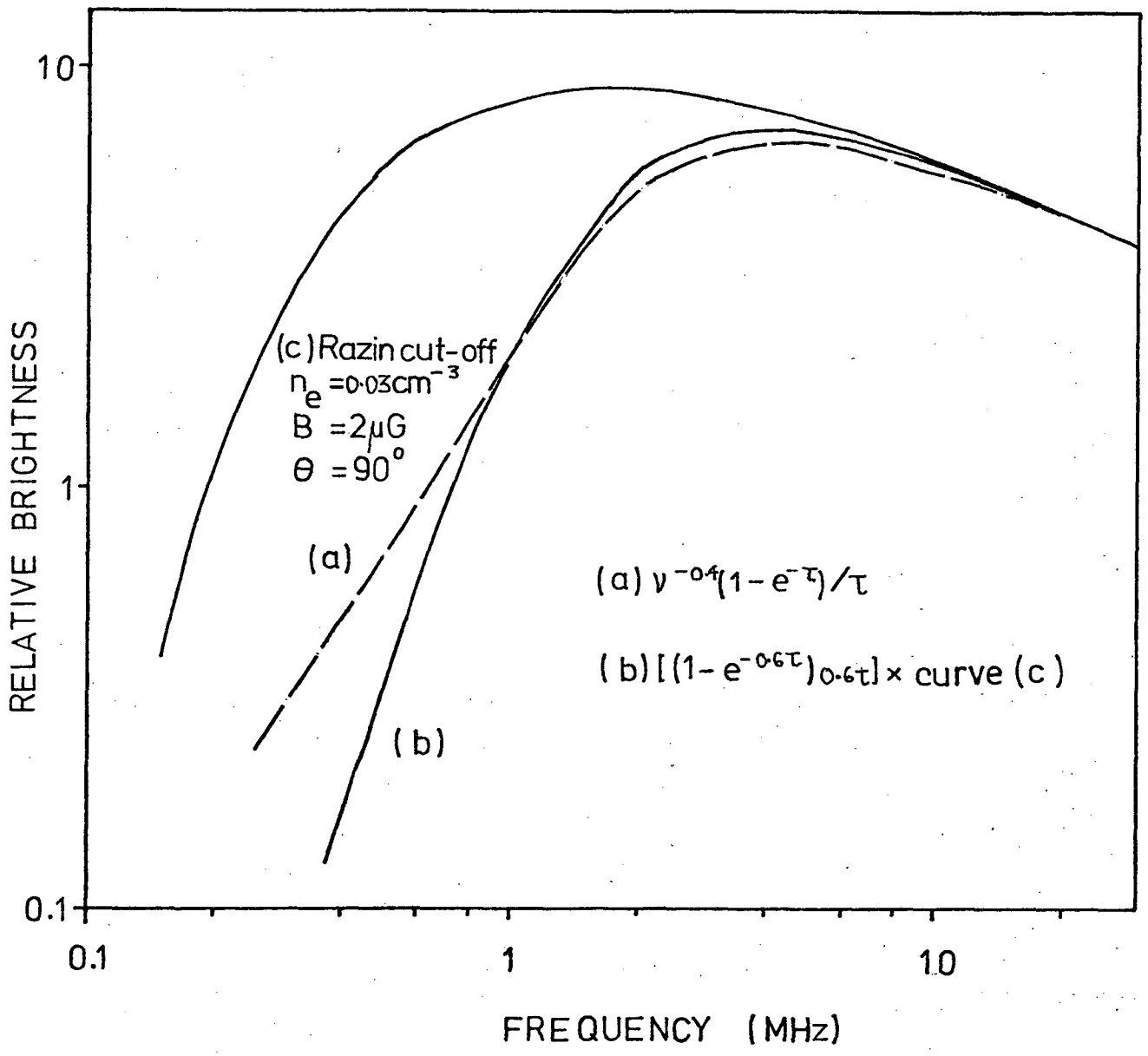
10
1
0.1
0.1
1
10
RELATIVE BRIGHTNESS
FREQUENCY (MHz)
(c) Razin cut-off
$n_e = 0.03 cm^{-3}$
$B = 2 \mu G$
$\theta = 90^\circ$
(a)
(b)
(a) $\nu^{-0.4}(1-e^{-\tau})/\tau$
(b) $[(1-e^{-0.6\tau})_{0.6\tau}] \times$ curve (c)

FIGURE 2.4

REFERENCES FOR CHAPTER 2

GINZBURG, V.L. 1953 Usp. Fiz. N auk. 51 343.

GINZBURG, V.L. 1960 'Propagation of Electromagnetic Waves in Plasmas' (Gordon and Breach, N.Y.)

GINZBURG, V.L. and SYROVATSKII, S.I. 1964 'The Origin of Cosmic Rays' (Pergamon, Oxford).

GINZBURG, V.L. and SYROVATSKII, S.I. 1965 Ann. Rev. of Ast. Astro. 3 297.

HAMILTON, P.A. 1969 Ph.D. Thesis (University of Tasmania).

KIEPENHEUER, K.O. 1950 Phys. Rev. 79 738.

MEZGER, P.G. and HENDERSON, A.P. 1967 Astrophys. J. 147 471.

MOFFET, A.T. 1969 'Astrophysics and General Relativity' Vol. 1 (Gordon and Breach, N.Y.).

RAMATY, R. 1972 Astrophys. J. 174 157.

RAZIN, V.A. 1960 Radiofizika 3 584.

SHKLOVSKY, I.S. 1960 'Cosmic Radio Waves' (Univ. Press, Harvard, Cambridge).

TURTLE, A.J. 1963 Mon. Not. R. astr. Soc. 126 31.

TSYTOVICH, V.N. 1951 Vestn. Mosk. Univ. 11 27.

WESTFOLD, K.C. 1959 Astrophys. J. 130 241.

CHAPTER 3

LIMITATIONS TO LOW FREQUENCY ASTRONOMY

Introduction

The great activity in background radiation studies in the 1960's seems to have faded with the discovery of pulsars and molecular lines; measurements that are made are usually at high frequencies where very high resolutions are now attainable. However, at low frequencies certain important measurements can be made and several phenomena manifest themselves. For example, comparisons between the cosmic ray electron spectrum and non-thermal background spectra must be made at low frequencies where the contribution of a thermal background may be neglected. The distribution of ionized hydrogen in the Galaxy may be investigated by low frequency observations since at these frequencies free-free absorption takes place. At low frequencies emission mechanisms other than the synchrotron process may become dominant under certain conditions. Yet,because of the difficulties involved many observations have not been made.

For ground-based observations there are three main difficulties:

"(1) Antennas of several kilometres extent are required for resolution better than 1 degree. Dashed lines in Figure 1 illustrate the resolution attainable with apertures of 3, 10 and 30 km width.

(2) Conditions in the Earth's ionosphere vary with time of day, time of year, and solar activity. Observing is possible only when the electron density in the F-region is sufficiently low and relatively free of irregularities on the kilometre scale.

(3) There are no frequency allocations for radio astronomy below 20 MHz. World radio communications make extensive use of these frequencies for propagation via ionospheric reflections. For this reason it is extremely difficult to find sites on the Earth sufficiently remote from interfering signals. It is significant that the few ground-based measurements below 10 MHz have been made from Tasmania which from an interference point of view can be regarded as relatively remote".

The above is extracted from a C.C.I.R. document (1975) on ground-based radio astronomy below 20 MHz. Figure 3.1 (from this document) shows the angular resolution of telescopes which have been used or are in use below 100 MHz.

Observations are also made from above the Earth's ionosphere from satellites and rockets. In recent years the NASA programme has contributed greatly to our knowledge of the low resolution, low frequency spectra. However, there are also limitations to this type of observation, in addition to the obvious short comings of rocket observations viz. the limited observing period. These are:-

(1) The lack of resolution -aerial beams are typically 100^{o}.

(2) The problem of determining the direction in which the aerial is pointing.

(3) In addition to man-made interference the aerial picks up exospheric emissions.

(4) Varying aerial impedance.

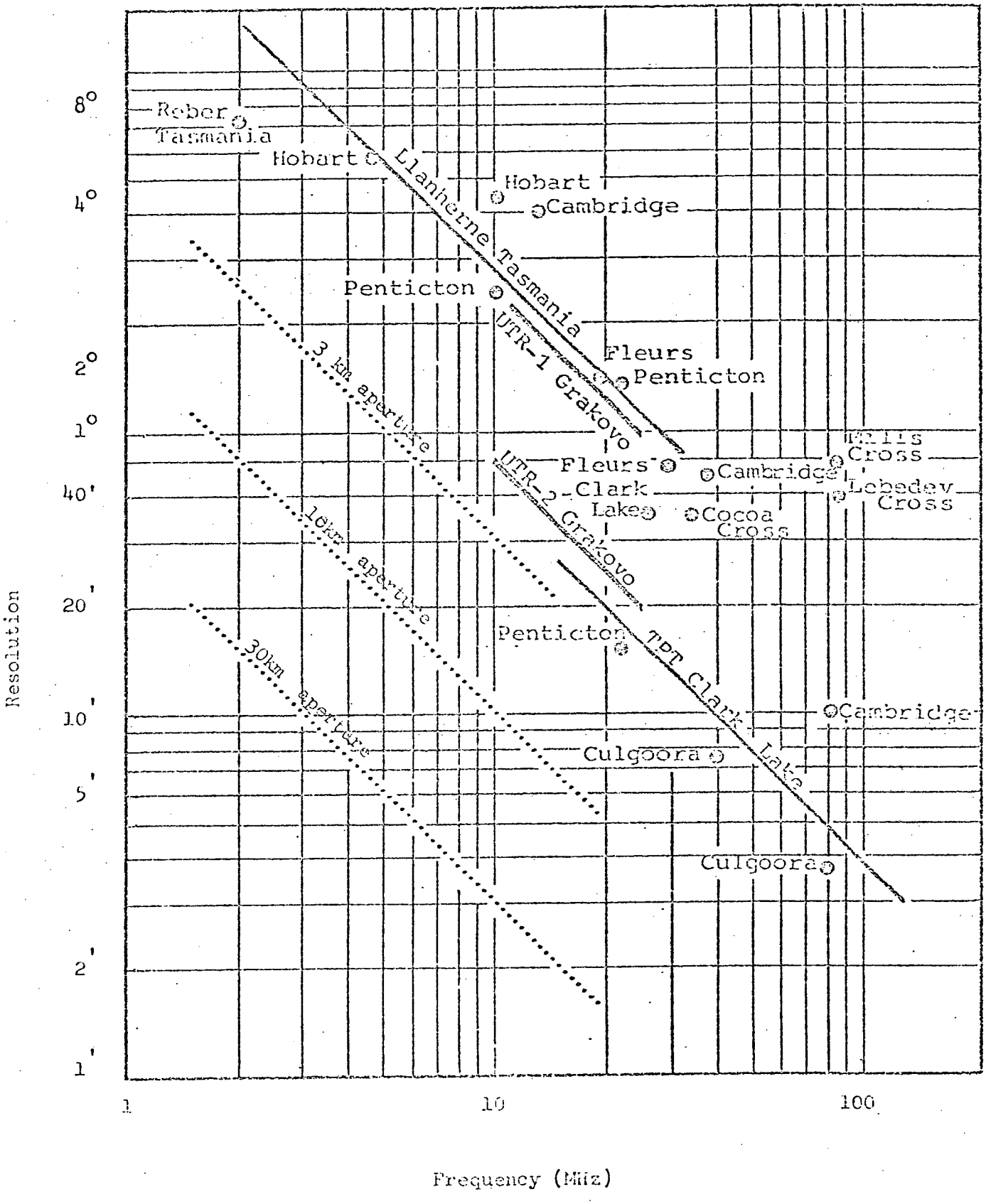
8°
4°
2°
1°
40'
20'
10'
5'
2'
1'
Resolution
1
10
100
Frequency (MHz)
Reber
Tasmania
Hobart
Llanherne Tasmania
Hobart
Cambridge
Penticton
UTR-1 Grakovo
Fleurs
Penticton
3 km aperture
Fleurs
Cambridge
Mills Cross
Lebedev
Cross
UTR-2 Grakovo
Clark
Lake
Cocoa
Cross
10km aperture
Penticton
TPT Clark Lake
Cambridge
30km aperture
Culgoora
Culgoora

FIGURE 3.1

Ionospheric Limitations

Ground-based observations are only possible when the cosmic radio emissions can propagate through the ionosphere and this occurs when the critical penetration frequency of the ionosphere f_oF_2 is less than the observing frequency. Such observing conditions can be realized at very low frequencies ($\lesssim$ 1.5 MHz) but only under strict limitations.

Firstly, observations must be made at night time during the 4-5 years around sunspot minimum.

Secondly, the world contours of f_oF_2 illustrate that there are geographic limitations and that a minimum in the F-region electron density exists at geomagnetic latitudes 40^o-50^o. Figure 3.2 (taken from Ellis and Hamilton, 1965) shows the variation of f_oF_2 with geographic latitude observed by the Alouette I satellite (Muldrew, 1965).

In the winter months at mid-latitude stations up to 9 hours of available observing time at 3 MHz can occur. But at the same time there are probably no hours when interfering signals can not propagate by reflection. Figure 3.3 shows the average number of hours per night that f_oF_2 was less than 4 MHz for the years 1973-1976 at Hobart. Figure 3.4 shows the same information for the years 1961-1964 (taken from Ellis, 1965) illustrating the variation of conditions from one solar cycle to the next.

Even when the critical frequencies are low ionospheric absorption can occur. Ellis (1965) discusses fully the effect of ionospheric absorption and screening due to ionospheric refraction. Figure 3.5 (taken from Ellis, 1965) shows the total calculated attenuation as a function of f_oF_2 for different observing frequencies.

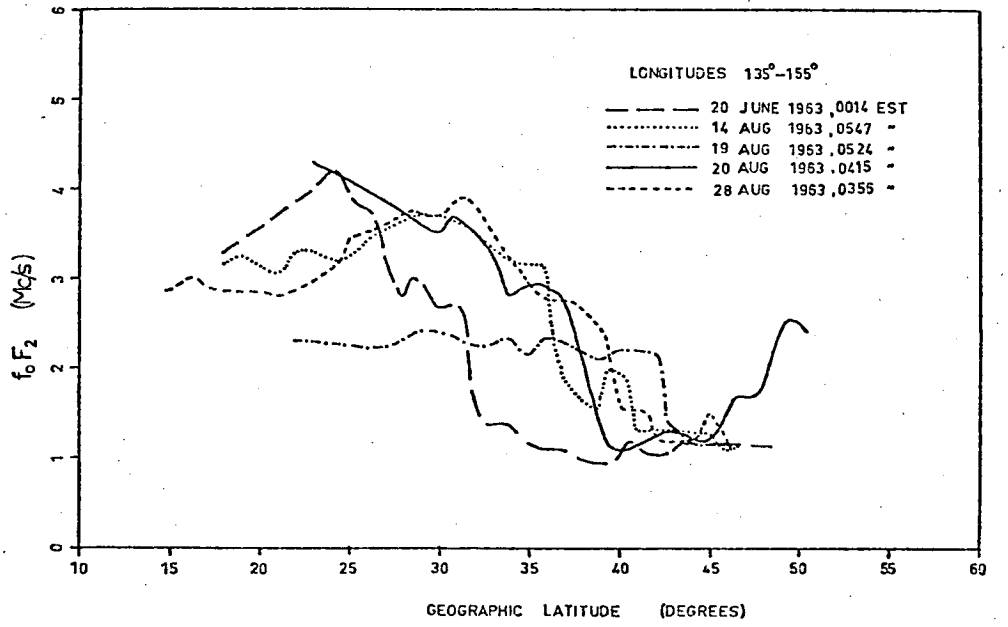

Sample curves showing the variation of ionospheric critical frequency f_0F_2 with geographic latitude observed by Alouette satellite.

FIGURE 3.2

after Ellis and Hamilton (1966)

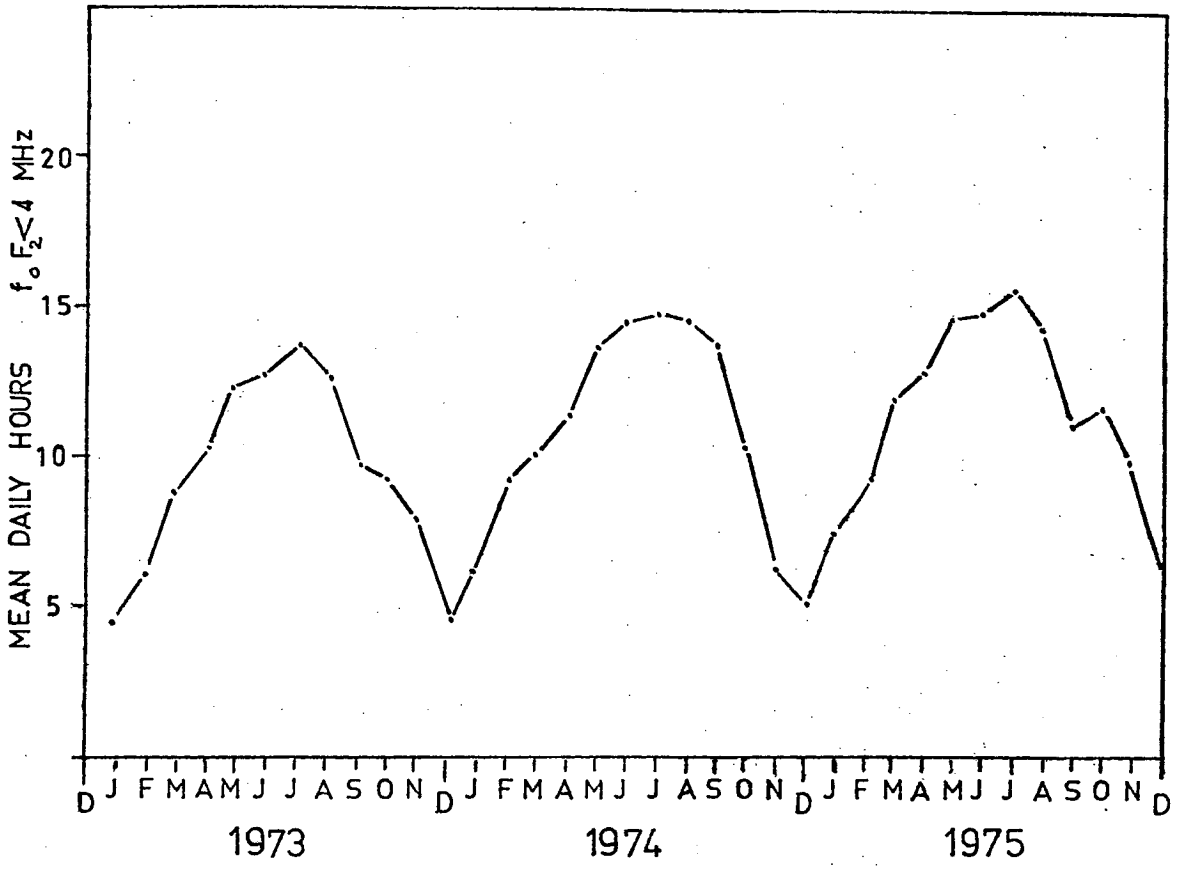

FIGURE 3.3

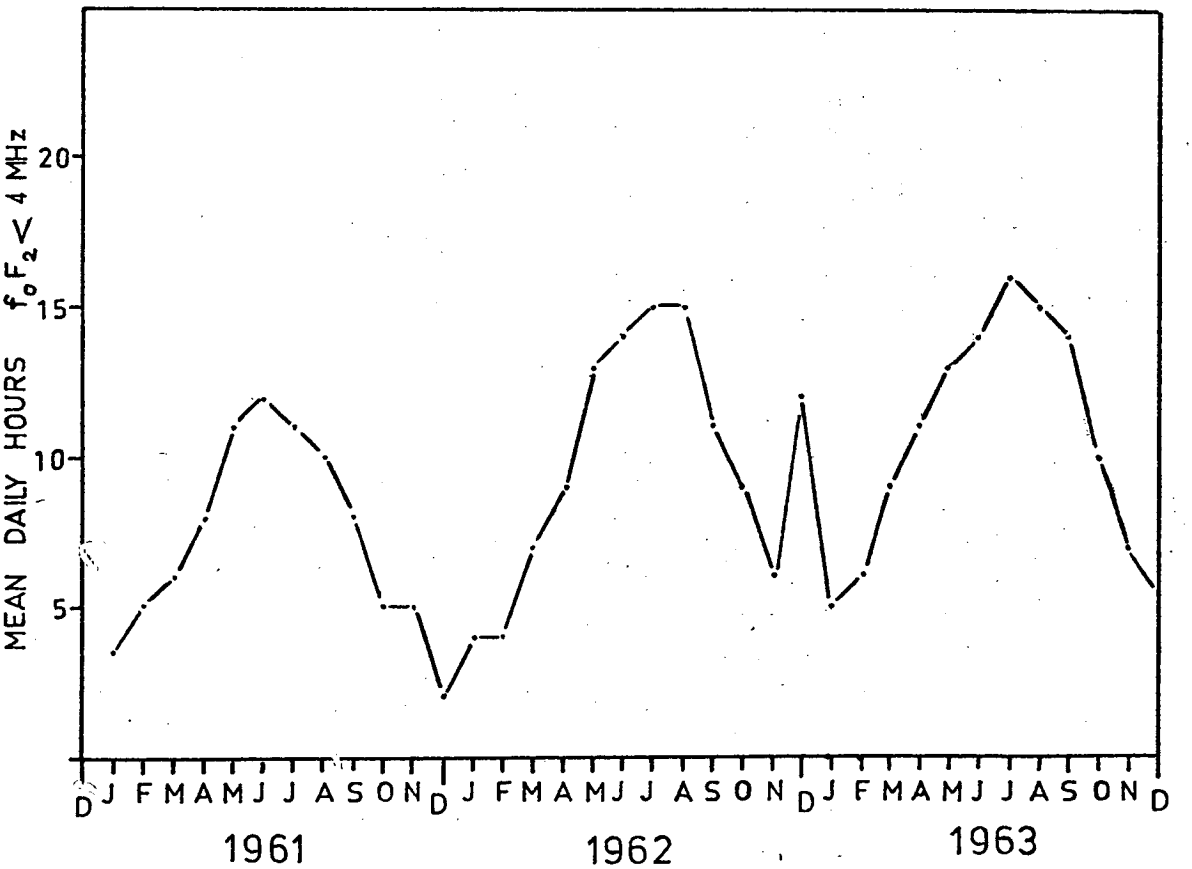

FIGURE 3.4

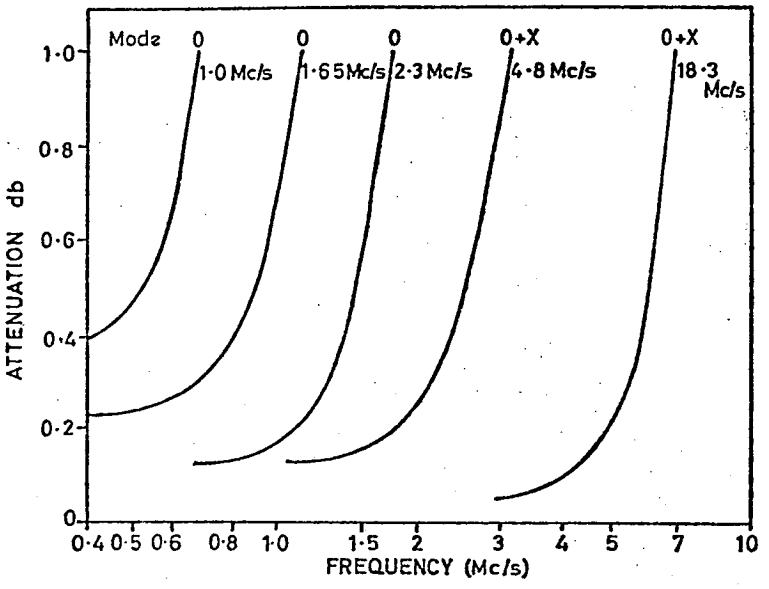

Variation of total attenuation with f_0F_2.

FIGURE 3.5

after Ellis (1965)

Transmitting Station Interference

Unless the critical frequency is less than 0.3 of the transmitting frequency, reflection of transmitting station signals takes place and given the signals have sufficient radiating power they may reach a radio telescope after multiple hops from almost anywhere on the Earth's surface.

Because the above condition is not often realized at low frequencies a technique has been developed to reduce the effects of this interference. This is the minimum reading technique discussed in Appendix I. By careful selection of the observing frequency the problem can be minimized and in addition, for sky surveys at least, during observations the frequency can be altered slightly to avoid transmitting stations. However, the only way to obtain reliable information is by the duplication of records.

Limitations on Absolute Calibrations

Calibration Sources

At frequencies less than 20 MHz no suitable primary standard exists and a secondary standard must be used. This standard must provide equivalent temperatures in the range 10^5 - 10^6 K.

Above 100 MHz thermal loads are used but they do not provide large enough signals at lower frequencies. Between ~ 20 and 100 MHz the accepted standard is the temperature saturated noise diode (described by Van der Ziel, 1955) which can give equivalent temperatures up to 10^5 K. These must be calibrated against a thermal source.

The secondary standard used in the present work was a Zener diode calibrated against a temperature saturated noise diode. This noise generator could provide temperatures greater than 10^7K.

Antenna Gain

The calibration of a radio telescope involves replacing the aerial with a calibration source of the same impedance. However, this only gives the relative calibration of receiver gains and to obtain sky temperatures one needs to know the antenna gain as a function of zenith angle.

The antenna gain is mainly determined by the losses in the aerial feeder cables. In addition, account must be taken of the ground radiation, if significant, and the power loss from imperfectly reflecting ground screens.

At low frequencies with large arrays these calculations are not simple and usually a semi-empirical derivation is performed. This is achieved by using 'expected' values of point source intensities obtained from extrapolation of higher frequency data. There are a limited number of sources observable at low frequencies so that as an alternative the 'expected' response to background emissions in regions of minimal variation is used. This can involve extrapolating higher frequency data which necessitates the assumption of a spectral index. But in Tasmania it has become practice to use low resolution measurements of the south galactic pole to estimate antenna gains.

REFERENCES FOR CHAPTER 3

C.C.I.R. 1975 Proposed New Report Doc. 2/9-E

ELLIS, G.R.A. 1965 Mon. Not. R. astr. Soc. 130 429.

ELLIS, G.R.A. and HAMILTON, P.A. 1966 Astrophys. J. 143 227.

MULDREW, D.B. 1965 J. Geophys. Res. 70 2635.

VAN DER ZIEL, A. 1955 'Noise' (Chapman and Hall, London).

CHAPTER 4

THE INTERSTELLAR MEDIUM

Introduction

In Chapter 7 we derive a model of the Galaxy in which synchrotron emission and thermal absorption take place in spiral arms. Prior to this it is important to summarize the currently acceptable values for properties of the interstellar gas and the magnetic fields. We are reasonably certain about some of these values but for others we can only place limits. One of the greatest problems is that the observations measure different combinations of parameters. In many cases the measurement gives an integral along the line of sight and path lengths are uncertain.

The basic component of the interstellar gas is hydrogen and interstellar space is often divided into two regions depending on the state of the hydrogen. In HII regions the gas is ionized whereas it is predominately neutral in the HI region. The latter is further divided into cool dense clouds and a tenuous hot intercloud medium. Theories predict that both components are partially ionized.

In this chapter we will discuss the distribution of the interstellar gas and magnetic fields with particular emphasis on spiral and radial features. In addition, we summarize the observations of free electrons in the Galaxy, with particular reference to electron temperatures and densities.

HII Regions

If a hot star is surrounded by a cloud of interstellar gas the far ultra-violet radiation from the star ionizes the hydrogen. When the cloud is not small the radiation can only travel a certain

distance before it is completely absorbed so that there exists a zone of radius S_o beyond which the hydrogen remains neutral. The region of ionized hydrogen is called a Strömgren sphere. S_o, the Strömgren radius, can be shown to be dependent on the star's spectral class and inversely proportional to the gas density. Only O and B stars have Strömgren spheres of significant size.

HII regions can be observed in many ways. Their distribution is of considerable interest as they are excellent spiral arm tracers. A comprehensive review of the properties of HII regions is presented by Mezger (1972) and, in particular, he summarizes the interpretation of the radio observations. Below we summarize the basic results of the optical and radio observations.

(a) Optical Observations

HII regions emit all the hydrogen series lines but only the Balmer series are easily observed. A number of photographic Hα surveys have been made, of which the most recent and most extensive is that of Sivan (1974), which covers the whole galactic plane. The longitude distribution shows a clustering of regions in directions towards the galactic centre corresponding to the Sagittarius arm, and in the longitude range 98^o- 273^o corresponding to the Perseus and Orion arms.

Kinematic distances derived from interferometric studies of Hα emission, combined with photometric distances of the exciting stars have been plotted to give the radial distribution of HII regions (Courtes, 1973). The local spiral arms are well defined as seen in figure 4.1. However, optical measurements

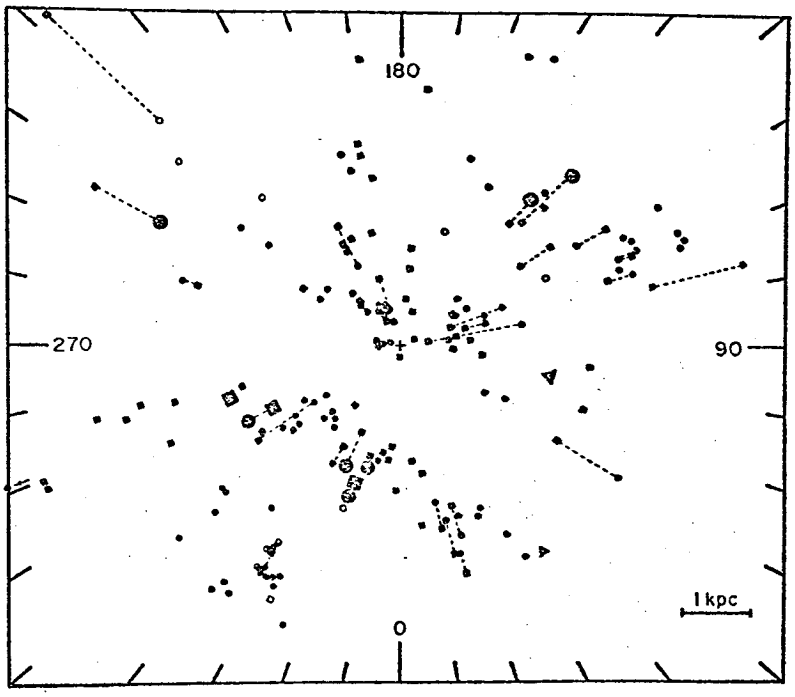

Distribution of H II-regions according to Courtès (1973). Kinematic distances of the H II-regions are indicated by dots, spectrophotometric distances of the exciting stars by squares

FIGURE 4.1

are limited to HII regions within about 3 kpc of the Sun owing to extinction by interstellar dust.

(b) Radio Observations

(i) Free-free transitions

In the GHz range many HII regions are seen as discrete sources on a background of radiation. The longitude distribution of thermal sources exhibits peaks in various directions which are interpreted to be directions in which we look tangentially along spiral arms. For northern hemispheres surveys the main peaks occur at $\ell = 25^{\circ}$ and $\ell = 50^{\circ}$. The latitude distribution is narrow and has a half-power width of less than 2°. A comparison of optical HII regions with thermal sources indicates that they pertain to different evolutionary stages. Strong thermal sources are usually young, compact HII regions. Most of the optically observed HII regions are only weak thermal sources.

At low radio frequencies HII regions absorb non-thermal radiation. It is found that there is a close correlation between optically observed HII regions and regions of discrete absorption on low frequency maps (see, for example, figure 6.16).

(ii) Radio recombination lines

This is the most useful measurement for observing the large scale distribution of HII regions. Several surveys of the H109α line have been made.

The basic results of such work are that the distribution of giant HII regions exhibits a maximum between 5 and 6 kpc from the galactic centre, a secondary maximum between 7 and 8 kpc and a virtual absence of giant HII regions beyond 12 kpc (Mezger, 1970).

The HI Distribution

Most of the interstellar matter is neutral hydrogen. The prediction and subsequent observation of the λ21 cm hyperfine transition opened up the way to studying the gas throughout the Galaxy. The first 'picture' of the large scale distribution of HI was the Leiden-Sydney map (Oort et al., 1958) which showed that the gas was concentrated into spiral arm features. The map displayed contours of the volume-density of the hydrogen in spatial co-ordinates with the density derivation based on the assumption of circular symmetry. This assumption is not really valid as there exist irregularities in velocity, density and temperature so that a direct transformation from velocity to distance is not possible. Nevertheless, certain features can be distinguished and these are discussed by Kerr (1969),(1970). A later review of the large scale HI distribution is given by Burton (1974).

Apart from the spiral structure of the HI distribution there are several other aspects which need to be considered. The accepted value for the average volume density of emitting H atoms is about 0.4 cm^{-3} with the density contrast between arm and interarm regions being between 3:1 and 7:1. The thickness of the layer increases in the outer regions of the Galaxy with the scale height between 4 and 9 kpc radius being about 200 pc.

Prior to 1965, models of the hydrogen distribution assumed a uniform temperature T_s = 125 K throughout the Galaxy. However absorption studies indicated that the temperature of the gas clouds was much lower than this and it was proposed by Clark (1965) that the gas was distributed into cold clouds (T_s < 100 K) embedded

in a hot medium with $T_s > 1000$ K. Since Clark's proposal there have been many theoretical discussions on the conditions in the two phases. An extensive review paper has been presented by Dalgarno and McRay (1972). The two models which have received the most attention are those of Field, Goldsmith and Habing (1969) and Hjellming, Gordon and Gordon (1969). Both models are based on heating by low energy cosmic rays and the main difference between them is the temperature of the intercloud medium. Field et al. predict a temperature greater than 8000 K in contrast to the 1000 K predicted by Hjellming et al.

Among the other heating sources that have been suggested are soft X-rays and bursts of hard ultraviolet radiation from supernovae. A comprehensive review of the heating and cooling of the HI gas is presented in the Dalgarno and McRay paper including the energy source problems raised by the observations. Various methods are presented for distinguishing between cosmic ray and X-ray heat sources.

Diffuse Ionized Hydrogen

Theories which predict heating of the interstellar gas also predict partial ionization. The predicted ionizations are $n_e/n_H \lesssim 0.2$ for the interlcoud and $n_e/n_H \lesssim 0.03$ for the clouds (Dalgarno and McRay, 1972). Electron densities in the range 0.01 cm^{-3} to 0.1 cm^{-3} are obtained. There are several effects which indicate the presence of free electrons. These are:-

1. Pulsar signal dispersion
2. The presence of a thermal radio background
3. The presence of background radio recombination lines

4. Hα emissions away from known HII regions
5. Free-free absorption of the radiation from sources and of the galactic background radiation
6. Faraday rotation of sources
7. Interstellar absorption lines

Although most of these effects have been attributed to free electrons in the HI gas, particularly at the time when the partial ionization of the HI gas was predicted, in latter years many authors have suggested that certain effects could take place in low density HII regions (e.g. Mezger, 1972; Walmsley and Grewing, 1971). Certainly this is likely for lines of sight close to the galactic plane but the presence of free electrons at heights much greater than 100 pc as indicated by pulsar measurements probably rules out HII regions as their source.

The uncertainty arises because of the difficulty in determining the properties of the ionized gas. There are three major problems associated with the derivation of electron densities from the above measurements.

(1) An all cases there is confusion as to the contribution of HII regions. In particular the properties of HII regions around B stars are not well known.

(2) For many of the observations the quantity determined is a function of temperature and electron density and the two parameters cannot be properly separated.

(3) Different measurements pertain to different regions of the Galaxy. For example, Hα emission measurements can only give information about the gas within a few kpc of the Sun whereas radio recombination line data is from the inner regions of the Galaxy.

Below we summarize the information obtained from each type of measurement.

1. Pulsar Observations

The dispersion of pulsar signals gives a measure of $\int_0^L n_e \, dl$ where L is the distance to the pulsar and n_e the electron density. A measure of $\langle n_e \rangle$ can be obtained if the distance to the pulsar is known. However distances can only be estimated except for those pulsars which are associated with supernova remnants. Limits can be placed on the distances of several pulsars from measurements of their 21 cm line absorption (eg. Manchester et al., 1969; Guelin and Gomez-Gonzalez, 1974) and the results indicate mean electron densities ranging from $\langle n_e \rangle = 0.03$ to 0.12 cm^{-3}. The contribution of HII regions to the dispersion is uncertain. Rees and Sciama (1969) maintain that pulsars with DM $\gtrsim 10 \text{ cm}^{-3}$ pc probably lie behind at least one HII region.

Assuming that the dispersion does take place in the HI gas two useful properties can be derived. Firstly, $n_e \approx 0.03 \text{ cm}^{-3}$ and is constant within a factor of two within a few kpc of the Sun. Secondly, the layer is thicker than 0.8 kpc (see Guelin, 1974).

2. Thermal Background

For two reasons we believe the thermal background is not produced in HI regions but rather in low density HII regions. Nevertheless, it is convenient to discuss the thermal background at this stage. The reasons for our conclusions are:-

(1) The longitude distribution indicates that the gas is confined to the central regions of the Galaxy where there is a high formation rate for HII regions.

(2) Electron temperatures can be obtained from radio recombination line data and these combined with the thermal brightness temperatures (assuming they are accurately evaluated) give electron densities at least 10 times those to be expected in the HI gas. Such a calculation has been made by Mathews et al. (1973) who maintain they can justify the assumption that the emitting gas is in the local thermodynamic equilibrium condition.

The actual proportion of the background radiation which is contributed by thermal emission is a very important quantity, particularly for the estimation of electron temperatures and emission measures from radio recombination line observations. The original continuum observed at 1.4 GHz by Westerhout (1958) was later resolved almost completely into individual sources.

Separations of the background into its thermal and non-thermal components by virtue of their differing spectral indices have been made by a number of observers eg. Westerhout (1958), Mathewson et al., (1962) and Komesaroff (1961), using data in the range 1420-20 MHz. They found a ridge of thermal emission of half-power width ~ 1^{o} and extending $\pm$ 40^{o} from the galactic centre. Presumably many discrete sources remained unresolved as

beam-widths of 0.5^{o} to 1.4^{o} were used.

High resolution observations at 15 GHz (resolution of 11' arc) by Hirabayashi et al. (1972) indicated that at this frequency about 80% of the brightness is from thermal emission.

The observations of GHz radiation which are most frequently quoted are those of Altenhoff et al. (1970) and Altenhoff (1968) at 1.4, 2.7 and 5.0 GHz made with 11' arc beamwidths. Altenhoff (1968) states that the observations "show that the unresolved background is non-thermal". The statement by Mathews et al. (1973) that Altenhoff was referring to the radiation "in the lowest temperature saddles" and not to all the galactic ridge is confusing and seems unfounded. However, Mathews et al. have analyzed the data and determined the thermal component of the 1.4 GHz continuum emission. It appears that at some longitudes considered by them the thermal contribution has been over estimated -they obtain values greater than 75%. An average of values for the other longitudes is 25%. This is in reasonable agreement with the Hirabayashi et al. estimation and the value obtained by Jackson and Kerr (1971), the latter estimate being derived from the Altenhoff data. We conclude that at 5 GHz 50% of the background radiation is thermal. As the emitting gas has an electron temperature of 6000 K and an emission measure of ~ 2700 cm^{-6} pc we conclude that the emission comes from low density HII regions.

3. Radio Recombination Lines

Deductions from radio recombination line measurements depend on the determination of the thermal contribution T_c to the background radiation. The electron temperature T_e of the emitting gas can be calculated from T_c and then from T_e and T_c the emission

measure $E = \int n_e^2 dl$ can be calculated.

Gottesman and Gordon (1970) attribute the emission to the intercloud medium as they obtain $T_e \lesssim 10^3$ K and $\langle E \rangle \simeq 610$ cm^{-6}pc under the assumption that at 1.6 GHz T_c contributes less than 10% to the background. However, Mathews et al.(1973) estimate T_c to be about 25% at 1.4 GHz which gives $T_e = 6000$ K and $\langle E \rangle \simeq 2700$ cm^{-6}pc. These parameters are typical of low density HII regions (Pedlar and Davies, 1972).

Cesarky and Cesarky (1971) and Gottesman and Gordon (1972) have argued that the recombination line emission comes from the cool clouds and that free-free emission comes from the hot gas. However a strong correlation between recombination line emission and thermal brightness is shown to exist by Mathews et al. and this correlation has also been noted by Mezger (1972). The fact that the recombination line emission and the thermal background are confined to galactic radii less than about 7 kpc supports the idea that they arise in low density HII regions.

4. Diffuse Hα Emission

Diffuse Hα emission has been observed between known bright HII regions (Reynolds et al., 1973; Meaburn, 1972; Sivan, 1974). The detection of [NII] emission by Reynolds et al. means that the electron temperature must be greater than 3000 K and the intensity ratio [NII]/Hα suggests that the gas may be nearly totally ionized. They assume an electron temperature of 6000 K and calculate a mean square electron density $\langle n_e^2 \rangle \simeq 0.05$ cm^{-6} in the Orion arm and $\langle n_e^2 \rangle \simeq 0.1$ and 0.9 cm^{-6} in the Perseus and Sagittarius arms respectively. It is suggested that the

emission comes from low density HII regions.

5. Free-free Absorption

Free-free absorption causes the spectra of discrete sources and of the background radiation to turn over at low frequencies. The frequency at which the spectra turn over gives a measure of $\int n_e^2 T_e^{-1.35} dl$. We will summarize the observations and the properties derived for the two types of emmision separately and then present an overall summary. Since the optical depth is a function of n_e and T_e we can only place limits on certain properties of the absorbing gas.

(i) Discrete Sources

80 MHz observations of 20 supernova remnants have been made by Dulk and Slee (1972). Assuming a range of electron temperatures they obtain electron densities in excess of those predicted for the HI gas. However several of the absorbed sources lie behind visible HII regions and the line of sight to nearly every source passes through the region indicated by radio recombination line data to contain many HII regions. In fact it seems surprising that some sources have straight spectra.

The source observations at 10 MHz by Bridle (1969) can not be dismissed so easily. Firstly, the sources are not in the galactic plane (as were those observed by Dulk and Slee) and secondly, they lie in the anti-centre direction away from the concentration of HII regions in the inner regions of the Galaxy. Nevertheless, the two sources with optical depths >1 would appear to lie behind optically visible HII regions. For the remainder of the sources the average optical depth is 0.5 which implies

that $\int n_e^2 T_e^{-1.35} dl = 3.8 \times 10^{-4}$ cm^{-6}K$^{-1.35}$pc.

(ii) Non-Thermal Background Radiation

Later in this thesis we present galactic spectra for the longitude range 320^o -40^o but prior to this work the only directions in which spectra could be drawn with any certainty for frequencies less than 20 MHz were the galactic polar, the northern minimum and the anti-centre directions. These are illustrated in Chapter 5 where it is shown that the north and south polar spectra turn over at ~ 2 and 5 MHz respectively, whereas the anti-centre spectrum turns over at about 10 MHz. These values imply that $\int n_e^2 T_e^{-1.35} dl \simeq 2.6 \times 10^{-5}$ cm^{-6}K$^{-1.35}$pc for the polar directions, neglecting for the moment the differences between spectra of the different hemispheres, and $\int n_e^2 T_e^{-1.35} dl \simeq 1.8 \times 10^{-4}$ cm^{-6}K$^{-1.35}$pc for the anti-centre direction. These values assume the emission and absorption are uniformly mixed. If, however, the majority of the emission comes from behind the absorbing medium these values would be high by a factor of approximately 2.

(iii) Discussion

The absorption could be due to (a) low density HII regions presumably confined to spiral arms with T_e = 6000 K (b) the inter-cloud medium with $\langle n_e \rangle$ = 0.03 cm^{-3}, assumed to be uniform, or (c) cold dense clouds with $\langle n_e \rangle \simeq 0.03$ cm^{-3}.

We deal with case (c) first as it is believed this can be excluded. Although the original models of the two phase interstellar medium predicted that the absorption would occur overwhelmingly in the clouds many authors have considered that the uniformity of absorption across the sky can rule out this possibility.

Hamilton (1969) discusses this topic more fully.

Case (a) -Several authors have suggested the presence of low density HII regions to explain several types of observation of free electrons. Probably the presence of Hα emission away from HII regions combined with [NII] observations is the most convincing evidence. The half width of the medium would be ~ 100 pc and the temperature 6000 K. Putting these values in our estimates of $\int n_e^2 T_e^{-1.35} dl$ they imply mean square electron densities of about 0.09 cm^{-6} in the polar directions.

Case (b) -Pulsar observations indicate that the electron layer causing the dispersion is thicker than 0.8 kpc (Guelin, 1974; Falgarone and Lequeux, 1973; Lyne, 1974). If we assume $\langle n_e \rangle = 0.03$ cm^{-3} we obtain $T_e \simeq 750$ K in the polar direction.

It can be seen that it is not possible to differentiate between case (a) and case (b) as they both have properties consistent with other data. Probably the answer is a compromise with both types of medium contributing to the absorption.

6. Faraday Rotation

Faraday rotation of polarized radiation from radio sources gives a measure of $\int n_e B_L dl$ where B_L is the line of sight component of the magnetic field.

The latitude distribution of the rotation measures of extragalactic sources has been shown to be consistent with the presence of a uniform disk of electrons (Berge and Seilestad, 1967; Falgarone and Lequeux, 1973). Electron densities can be obtained by assuming a value for the galactic field strength and for the half thickness of the disk. Observations of the galactic field

will be discussed in the next section. They indicate that the field strength is approximately 2 μG.

The results of Berge and Seilestad give $\int n_e B_L dl = 20$ cm^{-3} μG pc in the galactic pole direction. Taking a half thickness of 400 pc we obtain $\langle n_e \rangle \simeq 0.02$ cm^{-3}. A similar model of Falgarone and Lequeux gives $\langle n_e \rangle = 0.025$ cm^{-3}.

Although these analyses ignore the possible rotation intrinsic to the source or taking place in the intergalactic medium and the possible complexity of the magnetic field they indicate that the rotation occurs in the same gas which causes the dispersion of pulsar signals.

7. Interstellar Absorption Lines

Information about free electrons within a few kpc of the Sun can be obtained from interstellar absorption lines in front of hot stars. The relative distribution of the stages of ionization can be used to estimate the electron density and to determine the possible sources of ionization.

From an analysis of the CaI to CaII ratio White (1973) derived electron densities in clouds of $n_e \simeq 0.03$ cm^{-3}. The main problem with this type of observation is the difficulty in separating out the contribution of the star's own HII region.

Summary

The observations indicate that there exists a uniform intercloud medium of mean electron density $\langle n_e \rangle \simeq 0.03$ cm^{-3} which extends to at least 400 pc above the galactic plane and is responsible for the observed effects of pulsar dispersion, Faraday rotation and low frequency absorption at high galactic latitudes. For lines

of sight near the galactic plane classical HII regions contribute greatly to the effects attributed to the intercloud medium. It is probable that within the spiral arms there exist low density HII regions which form an essentially continuous medium with mean square electron density of approximately 0.1 cm^{-6} and electron temperature 6000 K.

The Galactic Magnetic Field

The types of observation which enable estimates of the galactic magnetic fields are as follows:-

(i) Zeeman splitting of spectral lines,

(ii) Polarization of starlight,

(iii) Faraday rotation of linearly polarized radiation of radio sources,

and (iv) Polarization and magnitude of the galactic synchrotron radiation.

Although there exist inconsistencies when comparing data from the different observations a picture of the magnetic field emerges. This is that the field lies parallel to the galactic plane, has a field strength of approximately 2 μG and is directed towards longitudes $\ell = 50^{\circ} - 90^{\circ}$ (Whiteoak, 1974).

(i) Zeeman Splitting

This is the least useful measurement at this stage as the uncertainties in the measurements are too large. The values derived for the field are much higher than those yielded by other techniques and it is thought that they pertain to localized regions of compressed fields. A summary of the observations is given by Verschuur (1972).

(ii) Polarization of Starlight

This type of measurement does not allow an estimate of the field but gives the direction of the transverse field component. Measurements on thousands of stars have been made by Mathewson and Ford (1970) and the results plotted for stars in different distance groups. For most of the stars at distances greater than 2 kpc the radiation is strongly polarized and the results are consistent with a field parallel to the galactic plane and directed towards $\ell = 50^{\circ} - 80^{\circ}$. For stars within about 500 pc of the Sun the polarization is weaker and in addition to the field parallel to the plane there exist magnetic loops at high galactic latitudes. The most prominent loop, which cuts the equator at $\ell \simeq 40^{\circ}$, is probably associated with the North Polar Spur. Figure 4.2 shows the distribution of polarization vectors (taken from Whiteoak, 1974) that was analyzed by Mathewson (1968).

(iii) Faraday Rotation

Faraday rotation measurements on extragalactic sources and pulsars delineate a field parallel to the plane and directed towards $\ell \simeq 94^{\circ}$. For positive latitudes anomalies in the field are indicated and these are caused by loops of magnetic field. The distribution of rotation measures of sources is shown in figure 4.3 (taken from Whiteoak, 1974).

Pulsar observations are the most useful of all tools in determining the magnetic field. By dividing the rotation measure RM by the dispersion measure DM a direct estimate of the line of sight component of the magnetic field is obtained, without necessitating the assumption of an electron density. Unfortunately the sample is not large enough and the pulsars for which we have

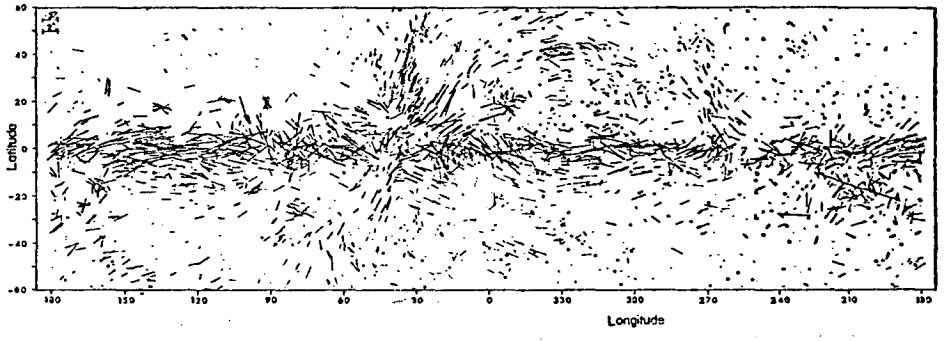

The distribution with galactic coordinates of the vectors of polarization of starlight (Mathewson and Ford, 1970a). The length of each vector is proportional to the percentage polarization P. Small circles are drawn about stars with $P<0.08\%$.

FIGURE 4.2

after Whiteoak (1974)

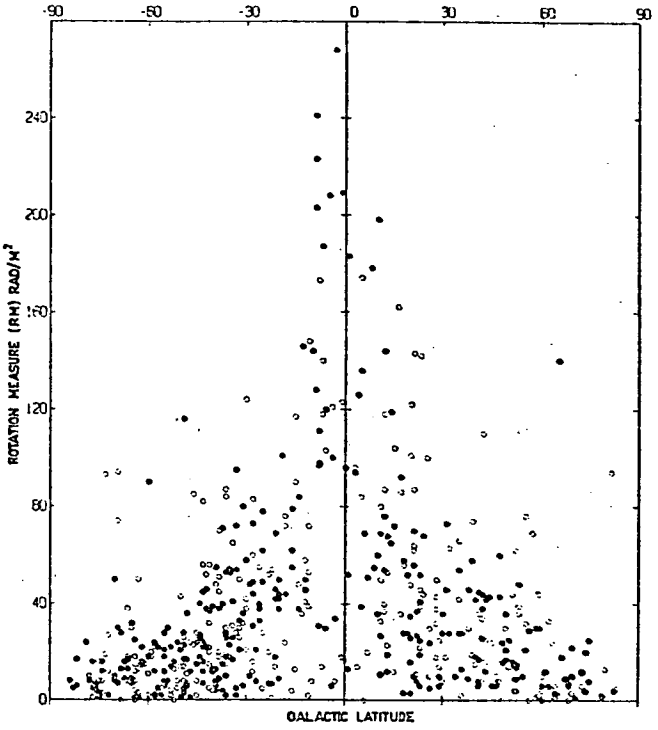

The distribution with galactic latitude of the rotation measures for sources observed at Parkes. The open circles represent negative values, the closed circles show positive values. Positive values correspond to line-of-sight magnetic fields directed toward the observer.

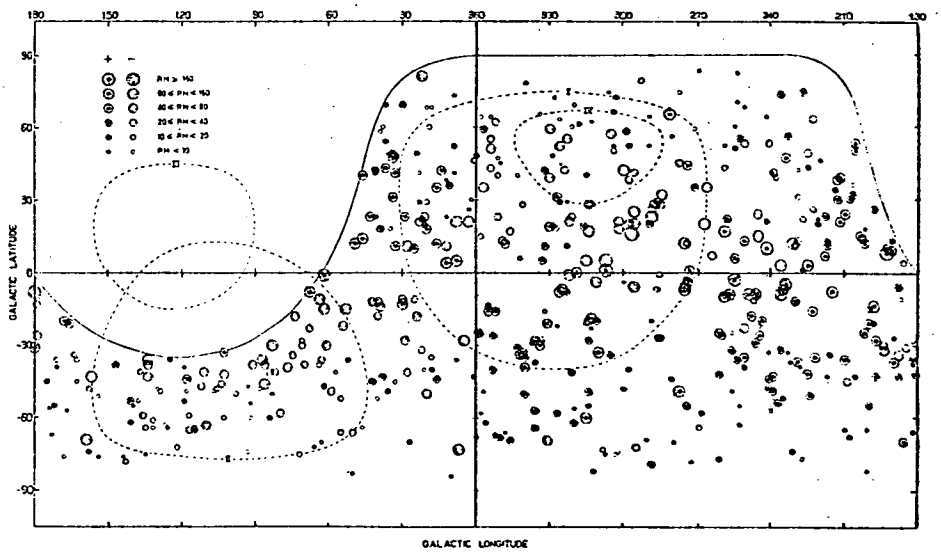

The distribution with galactic coordinates of the rotation measures for sources observed at Parkes. Positive rotation measures correspond to line-of-sight magnetic fields directed toward the observer. The continuous line shows the limits of observation of the 64-m telescope. The broken lines show the loops of radio emission according to Haslam *et al.* (1971).

FIGURE 4.3

after Whiteoad (1974)

values of RM and DM are largely confined to the equator. For the pulsars near the galactic plane and with calculated distances less than 2 kpc a large scale field of 2.2 μG aligned parallel to the plane is delineated (Manchester, 1975). Figure 4.4 illustrates the distribution of RM/DM for the 59 pulsars measured to date. The unpublished data was provided by Hamilton.

(iv) Galactic Synchrotron Emission

Observations of the polarization of synchrotron background emission give information about the magnetic field transverse to the line of sight within a few hundred parsec of the Sun. Investigations indicate a field aligned parallel to the galactic plane and directed towards $\ell \simeq 50^{\circ} - 70^{\circ}$. In directions of the radio spurs the observations are consistent with a magnetic field along the spurs, as indicated by stellar polarization.

From the half thickness of the non-thermal background radiation at about 100 MHz it is estimated that the scale height of the magnetic field in the solar neighbourhood is in the range 300-1000 pc (Mills, 1971).

Discussion

There is one aspect of the above brief summary which requires further mention. This is that the direction of the large scale field as indicated by Faraday rotation of sources is different from the direction indicated by the polarization of starlight and the polarization of the galactic background radiation. Whiteoak (1974) suggests that "the spatial distribution of the thermal electrons responsible for the Faraday rotation may not be the same as that of the relativistic electrons producing the

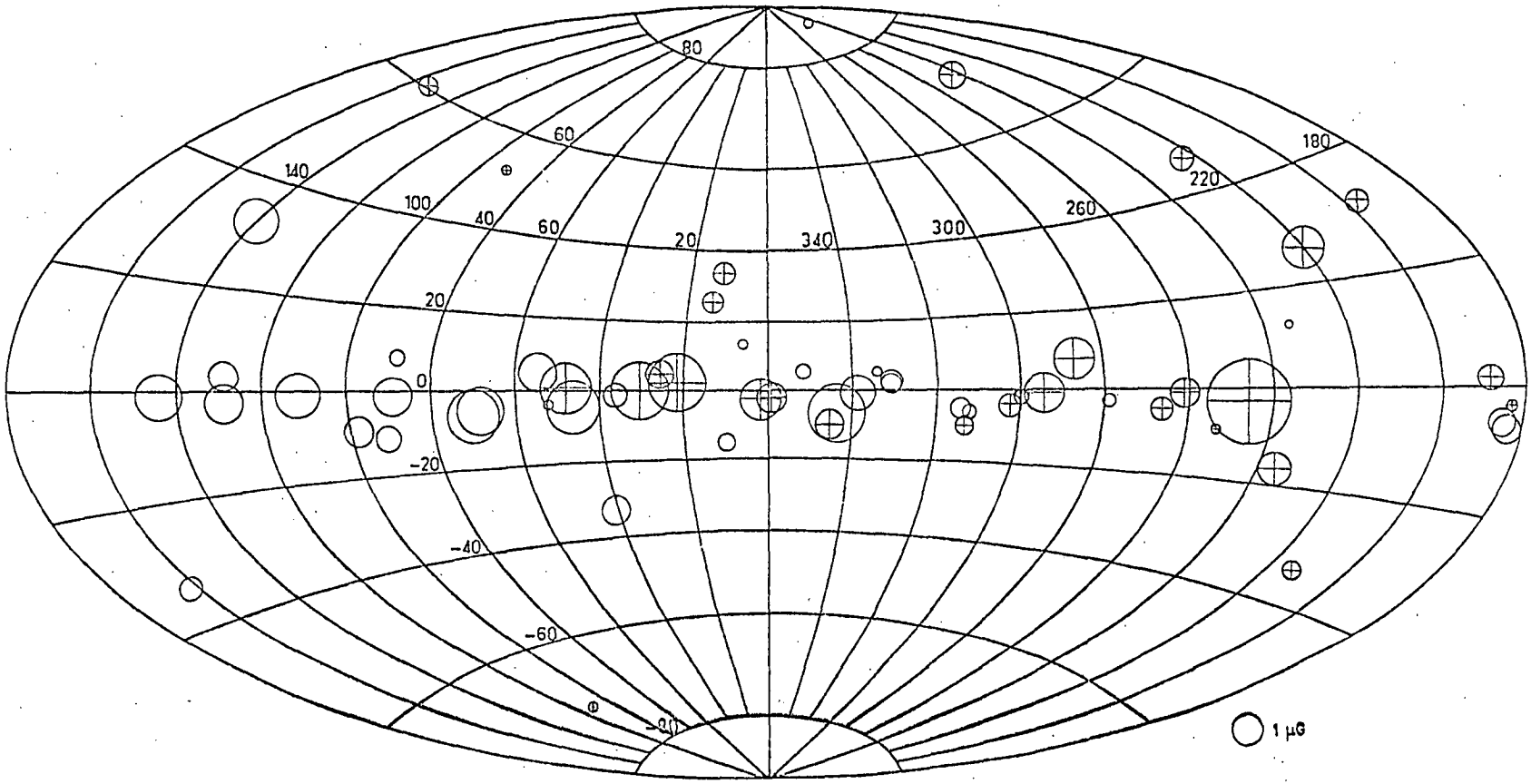

Line-of-sight magnetic-field components in the direction of 59 pulsars. For fields greater than 0.1 microgauss the area of the circle is proportional to the field strength and for fields directed towards the observer a plus sign is enclosed. A circle representing a 1 microgauss field is shown at the lower right of the figure.

FIGURE 4.4

synchrotron radiation" and that "the interstellar dust producing the optical polarization is differently distributed with respect to the synchrotron emission and the magnetoionic plasma".

Taking this suggestion further, perhaps these results are observational evidence for the results of the two-armed spiral shock pattern (Roberts, 1969) that the dust lanes and the magnetic fields lie on the inner side of bright optical arms, where the majority of the thermal electrons would be expected to be. In figure 4.5 we show a photograph from Roberts (1975) which illustrates that this type of distribution has been observed (by Mathewson et al., 1972) in the external galaxy M51.

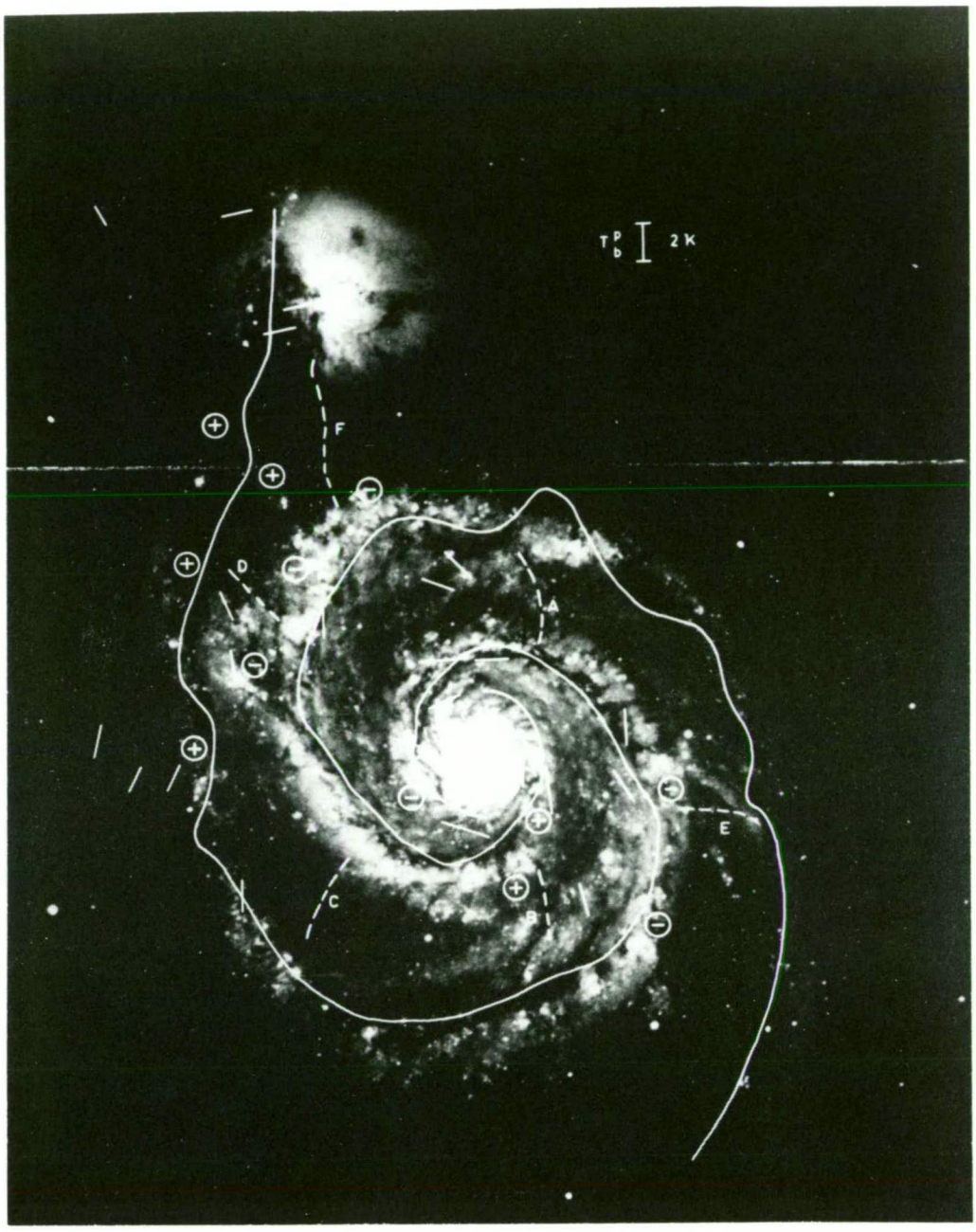

The ridges of the 1415 MHz emission from the radio spiral arms of M 51 drawn on a photograph of M 51 and NGC 5195 reproduced from a blue plate taken by Humason with the Palomar 200-inch telescope.

FIGURE 4.5

after Roberts (1975)

77/1/82

REFERENCES FOR CHAPTER 4

ALTENHOFF, W.J. 1968 'Interstellar Ionized Hydrogen', Ed. Y. Terzian, p. 519, (W.A. Benjamin, Inc., New York).

ALTENHOFF, W.J., DOWNES, D., GOAD, L., MAXWELL, A. and RINEHART, R. 1970 Astron. Astrophys. Suppl. 1 319.

BERGE, G.L. and SEIELSTAD , G.A. 1967 Astrophys. J. 148 367.

BRIDLE, A.H. 1969 Nature 221 648.

BURTON, W.B. 1974 IAU Symposium 60 551.

CESARSKY, C.J. and CESARSKY, D.A. 1971 Astrophys. J. 169 293.

CLARK, B.G. 1965 Astrophys. J. 142 1398.

COURTES, G. 1973 Vistas in Astron. Ed. A. Beer. 14 81.

DALGARNO, A. and McCRAY, R.A. 1972 Ann. Rev. Astron. Astrophys. 10 375.

DAVIES, R.D. 1969 Nature 223 355.

DULK, G.A. and SLEE, O.B. 1972 Aust. J. Phys. 25 429.

FALGARONE, E. and LEQUEUX, J. 1973 Astron. Astrophys. 25 253.

FIELD, G.B., GOLDSMITH, D.W. and HABING, H.J. 1969 Astrophys. J. Letters 155 L149.

GOTTESMAN, S.T. and GORDON, M.A. 1970 Astrophys. J. Letters 162 L93.

GREWING, M. and WALMSLEY, C.M. 1971 Astron. Astrophys. 11 65.

GUELIN, M. 1974 IAU Symposium 60 51.

GUELIN, M. and GOMEZ-GONZALEZ, J. 1974 Astron. Astrophys. 32 441.

HIRABAYASHI, H., YOKOI, H. and MORIMOTO, M. 1972 Nature 237 54.

HJELLMING, R.M., GORDON, C.P. and GORDON, K.J. 1969 Astron. Astrophys. 2 202.

JACKSON, P.D. and KERR, F.J. 1971 Astrophys. J. 168 29.

KERR, F.J. 1969 Ann. Rev. Astron. Astrophys. 7 39.

KERR, F.J. 1970 IAU Symposium 38 95.

KOMESAROFF, M.M. 1961 Aust. J. Phys. 14 515.

LYNE, A.G. 1974 IAU Symposium 60 87.

MANCHESTER, R.N., MURRAY, J.H. and RADHAKRISHNAN, V. 1969 Astrophys. Letters 4 229.

MATHEWS, H.E., PEDLAR, A. and DAVIES, R.D. 1973 Mon. Not. R. astr. Soc. 165 149.

MATHEWSON, D.S. 1968 Astrophys. J. Letters 153 L47.

MATHEWSON, D.S., HEALEY, J.R. and ROME, J.M. 1962 Aust. J. Phys. 15 269.

MATHEWSON, D.S. and FORD, V.L. 1970 Mem. R. astr. Soc. 74 (5) 139.

MATHEWSON, D.S., VAN DER KRUIT, P.C. and BROUW, W.N. 1972 Astron. Astrophys. 17 468.

MEABURN, J. 1972 Astrophys. Space Sci. 17 499.

MEZGER, P.G. 1970 IAU Symposium 38 107.

MEZGER, P.G. 1972 'Interstellar Matter' Astronomical Institute, University of Basel ed., Geneva Observatory, Sauverny, Switzerland.

MILLS, B.Y. 1971 (Invited Paper) Proc. 12th Int. Cosmic Ray Conf. (Hobart).

OORT, J.H. KERR, F.J. and WESTERHOUT, G. 1958 Mon. Not. R. astr. Soc. 118 379.

PEDLAR, A. and DAVIES, R.D. 1972 Mon. Not. R. astr. Soc. 159 129.

REYNOLDS, R.J., SCHERB, F. and ROESLER, F.L. 1973 Astrophys. J. 185 869.

REES, M.J. and SCIAMA, D.W. 1969 Comments. Astrophys. Space Sci. 35.

ROBERTS, W.W. 1975 Vistas in Astron. Ed. A. Beer. 19 91.

SHAIN, C.A., KOMESAROFF, M.M. and HIGGINS, C.S. 1961 Aust. J. Phys. 14 508.

SIVAN, J.P. 1974 Astron. Astrophys. Suppl. 16 163.

VERSCHUUR, G.L. 1972 Review Paper IAU Colloquim 23.

WALMSLEY, C.M. and GREWING, M. 1971 Astrophys. Lett. 9 185.

WESTERHOUT, G. 1958 Bull. astr. Inst. Nethl. 14 215.

WHITE, R.E. 1973 Astrophys. J. 183 81.

WHITEOAK, J.B. 1974 IAU Symposium 60 137.

CHAPTER 5

Introduction

This chapter presents a summary of the observations of the galactic background radiation at frequencies less than approximately 500 MHz and an assessment of the information obtained from such measurements.

In PART I the properties of all the surveys with beamwidths less than approximately 10^{o} (but greater than 45') are summarized. It is believed that this has never been done before and it is felt that it would be a useful contribution as many sky surveys have odd contour units and zero levels whose values are often hidden within the manuscript presenting the survey. In addition, new composite maps at 10 and 30 MHz are presented. A summary is made of the basic features of sky surveys at frequencies between 10 and 420 MHz and the components which contribute to this distribution are discussed.

In PART II the measurements of the galactic poles which have been made since Hamilton's 1969 review are presented. New spectra for the north and south galactic poles (NGP and SGP) are compiled. In addition, measurements in the anti-centre and northern minimum directions are compiled and spectra are defined.

PART III. Equipped with the information from PARTS I and II the variation of the spectral index of the non-thermal radiation across the sky and with frequency is discussed.

PART IV. Finally a new assessment of the synchrotron emissivity is undertaken. The results are discussed in terms of the spiral structure of the Galaxy and with respect to measurements of the cosmic ray electron flux in the solar neighbourhood.

PART I

GALACTIC BACKGROUND RADIATION

Sky Surveys

It is intended to outline the basic features of each survey. Table 5.1 presents the details of the surveys where they are numbered in descending order of observation frequency and, for the same frequency, in chronological order.

The basic features are (a) the beamwidth of the observing instrument, (b) the contour unit of the map and (c) the zero level of the map. In addition, we have attempted to give an estimate of the extent of the survey in galactic co-ordinates but the limits are only approximate as observations are made in right ascension and declination. Many of the northern hemisphere maps are presented in equatorial co-ordinates only. Included are some comments, where applicable on the incompatibility of the data with other surveys.

Table 5.2 lists the observers.

From henceforth throughout this thesis a referencing system will be used based on column 1 of Table 5.1 . This will avoid the necessity of referring to observers when surveys are mentioned. For example, when discussing the 30 MHz survey of Mathewson et al. (1965) we will refer to survey S20.

TABLE 5.1

DETAILS OF GALACTIC SURVEYS

Survey Number	Observing Frequency (MHz)	Beamwidth (degrees)	Contour Unit (K)	Zero Level (K)	Extent in Galactic Longitude	Extent in Galactic Latitude	Comments
1	408	0.67 × 0.9	43	80	350,56	-6, 6	
2	408	0.79	34.7	16	280,355	-6, 6	
3	408	0.75	1	0	150,240	-30, 70	
4	404	7.5		0	0,230	-80, 90	Not comparable with other surveys close to galactic plane
5	240	1	0	0	10, 50	10, 45	
6	240	1	10	0	230,340	20, 55	
7	237	1.1 × 1.2	1	0	186,210	-15, 15	
8	178	4.6	1	0	30,200	-40, 90	
9	153	2	1	0	200,45	-90, 20	
10	150	2.2	1	0	290,60	-8, 8	
11	150	2.2 × 2.2	1	0	190,220 220, 30 5, 60 40,180	-30, 30 30, 70 -30, 30 -70,-30	

TABLE 5.1 continued

Survey Number	Observing Frequency (MHz)	Beamwidth (degrees)	Contour Unit (K)	Zero Level (K)	Extent in Galactic Longitude	Extent in Galactic Latitude	Comments
12	85.5	0.83	10^3	0	255, 45	-5, 5	
13	85	3.5 × 3.8	1	0	240, 10	-90, 30	
14	85	3.7	1	0	290, 60	-10, 10	
15	85	3.8 × 3.5	1	0	190,220 220, 30 5, 60 40,180	-30, 30 30, 70 -30, 30 -70,-30	
16	38	2.2 × 2.3	10^3	0	180,230 180, 30 30,180	-50, 40 40, 90 -70, 90	Temperatures too high for $\|b\| \leq 20^o$ towards the galactic centre
17	38	1	900	0	45, 55 160, 195	-2, 10 -10, 10	
18	38	0.75	837	0	120,190	-30, 90	
19	38	7.5	100	0	20,100 120,220	-90, 90 -90, 90	

TABLE 5.1 continued

Survey Number	Observing Frequency (MHz)	Beamwidth (degrees)	Contour Unit (K)	Zero Level (K)	Extent in Galactic Longitude	Extent in Galactic Latitude	Comments
20	30	11	1800	1.3×10^4	215, 30	-90, 40	Temperatures should be lowered by a factor of 0.7 and zero level taken as $1.5\ 10^4$ K if temperatures to agree with SGP spectrum
21	30	0.8	1470	0	225, 30	-15, 15	Contour unit should be 1000 K
22	19.7	1.4	10^5	0	256, 48	-4, 5	
23	16.5	1.5	10^5	0	330, 30	-20, 17	Contour unit should be 7.3×10^4 K
24	13.1	2.7 × 6.3	10^3	0	140,185	-30, 80	Steep gradient across $\ell = 200^o$ not seen on any other maps - this is the centre of the northern minimum
25	10	4 × 5	2×10^5	0	270,30	-90, 30	Contour unit should be 8×10^4 K according to revised SGP spectrum

TABLE 5.1 continued

Survey Number	Observing Frequency (MHz)	Beamwidth (degrees)	Contour Unit (K)	Zero Level (K)	Extent in Galactic Longitude	Extent in Galactic Latitude	Comments
26	10	2	10^5	0	120,200 all	-60, 20 b > 50	
27	4.7	3 × 10	7.5×10^5	0	240,20	-90, 30	Contour unit should be 7.2×10^5 K according to revised SGP spectrum
28	2.1	8	relative brightness only	0	240, 35	-90, 30	Contour unit should be 3.8×10^5 K according to revised SGP spectrum

TABLE 5.2

LIST OF OBSERVERS

1	Large, Mathewson and Haslam (1961)
2	Komesaroff (1966)
3	Haslam, Quigley and Salter (1970)
4	Pauliny-Toth and Shakeshaft (1962)
5	Haslam, Large and Quigley (1964)
6	Large, Quigley and Haslam (1966)
7	Davies and Hazard (1962)
8	Turtle and Baldwin (1962)
9	Hamilton and Haynes (1969)
10	Wielebinski, Smith and Garzon-Cardenas (1968)
11	Landecker and Wielebinski (1970)
12	Hill, Slee and Mills (1958)
13	Yates, Wielebinski and Landecker (1967)
14	Wielebinski, Smith and Garzon-Cardenas (1968)
15	Landecker and Wielebinski (1970)
16	Blythe (1957)
17	Kenderdine (1963)
18	Williams, Kenderdine and Baldwin (1966)
19	Milogradov-Turin and Smith (1973)
20	Mathewson, Broton and Cole (1965)
21	Jones and Finlay (1974)
22	Shain, Komesaroff and Higgins (1961)
23	Cane (1975)
24	Andrew (1969)
25	Hamilton and Haynes (1968)
26	Caswell (1976)
27	Ellis and Hamilton (1966)
28	Reber (1968)

The 10 MHz Composite Map

The 10 MHz composite map was derived from a northern survey at 10 MHz (S26), a southern survey at 10 MHz (S25) and 13 MHz data obtained by the author. The southern survey was made with a 4° x 5° beam whereas the rest of the data was obtained with beams of approximately 2°.

The northern data was convolved to a resolution of 5° and contours drawn on the Hammer equal-area projection. This enabled direct comparisons with the southern survey. The northern temperatures were much lower than the southern temperatures in the regions where the surveys overlapped.

The overall temperatures of the southern survey were reduced by a factor of 1.25 to bring temperatures in the region of the south galactic pole into agreement with the revised south galactic pole spectrum. With this reduction in temperatures the northern and southern 10 MHz maps agreed in the overlap region Dec. -2.5°, R.A. 03^h to 05^h (i.e. $-20° \lesssim b \lesssim 40°$, $180° \lesssim \ell \lesssim 200°$). However for the overlap region Dec. -2.5°, R.A. 10^h to 13^h the features presented by the two maps are not the same. Thus recourse was made to the new 13 MHz data.

The 13 MHz data was in the form of declination scans for each declination. As these showed no significant structure on a scale of less than 5° the data were assembled on a 5° x 5° grid and contours drawn. 10 MHz contours were then "derived" from the 13 MHz contours by assuming a temperature spectral index of 2.6. The resulting contours agreed with the northern 10 MHz map in the region where the two 10 MHz maps disagreed. On the basis of this

the 13 MHz data was used to alter contours in the region $280° \lesssim \ell \lesssim 350°$, $b > 0°$. In addition the 13 MHz data was used to extend the southern survey.

The final map is presented in figure 5.1. The contour unit is 8×10^4K. In some regions contours have been closed with broken lines in a manner consistent with the structure seen in higher frequency maps (S8 and S13) at 178 and 85 MHz. Dec. -5° is dotted in so that the extent of the northern data will be apparent.

Caswell discusses the specific details of his map and the features of the southern survey near the galactic centre will be discussed in Chapter 7. As the overall distribution of non-thermal radiation will be discussed in a later section at this stage only the specific features of the 13 MHz section of the map will be mentioned.

Firstly, the region of minimum brightness is centred at approximately $\ell = 220°$, $b = -40°$. At 30 MHz the minimum in the southern hemisphere is also centred at $\ell = 220°$ whereas at higher frequencies (e.g. 85 and 153 MHz) the minimum is centred at $\ell = 240°$. At 10 MHz it is observed that the minimum temperature in the southern hemisphere is equal to the minimum temperature in the northern hemisphere. At higher frequencies it is also observed that the northern and southern minima have the same temperature.

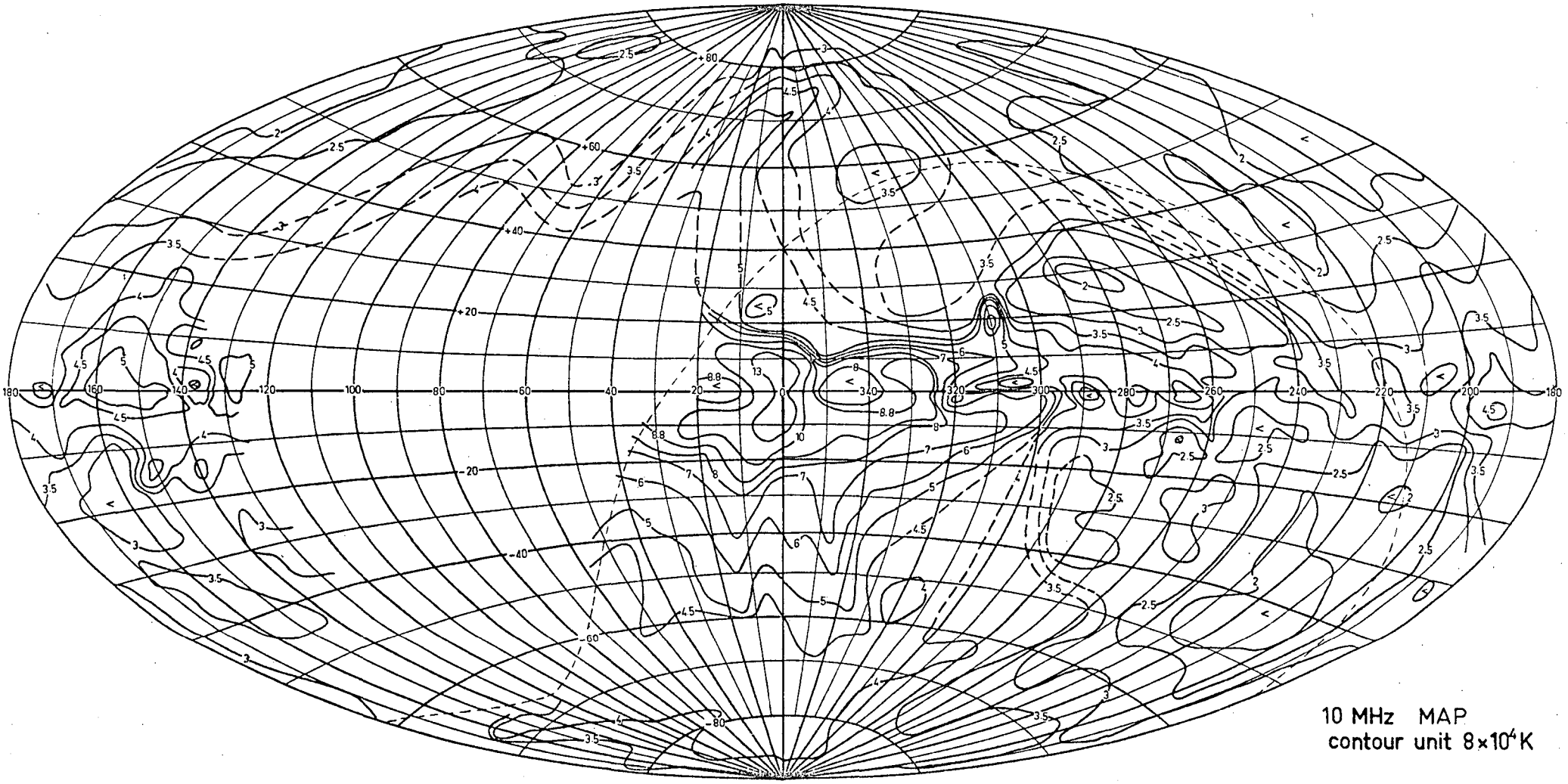

FIGURE 5.1

Secondly, there are discrete regions of absorption due to the m Centauri nebula (ℓ = 306°), the η Carina nebula (ℓ = 288°) and the Gum nebula (ℓ = 250° - 270°).

The 30 MHz Composite Map

The data for this map was provided by a northern 38 MHz 7.5° survey (S19) and a southern 30 MHz 11° survey (S20). The factor for conversion of the 38 MHz temperatures to 30 MHz temperatures was derived from a comparison of the two surveys over the region where they overlap. This comparison was made after the contour unit and zero level of the 30 MHz survey had been adjusted to bring temperatures in the vicinity of the SGP into agreement with the low resolution spectrum of this region. If a spectral index of 2.6 is assumed at these frequencies then the 38 MHz temperatures appear to be about 10% too low.

In directions close to the galactic centre the 30 MHz temperatures have been used and for these directions the difference in resolution of the surveys becomes significant. Thus in the longitude range 20° - 50° for latitudes close to the galactic plane, a region not covered by the 30 MHz survey, we have not included the detail provided by the 38 MHz survey.

In one region not covered by the 38 MHz survey contours have been closed with broken lines in a manner consistent with the features seen in the 178 MHz (S8) survey.

The features of the 30 MHz composite map (see figure 5.2) are essentially the same as those presented by the 85 MHz composite map of Yates (1968) and these will be discussed in the next section.

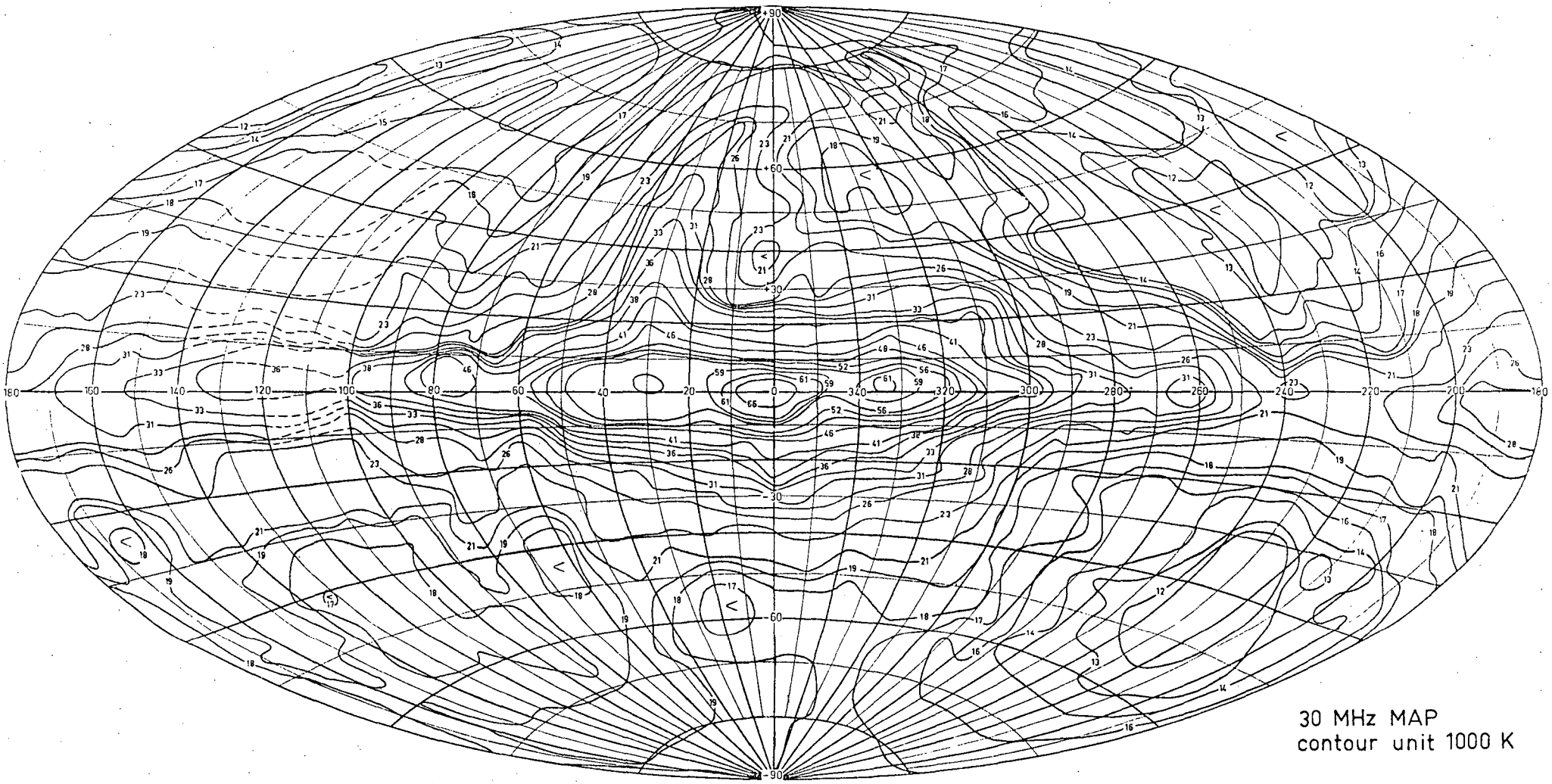

30 MHz MAP
contour unit 1000 K

FIGURE 5.2

The Distribution of Non-Thermal Background Radiation

When discussing the fundamental characteristics of the background radiation it is preferable to have all-sky maps. Prior to this thesis, two such maps had been prepared; at 150 MHz (Landecker and Wielebinski, 1970) and 85 MHz (Yates, 1968). Both rely on the 178 MHz data (S8) in the northern hemisphere and 85 MHz data (S8) in the southern hemisphere and care should be taken in deriving spectra from these maps. The 85 MHz map is presented in figure 5.3 - not in its original form but redrawn on the same projection as used for most of the other maps presented in this thesis. It can be seen that the brightness distribution of the background radiation is irregular but that in its simplest form the emission can be described as having a concentration towards the galactic plane but still being substantial at high latitudes. However models describing the emission usually have four components; the galactic disk, the spurs, the halo and the extra-galactic radiation. These are discussed below.

1. The Galactic Disk

The variation with longitude of the radiation near the galactic plane is irregular and there is a concentration of emission to longitudes within 40° of the galactic centre. Even at 10 MHz this concentration exists although the effect is not so pronounced. The irregularities are due partially to discrete sources, particularly in regions away from the galactic centre, but also because the constituents of the Galaxy tend to be distributed into spiral arms. Although it was anticipated that

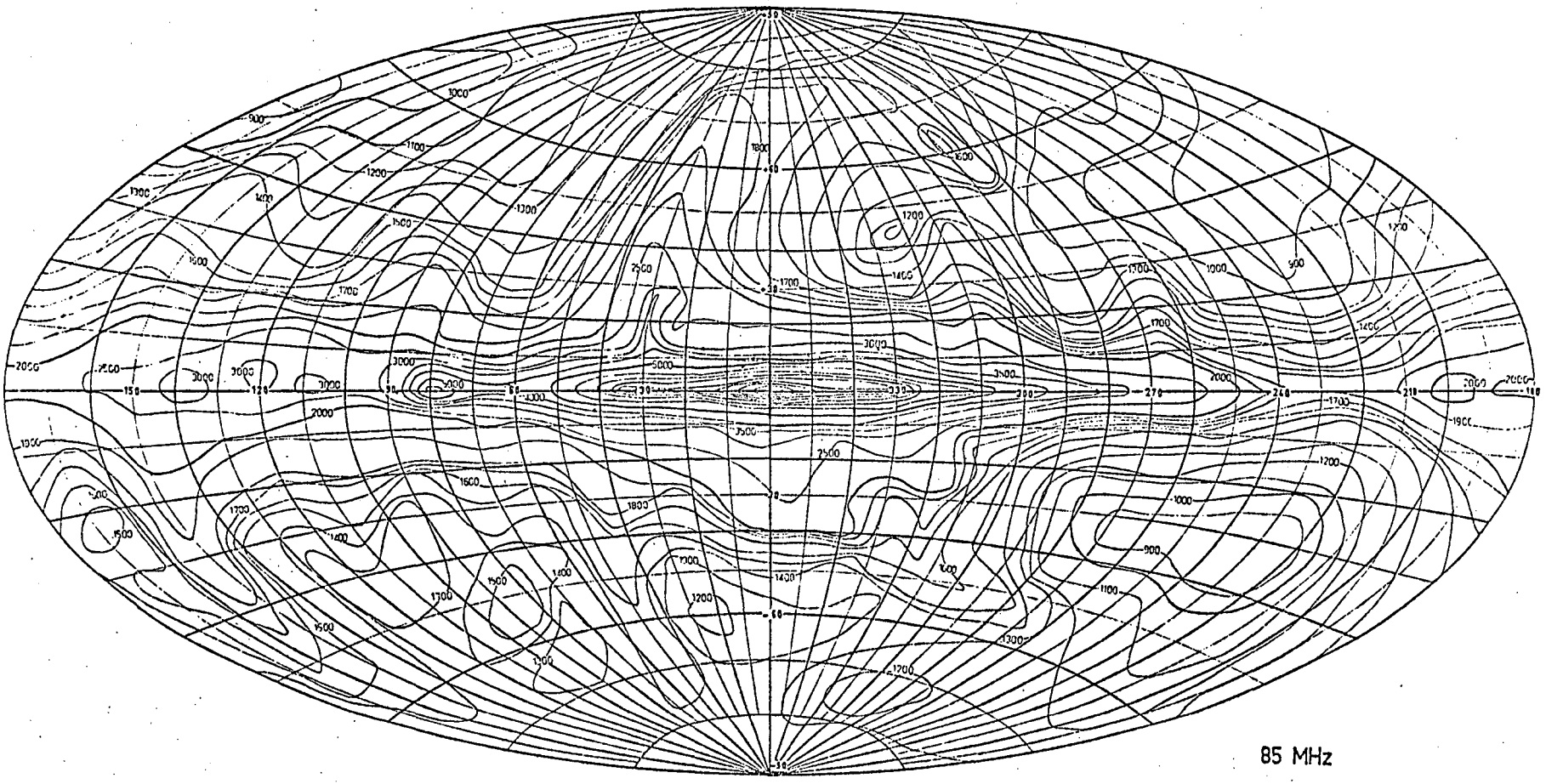

FIGURE 5.3

after Hamilton (1969)

peaks would occur in directions tangential to spiral arms, this is not observed. Instead, there are 'steps' in the brightness distribution, the most pronounced ones being at 325^{o} and 35^{o}. This is illustrated in figure 5.4 where the longitude distribution at $b = +2^{o}$ for 408 and 85 MHz (S1, S2 and S12) is shown.

The maximum intensity at frequencies greater than approximately 100 MHz is at longitude $\ell = 0^{o}$ where the intense source Sagr A is situated. Below 100 MHz absorption in the HII regions in the galactic centre region takes place and the maximum occurs at $\ell = 2.5^{o}$. The minimum along the galactic plane is seen to be in the range $210^{o} \lesssim \ell \lesssim 240^{o}$ rather than $\ell = 180^{o}$ as might be expected.

The latitude variation of the emission is affected by the distribution of ionized hydrogen. At frequencies above approximately 30 MHz profiles across the galactic plane exhibit a peak, usually at $b = 0$. At higher frequencies for profiles in the longitude range $320^{o} \lesssim \ell \lesssim 40^{o}$ this peak is very pronounced but decreases with decreasing frequency until at about 30 MHz profiles exhibit a plateau for $b < 2.5^{o}$ provided the profile does not cross the line of sight to a nearby HII region. This behaviour is illustrated in figure 5.5. where an example of a pair of profiles of normalized temperature at 29.9 MHz (S21) and 1410 MHz (Hill, 1968) is shown for longitude 347^{o}. Figure 5.6 shows profiles of normalized temperature at 153 MHz (S9), 85 MHz (S15) and 29.9 MHz (S21) for longitude 20^{o}.

At frequencies less than about 30 MHz the effect of ionized hydrogen becomes pronounced. Even at 30 MHz with an 11^{o} beam the effect of regions of ionized hydrogen at $\ell = 345^{o}$ can

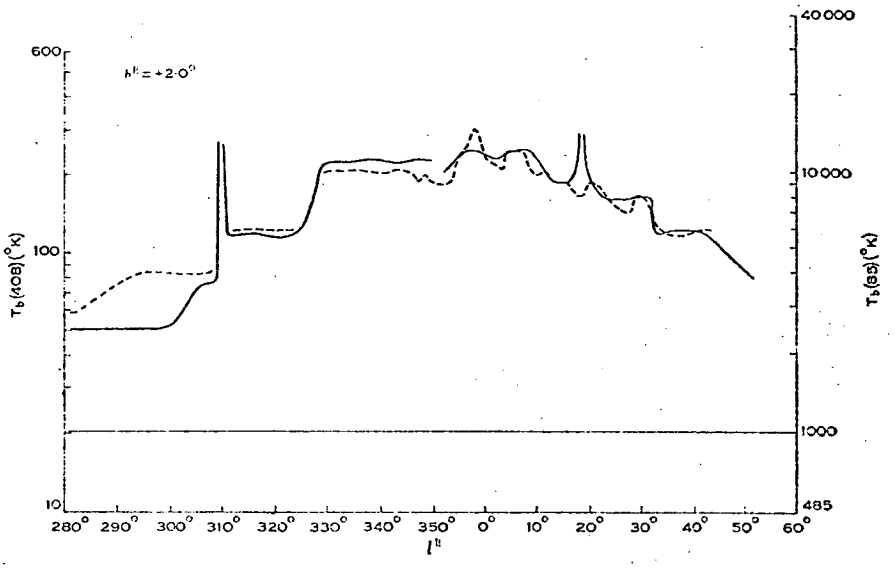

Variation of brightness temperature with l^{II}, at $b^{II} = +2°$, for 85 and 408 Mc/s. Identical logarithmic scales of brightness temperature have been used for both frequencies, but their relative heights have been adjusted (see Section V). Where the results of other surveys are shown, the curves have been derived from the published isophotes. 408 Mc/s: —— present survey, ---- Large, Mathewson, and Haslam (1961); 85·5 Mc/s: – – – – Hill, Slee, and Mills (1958).

FIGURE 5.4

after Komesaroff (1966)

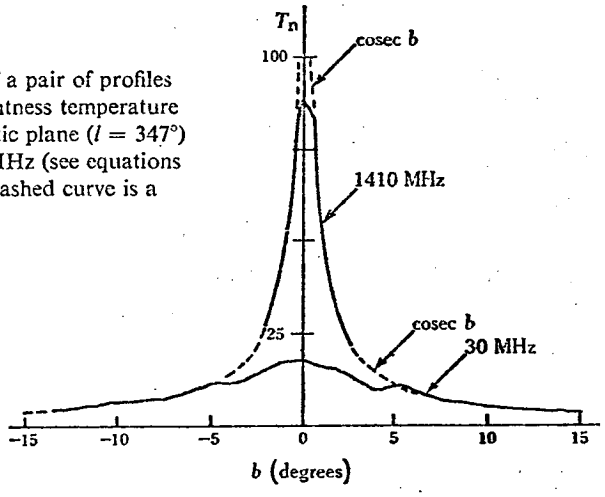

Example of a pair of profiles of normalized brightness temperature T_n across the galactic plane ($l = 347°$) at 29·9 and 1410 MHz (see equations (1) and (2)). The dashed curve is a plot of cosec b.

FIGURE 5·5

after Jones and Finlay (1974)

Profiles of normalized brightness temperature T_n across the galactic plane ($\ell = 20°$) at 153 MHz ___ (S15), 85 MHz ---- (S15) and 30 MHz _ _ (S21).

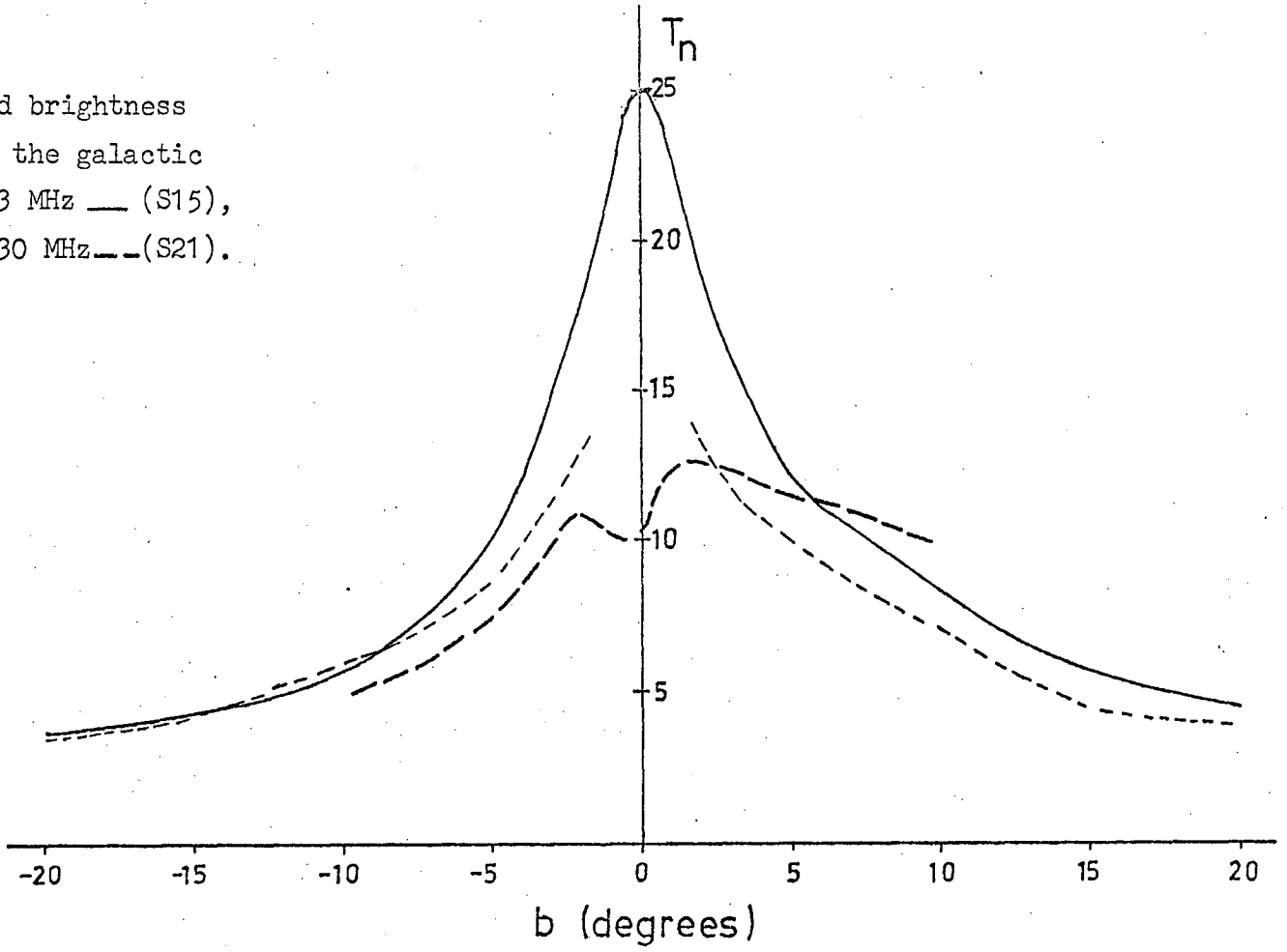

FIGURE 5.6

be seen. At 10 MHz two pronounced absorption troughs exist centred at $\ell = 345^{o}$ and $\ell = 18^{o}$. Many other discrete regions of absorption can be seen at latitudes within approximately 30^{o} of the plane at all longitudes.

Profiles across the galactic plane in the anti-centre direction exhibit a different behaviour. This is illustrated in figure 5.7 where we show profiles of normalized temperature at 408 MHz (S3), 178 MHz (S8) and 10 MHz (S26) for longitude 180^{o}. The temperature normalization used for this diagram is almost the same as that used for figure 5.6. It can be seen that in the anti-centre direction the peaking is less pronounced and the normalized height is only weakly dependent on frequency.

2. The Spurs

The most prominent feature of the galactic continuum maps apart from the ridge of emission along the plane is the North Polar Spur, a finger of emission perpendicular to the plane at about $\ell = 40^{o}$ extending to the north galactic pole. There are two other prominent spurs and several smaller, similar features. It is thought that they all form parts of arcs of circles and these objects have been named loops.

In figure 5.8 the circles are drawn onto the 85 MHz whole sky map following Haslam et al. (1971). It can be seen that all these features are also visible on the 30 MHz composite map. On the 10 MHz composite map several spurs are evident and in particular the North Pole Spur region of Loop I is very prominent.

Profiles of normalized brightness temperature T_n across the galactic plane ($\ell = 180^{\circ}$) at 408 MHz ___ (S3), 178 MHz ____ (S8) and 10 MHz __ (S26).

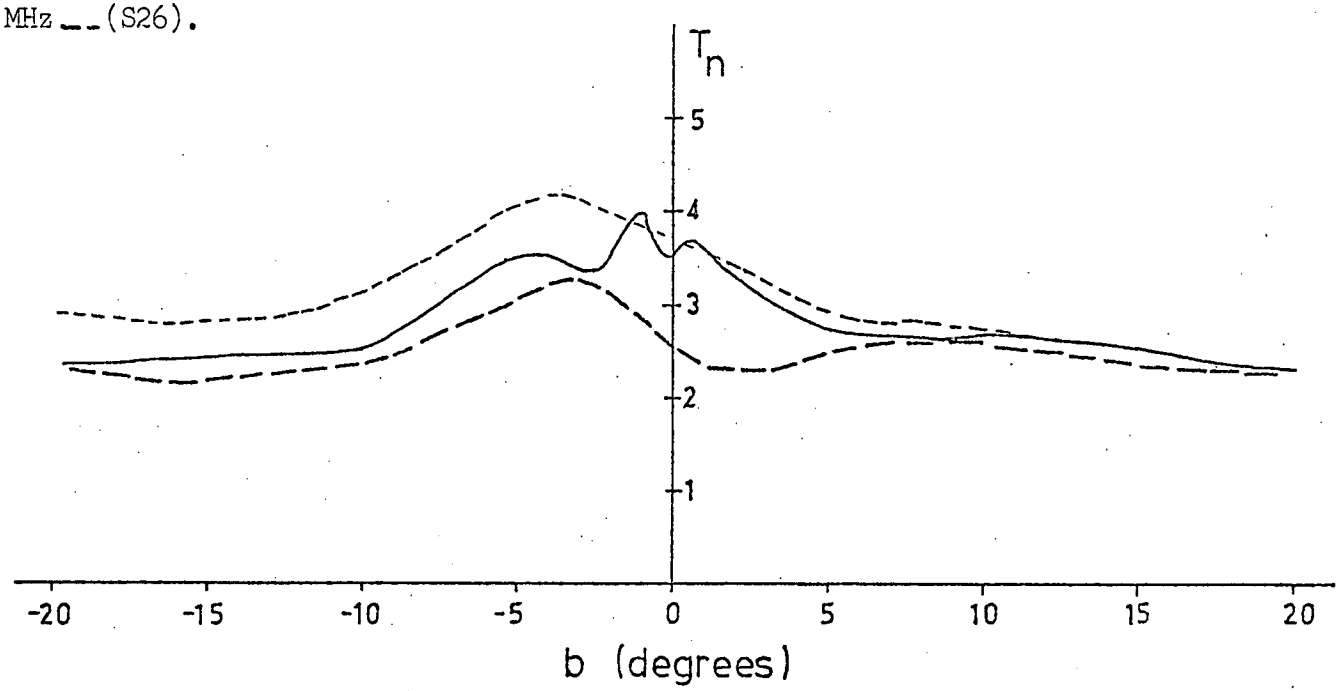

FIGURE 5.7

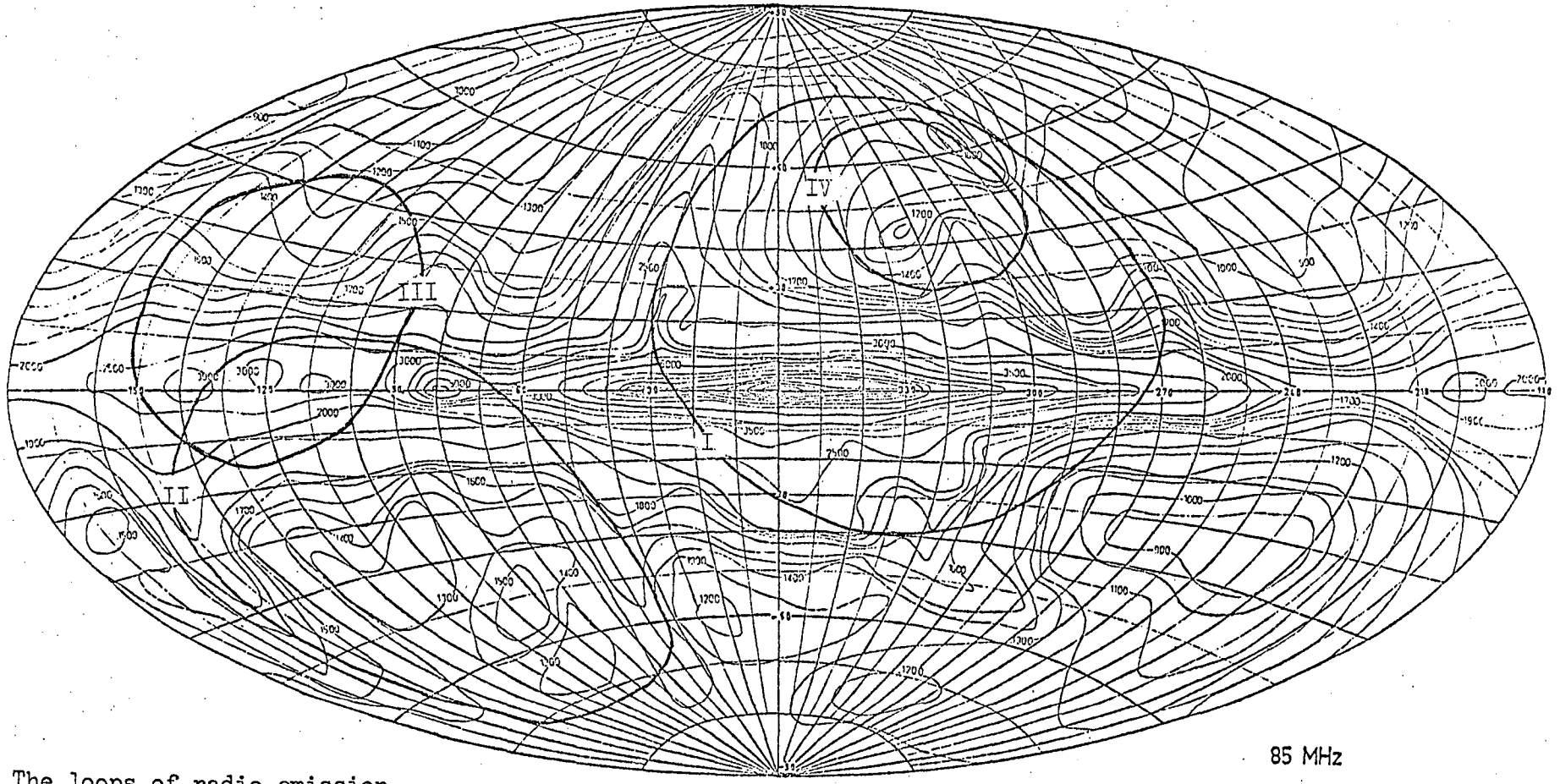

The loops of radio emission
according to Haslam et al. (1971)

FIGURE 5.8

Observations of the magnetic fields in the spurs and polarization of starlight indicate that the loops are local features. For example, the inferred distance to the North Polar Spur is 100 ± 20 pc (Bingham, 1967).

Probably the most widely accepted hypothesis for the origin of the loops is that they are supernova remnants. However, several other interpretations have been suggested including the postulate that they are features in the magnetic field structure of the local spiral arm.

3. High Latitude Emission

Emission at high latitudes consists of contributions from: the local region, the super-position of extra-galactic sources, a hypotheoretical galactic halo and the galactic spurs. Assessments of any one component are complicated as their individual contributions are not entirely separable. Perhaps it is easiest to assess the extra-galactic contribution, although only one experiment has been proposed which can measure this directly. This was by Shain (1959) who made observations of the emission nebula 30 Doradus in the large Magallanic cloud (LMC) and compared these with observations in the neighbouring directions. Assuming total absorption in the nebula it is possible to separate the components of the emission generated in front and behind the LMC. The results are not conclusive as the beam used did not have sufficient resolution and the size of 30 Doradus is not known accurately.

Using a method based on certain assumptions, an estimate of the extra-galactic component has been made by Costain (1960), Turtle et al. (1962), Yates and Wielebinski (1966) and Bridle (1967). The assumptions are that the spectral index of the galactic component is constant across the sky and is different from the spectral index of the extra-galactic component. Although the spectral index of the galactic component is not constant the variation across the sky is not rapid so that the method is useful in the absence of alternative direct estimates.

Any estimate of the temperature of the extra-galactic component requires the assumption of a spectral index. Observations of extra-galactic sources indicate a mean spectral index of 2.75 (Bridle, 1967) and with this value Table 5.3 lists the various estimates that have been made of the extra-galactic component scaled to 85 MHz. An average value is ~ 280 K which is less than one-third the minimum temperature as seen in figure 5.3. This leaves a substantial amount of radiation to be explained.

This excess radiation was, until the late 60's attributed to a galactic radio halo, a concept introduced in the early 50's. However, with the identification of the spurs as local features it became obvious that much of the high latitude emission comes from the local arm.

The observations and interpretations which led to the belief in a radio halo should be discussed.

The radio astronomical evidence for a radio halo as discussed by Shklovskii (1952), Baldwin (1955) and Mills (1959) was the high level of emission at high latitudes. As has been

TABLE 5.3

EXPERIMENTAL DETERMINATIONS OF THE EXTRA-GALACTIC COMPONENT ASSUMING A SPECTRAL INDEX OF 2.75

Observer	$T_{eg},85$ (K)
Shain	126 - 395
Costain	<100
Turtle et al.	185 - 296
Yates and Wielebinski	100 - 200
Bridle	176 - 282

mentioned this is now partially explained by the local nature of the loops. Furthermore, it was realized by Baldwin (1963) that the low resolution instruments used could have significant sidelobe response in the galactic plane.

In 1967 Baldwin suggested that the only observational evidence for a radio halo was the relative brightness temperatures of the four points $\ell = 180^{\circ}$, $b = \pm 45^{\circ}$ and $\ell = 0^{\circ}$, $b = \pm 45^{\circ}$. He had shown in 1955 that

$$R = T_B\ (\ell = 0^{\circ},\ b = \pm 145^{\circ})\ /\ T_B(\ell = 180^{\circ}\ ,\ b = \pm 45^{\circ}) = 3$$

which was consistent with a spherical halo. However experiments by Burke (1967) and Wielebinski and Peterson (1968), which allowed for the extra-galactic contribution and spur effects, showed that $R \simeq 1$ as expected in the absence of a halo. Of course, if a radio halo does exist then the existence of a "cosmic-ray" halo is implicit. That is, a region surrounding the Galaxy filled with low-density gas, magnetic fields and cosmic rays. Biermann and Davis (1958) postulated that such a region would be required to produce the observed isotropy of cosmic rays and this has been used as supporting evidence for the radio halo. But, as pointed out by Ginzburg (1970), it is possible for there to be a "cosmic-ray" halo without there being a radio halo. Moreover, studies have been completed on models in which cosmic rays are produced, isotropized and confined in the galactic disk.

Thus neither radio astronomical or cosmic ray data require the existence of a radio halo, although its existence cannot be ruled out completely. Price (1974) maintains that any "large-scale spherical component could not have a volume emissivity greater than

1.5% of the average volume emissivity of the disk at metre wavelengths". Observations of external spiral galaxies show that they seldom have associated large-scale haloes.

The problem could be solved if it would be possible to separate the local irregularities and extra-galactic contributions. An attempt to do this has been made by Yates (1968) who finds he can account for the brightness distribution without the introduction of a spherical halo. The small excess of radiation after allowing for all other components was attributed to a disk-shaped 'halo'.

An assessment of the magnitude of the background radiation from the local arm requires a knowledge of the magnitude and form of the magnetic field and of the electron distribution. In Chapter 4 the observations of the galactic magnetic field were summarized. Stellar polarization measurements indicate that within a few hundred parsecs of the Sun the field is directed towards $\ell = 50^{\circ}$. Although the large-scale field has a magnitude of ~ 2 μG there are regions of irregularities with much higher fields.

It will be shown in Part IV that the electron flux observed at Earth is not typical of the average flux in the local arm and thus attempts to calculate the local arm emission from the observed flux and an assumed field value are not valid. However certain properties of the background brightness distribution can be attributed to the local emission and indicate its great intensity.

It is observed that the brightness distribution

(a) is not symmetrical about the plane $\ell = 0^{\circ}$;

(b) has minima at $\ell = 191^{\circ}$, $b = 45^{\circ}$ and $\ell = 230^{\circ}$, $b = -30^{\circ}$;

(c) is asymmetrical relative to the plane at $\ell = 180^{\circ}$.

It is profitable to attribute certain parameters to the local arm, construct a model to explain the observed background distribution and compare the derived properties with the observations of these properties. This method will be persued in Chapter 7 and further discussion of this topic will be left until then.

PART II

GALACTIC SPECTRA

The Spectra of the Galactic Polar Regions

In his Ph.D. thesis Hamilton (1969) devoted a complete chapter to low resolution (i.e. beamwidth > 25°) measurements of the galactic poles. He summarized each experiment, assessed the measurements and discussed the implications. He also discussed the general problems of comparing different results and the reader is referred to this thesis for these useful comments. The author reiterates a plea by Hamilton, that measurements be presented numerically in terms of equivalent aerial temperature. Of all the recent satellite measurements in all but two instances the data have been presented only in graphical form.

Hamilton plotted the spectra for the two hemispheres separately and found that differences existed between them. He would appear to be the first person to notice these differences and in the literature to date there has been no attempt to discern why they exist.

In this section the data for the two poles are presented separately and the experiments which have been performed since Hamilton's compendium are listed, in the same format. Graphs of the experimental points for each pole are compiled and then the spectra which are thought to be the best fit to the data are presented. A south galactic pole spectrum needs to be defined for normalizing the data presented in Chapter 6.

Northern Hemisphere Observations

Alexander et al. 1969, 1970:

These measurements form part of a continuing programme in low frequency astronomy at the Goddard Space Flight Centre. Observations were made from the Radio Astronomy Explorer Satellite (RAE-1) which was launched in 1968 and was the first spacecraft designed exclusively for radio astronomical studies. The satellite has two 229 m travelling-wave V antennas and a 37 m dipole. The results presented here were from the latter, which has a beamwidth of approximately 100^{o}. In-flight calibration was against a solid-state noise source calibrated before flight against a temperature-limited noise source. At no time have these data been presented numerically. The paper in 1969 presents the spectrum of the northern halo minimum whereas the later paper presents spectra for the galactic centre, anti-centre and "poles".

Brown, 1973:

Observations were made at frequencies between 0.13 and 2.6 MHz from the IMP-6 spacecraft. Two 46 m monopole antennas were used and after the signals from these were amplified separately they were combined to electronically form a 91 m dipole antenna with a beamwidth of the order of 100^{o}. Calibration sources were the same as for the RAE-1 with an additional check on the high-level source.

A table gives the brightness at each frequency (22 in all) and a list of all the errors and their contributions. No definite direction could be assigned to the spectrum and the data is not included in the final spectra.

Getmansev et al., 1969:

Measurements were made at several frequencies in the range 6.3 to 40 MHz using scaled arrays with beamwidths $25^{o} \times 35^{o}$. Calibrations were against a noise generator. Brightness and effective temperature are given for several right ascensions for declination $+56^{o}$. The values at 13^{h} have been selected, corresponding to $\ell \simeq 120^{o}, b \simeq 60^{o}$.

Novaco, 1976:

This was a private communication in which the author received graphs of RAE-2 spectra for the north and south galactic poles. The system is similar to that of RAE-1. The data was indicated as being preliminary and further analysis was underway.

Parthasarathy, 1968:

These measurements, at 2 and 3 MHz, are an extension of the earlier work (Parthasarathy and Lerfeld, 1965) using scaled antennas with 70^{o} beamwidths. Calibrations were done by means of diode noise generators. The measurements refer to $\ell \simeq 120^{o}$, $b \simeq 55^{o}$ and are presented graphically only.

Weber, 1972:

Measurements were made at frequencies in the range 0.54-4.17 MHz from an Astrobee sounding rocket using two 50 m dipoles (beamwidth $\sim 100^{o}$). The spectrum obtained was for $\ell = 75^{o}, b = 0^{o}$ and it was shown to be comparable with a revised version of the RAE-1 northern halo minimum spectrum. The revision only affected the spectrum below 1 MHz, where the brightness was reduced. It is

puzzling to note that above this frequency the spectrum is not the same as that presented by Alexander et al. (1969). A table is given of Astrobee and revised RAE-1 brightness values. These measurements are not included in the final spectra.

Southern Hemisphere Observations

Alexander et al. 1969 b:

The author has not seen this paper but it was referred to by Stephens (1971) and a graph was presented.

Novaco, 1976:

Private communication of data for RAE-2.

Summary

The observations in the two hemispheres are summarized in Table 5.4 and Table 5.5. Table 5.6 gives the list of observers.

To convert temperature to brightness the following relationship has been used

Brightness $S = 2 k T / \lambda^2$ ($k = 1.38 \times 10^{-23}$ joule/K)

$= 3.068 \times 10^{-28} T\nu^2$

where T = temperature, K

ν = frequency, MHz

The data is presented in figures 5.9 -5.12. The diagrams have been taken from Hamilton's thesis and the new data added. The "five less satisfactory points" have been removed.

TABLE 5.4

SPECTRAL MEASUREMENTS OF NORTH GALACTIC POLE

FREQUENCY (MHz)	EQUIVALENT AERIAL TEMPERATURE (K)	SKY BRIGHTNESS ($W\ m^{-2} Hz^{-1} ster^{-1}$)	OBSERVER
0.25	7.3×10^{6}	1.4×10^{-22}	15
0.29	1.1×10^{7}	2.9×10^{-22}	15
0.36	1.5×10^{7}	5.8×10^{-22}	15
0.43	1.6×10^{7}	9.0×10^{-22}	15
0.45	1.6×10^{7}	9.9×10^{-22}	15
0.45	4.0×10^{7}	2.5×10^{-21}	3
0.47	1.5×10^{7}	9.9×10^{-22}	15
0.55	3.8×10^{7}	3.5×10^{-21}	3
0.6	1.6×10^{7}	1.8×10^{-21}	15
0.69	1.7×10^{7}	2.5×10^{-21}	15
0.7	3.5×10^{7}	5.2×10^{-21}	3
0.72	3.3×10^{7}	5.2×10^{-21}	5
0.73	1.8×10^{7}	2.9×10^{-21}	15
0.85	2.7×10^{7}	6×10^{-21}	3
0.87	1.8×10^{7}	4.1×10^{-21}	15
0.88	1.7×10^{7}	4.1×10^{-21}	15
1.0	2.3×10^{7}	7×10^{-21}	3
1.05	1.6×10^{7}	5.5×10^{-21}	15
1.1	2.2×10^{7}	8.0×10^{-21}	5
1.25	1.5×10^{7}	7.4×10^{-21}	15
1.25	2.3×10^{7}	1.1×10^{-20}	10
1.3	1.5×10^{7}	7.5×10^{-21}	15
1.3	1.5×10^{7}	8×10^{-21}	3
1.45	1.5×10^{7}	9.5×10^{-21}	15
1.5	2.2×10^{7}	1.5×10^{-20}	10
1.6	1.1×10^{7}	8.7×10^{-21}	5
1.75	1.6×10^{7}	1.5×10^{-20}	10
1.8	1.3×10^{7}	1.25×10^{-20}	15
1.91	2.0×10^{7}	2.2×10^{-20}	2
2.0	1.1×10^{7}	1.3×10^{-20}	10
2.0	6.2×10^{6}	7.6×10^{-21}	13
2.2	8.1×10^{6}	1.2×10^{-20}	15
2.2	9.4×10^{6}	1.4×10^{-20}	15
2.2	7.7×10^{6}	1.15×10^{-20}	3

TABLE 5.4 continued

FREQUENCY (MHz)	EQUIVALENT AERIAL TEMPERATURE (K)	SKY BRIGHTNESS ($W\ m^{-2} Hz^{-1} ster^{-1}$)	OBSERVER
2.2	9.4×10^{6}	1.4×10^{-20}	11
2.5	7.3×10^{6}	1.4×10^{-20}	10
2.7	5.4×10^{6}	1.2×10^{-20}	3
2.8	5.4×10^{6}	1.3×10^{-20}	15
2.85	1.1×10^{7}	2.7×10^{-20}	2
3.0	5.1×10^{6}	1.4×10^{-20}	10
3.0	2.6×10^{6}	7.1×10^{-21}	13
3.4	4.9×10^{6}	1.8×10^{-20}	10
3.6	4.3×10^{6}	1.7×10^{-20}	2
3.9	2.8×10^{6}	1.3×10^{-20}	15
4.0	3.1×10^{6}	1.5×10^{-20}	3
4.5	2.3×10^{6}	1.45×10^{-20}	3
4.7	3.2×10^{6}	2.2×10^{-20}	2
4.7	1.9×10^{6}	1.3×10^{-20}	15
5.0	1.1×10^{6}	8.1×10^{-21}	12
6.3	6.5×10^{5}	7.9×10^{-21}	8
7.5	6.7×10^{5}	1.15×10^{-20}	15
9.0	2.8×10^{5}	7.1×10^{-21}	8
9.1	4.0×10^{5}	1.02×10^{-20}	15
10.0	2.3×10^{5}	6.9×10^{-21}	4
10.0	2.9×10^{5}	8.9×10^{-21}	12
13.0	1.1×10^{5}	5.7×10^{-21}	8
13.1	1.0×10^{5}	5.4×10^{-21}	4
13.15	9.0×10^{4}	4.8×10^{-21}	14
17.5	5.4×10^{4}	5.0×10^{-21}	4
17.5	4.8×10^{4}	4.5×10^{-21}	14
18.6	4.3×10^{4}	4.5×10^{-21}	8
20.0	4.3×10^{4}	5.2×10^{-21}	12
25.0	2.6×10^{4}	5.0×10^{-21}	7
25.0	1.9×10^{4}	3.7×10^{-21}	8
26.3	1.8×10^{4}	3.7×10^{-21}	14
26.5	2.0×10^{4}	4.2×10^{-21}	4
30.0	1.7×10^{4}	4.7×10^{-21}	12
35.0	1.1×10^{4}	4.1×10^{-21}	7

TABLE 5.4 continued

FREQUENCY (MHz)	EQUIVALENT AERIAL TEMPERATURE (K)	SKY BRIGHTNESS ($W\ m^{-2} Hz^{-1} ster^{-1}$)	OBSERVER
38.0	9.7×10^{3}	4.3×10^{-21}	1
38.0	8.0×10^{3}	3.5×10^{-21}	4
38.0	7.0×10^{3}	3.1×10^{-21}	6
38.0	7.8×10^{3}	3.5×10^{-21}	14
40.0	5.8×10^{3}	2.8×10^{-21}	8
50.0	5.0×10^{3}	3.8×10^{-21}	7
50.0	4.3×10^{3}	3.3×10^{-21}	12
75.0	1.8×10^{3}	3.1×10^{-21}	7
81.5	1.5×10^{3}	3.0×10^{-21}	1
81.5	1.1×10^{3}	2.3×10^{-21}	14
81.5	1.2×10^{3}	2.4×10^{-21}	6
110.0	700	2.6×10^{-21}	7
175.0	266	2.5×10^{-21}	1
178.0	169	1.6×10^{-21}	14
178.0	185	1.8×10^{-21}	6
404.0	17.9	9.0×10^{-21}	14

TABLE 5.5

SPECTRAL MEASUREMENTS OF SOUTH GALACTIC POLE

FREQUENCY (MHz)	EQUIVALENT AERIAL TEMPERATURE (K)	SKY BRIGHTNESS ($W\ m^{-2} Hz^{-1} ster^{-1}$)	OBSERVER
0.25	7.8×10^6	1.5×10^{-22}	15
0.29	1.24×10^7	3.2×10^{-22}	15
0.36	1.7×10^7	6.7×10^{-22}	15
0.42	1.85×10^7	1×10^{-21}	15
0.42	4.4×10^7	2.4×10^{-21}	16
0.44	2.2×10^7	1.3×10^{-21}	15
0.48	1.9×10^7	1.35×10^{-21}	15
0.55	3.8×10^7	3.5×10^{-21}	16
0.6	2.0×10^7	2.2×10^{-21}	15
0.7	1.9×10^7	2.9×10^{-21}	15
0.7	4.1×10^7	6.2×10^{-21}	16
0.7	4.7×10^7	7.0×10^{-21}	16
0.73	1.8×10^7	3.0×10^{-21}	15
0.87	1.7×10^7	4×10^{-21}	15
0.9	1.8×10^7	4.5×10^{-21}	15
0.9	2.2×10^7	5.5×10^{-21}	16
0.9	1.8×10^7	4.5×10^{-21}	21
1.0	2.4×10^7	7.2×10^{-21}	16
1.0	1.7×10^7	5.3×10^{-21}	15
1.26	1.3×10^7	6.2×10^{-21}	15
1.3	1.3×10^7	6.9×10^{-21}	15
1.3	1.6×10^7	8.2×10^{-21}	16
1.43	1.1×10^7	6.6×10^{-21}	21
1.45	1.2×10^7	7.9×10^{-21}	15
1.65	1.0×10^7	8.6×10^{-21}	18
1.7	8.9×10^6	7.9×10^{-21}	16
1.85	9.0×10^6	9.5×10^{-21}	15
2.13	7.9×10^6	1.1×10^{-20}	21
2.2	7.1×10^6	1.05×10^{-20}	15
2.2	7.4×10^6	1.1×10^{-20}	15
2.3	8×10^6	1.3×10^{-20}	16
2.3	8×10^6	1.3×10^{-20}	18
2.7	5.4×10^6	1.2×10^{-20}	16

TABLE 5.5 continued

FREQUENCY (MHz)	EQUIVALENT AERIAL TEMPERATURE (K)	SKY BRIGHTNESS ($W\ m^{-2}\ Hz^{-1}\ ster^{-1}$)	OBSERVER
2.8	5.4×10^6	1.29×10^{-21}	15
3.8	4×10^6	1.8×10^{-20}	17
3.9	2.7×10^6	1.28×10^{-20}	15
3.9	2.9×10^6	1.35×10^{-20}	15
4.0	3.7×10^6	1.8×10^{-20}	16
4.4	2.9×10^6	1.7×10^{-20}	17
4.5	2.4×10^6	1.5×10^{-20}	16
4.7	1.8×10^6	1.25×10^{-20}	15
4.7	1.9×10^6	1.31×10^{-20}	15
4.8	3.0×10^6	2.1×10^{-20}	18
5.65	1.8×10^6	1.8×10^{-20}	17
6.5	8.5×10^5	1.1×10^{-20}	15
9.15	6×10^5	1.5×10^{-20}	20
9.2	3.9×10^5	1.0×10^{-20}	15
9.2	3×10^5	8.4×10^{-21}	15
9.6	7.2×10^5	2.0×10^{-20}	18
10.05	3.8×10^5	1.2×10^{-20}	17
14.1	1.3×10^5	7.7×10^{-21}	23
18.3	7.5×10^4	7.7×10^{-21}	22
20.0	5.5×10^4	6.7×10^{-21}	23
30.0	1.7×10^4	4.8×10^{-21}	23
48.5	5.1×10^3	3.7×10^{-21}	23
85.0	1.2×10^3	2.7×10^{-21}	23
153.0	240	1.7×10^{-21}	19

TABLE 5.6

LIST OF OBSERVERS

1	Adgie and Smith (1956)
2	Alexander and Stone (1965)
3	Alexander (1970)
4	Andrew (1966)
5	Benediktov et al. (1965)
6	Costain (1960)
7	Cottony and Johler (1952)
8	Getmantsev et al. (1969)
9	Hartz (1964)
10	Hugill and Smith (1965)
11	Papagiannis (1964)
12	Parthasarathy and Lerfald (1965)
13	Parthasarathy (1968)
14	Purton (1966)
15	Novaco (1976)
16	Alexander et al. (1969 b)
17	Ellis (1957)
18	Ellis (1965)
19	Hamilton and Haynes (1969)
20	Higgins and Shain (1954)
21	Reber and Ellis (1956)
22	Shain and Higgins (1954)
23	Yates and Wielebinski (1966)

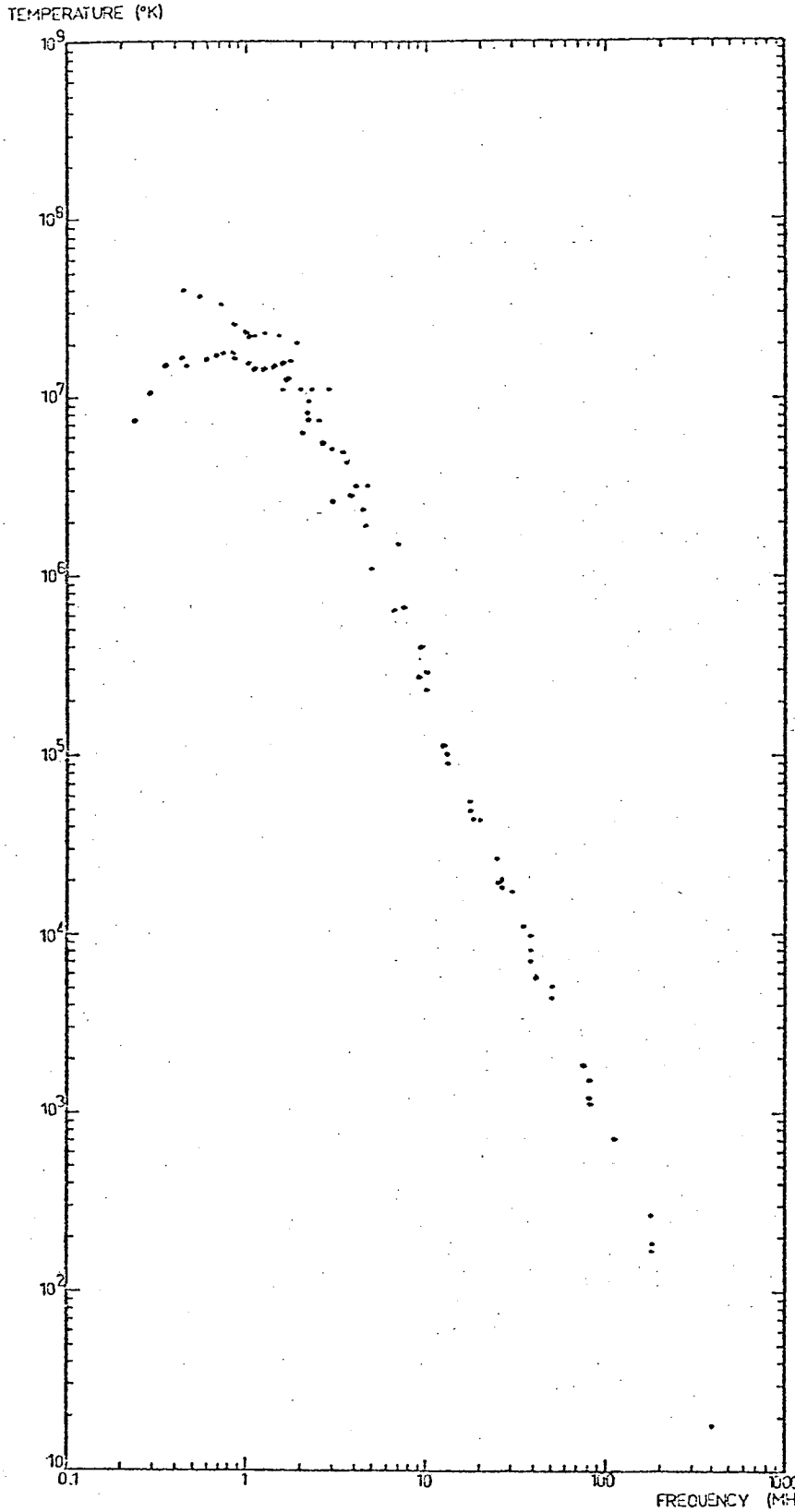

SPECTRUM OF NORTH GALACTIC POLAR REGION

FIGURE 5.9

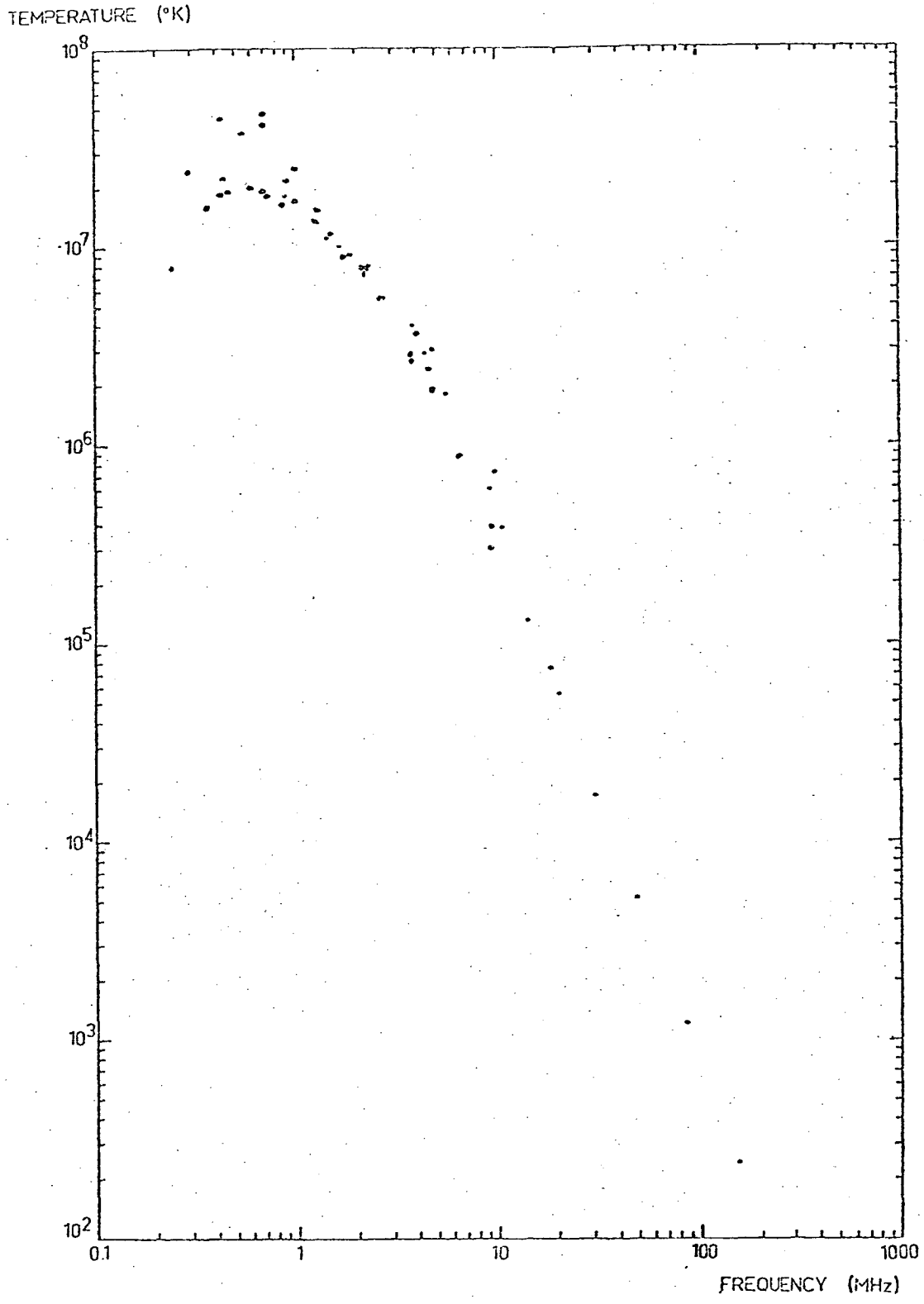

SPECTRUM OF SOUTH GALACTIC POLAR REGION

FIGURE 5.10

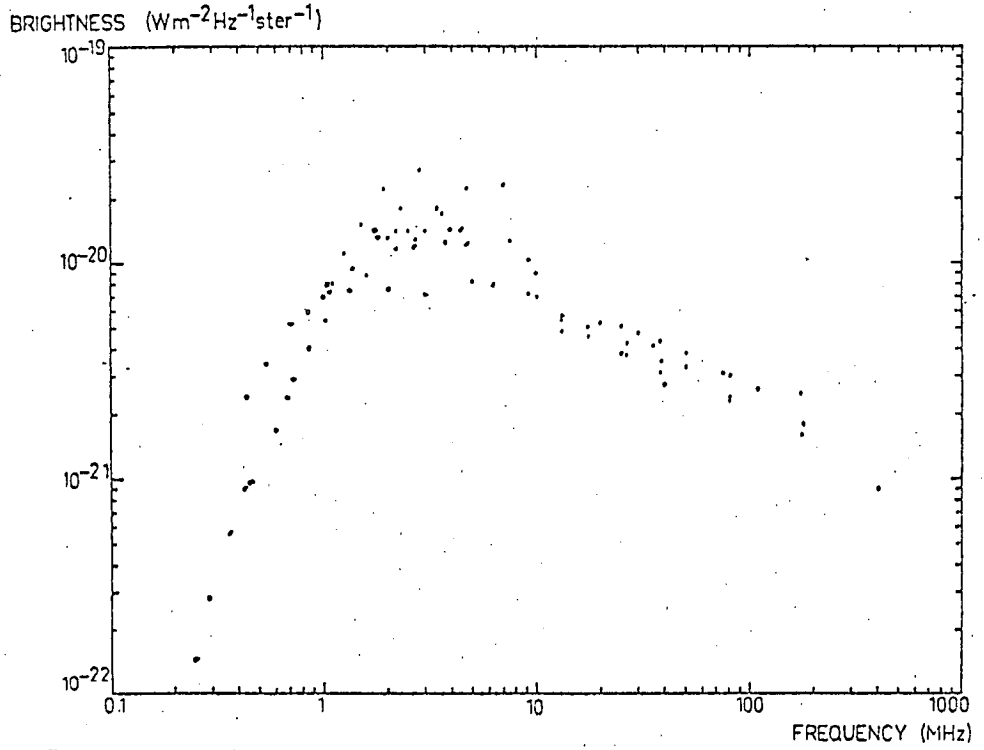

SPECTRUM OF NORTH GALACTIC POLAR REGION

FIGURE 5.11

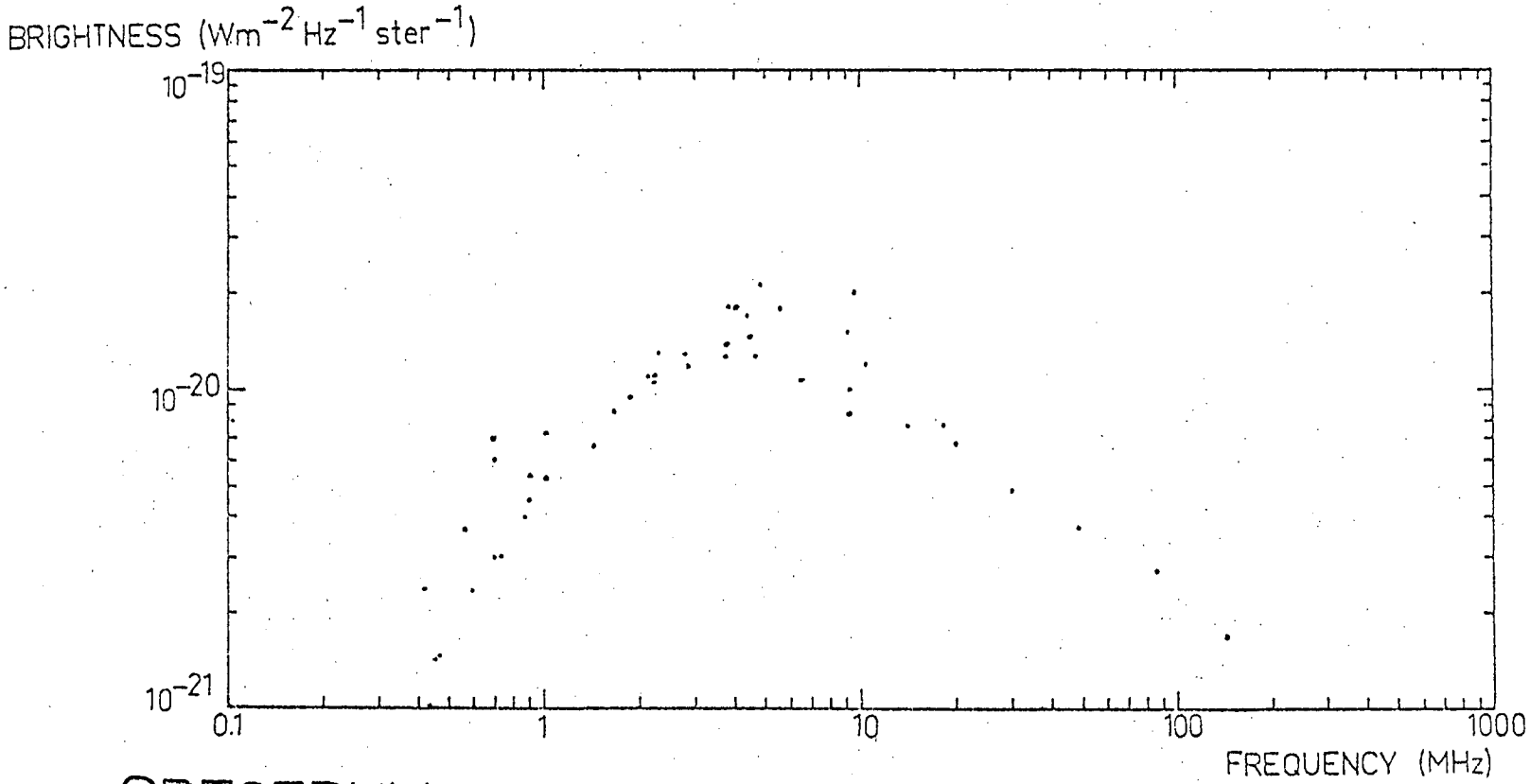

SPECTRUM OF SOUTH GALACTIC POLAR REGION

FIGURE 5.12

Discussion

With the addition of the recent data the galactic polar spectra have become better defined. The differences between the north and south spectra still exist but the shapes of the spectra are more readily explained by known mechanisms.

Above 10 MHz the variation of brightness S with frequency ν is given by

$$S \propto \nu^{-\alpha}$$

where the spectral index α has the values

$\alpha \simeq 0.5$ (north galactic pole),

$\alpha \simeq 0.6$ (south galactic pole).

There is some evidence of a steepening of the spectral indices above 80 MHz. This steepening is more obvious above 100 MHz.

Smooth curves can be drawn through both sets of points as shown in figure 5.13. However, it is important to note that with the present data there is some latitude in defining smooth curves. For example, Webber (private communication) prefers to define the curves in such a way that at 10 MHz the intensity in the south pole direction is 8.4×10^{-21} watts m^{-2} Hz^{-1} $ster^{-1}$ and the intensity in the north pole direction is 7×10^{-21} watts $m^{-2}Hz^{-1}ster^{-1}$. These values are below those defined by figure 5.13. The sharp increase in brightness in the range 6-10 MHz discussed by Hamilton was probably instrumental in origin, although there is still some evidence of an increase in the north pole spectrum.

Below about 6 MHz both the spectra turn over and this has been attritubed to free-free absorption. The south pole spectrum reaches a maximum intensity of 1.3×10^{-20} watts $m^{-2}Hz^{-1}ster^{-1}$

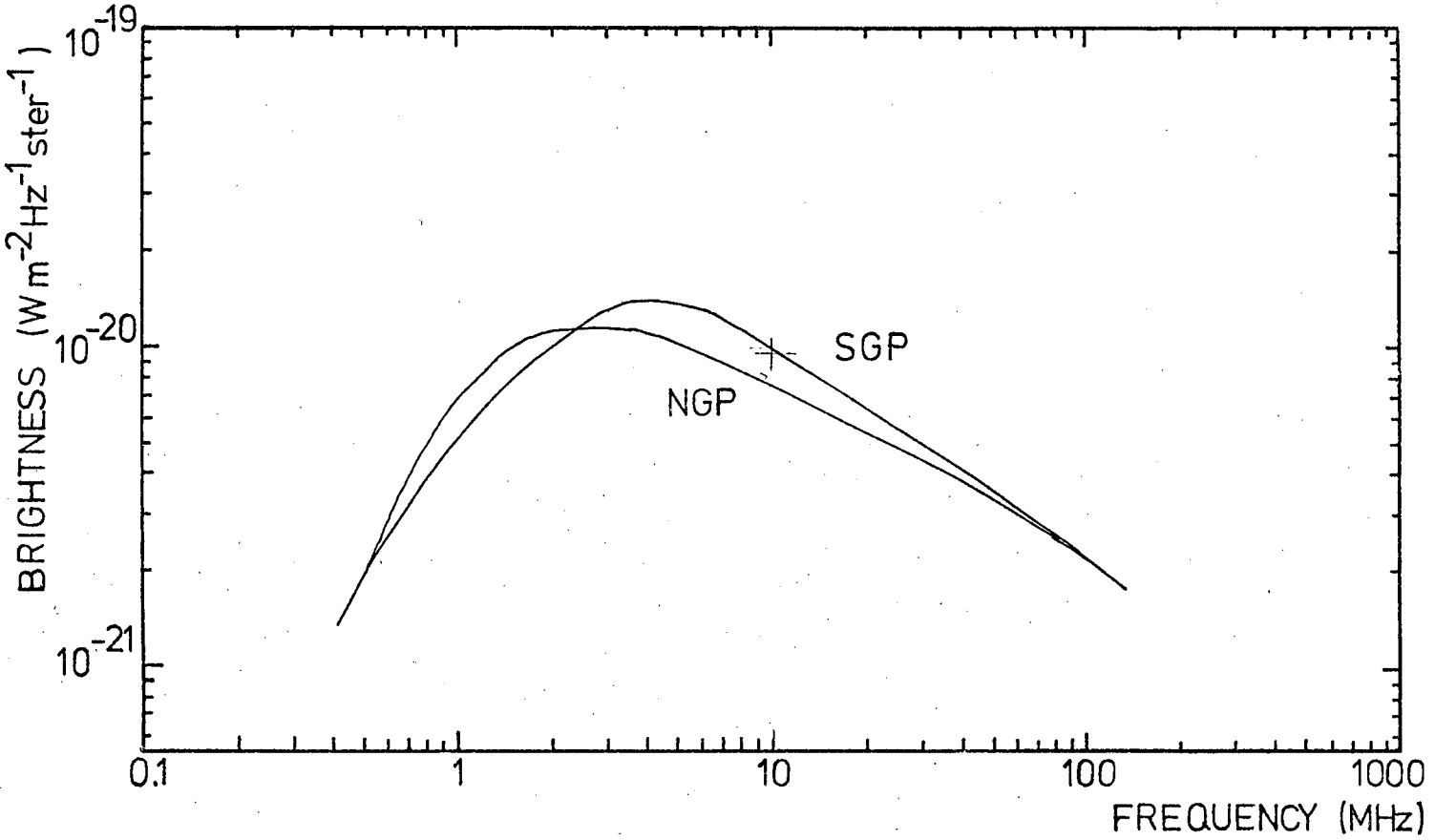

SPECTRA OF THE GALACTIC POLES

FIGURE 5.13

at 5 MHz whereas the north pole spectrum reaches a maximum intensity of 1.2×10^{-20} watts $m^{-2} Hz^{-1}$ $ster^{-1}$ at about 2 MHz. A model with a small amount of emission behind a region of combined emission and absorption will satisfy the data down to about 1 MHz but below this frequency the spectra fall off more rapidly. This has been attributed to the Razin effect (eg. Brown, 1973). The example shown in figure 2.4(b) illustrates that the observed spectral shapes could be the result of the Razin effect.

There are two features of the polar spectra which are unexpected. Firstly, the observation that the spectra turn over at different frequencies. If the turn-over is attributed solely to free-free absorption then the simplest explanation is differing distributions of ionized hydrogen. If the ionized hydrogen is mainly in the form of HII regions then it is unlikely that the distribution would be uniform. However, the optical depth in the south pole direction is approximately twice that in the north pole direction and this would require that the average value of any one of the parameters n_e, T_e or L or a combination of them would need to differ by a factor of 2.

Alternatively, if the Razin effect is taking place then the parameters which determine this effect may be different in the different hemispheres. For example, if for the line of sight $b = -90^o$ the magnetic field is observed at a much smaller angle than for the line of sight $b = +90^o$ then the polar spectra could turn-over at different frequencies.

Of course, it is possible that the discrepancy has been introduced by the data and the situation will not be clarified until the spectra are better defined. At present there is still considerable latitude in defining the polar spectra.

The second feature of the polar spectra is the difference in spectral indices below 100 MHz and this will be discussed in Part III.

Galactic Spectra in Other Directions

In Figure 5.14 we show the north and south galactic pole spectra together with spectra of two other regions of interest. These are the region of minimum brightness in the northern hemisphere ($\ell \simeq 200°$, $b \simeq 45°$) and the anti-centre direction. The scaled array experiments of Turtle et al. (1962), Purton (1966) and Bridle (1967) covered these regions and so do several surveys. Tables 5.7 and 5.8 list the high resolution measurements in the northern minimum and anti-centre directions respectively.

We have fitted straight lines to the spectral points in the northern minimum and anti-centre directions. The slopes of these lines imply spectral indices as follows:

$$\alpha = 0.54 \pm 0.04 \quad \text{(northern minimum)}$$

and

$$\alpha = 0.43 \pm 0.04 \quad \text{(anti-centre)}.$$

The 10 MHz and 13.1 MHz data points at the low frequency end of the anti-centre spectrum are not consistent. Since the 13.1 MHz map is in disagreement with higher frequency surveys (as discussed in Part I) whereas the 10 MHz composite map is in agreement the 10 MHz point should probably be given more weight.

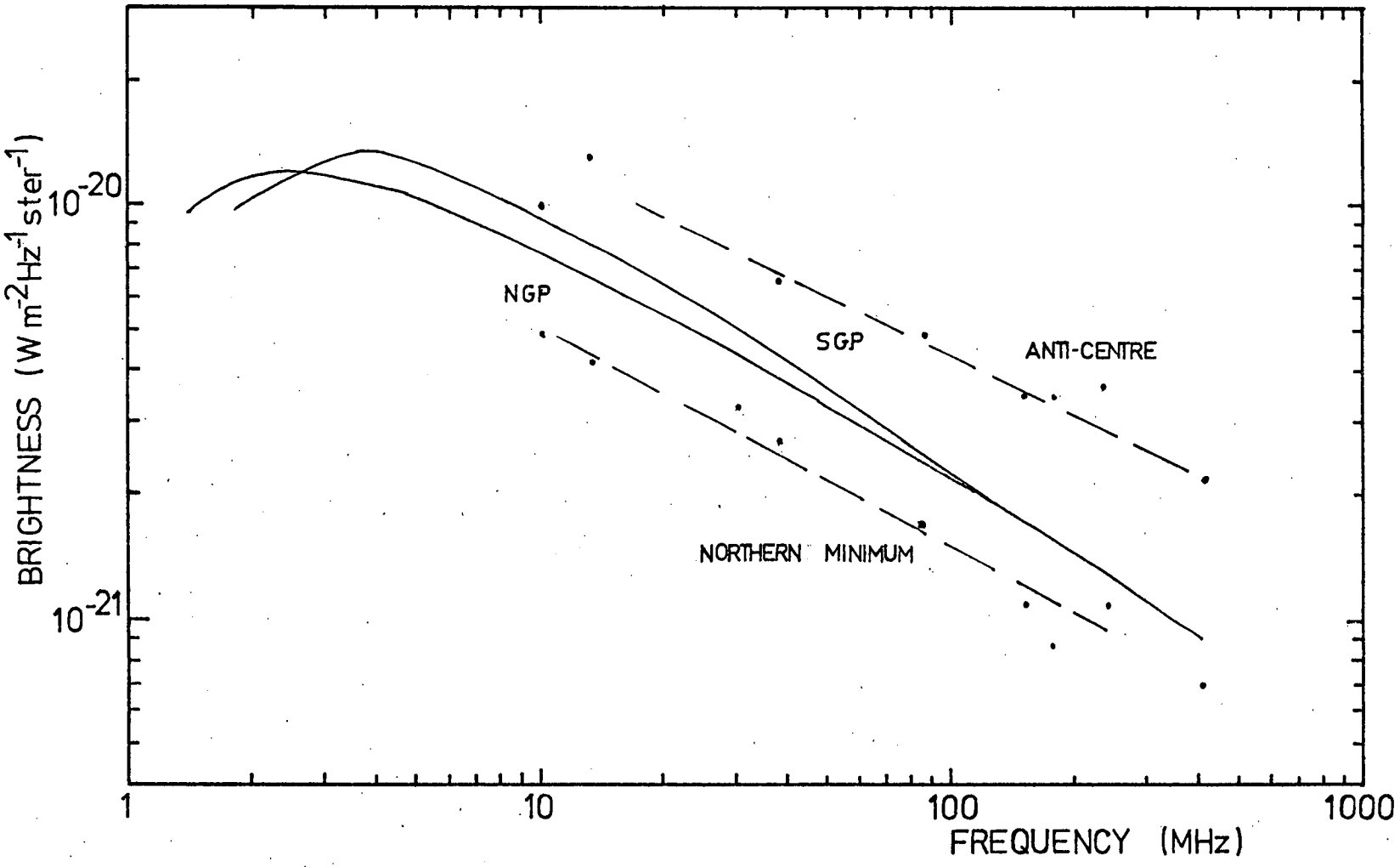

GALACTIC SPECTRA

FIGURE 5.14

TABLE 5.7

MEASUREMENTS OF NORTHERN MINIMUM

FREQUENCY (MHz)	EQUIVALENT AERIAL TEMPERATURE (K)	SKY BRIGHTNESS ($W\ m^{-2} Hz^{-1} ster^{-1}$)	OBSERVER
10.0	1.6×10^5	4.9×10^{-21}	S27
13.1	8×10^4	4.2×10^{-21}	S25
30.0	1.2×10^4	3.3×10^{-21}	S20
38.0	6×10^3	2.7×10^{-21}	S19
85.0	750	1.7×10^{-21}	S15
150.0	160	1.1×10^{-21}	S11
178.0	90	8.7×10^{-22}	S8
240.0	60	1.1×10^{-21}	S6
404.0	14.2	7.0×10^{-22}	S4

TABLE 5.8

MEASUREMENTS IN THE ANTI-CENTRE DIRECTION

FREQUENCY (MHz)	EQUIVALENT AERIAL TEMPERATURE (K)	SKY BRIGHTNESS ($W\ m^{-2} Hz^{-1} ster^{-1}$)	OBSERVER
10.0	3.4×10^5	1.0×10^{-20}	S27
13.1	2.5×10^5	1.3×10^{-20}	S25
38.0	1.5×10^4	6.6×10^{-21}	S19
85.0	2200	4.9×10^{-21}	S15
150.0	500	3.5×10^{-21}	S11
178.0	360	3.5×10^{-21}	S8
237.0	220	3.7×10^{-21}	S7
408.0	44	2.2×10^{-21}	S3

In summary, the north and south galactic pole spectra have been updated and it is found that they are not the same. It is suggested that the shape of these spectra is compatible with known mechanisms and that at low frequencies the spectra turn over due to absorption in ionized hydrogen and the Razin effect. The diagrams illustrate the need for more high resolution low frequency observations particularly in the anti-centre direction.

PART III

SPECTRAL INDEX VARIATIONS

Introduction

The variation of the non-thermal spectrum with direction has not been fully investigated. Ideally such investigations should be made with scaled arrays but such measurements have been concentrated on the polar regions and the northern minimum. Most of this work has been summarized in the previous section.

The emission spectral index (see Chapter 2) is found to lie in the range 0.4 - 0.9 with values greater than 0.7 applying at frequencies>200 MHz. For decametric frequencies the index varies between 0.4 and 0.7. However, some of the variation in values quoted is due to the method of analysis used by the observer. Many of the scaled array measurements have been analyzed by a method which eliminates an extra-galactic component and the "differential spectral index" quoted is for the "galactic" component only. As the extra-galactic component is taken to have a steeper spectral index than the galactic component, differential spectral indices will be less than total background spectral indices (α_T). If plots of the α_T shows an anti-correlation with brightness temperature then changes in the α_T may only reflect variations in intensity of a galactic component of constant spectral index i.e. the α_T would take high values in regions where the total sky brightness is small and thus the galactic component contributes little radiation. However in the previous section it was shown that α_T was 0.5 for the region of minimum brightness whereas towards the south galactic pole α_T was 0.6. These variations must reflect variations in the galactic spectral index and so plots of the total background will provide information on this variation. Below

we briefly summarize the results of previous investigations and then introduce a new visual approach to determining the variation of the temperature spectral index using all-sky maps. The temperature spectral index β is related to the emission spectral index α as follows

$$\beta = \alpha + 2.0$$

The Measurements

Most studies of background spectra have interpreted the variation of spectral indices across the sky as due to the superposition of a varying intensity galactic component of constant temperature spectral index β_1 and an isotropic component having a different spectra index β_0. If temperatures at one frequency are plotted against temperatures at the same positions at another frequency then the plots should be a straight line of slope β_1 - the differential spectral index - and the intercept on the lower frequency axis is a measure of the extra-galactic component. Such a graph has been called a T-T plot and was introduced by Turtle et al. (1962).

Using this method Purton (1966) obtained a β_1 of 2.38 at frequencies in the range 13 - 100 MHz for the halo and anti-centre regions - the former being defined by R.A. 10^h - 17^h and Dec. $+20^\circ$ and $+60^\circ$. Similarly, Andrew (1966) obtained a β_1 of 2.43 for the halo region. However, the work of Bridle (1967), and the later work of Sironi (1974), revealed that the galactic spectral index was not constant. Since the T-T plot assumes a constant temperature spectral index it was apparent that the method should be applied to smaller regions. Bridle and Sironi drew up T-T plots for several regions and found that β_1 was less in Region 1 than in Region 2 where the radiation from Region 1 was expected to come from the local arm and

that from Region 2 from the interarm region. They correspond roughly to the northern minimum and northern galactic pole directions. Bridle's work covered the frequency range 13 - 178 MHz and he found spectral indices of 2.38 and 2.46 for Regions 1 and 2 respectively. Bridle concluded that for Region 1 slight curvature over the whole range from 178 to 13.15 MHz was possible within the error limits. The later paper of Sironi concluded that spectra do increase in steepness over the whole range 17.5 to 408 MHz.

Some other work at decametric frequencies is that of Komesaroff (1961) who used data in the frequency range 19.7 to 1390 MHz to obtain spectra in directions towards the galactic centre. He drew straight spectra over this whole frequency range and obtained an average α_T of 0.6. For these directions α_T approximates the galactic spectral index. For similar directions, although slightly further from the galactic centre, Wielebinski et al. (1968) obtained $\alpha_T = 0.5$ from measurements at 85 and 150 MHz. Along the galactic plane they found an average α_T of 0.2 and this was attributed to the presence of a thermal component. Early workers (e.g. Westerhout, 1958) assumed that spectral variations near the galactic plane were due entirely to thermal absorption in ionized hydrogen and variations in the spectral index were used to seperate out the thermal background from the non-thermal background. However, the reduction of the spectral index from 0.5 to 0.2 over the frequency range 150 - 85 MHz necessitates a much larger proportion of thermal background than has been deduced by other methods and we believe that the variation is real.

To conclude there exist variations in the total background spectral index which reflect variations in the galactic spectral index. The latter takes a value of approximately 0.5 at high latitudes in the northern hemisphere and approximately 0.6 towards the galactic

centre. There is evidence of a flattening of the spectrum close to the galactic plane.

Variations of the Total Background Temperature Spectral Index

Variations of the total background temperature spectral index can be illustrated using all-sky maps. The method can only be used to show general trends. Since the 85 and 150 MHz maps are based on the same data over much of the sky one should use one or the other, but not both, for illustrating spectral variations. Consequently, we choose the 85 MHz map as, together with the new 30 and 10 MHz composite maps an even coverage over a decade in frequency can be achieved.

On the 85 MHz map a contour (e.g. 1600 K) is emphasized by some method or another and here we will use coloured pencils. Assuming a temperature spectral index, say 2.6, the corresponding temperatures are calculated at 30 and 10 MHz. They are 24×10^3 K and 4.2×10^5 K (i.e. $5.2 \times 8 \times 10^4$ K) respectively and these levels are emphasized on the respective maps. By comparing the three maps it is apparent whether our choice of spectral index was correct or not. If the coloured line on any pair of maps match in placement with respect to galactic longitude and latitude then the assumed spectral index is correct. In Figures 5.15, 5.16 and 5.17 three levels are emphasized on each map, the levels being chosen to give a reasonable coverage of the sky. The corresponding levels at each

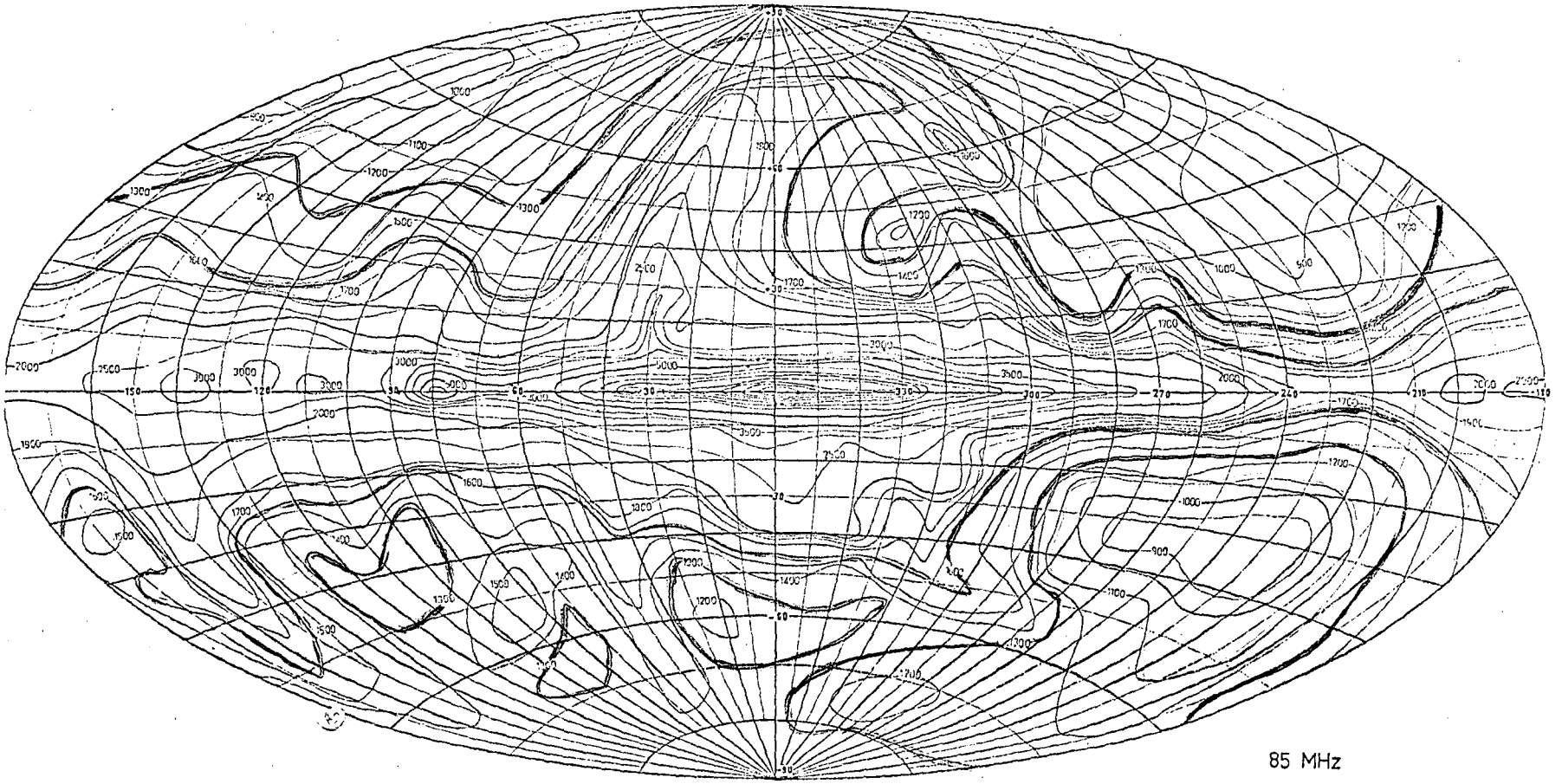

FIGURE 5.15

$\beta = 2.6$

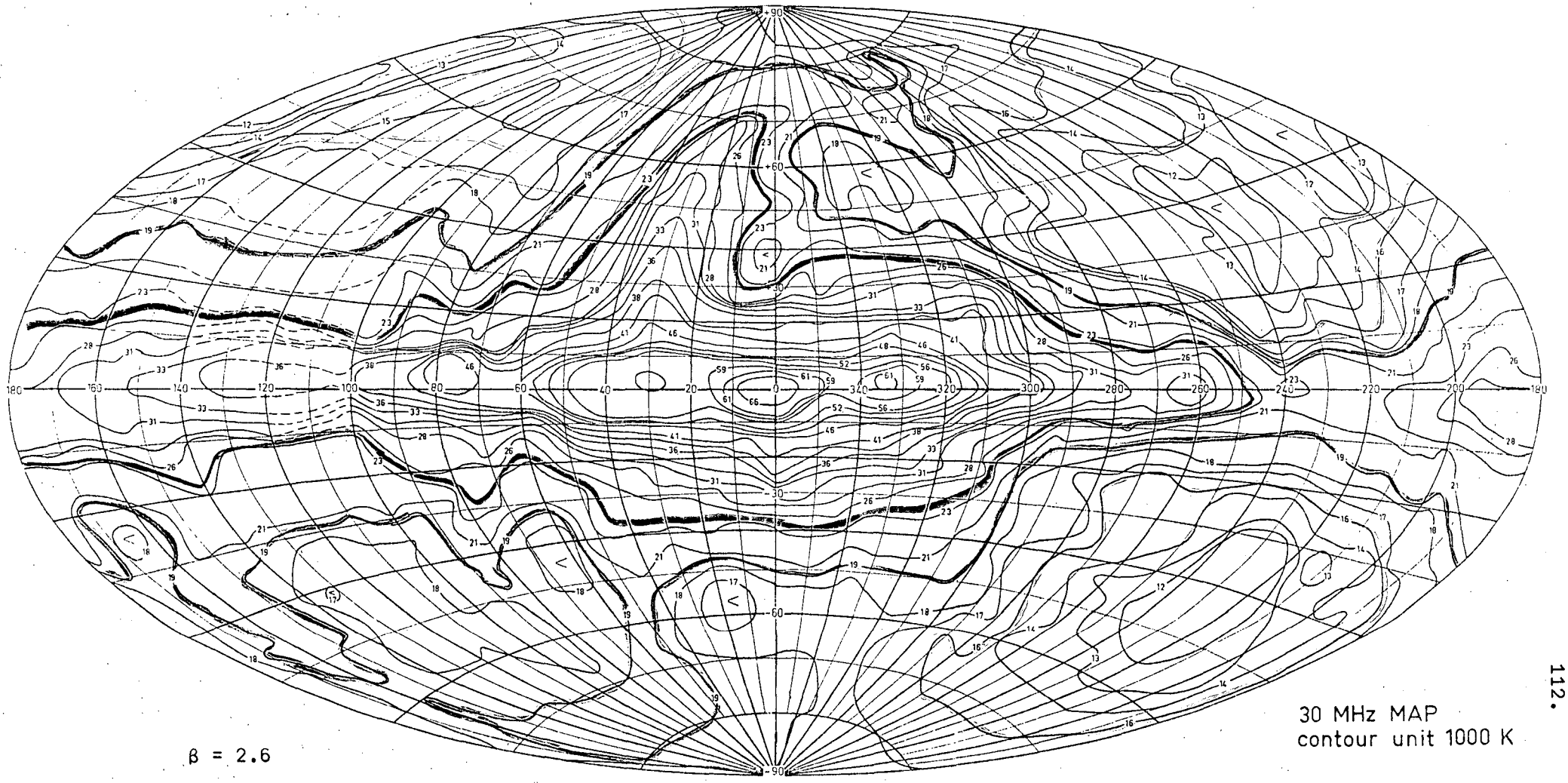

$\beta = 2.6$

30 MHz MAP
contour unit 1000 K

FIGURE 5.16

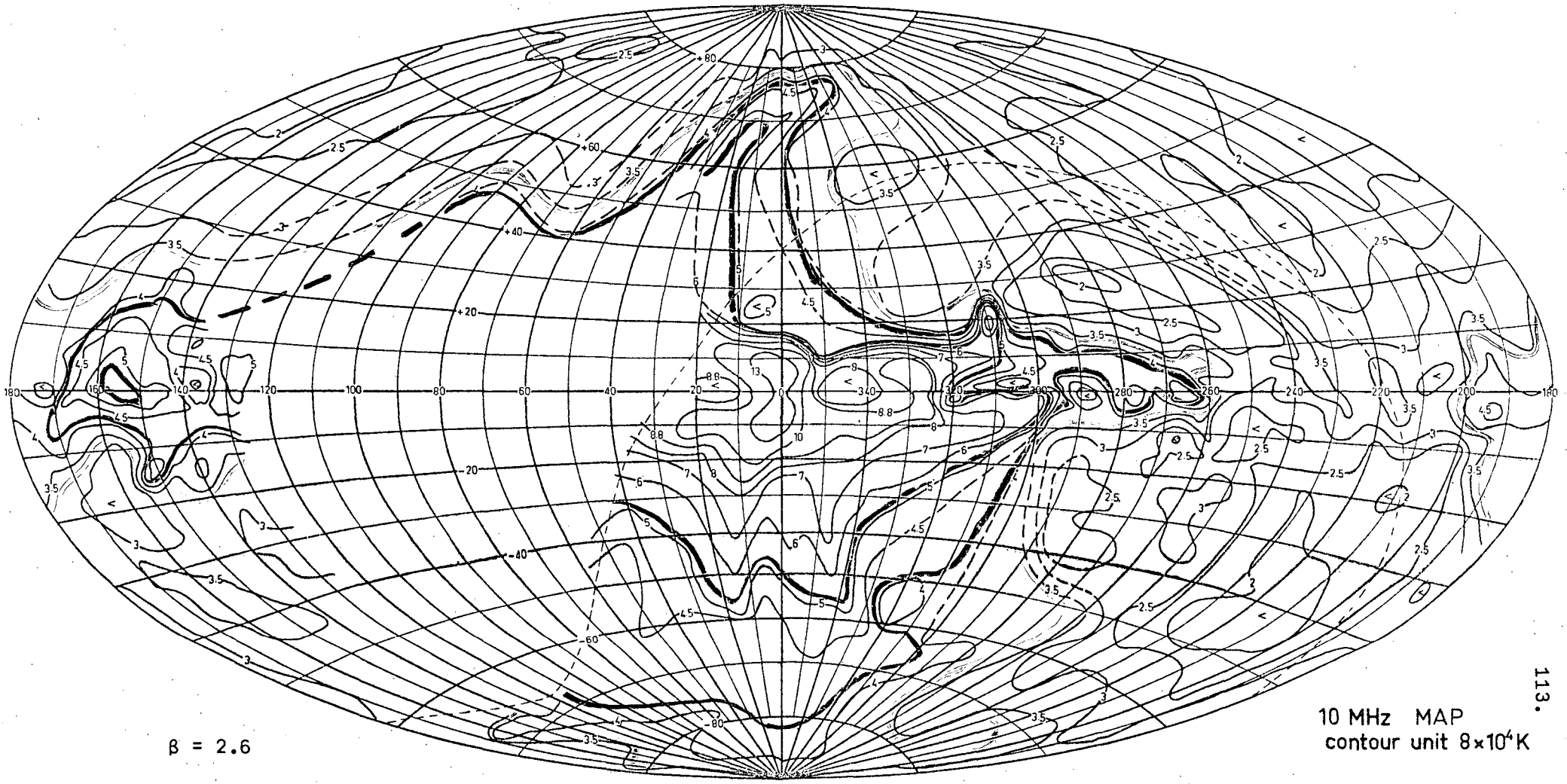

FIGURE 5.17

frequency are of the same colour, where a spectral index of 2.6 is assumed.

Comparing the 85 and 30 MHz maps reveals that the levels more or less pass through the same co-ordinates. When one compares the 85 and 10 MHz maps the result is different and the differences across the sky stand out. The most outstanding feature is the low 10 MHz temperatures at high latitudes in the northern hemisphere. The spectral index must be less than 2.6 for these directions. The low values along the galactic plane are partially due to absorption in ionized hydrogen but may also be due to a change in spectral index with frequency.

In Figure 5.18 we show a plot at 10 MHz assuming a spectral index of 2.45. This shows that a reasonable agreement is obtained between the 85 and 10 MHz maps in the northern hemisphere and in the low temperature regions but it is apparent that near the south galactic pole and near the galactic centre a higher value for the spectral index is appropriate. If a spectral index of 2.6 is appropriate between 85 MHz and 30 MHz and a smaller value is appropriate between 85 MHz and 10 MHz then a curved spectrum is implied. The results of the analysis suggest that for many lines of sight curved spectra may be more appropriate than straight spectra.

There is another aspect of Figures 5.15 - 5.17 which deserves mention. This is that the highlighting of contours makes the features of the maps stand out. Notice, firstly, that all three maps show that the polar regions in the opposite hemispheres do not have the same temperature and secondly, that the sky is not symmetrical about the plane $\ell = 0°$.

Figure 5.19 is an alternative presentation of the information contained in Figures 5.15 - 5.18. Here spectra in various directions are shown on a grid of galactic co-ordinates. Squares without asterisks cover the same frequency and brightness range so that the figure shows intensity variation as well as spectral shape. The scale of the squares is

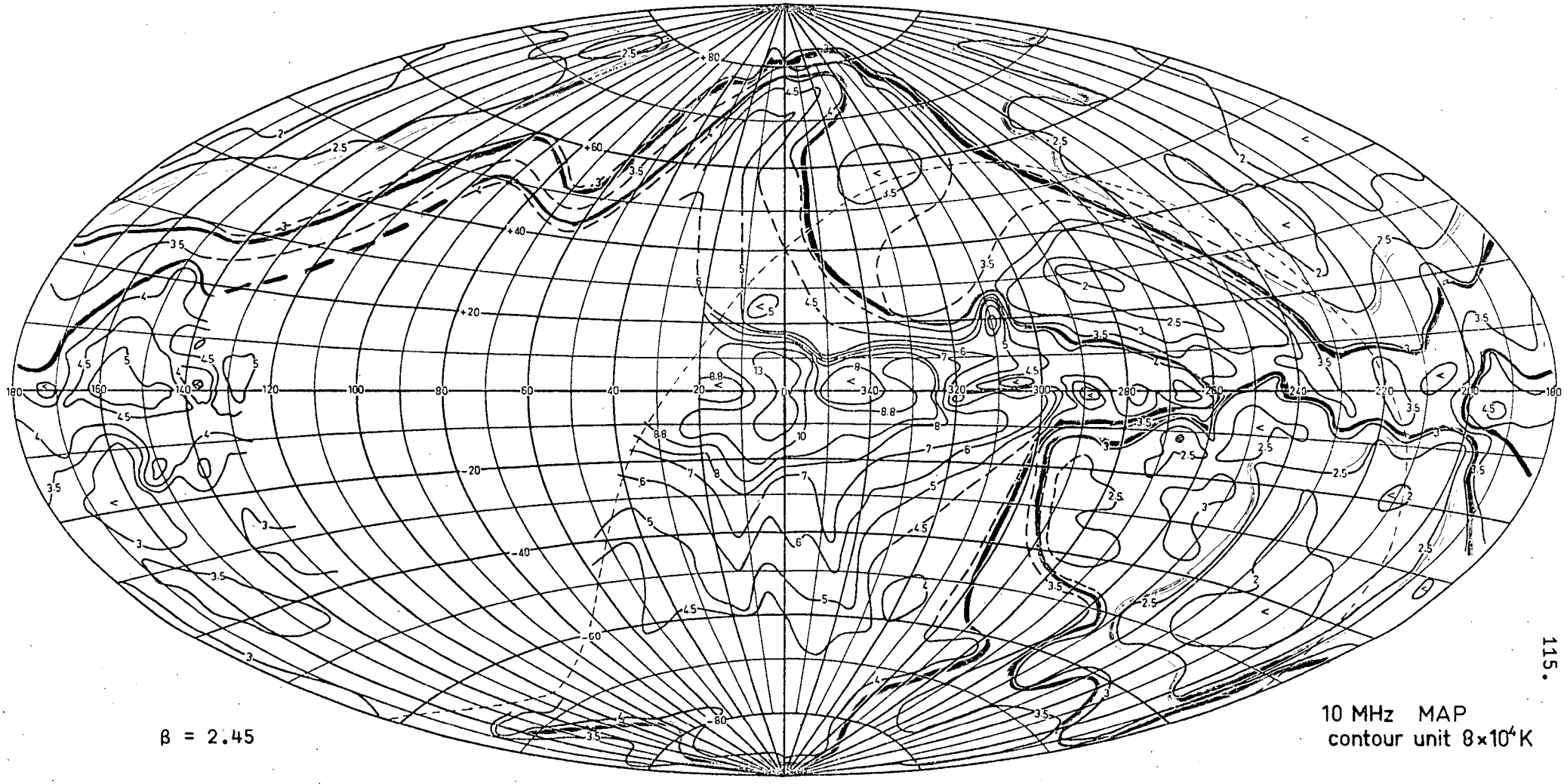

FIGURE 5.18

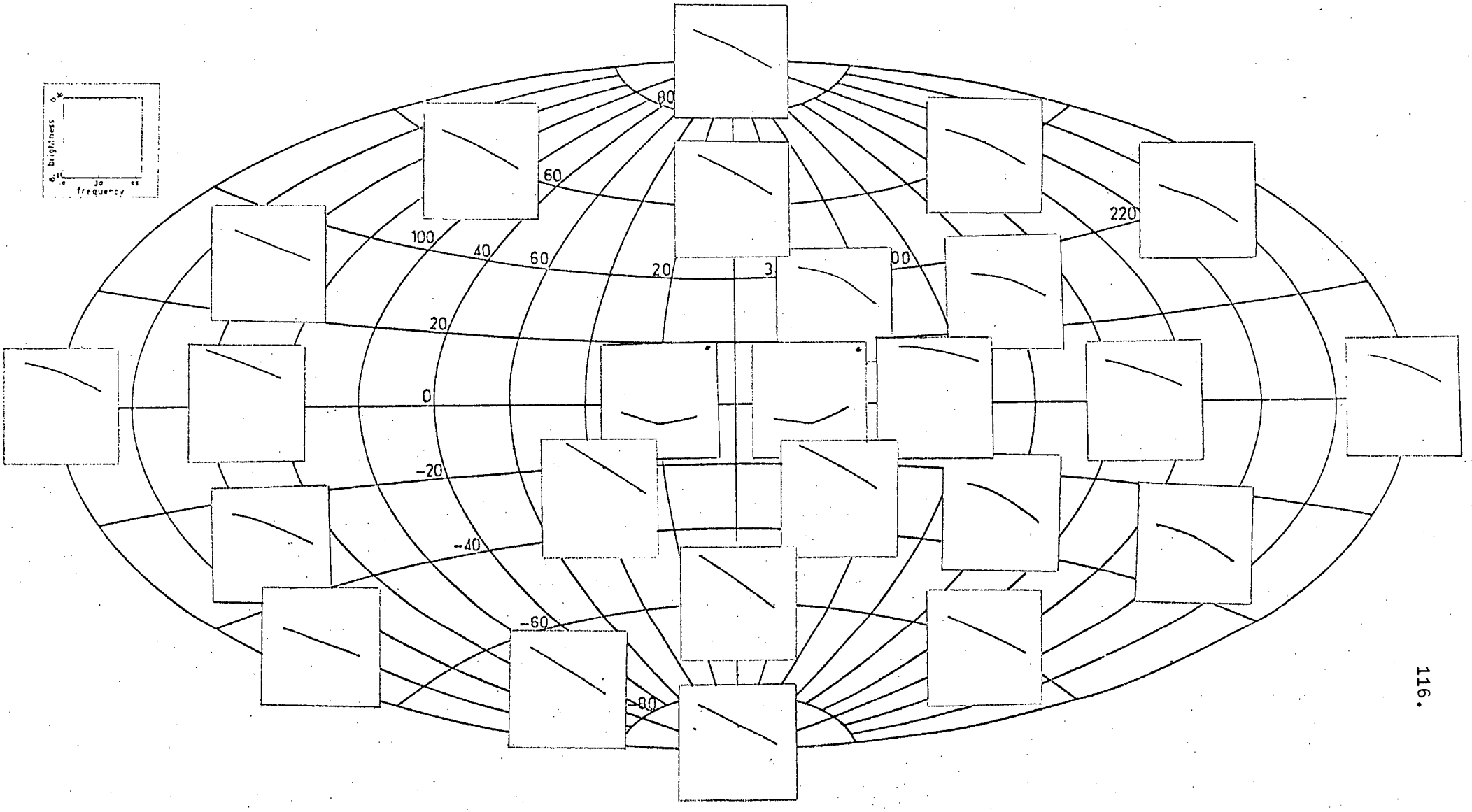

FIGURE 5.19

shown top left of the figure. The peculiar shape of the galactic plane spectra near the galactic centre is partially due to the low resolution of the 30 MHz survey relative to the other surveys. However spectra in these directions will be discussed in Chapter 6.

The suggestion is that curved spectra predominate in the range $180° \leq \ell \leq 360°$ and that straight spectra tend to occur in a diagonal band crossing the galactic plane at about $\ell = 120°$. Such a situation could arise if, for example, the loops have straighter spectra than the remaining galactic component. It would be expected that the regions furthest away from the loops, i.e. the minima and the anti-centre directions, would have curved spectra. It has been stated by Berkhuijsen (1971) that the minima "should probably be considered as regions where there happen to be no loops". Berkhuijsen has found that the loops have steeper spectra than the underlying background component.

However, the present data is not accurate enough and the number of frequencies too small to carry this investigation further but the topic deserves more attention and more high resolution, calibrated observations are required.

In summary the spectral index of the non-thermal galactic background radiation varies across the sky and with frequency. In the frequency range 10 - 85 MHz the spectral index varies between approximately 0.4 and 0.6. There is some evidence that the loops have straight spectra and that the remaining background has curved spectra.

PART IV

NON-THERMAL EMISSIVITY

Introduction

The non-thermal emissivity has been derived by a variety of methods but observations of HII regions at low frequencies provide the best, direct estimates. It is found that emissivities deduced from radio astronomical observations are substantially above those deduced from observations of the cosmic ray electron flux in the solar neighbourhood. We will review the radio observations and deduce an average emissivity for the local arm. As 10 MHz is in the frequency range pertinent to the model discussed in Chapter 7, emissivities will be quoted at this frequency, assuming a spectral index of 0.5.

The Measurements

Non-thermal spectra may be directly converted to volume emissivities $\eta(\nu)$ since

$$I(\nu) = \int \eta(\nu) dr \ ,$$

for frequencies where free-free absorption is insignificant. Average emissivities have been derived by several authors (e.g. Webber, 1968; Goldstein et al., 1970) by considering a uniform emissivity over 5 kpc in the anti-centre direction. Webber obtains

$$\eta(10) = 1 \times 10^{-40} \text{ watts m}^{-3} \text{ Hz}^{-1} \text{ ster}^{-1}$$

However, the distance of 5 kpc is very uncertain and the method takes no account of spiral arm features.

At a high frequency where absorption may be neglected, an estimate of the emissivity in the polar directions can be made, after allowing for the extra-galactic radiation, and assuming there is no radio halo. For the south galactic pole the observed

brightness temperature at 10 MHz is 2.8×10^5 K. Allowing for an extra-galactic contribution of 10^5 K (as obtained in Part I) and assuming a half-thickness for the disk of 450 pc one obtains

$$\eta(10) = 4 \times 10^{-40} \text{ watts m}^{-3} \text{ Hz}^{-1} \text{ ster}^{-1}$$

The comparison between this value and the previous one indicates that 5 kpc is an overestimate for the distance in the disk in the anti-centre direction.

The method used by Alexander et al. (1970) is not conclusive but a lower limit can be obtained. The method uses the fact that for a region of uniform emission and absorption with optical depth τ greater than approximately 2, the observed brightness at a frequency ν is

$$I(\nu) = \eta L/\tau$$

where η is the volume emissivity of the non-thermal radiation and L is the path length over which the emission occurs. Optical depths can be calculated from the shape of the background spectra and estimates of L must be made. A lower limit to the emissivity can be obtained by assuming that the radiation is generated over the half-thickness of the disk in the polar directions. Taking $\tau = 5$, $L = 400$ pc and $I(1 \text{ MHz}) = 5 \times 10^{-21}$ watts m^{-3} Hz^{-1} ster^{-1} gives

$$\eta(1) = 2 \times 10^{-39} \text{ watts m}^{-3} \text{ Hz}^{-1} \text{ ster}^{-1}$$

or assuming a straight spectrum with $\alpha = 0.5$

$$\eta(10) = 6.3 \times 10^{-40} \text{ watts m}^{-3} \text{ Hz}^{-1} \text{ ster}^{-1}$$

Emissivities can also be calculated from models of the Galaxy proposed to explain latitude and/or longitude intensity variations. The model proposed by Hamilton (1969) gives a disk emissivity of

$$\eta(10) = 5.7 \times 10^{-40} \text{ watts m}^{-3} \text{ Hz}^{-1} \text{ ster}^{-1}$$

for directions within 30° of the galactic centre assuming a uniform emissivity throughout the disk.

Probably the best method for determining the local emissivity is from observations of the non-thermal emission in front of HII regions. A direct conversion from foreground brightness to emissivity can be made if it can be assumed that all the background radiation is absorbed in the HII region and that the beam of the observing telescope is sufficiently small that it is filled by the HII region.

Calculations of this type have been made by Caswell (1976) and Bridle (1968) at 10 MHz, Andrew (1969) at 13 MHz and Jones (1973) at 30 MHz.

Shain (1959) performed the calculations for 19.7 MHz observations but he took into account the fraction of the beam filled by the HII region and assumed an optical depth and an electron temperature.

At higher frequencies more complicated analyses have been carried out by Roger (1969) and Parrish (1972) who used measurements at a number of frequencies and calculated the electron temperature of HII regions and the foreground emission.

In Figure 5.20 all the estimates are plotted, with points joined by dotted lines being measurements on the same object. Table 5.9 gives the details of the observations of HII regions used to obtain the emissivity estimates. Included are estimates based on the 13 MHz data used for the 10 MHz composite map. The crosses in Figure 5.20 are the emissivities derived by the other methods as discussed previously.

The scatter of points and the inconsistencies between measurements on the same object indicate that some of the assumptions made are incorrect. Certainly, the distances to some of the objects are

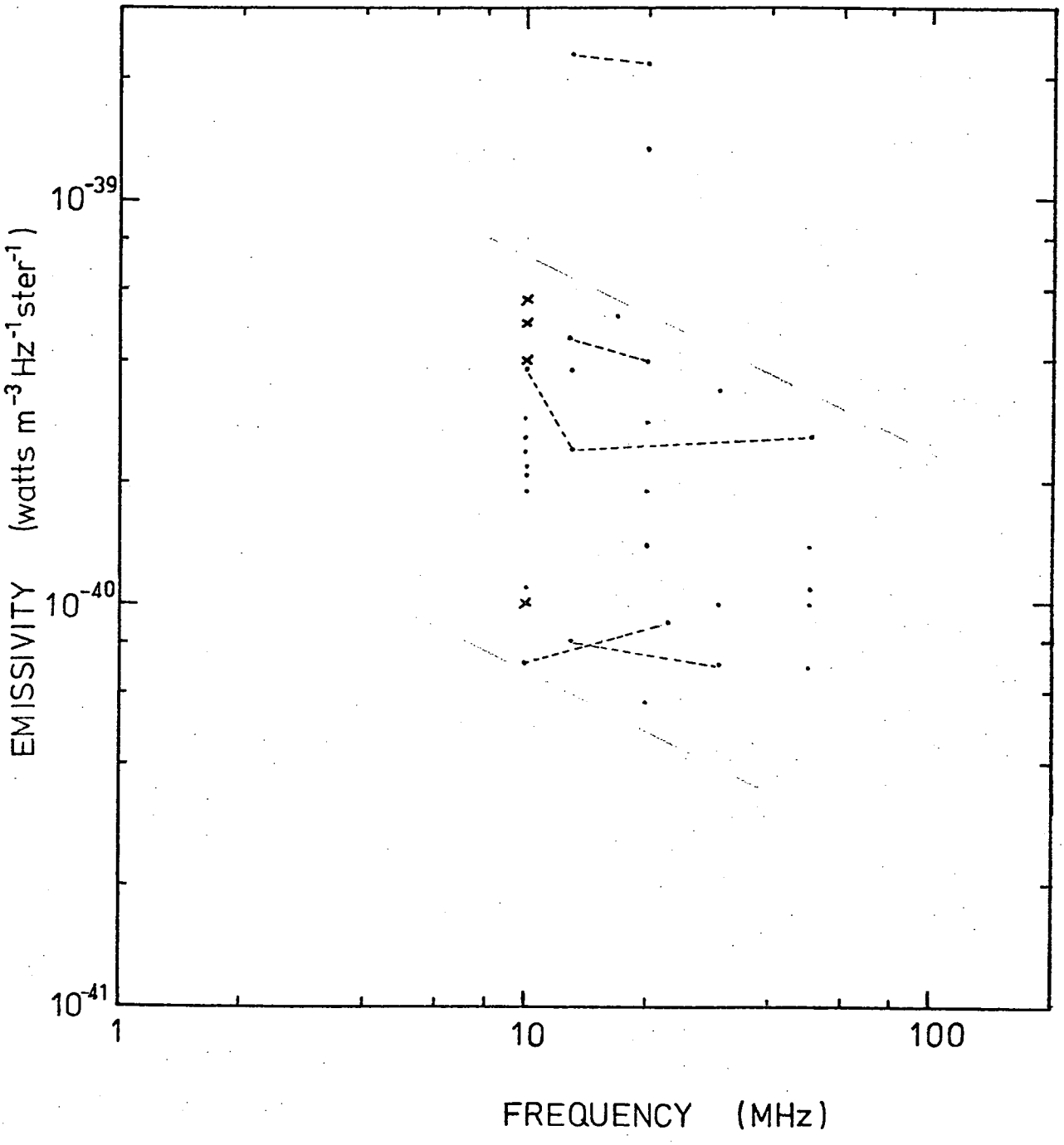
EMISSIVITY (watts m^{-3} Hz^{-1} ster^{-1})
10^{-39}
10^{-40}
10^{-41}
1
10
100
FREQUENCY (MHz)

FIGURE 5.20

TABLE 5.9

EMISSIVITY ESTIMATES

FREQUENCY (MHz)	GALACTIC CO-ORDINATES ℓ	b	OBJECT	DISTANCE (pc)	EMISSIVITY $\times 10^{40}$ (W $m^{-3}Hz^{-1}ster^{-1}$)	EMISSIVITY AT 22 MHz $\times 10^{40}$ (W $m^{-3}Hz^{-1}ster^{-1}$)	OBSERVER
10.0	118.0	5.0	NGC 7822	850	1.9	1.3	Caswell (1976)
	134.5	1.0	IC 1805	2200	0.7	0.5	
	149.5	-1.0	-	850	3.9	2.6	
	160.5	-12.5	NGC 1499	440	2.6	1.8	
	172.5	-1.5	IC 405+	650	2.9	2.0	
	189.0	4.0	-	1900	1.1	0.7	
	196.0	-12.0	λ Ori. neb.	500	2.4	1.6	
	203.0	2.5	NGC 2264	710	2.2	1.5	
	208.0	-20.0	Barnard Loop	500	2.1	1.4	
13.0	268	-12	Gum neb.	300	4.5	3.5	Cane
	287	-1	Carina neb.	2500	0.8	0.6	
	6	24	ζ Ophiuchi neb.	150	23	18	

TABLE 5.9 (continued)

FREQUENCY (MHz)	GALACTIC CO-ORDINATES ℓ	b		DISTANCE (pc)	EMISSIVITY × 10^{40} (W $m^{-3}Hz^{-1}ster^{-1}$)	EMISSIVITY AT 22 MHz × 10^{40} (W $m^{-3}Hz^{-1}ster^{-1}$)	OBSERVER
13.1	160.5	-12.5	NGC 1499	440	2.4	1.9	Andrew (1969)
	172.5	1.2	IC 405+	650	3.8	1.2	
19.7	355.4	0.2	RCW 132	1400	1.4	1.3	Shain (1958)
	341.0	-0.8	RCW 110	1250	1.9	1.8	
	6.0	23.0	ζ Ophiuchi neb.	150	22	21	
	262.0	-8.0	Gum neb.	200	4.0	3.8	
	351.9	12.7	τ Scorphii neb.	200	13.4	12.7	
	6.6	-1.5	RCW 146	1300	2.8	2.7	
	17.0	0.8	RCW 165	2300	0.57	0.54	
22.0	134.5	1.0	IC 1805	2200	0.9	0.9	Roger (1969)
29.9	287	-0.6	Carina neb.	2500	0.82	0.96	Jones (1973)
	287	-1.5					
	337	0	RCW 108	1300	3.4	4.0	Jones and Finaly (1974)

TABLE 5.9 (continued)

FREQUENCY (MHz)	GALACTIC CO-ORDINATES ℓ	b	OBJECT	DISTANCE (pc)	EMISSIVITY × 10^{40} (W $m^{-3}Hz^{-1}ster^{-1}$)	EMISSIVITY AT 22 MHz × 10^{40} (W $m^{-3}Hz^{-1}ster^{-1}$)	OBSERVER
50.0	49		W 51	6100	1.4	2.1	Parrish (1972)
	59		NGC 6820	2000	1.0	1.5	
	158	-12	NGC 1499 ✓	440	2.6	3.9	
	175		IC 410 ✓	2000	0		
	190		NGC 2175	2000	0.7	1.1	
	200		NGC 2244	1500	1.1	1.7	

not accurately known. For example, the distance to IC 405+ is given as 1600 ± 600 pc by Andrew, whereas Caswell quotes 650 pc. Shain takes a distance of 600 pc to RCW 132 whereas Georgelin and Georgelin (1970) give a distance of 1400 pc.

Nevertheless, it is worthwhile to investigate these results further as it is likely that the scatter is partially due to real variations in emissivity. From Figure 5.20 it can be seen that a reasonable value for the spectral index is 0.5 and this value is consistent with the conclusions of the previous section over most of the frequency range discussed here. Using this value all the estimates from observations of HII regions have been scaled to the same frequency so that comparisons can be made with respect to galactic longitude and distance. To avoid extrapolating any result over a large frequency range, the results are scaled to a frequency in the centre of the range covered, namely 22 MHz. The calculated emissivities are given in Table 5.9.

Figure 5.21 shows an average emissivity along the line of sight to each HII region. The line for each object is plotted against its galactic longitude and the length of the line is proportional to the distance to the HII region.

The approximate locations of the Orion and Sagittarius arms as defined by HII regions (see Figure 4.1) are sketched in. Figure 5.22 illustrates the emissivity against distance to the object. This latter diagram shows that higher emissivities are obtained from observations of close objects. If the synchrotron emissivity is less in the interarm regions than in the arms, as is predicted (Mills, 1951), then it is expected that the emissivity should fall off with distance for lines of sight passing out of

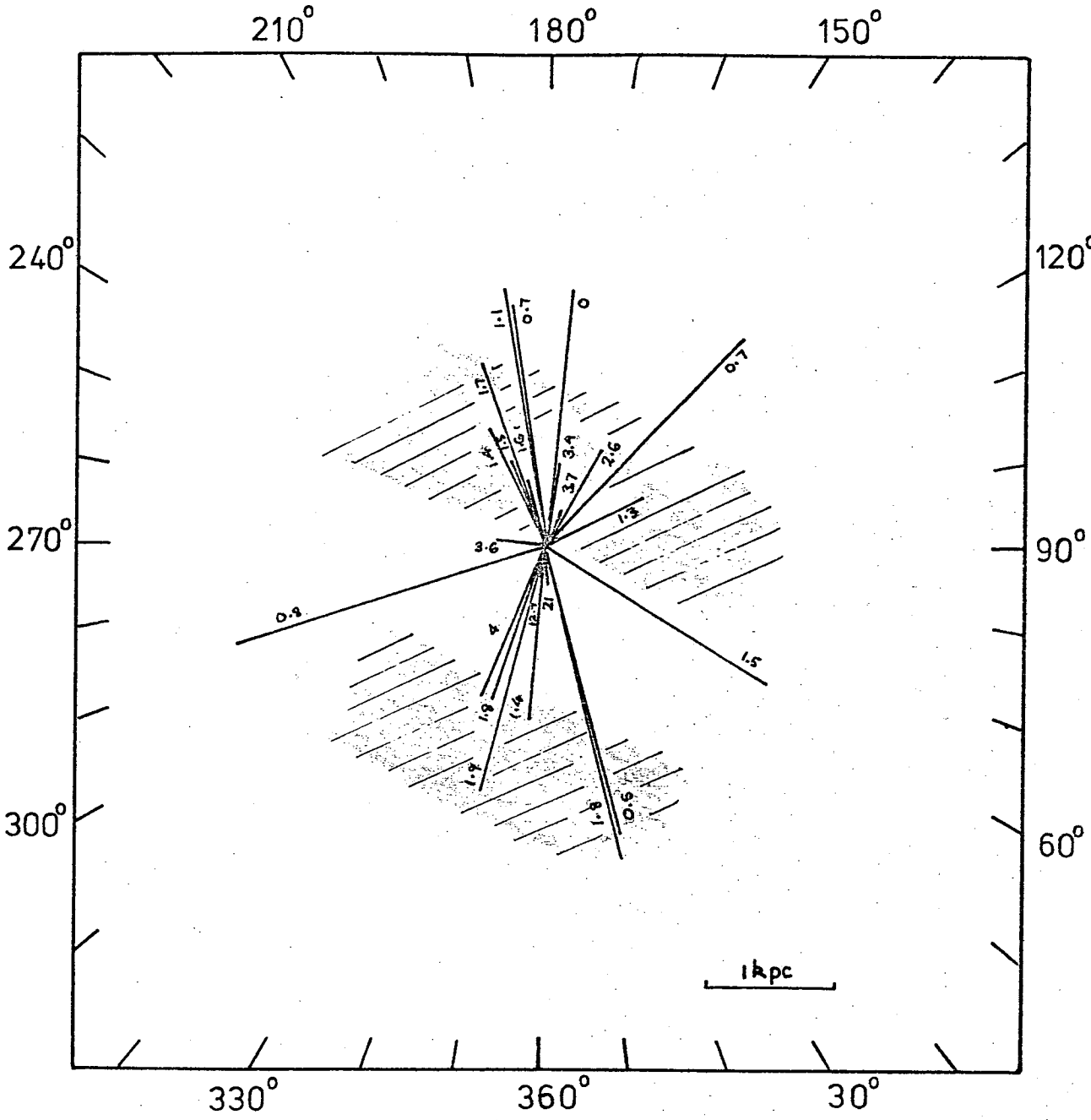
210°
180°
150°
240°
120°
270°
90°
300°
60°
330°
360°
30°
1.1
0.7
0
0.7
1.7
1.9
1.4
3.4
3.7
2.6
1.3
3.6
0.3
4
12
1.5
1.9
1.4
1.4
0.5
1.8
1kpc

FIGURE 5.21

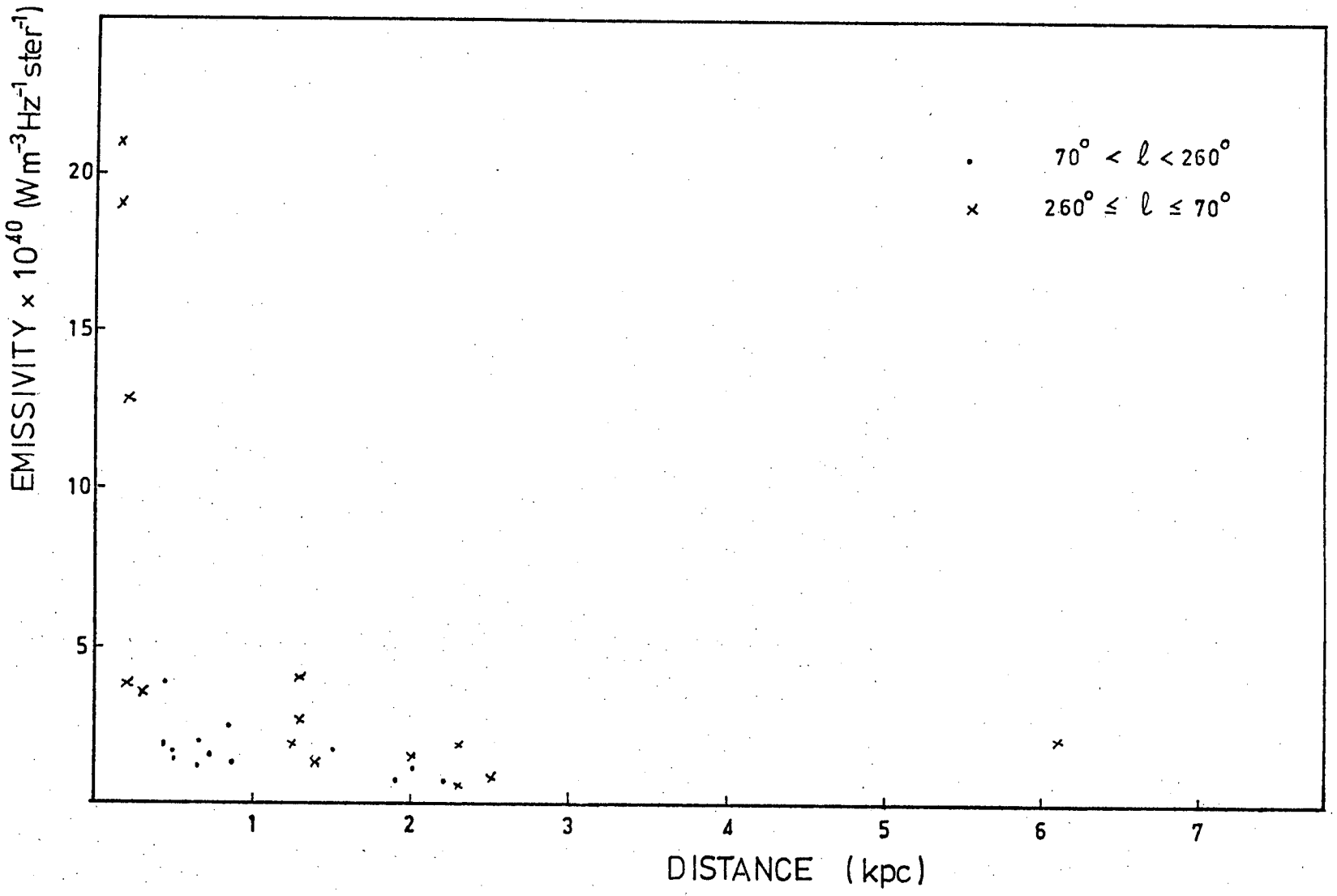
EMISSIVITY × 10^40 (W m^-3 Hz^-1 ster^-1)
20
15
10
5
1
2
3
4
5
6
7
DISTANCE (kpc)
70° < ℓ < 260°
260° ≤ ℓ ≤ 70°

FIGURE 5.22

the local arm. The distance at which the emissivity begins to decrease would not be the same for all longitudes. This feature is not apparent from Figure 5.22 but nevertheless the emissivity does fall off with distance. It would appear that on the average higher emissivities are obtained from objects in the longitude range $260^{\circ} \leq \ell \leq 70^{\circ}$. One could interpret this as an indication that the Sun is displaced towards the outer edge of the local arm. That is for path lengths of about 1 kpc at all longitudes, lines of sight in the range $260^{\circ} \leq \ell \leq 70^{\circ}$ pass through more arm region than do lines of sight for other longitudes. It is tempting to interpret the high values in the longitude range 150° - 170° as being due to the presence of Loop III. Similarly, the high value towards the Gum Nebula could be due to Loop I.

However, with the large variation in values it is over ambitious to derive too much from the data. We conclude that the average local emissivity is in the range

$$4.5\text{-}2.5 \times 10^{-40} \text{watts m}^{-3} \text{ Hz}^{-1} \text{ ster}^{-1}$$

at 22 MHz with the upper and lower levels being obtained in the centre and anti-centre directions respectively. The corresponding range at 10 MHz is

$$6.7\text{-}3.7 \times 10^{-40} \text{ watts m}^{-3} \text{ Hz}^{-1} \text{ ster}^{-1}$$

Nevertheless, we consider that the very high values towards the ζ Ophiuchi nebula and towards the nebula around τ Scorpii are probably real and these need to be explained. Shain (1959) suggested that they could be due to a source of emission close to the Sun, but it would need to be more extensive than he suggested. He appears to have made a numerical error when calculating the emissivity towards τ Scorpii and the value is much higher than he obtained. The new 19.7 MHz value is similar to the value obtained from the 10 MHz

composite map.

Emissivities From the Cosmic Ray Electron Spectrum

It was shown in Chapter 2 that the emissivity of synchrotron radiation

$$\eta(\nu) \propto B_{\perp}^{(\gamma+1)/2} \times n_o$$

where n_o is the co-efficient of the cosmic ray electron spectrum which has a spectral index γ. Thus synchrotron emissivities can be used to calculate electron spectra. The calculated spectra have been compared with the electron spectra deduced from observations at Earth and deductions made as to the magnitude of the local magnetic field and the modulation of electrons in the solar environment. Free-free absorption effects have also been examined by calculating the intrinsic low frequency spectrum from low energy electron data taking into account solar modulation. These investigations assumed that the electron flux observed at Earth is the same as that in near interstellar space. It is now apparent that this is not so for energies $\lesssim$ 3 Gev.

In Figure 5.23 we show the recent measurements of the total electron ($e^+ + e^-$) spectrum. Down to about 3 Gev this spectrum can be represented by a differential spectrum

$$\frac{dj}{dE} = 150\ E^{-3\cdot0}\ \text{el. m}^{-2}\ \text{ster}^{-1}\ \text{sec}^{-1}\ \text{Gev}^{-1}$$

Below $\sim$ 3 Gev the electron spectrum flattens and this is partially due to solar modulation effects. The lower curve shows the flux measured in 1969 during sunspot maximum whereas the highest intensities were observed during the sunspot minimum of 1965-66.

Also shown in Figure 5.23 is the measured $\frac{e^+}{e^+ + e^-}$ ratio. Webber (1976) shows that the application of a relationship between

this ratio and the $\frac{e^+}{e^+ + e^-}$ fraction of secondary radiation (determined by nuclear physics) gives the total interstellar flux as being about twice the secondary spectrum. This latter spectrum can be calculated for a given matter traversal. In Figure 5.23 the secondary spectrum for 5 g cm^{-2} of matter traversal is shown together with an estimation of the total interstellar electron flux. It can be seen that the calculated total electron flux exceeds the flux observed at Earth.

It now remains to calculate the synchrotron emissivities predicted by these electron fluxes. The calculation involves the application of equation (2.3) where n_o the co-efficient of the electron spectrum and γ its spectral index must be assigned values. In addition, the energy of the electrons which contribute most at any particular frequency must be determined.

For the spectrum of a single electron the frequency of maximum intensity is

$$\nu_m = 0.29\ \nu_c$$

where ν_c, the critical frequency is given in equation (2.1). This correspondence will also hold for a flat electron spectrum but not for the observed steep electron spectrum.

Using an electron spectrum with

$$\gamma = 2.5 \qquad E \geq 2 \text{ Gev}$$

$$\text{and } \gamma = 1.8 \qquad E < 2 \text{ Gev}$$

Cummings (1973) found that the frequency of maximum intensity was roughly half that predicted from the single electron spectrum. From Cumming's graph of frequency vs. energy it is found that for a 5 μG field, electrons of energy 0.32 Gev make the maximum contribution to the synchrotron intensity at 10 MHz. At this energy the observed electron flux j_e is approximately 100 el. m^{-2} $ster^{-1}$ sec^{-1} Gev^{-1} and the flux calculated from the observed $\frac{e^+}{e^+ + e^-}$

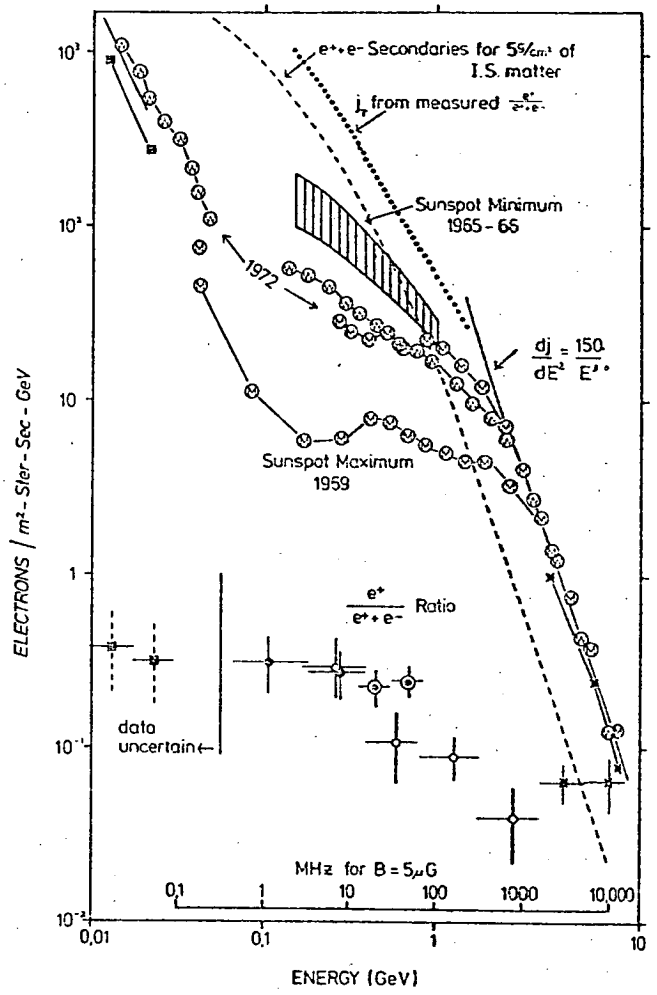

Recent measurements of the total electron intensity and the electron-positron ratio (lower). The curve labelled $e^+ + e^-$ secondaries for 5 g cm^{-2} of IS matter is from Ramaty (1974).

FIGURE 5.23

after Webber (1976)

ratio and secondary calculations is $\sim$ 400 el. m^{-2} $ster^{-1}$ sec^{-1} Gev^{-1}. Now

$$n_o = \frac{4\pi}{c} j_e E^{\gamma}$$

and taking $\gamma = 1.8$ we obtain

$$n_o = 3.12 \times 10^{-14} \text{ m}^{-2} \text{ joules}$$

using the observed electron flux.

With these values in equation (2.3) and assuming a field of 5 μG we obtain for the emissivity at 10 MHz

$$\eta(10) = 3.88 \times 10^{-41} \text{ watts m}^{-3} \text{ Hz}^{-1} \text{ ster}^{-1}$$

This value is approximately a factor of 10 below the lower limit determined from radio observations. The discrepancy is reduced to a factor of $\sim$ 2.5 if we use the calculated electron flux.

This discrepancy could be resolved if we assume a magnetic field of 10 μG but this value is significantly above the accepted value of 2 μG. Webber (1976) discusses the problem of relating the observed and predicted emissivities and although he suggests several possible causes for the discrepancy none can account for such a large difference. Although other workers (e.g. Goldstein et al. 1970) have attributed the difference to solar modulation effects, and in fact use the data to determine the magnitude of the solar modulation, Webber points out that such calculations have been based on data that was not normalized properly at high frequencies where the modulation would be expected to be small. He concludes that the electron flux must vary significantly on the scale of a spiral arm.

REFERENCES FOR CHAPTER 5

ADGIE,R. and SMITH,F.G., 1956 Observatory 76 181.

ALEXANDER,J.K. and STONE,R.G., 1965 Astrophys. J. 142 1327.

ALEXANDER,J.K., BROWN,L.W., CLARK,T.A., STONE,R.G. and WEBER,R.R., 1969a Astrophys. J. Letters 157 L163.

ALEXANDER,J.K., BROWN,L.W., CLARK,T.A., STONE,R.G. and WEBER,R.R., 1969b Presented at the American Astr. Soc. meeting held in New York, Dec. 8-11.

ALEXANDER,J.K., BROWN,L.W., CLARK,T.A., STONE,R.G., 1970 Astron. Astrophys. 6 476.

ANDREW,B.H., 1966 Mon. Not. R. astr. Soc. 133 463.

ANDREW,B.H., 1969 Mon. Not. R. astr. Soc. 143 17.

BALDWIN,J.E., 1955 Mon. Not. R. astr. Soc. 115 690.

BALDWIN,J.E., 1963 Observatory 83 153.

BALDWIN,J.E., 1967 IAU Symposium 31 337.

BENEDIKTOV,E.A., GETMANSEV,G.G., MITJAKOV,N.A., RAPOPORT,V.O., SAZONOV,J.A. and TARASOV,A.F., 1965 Space Research VI 110.

BIERMANN,L. and DAVIS,L., 1958 Astrophys. 51 19.

BINGHAM,R.G., 1967 Mon. Not. R. astr. Soc. 137 157.

BLYTHE,J.H., 1957 Mon. Not. R. astr. Soc. 117 652.

BRIDLE,A.H., 1967 Mon. Not. R. astr. Soc. 136 219.

BRIDLE,A.H., 1968 Mon. Not. R. astr. Soc. 138 251.

BROWN,L.W., 1973 Astrophys. J. 180 359.

BURKE,B.F., 1967 IAU Symposium 31 361.

CANE,H.V., 1975 Proc. Astron. Soc. Aust. 2 (6) 330.

CASWELL,J., 1976 Mon. Not. R. astr. Soc. 176 601.

COSTAIN,C.H., 1960 Mon. Not. R. astr. Soc. 120 248.

COSTAIN,C., 1976 Presented at the Canadian Astr. Soc. meeting.

COTTONY,H.V. and JOHLER,J.R., 1952 Proc. Instn. Radio Engrs. 40 1053.

CUMMINGS,A.C., 1973 Ph.D. Thesis (California Institute of Technology).

DAVIES,R.D. and HAZARD,C., 1962 Mon. Not. R. astr. Soc. 124 147.

ELLIS,G.R.A., 1957 J. Geophys. Res. 62 229.

ELLIS,G.R.A., 1965 Mon. Not. R. astr. Soc. 130 429.

ELLIS,G.R.A. and HAMILTON,P.A., 1966 Astrophys. J. 143 227.

GEORGELIN,Y.M. and GEORGELIN,Y.P., 1976 Astron. Astrophys. 49 57.

GETMANSEV,G.G., KARAVANOV,V.S., KOROBKOV,Yu.S. and TARASOV,A.F., 1969 Sov. Astr. - A.J. 12 5.

GINZBURG,V.L., 1970 Comments. Astrophys. Space Sci. 2 43.

GOLDSTEIN,M.L., RAMATY,R. and FISK,L.A., 1970 Phys. Rev. Letts. 24 1193.

HAMILTON,P.A., 1969 Ph.D. Thesis (University of Tasmania).

HAMILTON,P.A. and HAYNES,R.F., 1968 Aust. J. Phys. 21 895.

HAMILTON,P.A. and HAYNES,R.F., 1969 Aust. J. Phys. 22 839.

HARTZ,T.R., 1964 Ann. d'Astrophys. 27 823.

HASLAM,C.G.T., LARGE,M.I. and QUIGLEY,M.J.S., 1964 Mon. Not. R. astr. Soc. 127 273.

HASLAM,C.G.T., QUIGLEY,M.J.S. and SALTER,C.J.1970 Mon. Not. R. astr. Soc. 147 405.

HASLAM,C.G.T., KAHN,F.D. and MEABURN,J., 1971 Astron. Astrophys. 12 388.

HIGGINS,C.S. and SHAIN,C.A., 1954 Aust. J. Phys. 7 460.

HILL,E.R., 1968 Aust. J. Phys. 21 735.

HILL,E.R., SLEE,O.B. and MILLS,B.Y., 1958 Aust. J. Phys. 11 530.

HUGILL,J. and SMITH,F.G., 1965 Mon. Not. R. astr. Soc. 131 137.

JONES,B.B., 1973 Aust. J. Phys. 26 545.

JONES,B.B. and FINLAY,A.E., 1974 Aust. J. Phys. 27 687.

KENDERDINE,S., 1963 Mon. Not. R. astr. Soc. 126 41.

KOMESAROFF,M.M., 1961 Aust. J. Phys. 14 515.

KOMESAROFF,M.M., 1966 Aust. J. Phys. 19 75.

LANDECKER,T.L. and WIELEBINSKI,R., 1970 Aust. J. Phys. Astrophys. Suppl. 16 1.

LARGE,M.I., MATHEWSON,D.S. and HASLAM,C.G.T., 1961 Mon. Not. R. astr. Soc. 123 113.

LARGE M.I., QUIGLEY,M.J.S. and HASLAM,C.G.T., 1966 Mon. Not. R. astr. Soc. 131 335.

MANCHESTER,R.N., 1975 Astrophys. J. 188 637.

MATHEWSON,D.S., BROTIN,N.W. and COLE,D.J., 1965 Aust. J. Phys. 18 665.

MILLS,B.Y., 1959 IAU Symposium 9 431.

MILLS,B.Y., 1971 (Invited Paper) Proc. 12th Int. Cosmic Ray Conf. (Hobart)

MILOGRADOV-TURIN,F. and SMITH,F.G., 1973 Mon. Not. R. astr. Soc. 161 269.

NOVACO,J.C., 1976 Private Communication.

PAPAGIANNIS,M.D., 1964 Ph.D. Thesis (Harvard)

PARTHASARATHY,R. and LERFALD,G.M., 1965 Mon. Not. R. astr. Soc. 129 395.

PARTHASARATHY,R. 1968 Proc. Astron. Soc. Aust. 3 (1) 94.

PARRISH,A., 1972 Astrophys. J. 174 33.

PAULINY-TOTH,I.I.K. and SHAKESHAFT,J.R., 1962 Mon. Not. R. astr. Soc. 124 61.

PRICE,R.M., 1974 Astron. Astrophys. 33 33.

PURTON,C.R., 1966 Mon. Not. R. astr. Soc. 133 463.

REBER,G., 1968 J. Franklin Inst. 285 1.

REBER,G. and ELLIS,G.R.A., 1956 J. Geophys. Res. 61 1.

ROGER,R.S., 1969 Astrophys. J. 155 831.

SHAIN,C.A. and HIGGINS,C.S., 1954 Aust. J. Phys. 7 130.

SHAIN,C.A., 1959 IAU Symposium 9 451.

SHAIN,C.A., KOMESAROFF,M.M. and HIGGINS,C.S., 1961 Aust. J. Phys. 14 508.

SHKLOVSKII,I.S., 1952 Astron. Zh. 29 418.

SIRONI,G., 1974 Mon. Not. R. astr. Soc. 166 345.

STEPHENS,S.A. 1971 Astron. Astrophys 11 311.

TURTLE,A.J. and BALDWIN,J.E. 1962 Mon. Not. R.astr. Soc. 124 459.

TURTLE,A.J., PUGH,J.E., KENDERDINE,S. and PAULINY-TOTH,I.I.K. 1962 Mon. Not. R. astr. Soc. 124 297.

WEBBER,W.R. 1968 Aust. J. Phys. 21 845.

WEBBER,W.R. 1976 Proc. Astron. Soc. Aust. 3(1) 1.

WEBER,R.R. 1972 Astron. J. 77 707.

WESTERHOUT,G. 1958 Bull. astr. Inst. Neth. 14 215.

WIELEBINSKI,R., SMITH,D.H. and GARZON-CARDENAS,S. 1968 Aust. J.Phys. 21 185.

WEILEBINSKI,R. and PETERSON,C.E. 1968 Observatory 88 219.

WILLIAMS,P.J.S., KENDERDINE,S. and BALDWIN,J.E. 1966 Mem. R. astr. Soc. 70 53.

YATES,K.W. and WEILEBINSKI,R. 1966 Aust. J. Phys. 19 389.

YATES,K.W., WIELEBINSKI,R. and LANDECKER,T.L. 1967 Aust. J. Phys. 20 595.

YATES,K.W. 1968 Aust. J. Phys. 21 167.

CHAPTER 6

THE RESULTS

Introduction

In this chapter we present the data, both in the form of declination scans and maps. In addition, seven earlier southern continuum surveys are shown and these are combined with the new data to obtain galactic radio spectra in various directions. These spectra have been used to develop the model discussed in Chapter 7.

A preliminary report on the surveys has been given by Cane (1975) and some of the spectra have been presented by Cane (1976). The maps have been reported by Cane and Whitham (1977). In Table 6.1 we list the five frequencies at which observations were made.

Data Preparation

For all frequencies except 13 MHz the data were not sufficiently free from interference to permit computer analysis. The data were analysed manually as discussed in Appendix II. The set of records so obtained was digitized manually and transferred to paper tape. The sampling interval was chosen to comply with the Fourier Sampling Theorem. The sampling interval used for each frequency is shown in Table 6.1.

Some of the 13 MHz data were almost free from interference so that for declinations south of Dec. - 35° the final set of scans was obtained from a computerized average of suitable records and the data were transferred to magnetic tape.

Because of the large amount of data analysis involved in preparing southern surveys at five frequencies it was decided that only the five hours of right ascension near the galactic plane (viz. 1500^h to 2000^h) would be assembled into maps. The final maps were contained within the region $310° \leq \ell \leq 40°$ and $-27° \leq b \leq + 25°$.

TABLE 6.1

DETAILS OF MAPS

FREQUENCY (MHz)	SAMPLING INTERVAL (degrees)	CONTOUR UNIT (K)
3.7	3	5×10^5
5.6	3	7.9×10^5
5.6	2	7.4×10^5
8.3	2	5×10^5
13.0	1	7.9×10^4
16.5	1	7.3×10^4

Scans

In the first instance, scans were normalized by taking the region of low brightness near R.A. 0100^h for each declination to have the temperature of the south galactic pole as determined by low resolution observations.

Preliminary maps were plotted and then the normalization factors were adjusted to remove any discontinuities between neighbouring declination scans. When the final maps were obtained computer plots of the scans were drawn with their respective normalization factors taken into account. Due to the amount of space they would otherwise occupy the scans had to be overlapped. The scans are shown in figures 6.1 to 6.6 in ascending order of observation frequency. Zero levels for each scan are marked.

Maps

The maps are presented in figures 6.7- 6.12. Some further smoothing was performed when the maps were prepared from the computer plots. Figures 6.13 - 6.15 are the low frequency surveys at 2.1, 4.7 and 10 MHz made in Tasmania during the previous solar minimum. They have been prepared in the same form as the new maps to enable direct comparisons to be made. The original 4.7 MHz data presented by Ellis and Hamilton (1966) has been replotted. The 10 MHz map is in its original form to illustrate how it differs from the other maps, thus justifying the alterations made to it when preparing the composite map. The 10 MHz spectral points have been obtained from the new map.

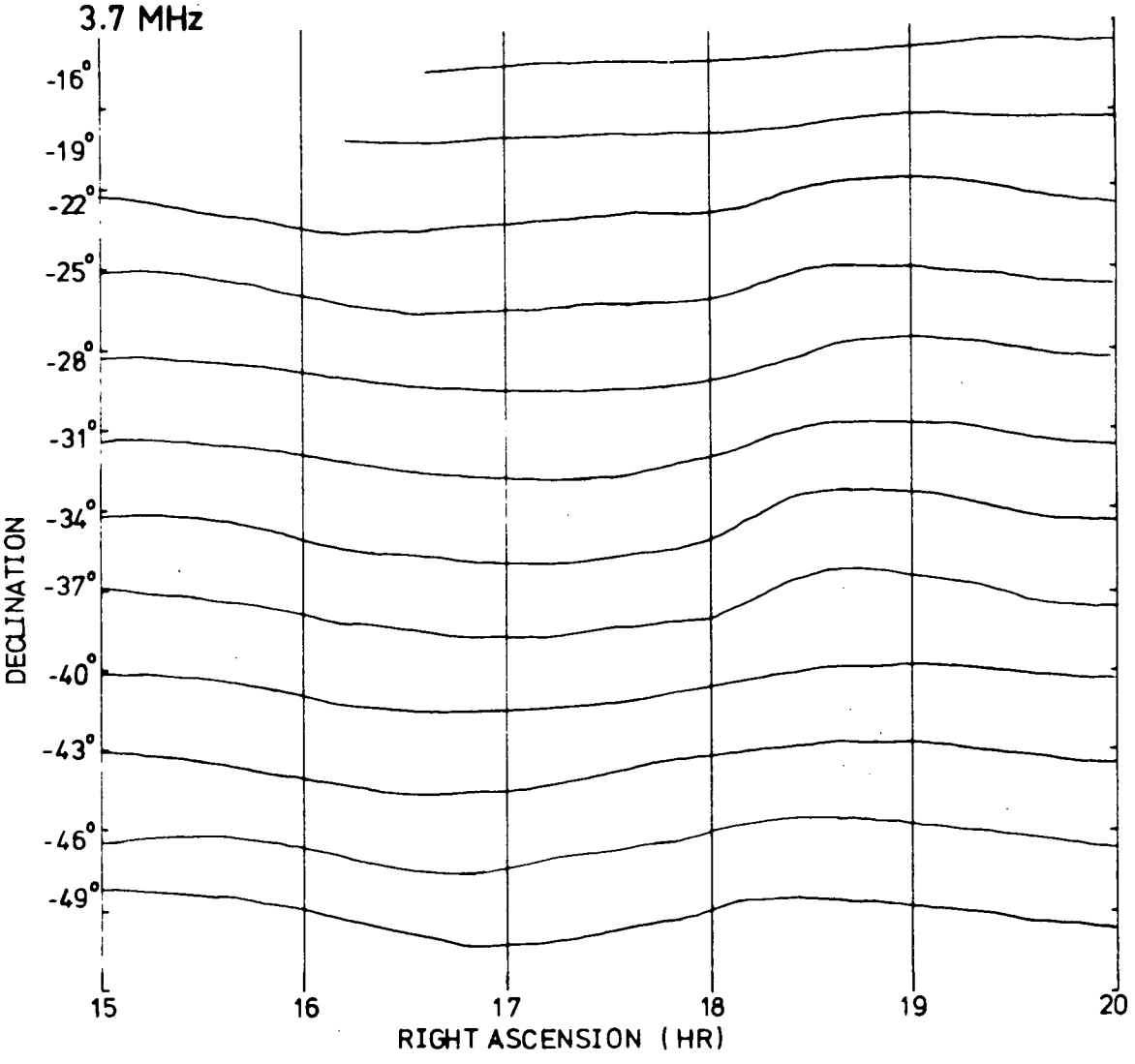
3.7 MHz
-16°
-19°
-22°
-25°
-28°
-31°
-34°
-37°
-40°
-43°
-46°
-49°
DECLINATION
15
16
17
18
19
20
RIGHT ASCENSION (HR)

FIGURE 6.1

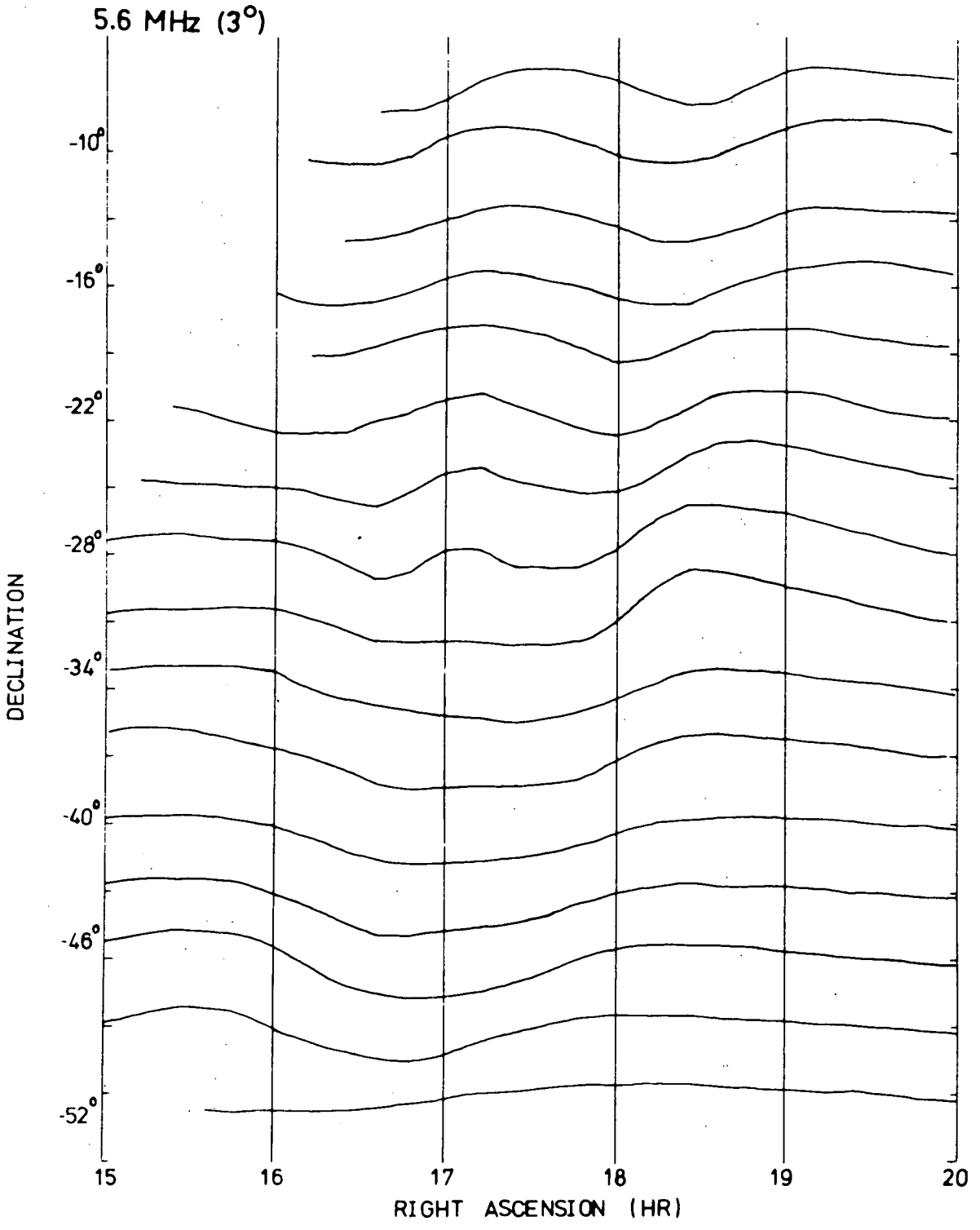
5.6 MHz (3°)
-10°
-16°
-22°
-28°
-34°
-40°
-46°
-52°
DECLINATION
15
16
17
18
19
20
RIGHT ASCENSION (HR)

FIGURE 6.2

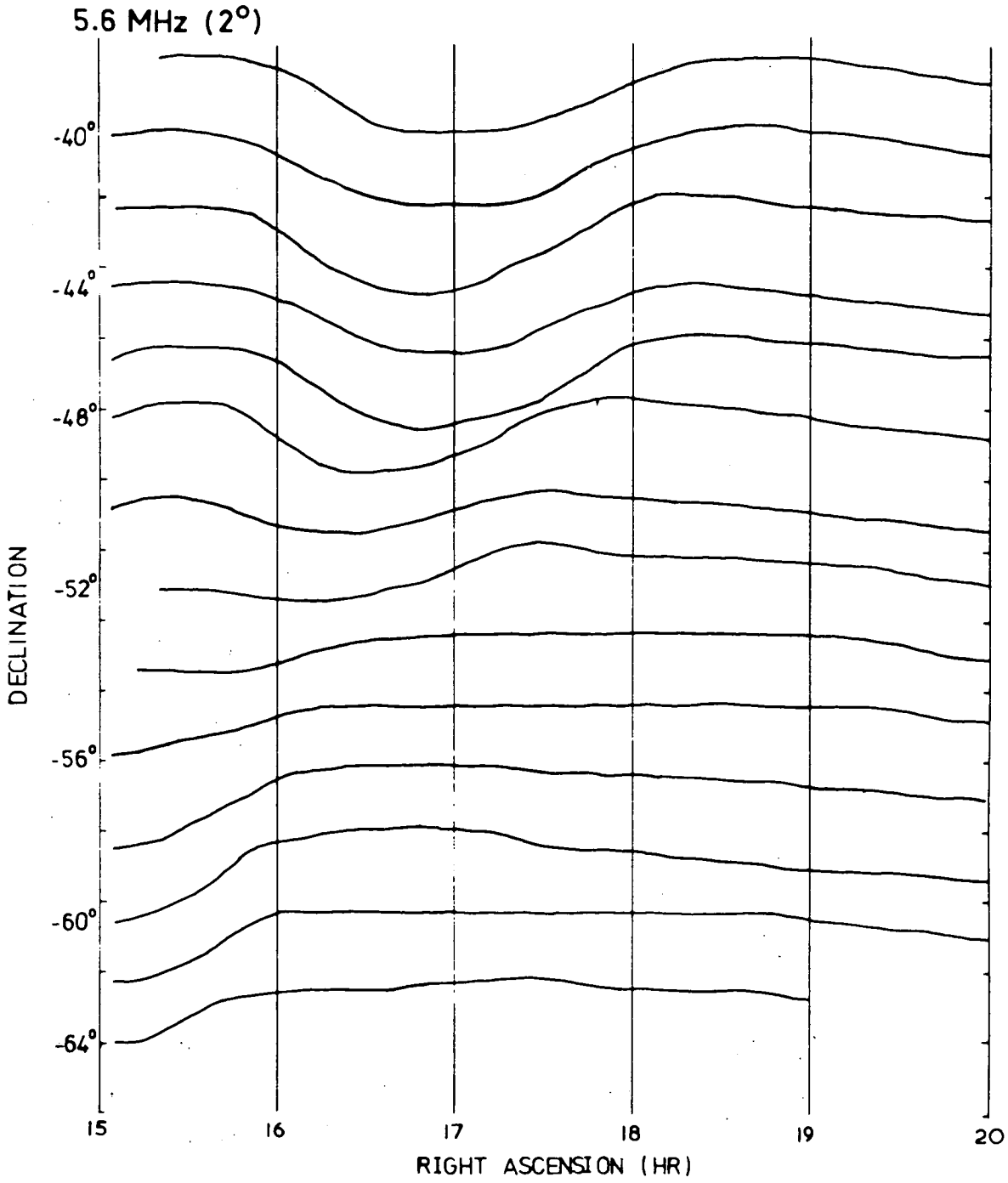
5.6 MHz (2°)
-40°
-44°
-48°
-52°
-56°
-60°
-64°
DECLINATION
15
16
17
18
19
20
RIGHT ASCENSION (HR)

FIGURE 6.3.1

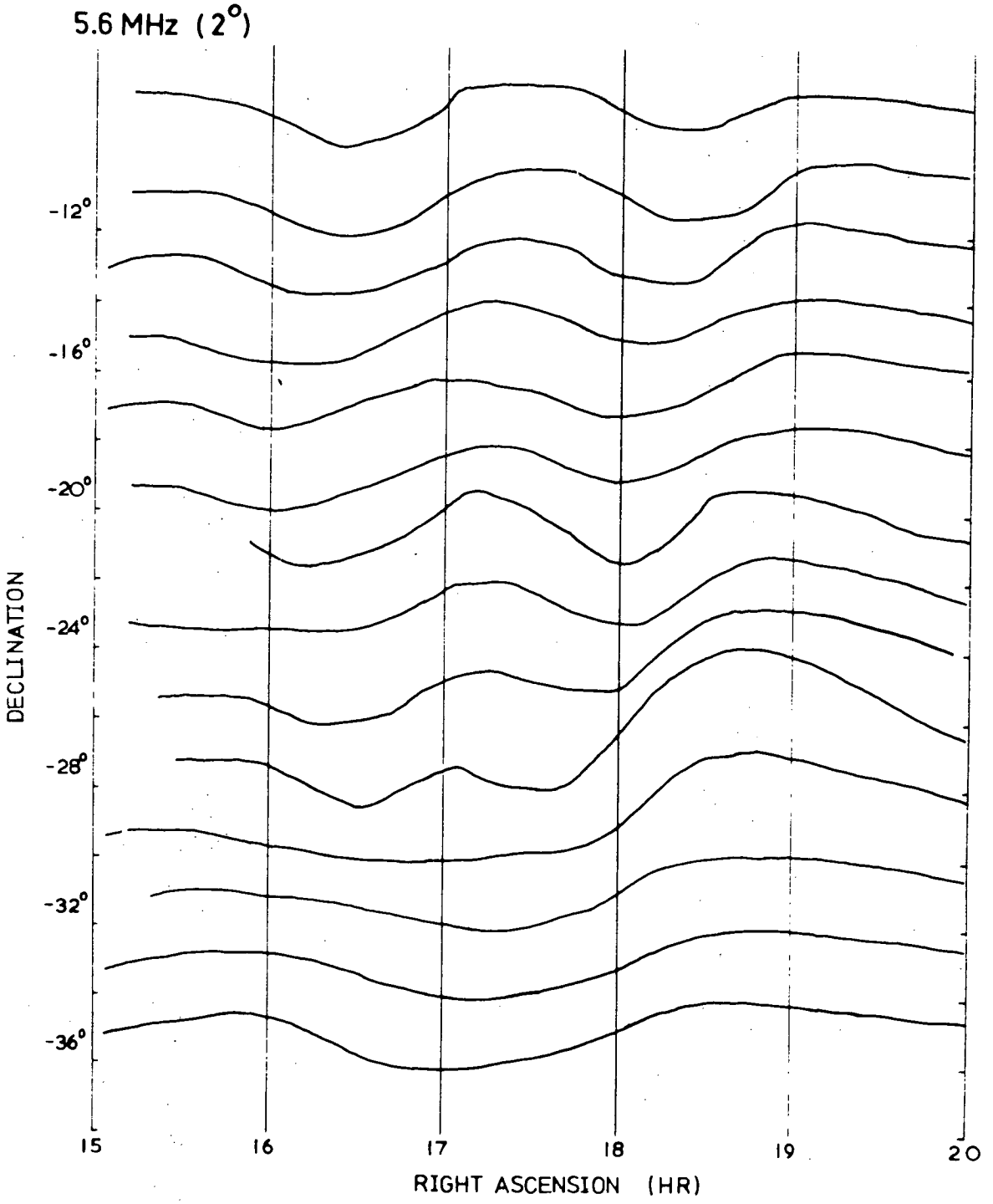
5.6 MHz (2°)
-12°
-16°
-20°
-24°
-28°
-32°
-36°
DECLINATION
15
16
17
18
19
20
RIGHT ASCENSION (HR)

FIGURE 6.3.2

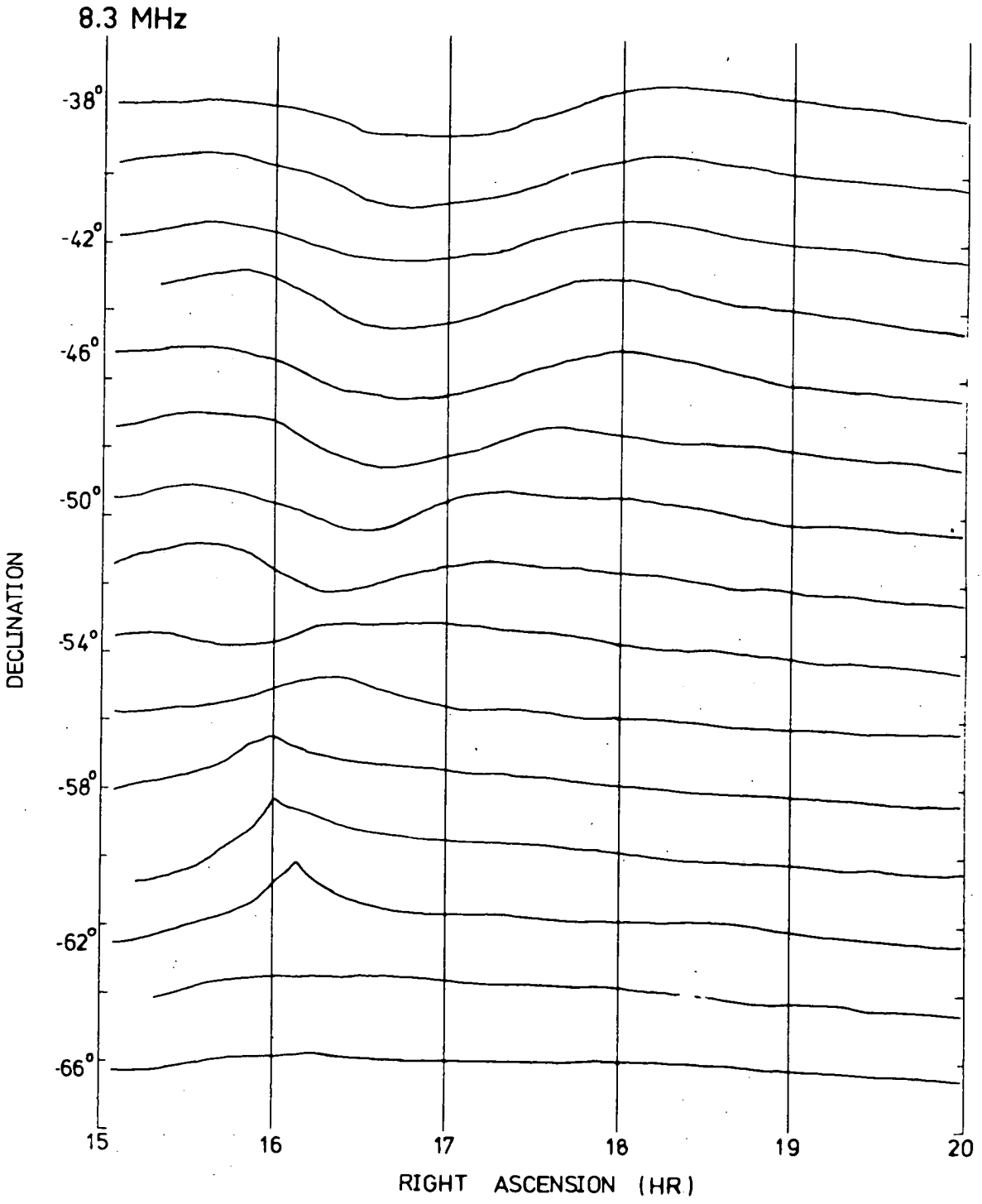
8.3 MHz
-38°
-42°
-46°
-50°
-54°
-58°
-62°
-66°
DECLINATION
15
16
17
18
19
20
RIGHT ASCENSION (HR)

FIGURE 6.4.1

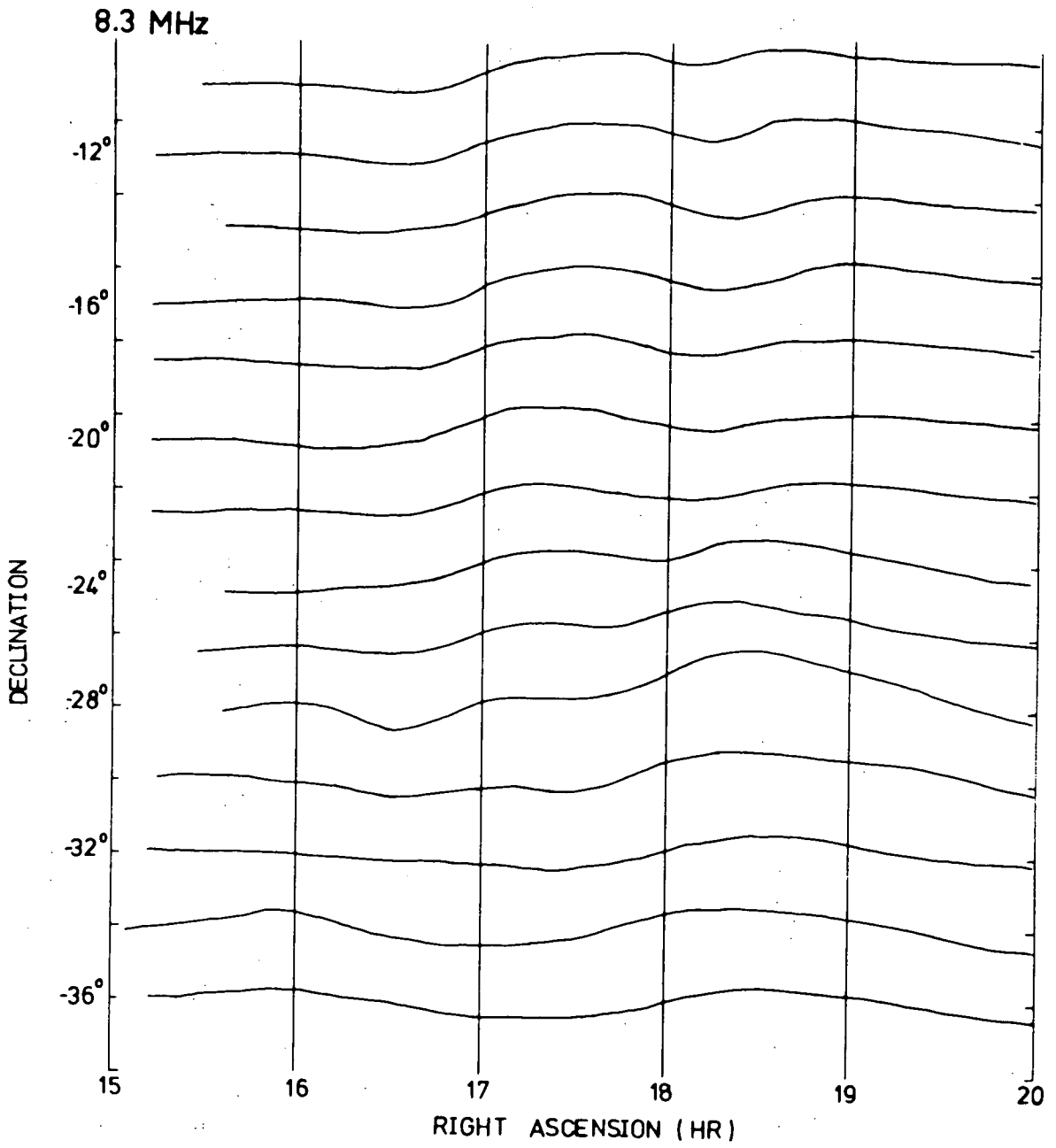
8.3 MHz
-12°
-16°
-20°
-24°
-28°
-32°
-36°
DECLINATION
15
16
17
18
19
20
RIGHT ASCENSION (HR)

FIGURE 6.4.2

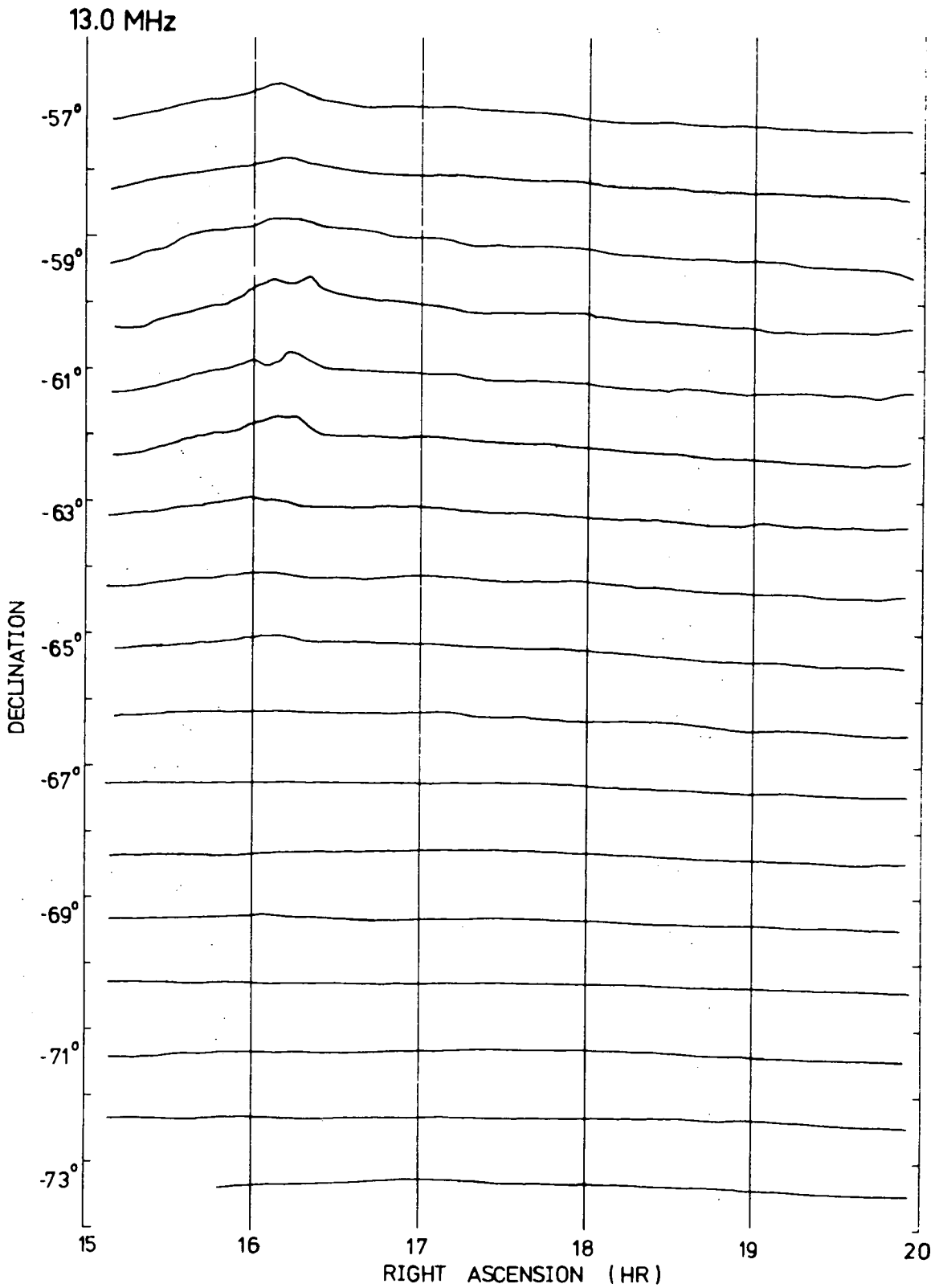
13.0 MHz
-57°
-59°
-61°
-63°
-65°
-67°
-69°
-71°
-73°
DECLINATION
15
16
17
18
19
20
RIGHT ASCENSION (HR)

FIGURE 6.5.1

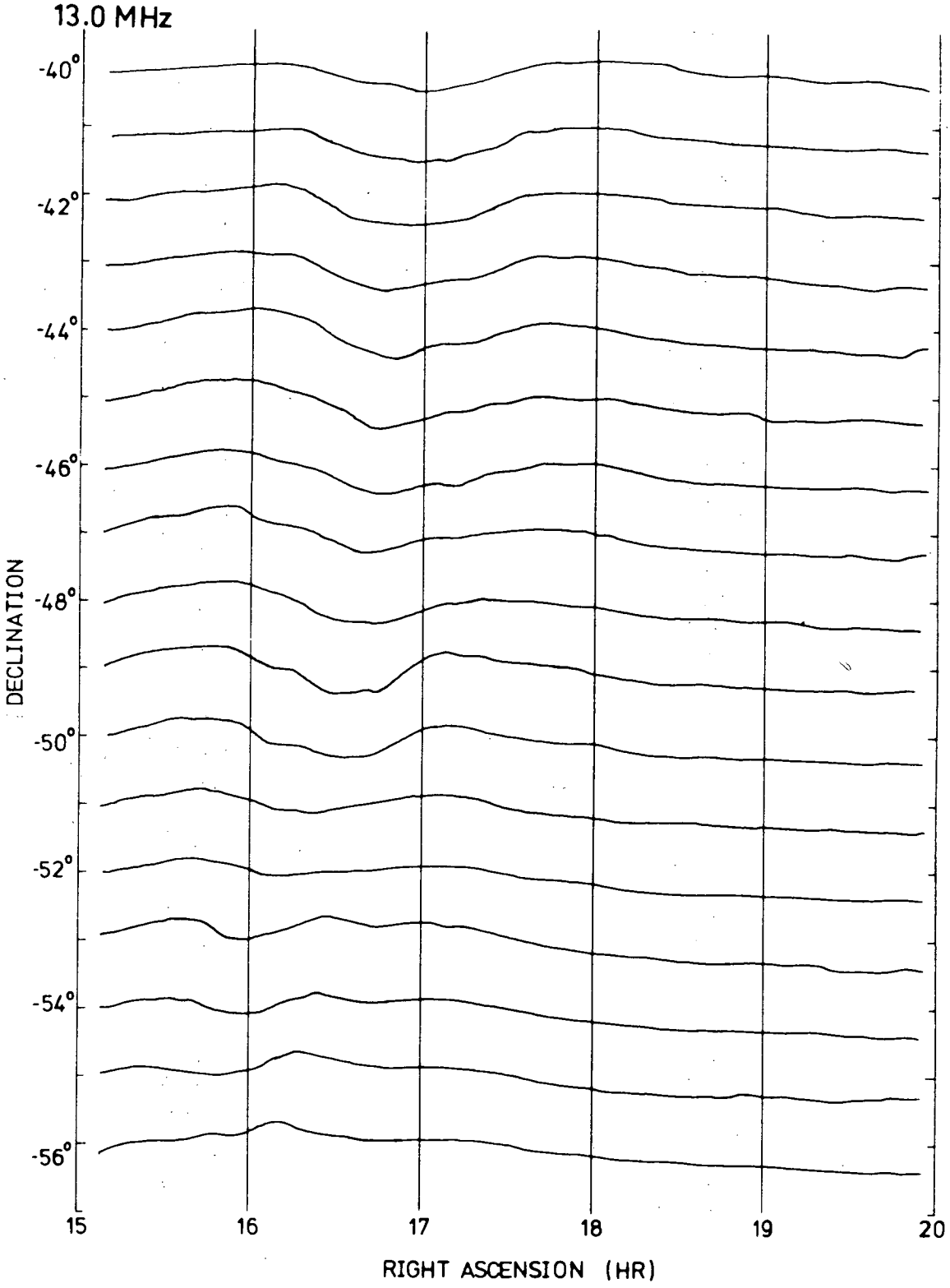
13.0 MHz
-40°
-42°
-44°
-46°
-48°
-50°
-52°
-54°
-56°
DECLINATION
15
16
17
18
19
20
RIGHT ASCENSION (HR)

FIGURE 6.5.2

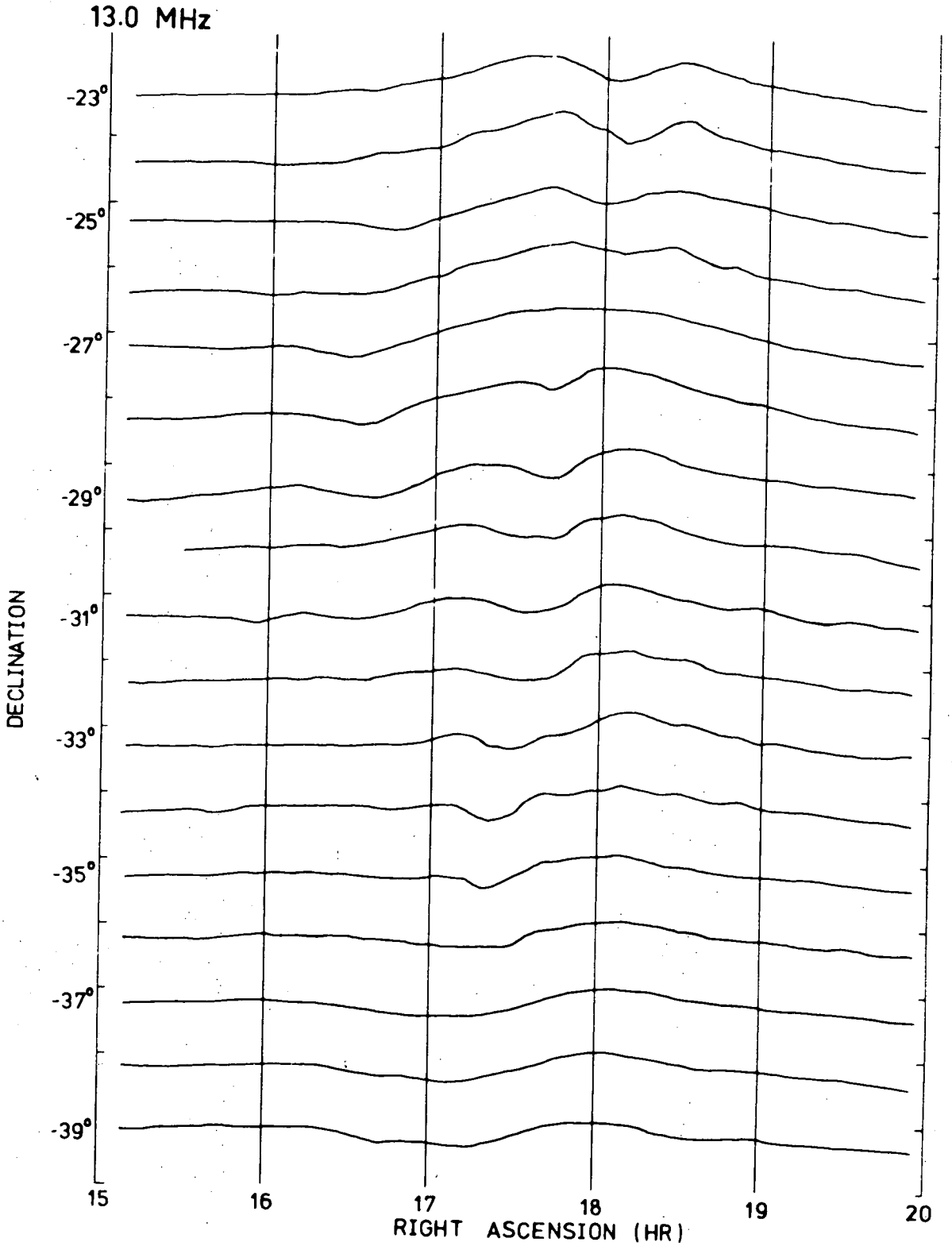
13.0 MHz
-23°
-25°
-27°
-29°
-31°
-33°
-35°
-37°
-39°
DECLINATION
15
16
17
18
19
20
RIGHT ASCENSION (HR)

FIGURE 6.5.3

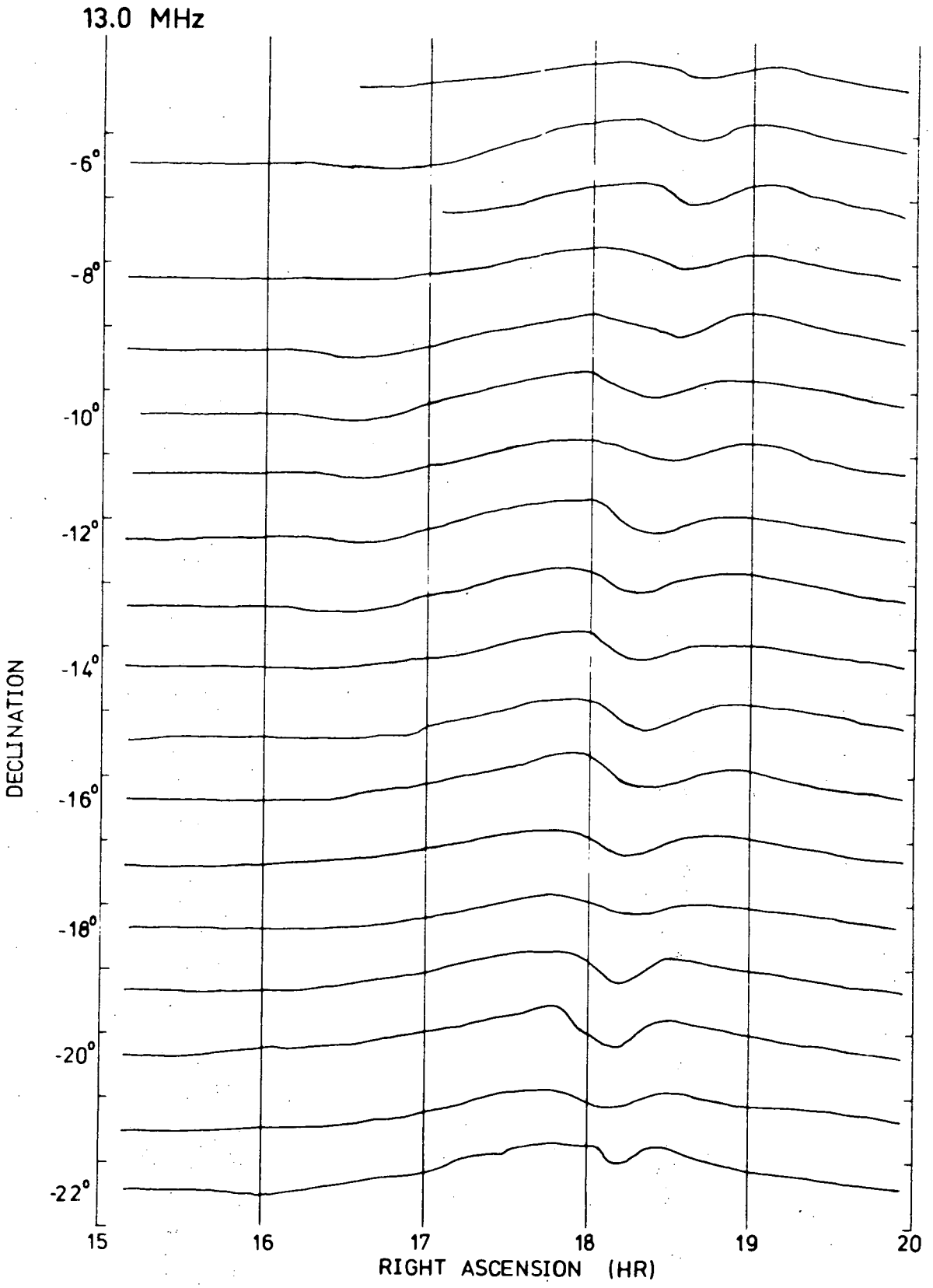
13.0 MHz
-6°
-8°
-10°
-12°
-14°
-16°
-18°
-20°
-22°
DECLINATION
15
16
17
18
19
20
RIGHT ASCENSION (HR)

FIGURE 6.5.4

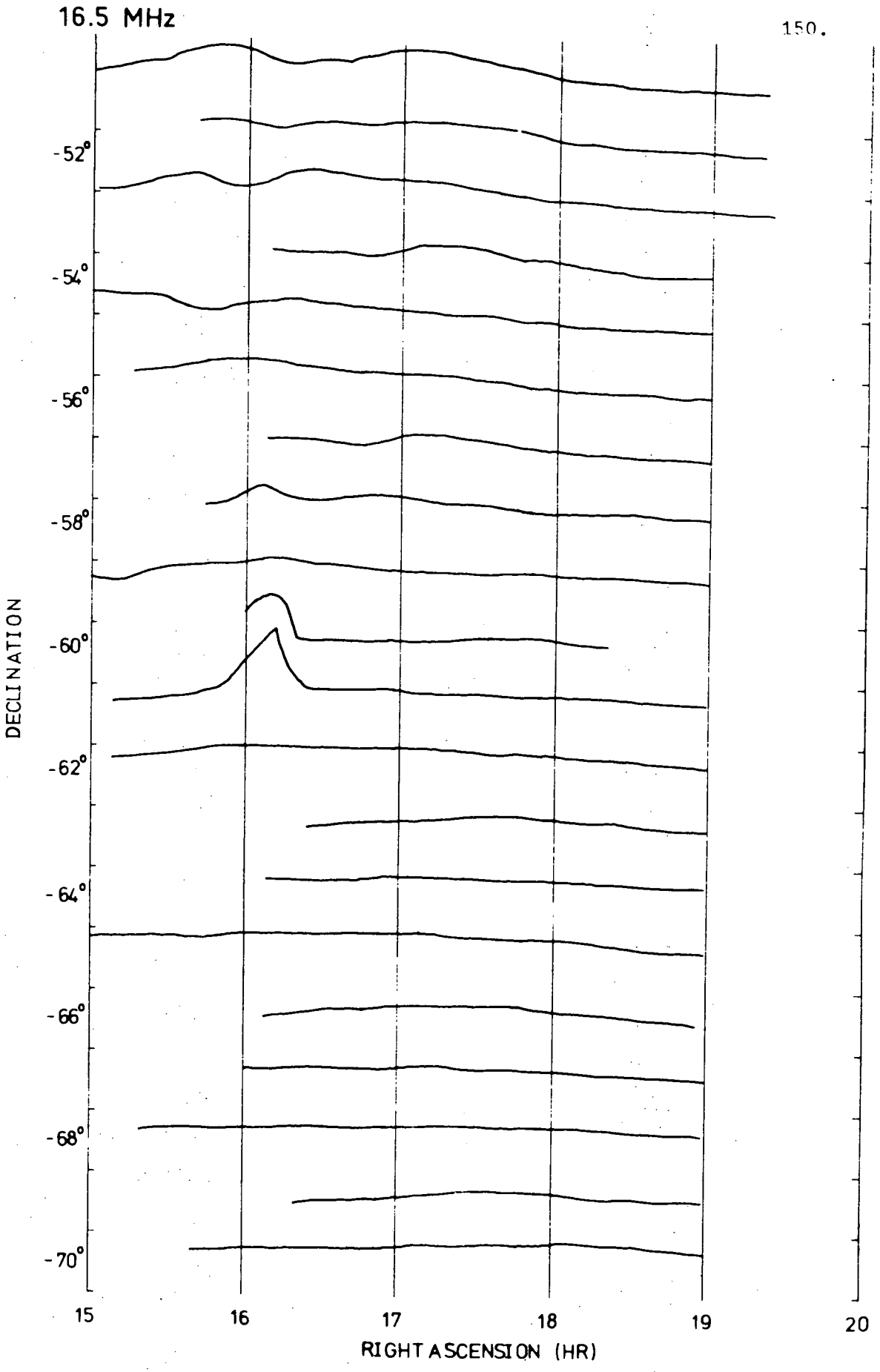
16.5 MHz
-52°
-54°
-56°
-58°
-60°
-62°
-64°
-66°
-68°
-70°
DECLINATION
15
16
17
18
19
20
RIGHT ASCENSION (HR)

FIGURE 6.6.1

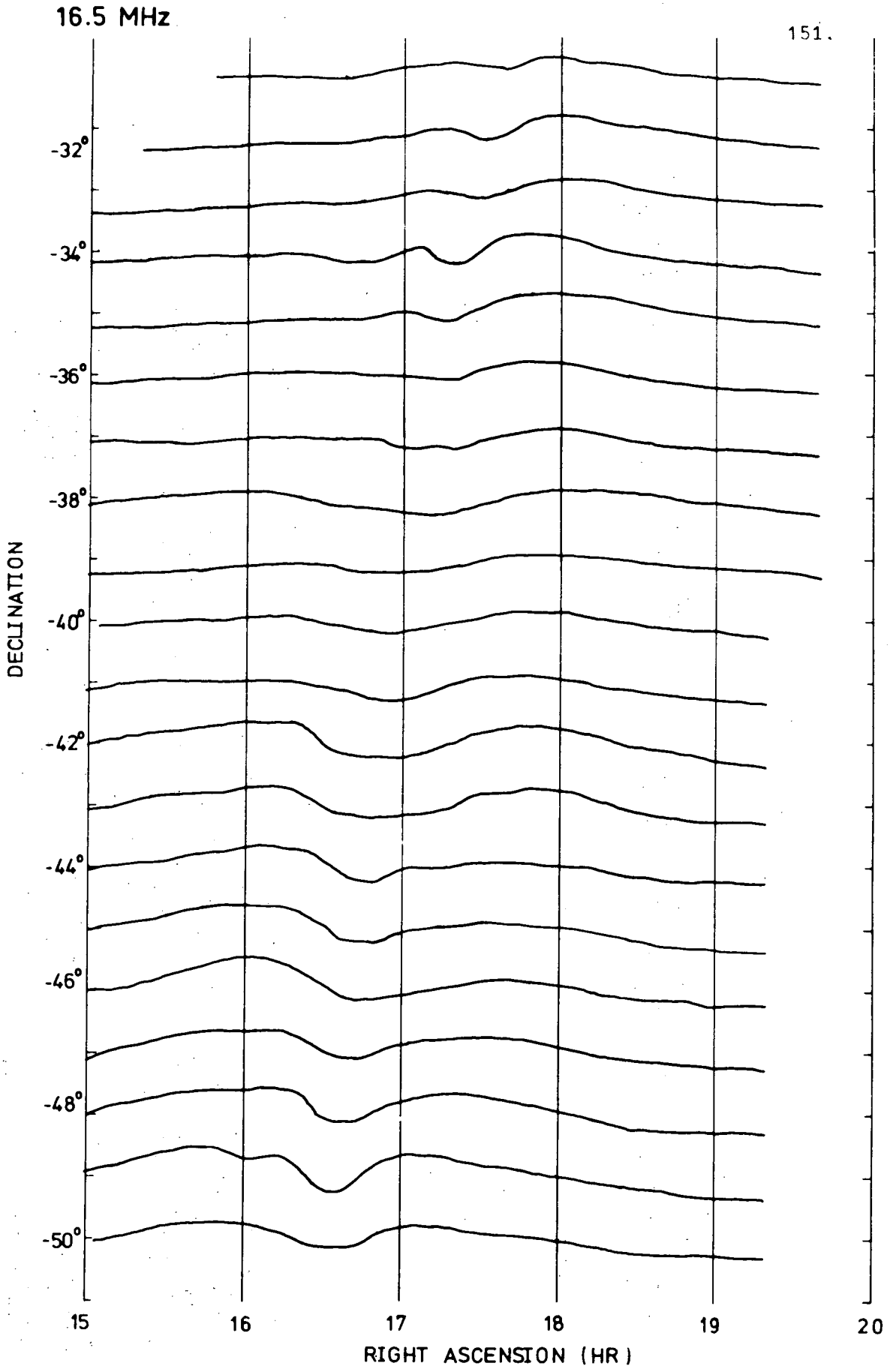
16.5 MHz
-32°
-34°
-36°
-38°
-40°
-42°
-44°
-46°
-48°
-50°
DECLINATION
15
16
17
18
19
20
RIGHT ASCENSION (HR)

FIGURE 6.6.2

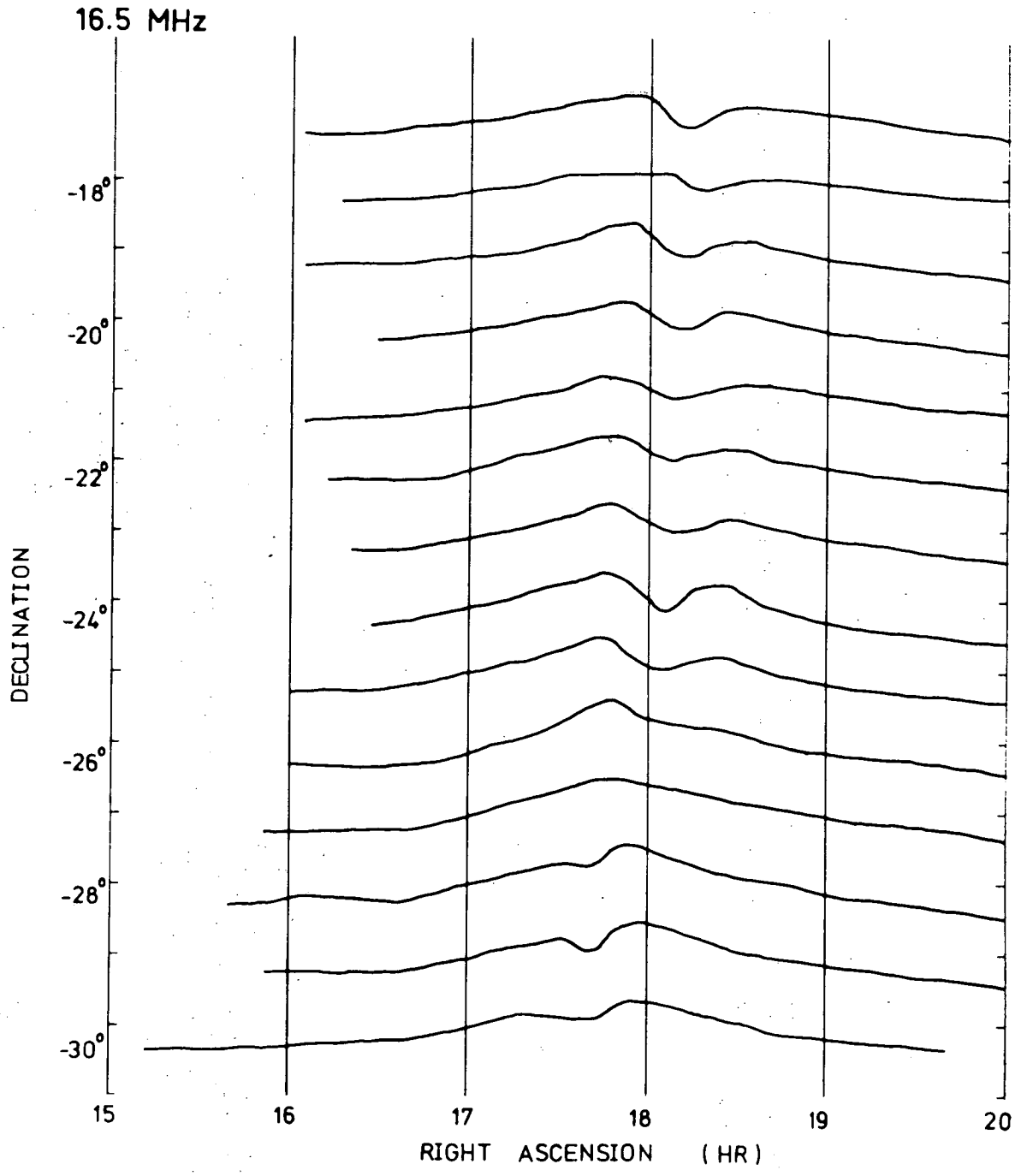
16.5 MHz
-18°
-20°
-22°
-24°
-26°
-28°
-30°
DECLINATION
15
16
17
18
19
20
RIGHT ASCENSION (HR)

FIGURE 6.6.3

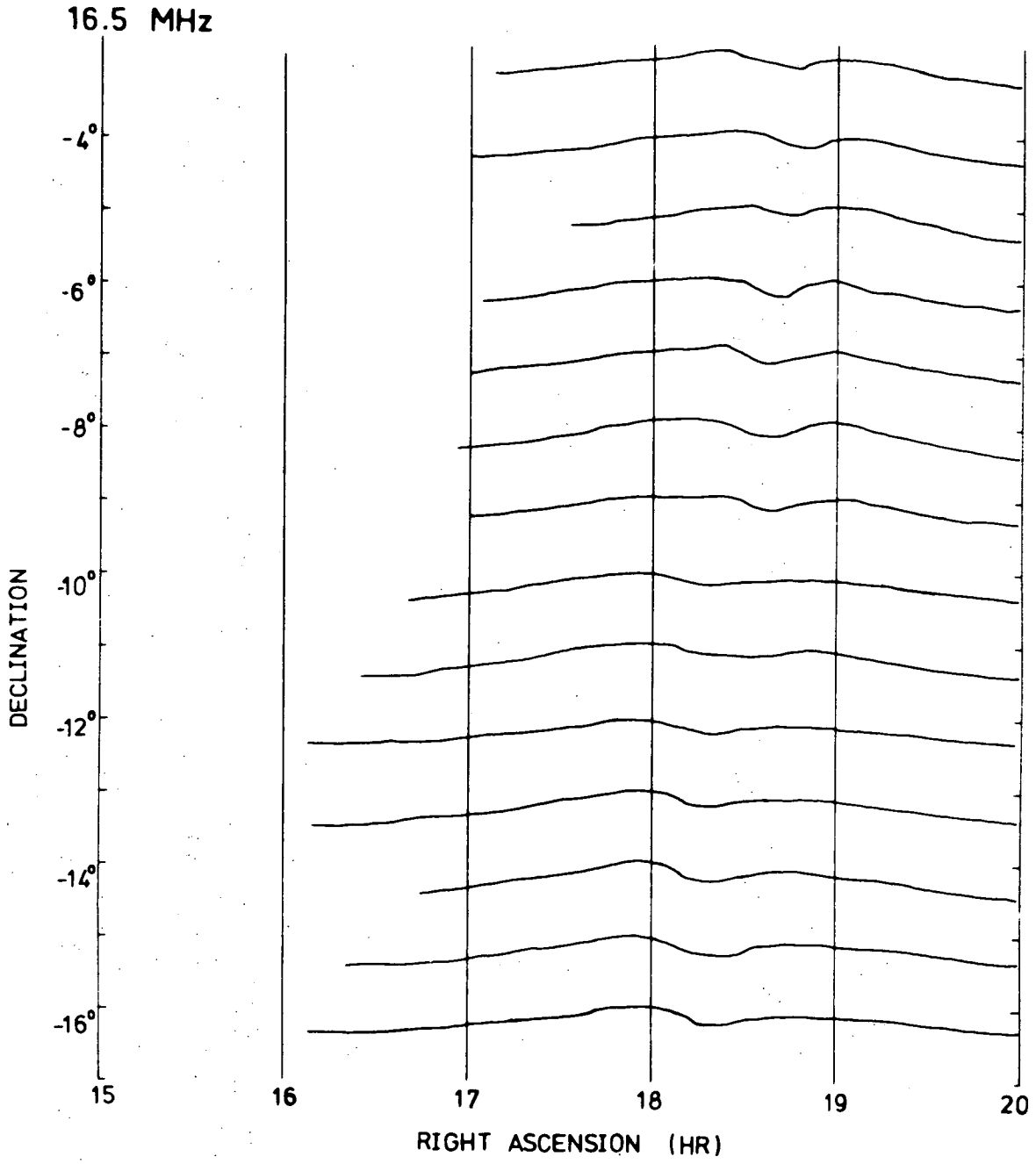
16.5 MHz
-4°
-6°
-8°
-10°
-12°
-14°
-16°
DECLINATION
15
16
17
18
19
20
RIGHT ASCENSION (HR)

FIGURE 6.6.4

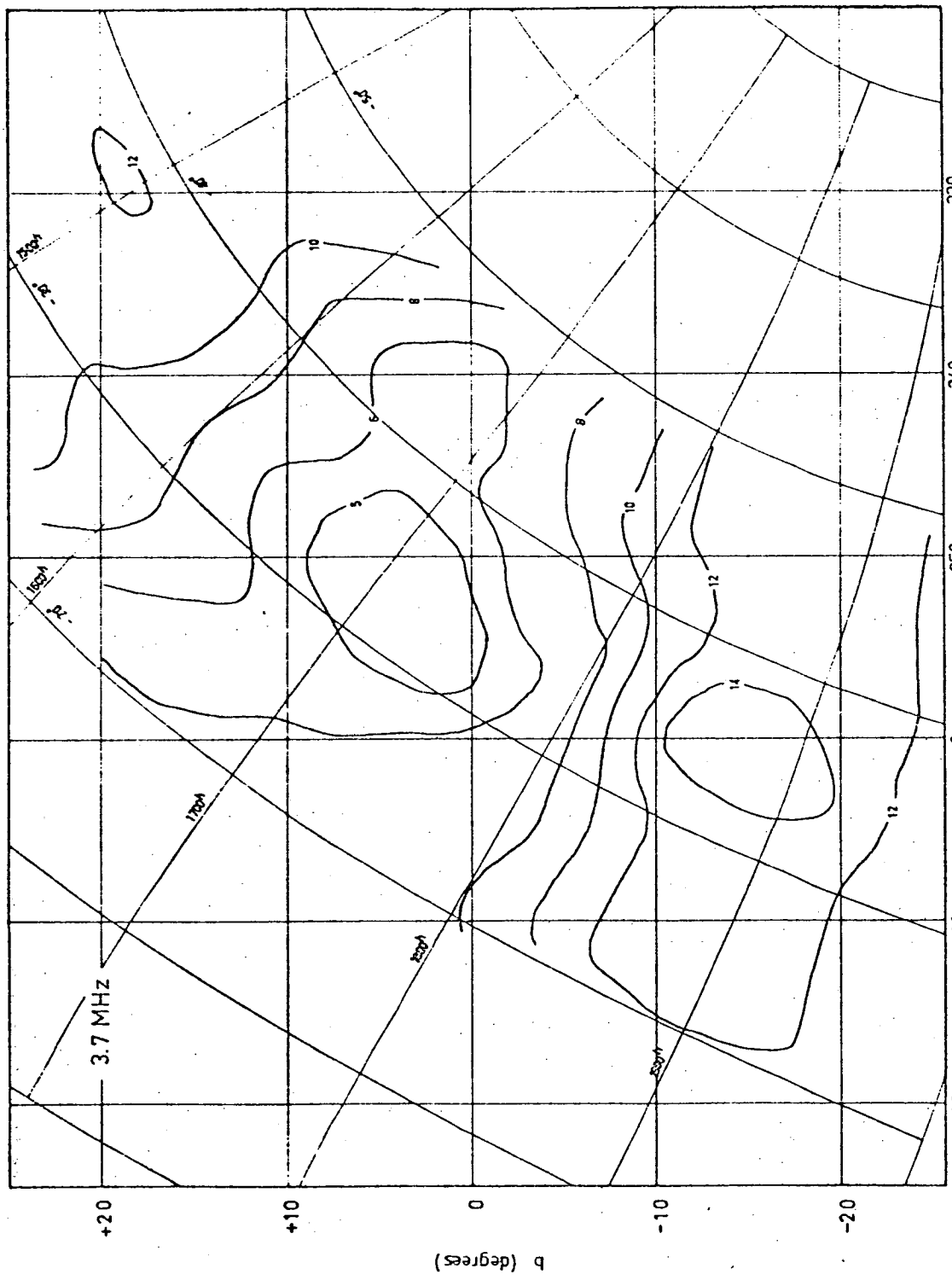
3.7 MHz
+20
+10
0
-10
-20
b (degrees)
330
340
350
0
10
20
l (degrees)
6
8
10
12
14

FIGURE 6.7

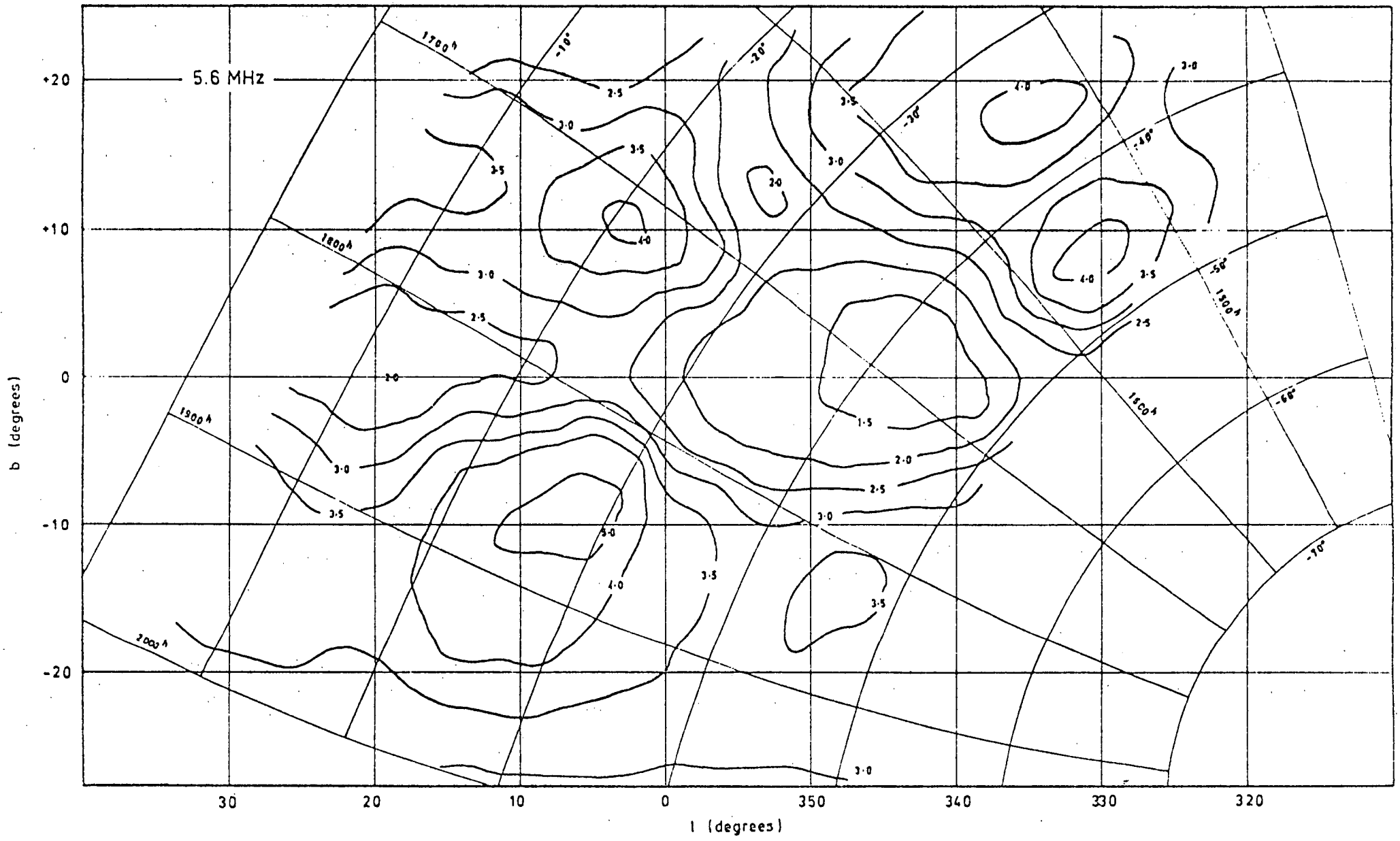
5.6 MHz
+20
+10
0
-10
-20
b (degrees)
30
20
10
0
350
340
330
320
l (degrees)
1700 h
1800 h
1900 h
2000 h
1500 h
-10°
-20°
-30°
-40°
-50°
-60°
-70°
2·5
3·0
3·5
4·0
2·0
1·5

FIGURE 6.8

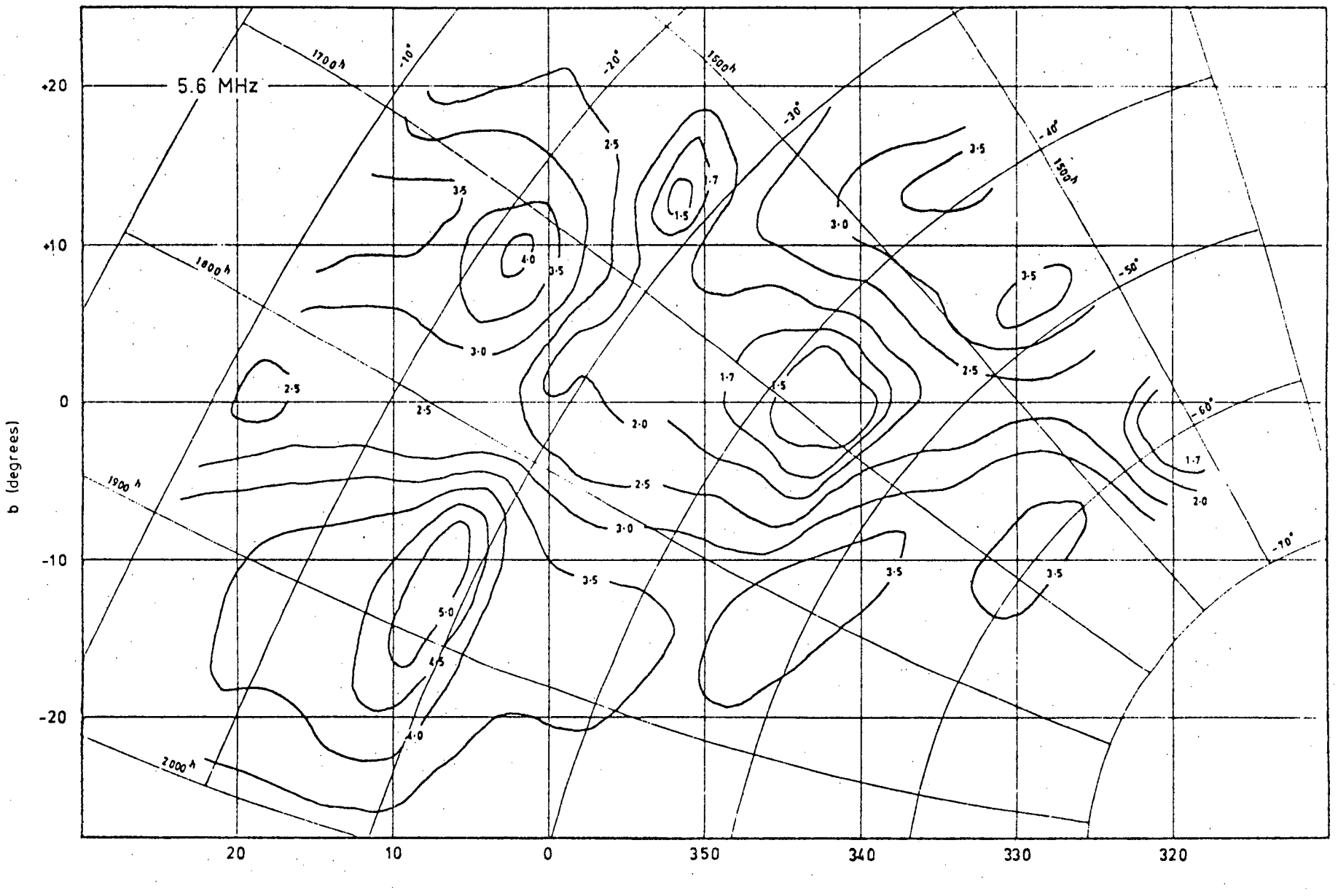
5.6 MHz
+20
+10
0
-10
-20
b (degrees)
20
10
0
350
340
330
320
l (degrees)
1700 h
1800 h
1900 h
2000 h
1500 h
-10°
-20°
-30°
-40°
-50°
-60°
-70°
2·5
3·5
1·7
1·5
3·0
4·0
2·0
5·0
4·5

FIGURE 6.9

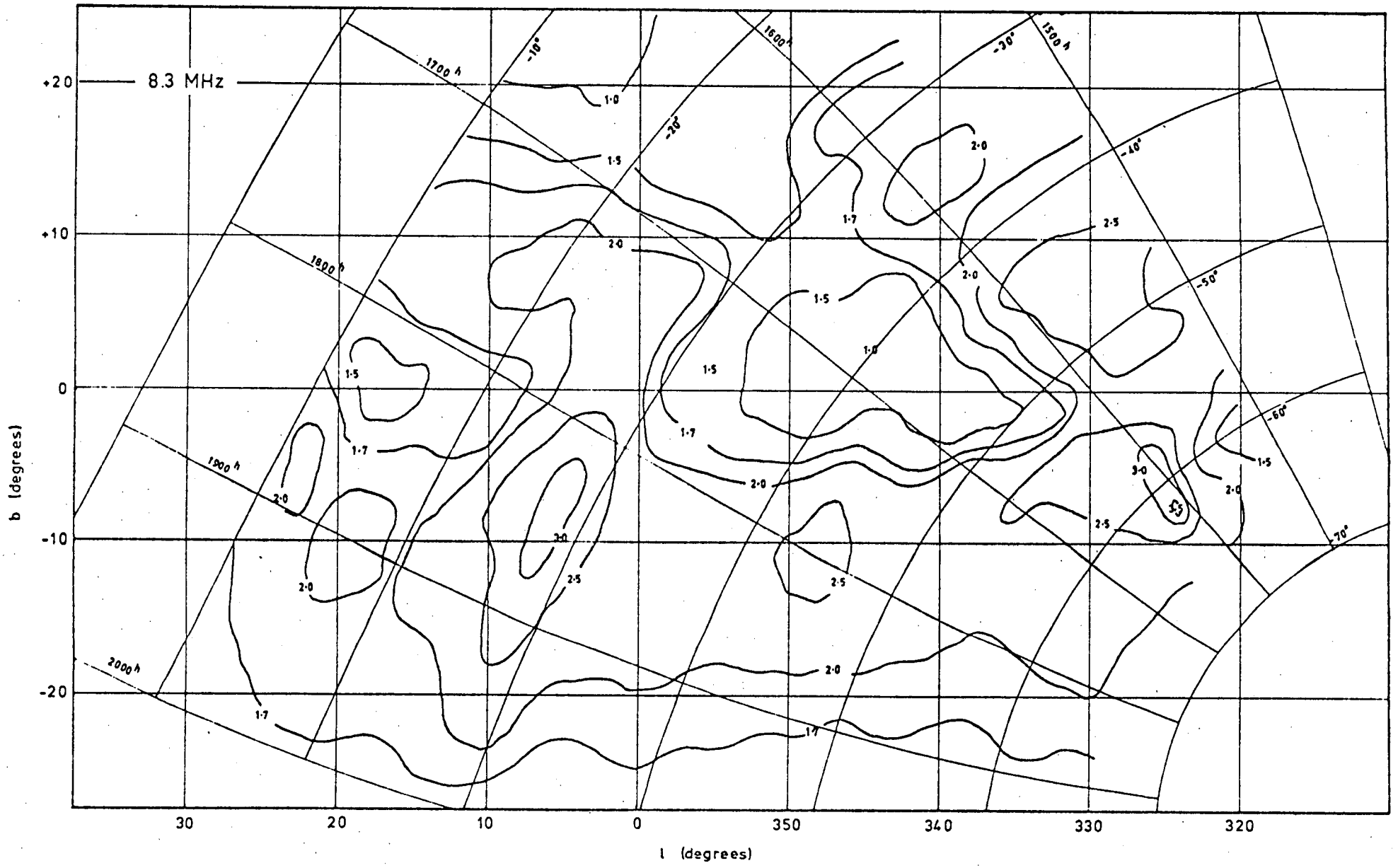
8.3 MHz
+20
+10
0
-10
-20
b (degrees)
30
20
10
0
350
340
330
320
l (degrees)
1700 h
1600 h
1500 h
1800 h
1900 h
2000 h
-10°
-20°
-30°
-40°
-50°
-60°
-70°
1·0
1·5
1·7
2·0
2·5
3·0
F3

FIGURE 6.10

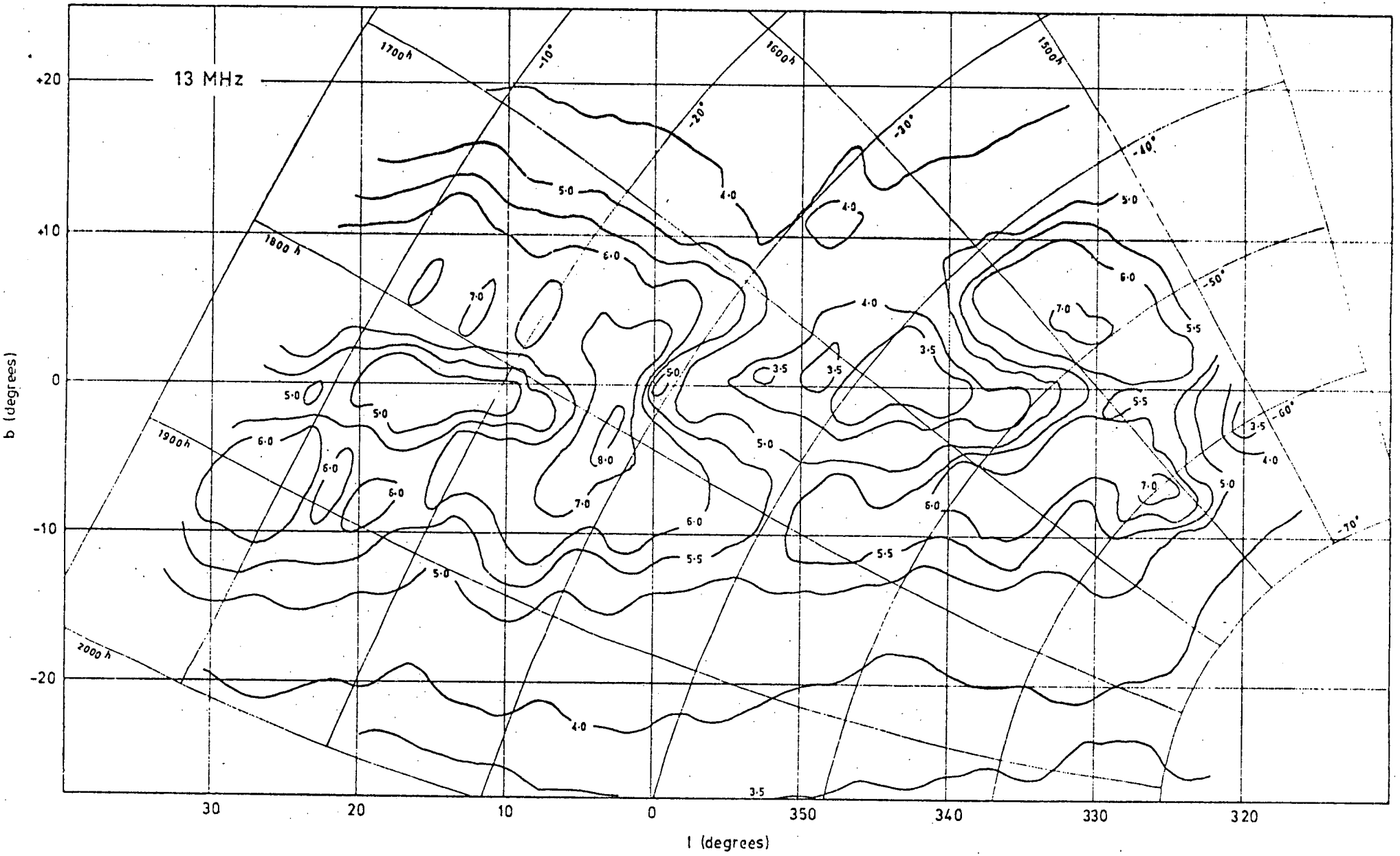
13 MHz
+20
+10
0
-10
-20
b (degrees)
30
20
10
0
350
340
330
320
l (degrees)
1700 h
1600 h
1500 h
1800 h
1900 h
2000 h
-10°
-20°
-30°
-40°
-50°
-60°
-70°
5·0
4·0
6·0
7·0
3·5
5·5
8·0

FIGURE 6.11

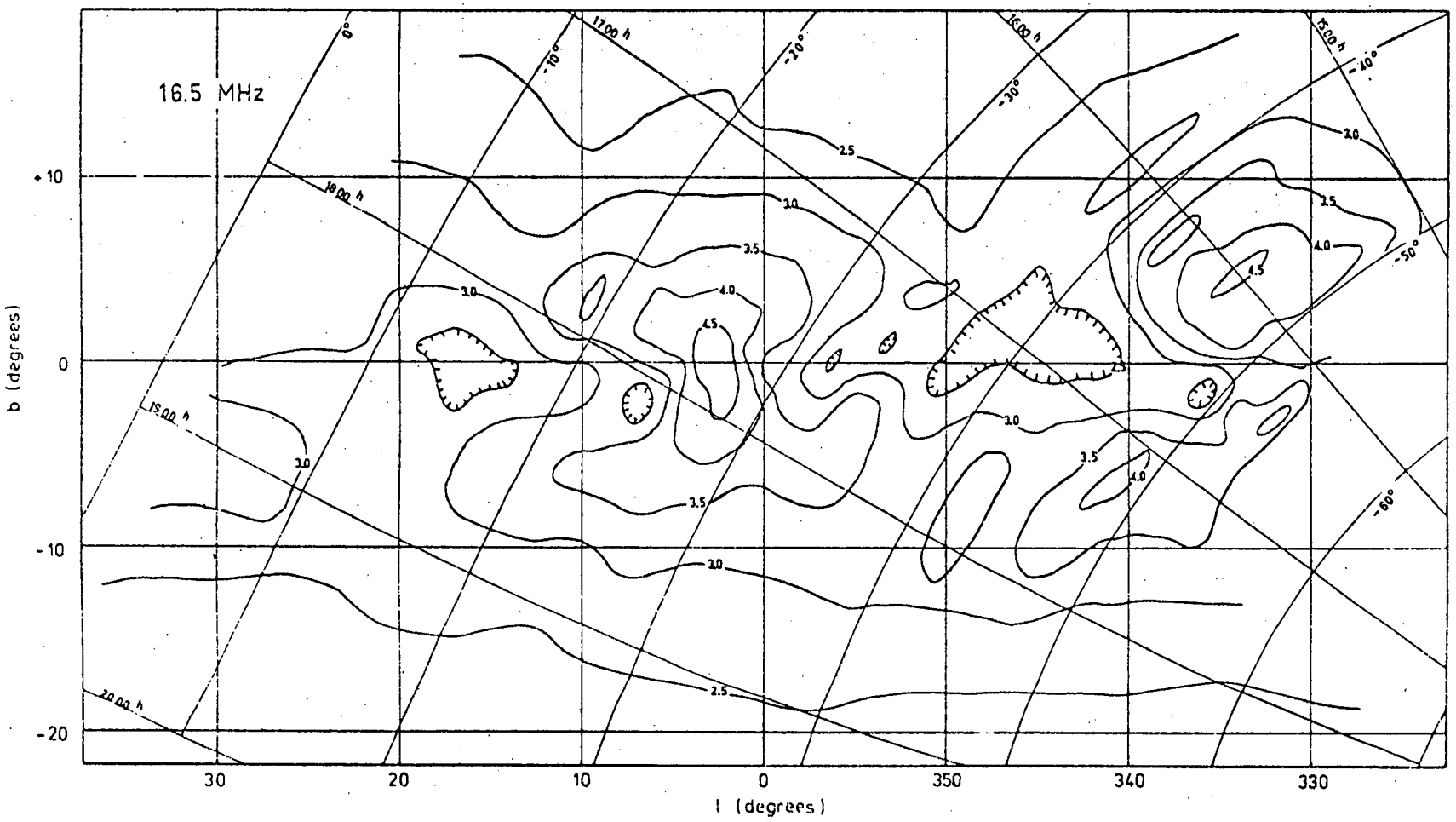
16.5 MHz
b (degrees)
l (degrees)
+10
0
-10
-20
30
20
10
0
350
340
330
0°
-10°
-20°
-30°
-40°
-50°
-60°
17.00 h
16.00 h
15.00 h
19.00 h
18.00 h
20.00 h
2.5
3.0
3.5
4.0
4.5

FIGURE 6·12

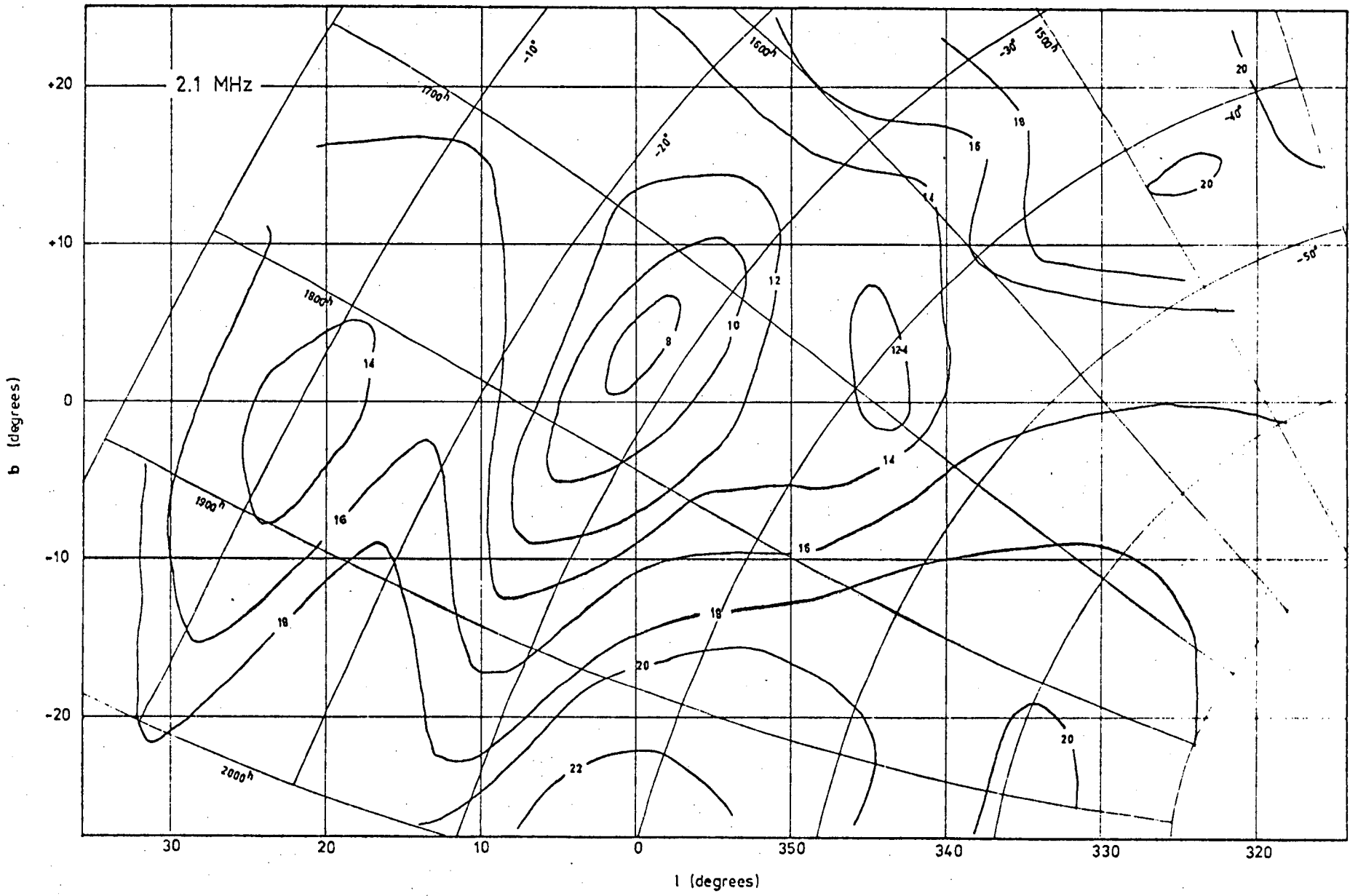
2.1 MHz
+20
+10
0
-10
-20
b (degrees)
30
20
10
0
350
340
330
320
l (degrees)
1700h
1800h
1900h
2000h
1600h
1500h
-10°
-20°
-30°
-40°
-50°
8
10
12
12-4
14
16
18
20
22

FIGURE 6.13

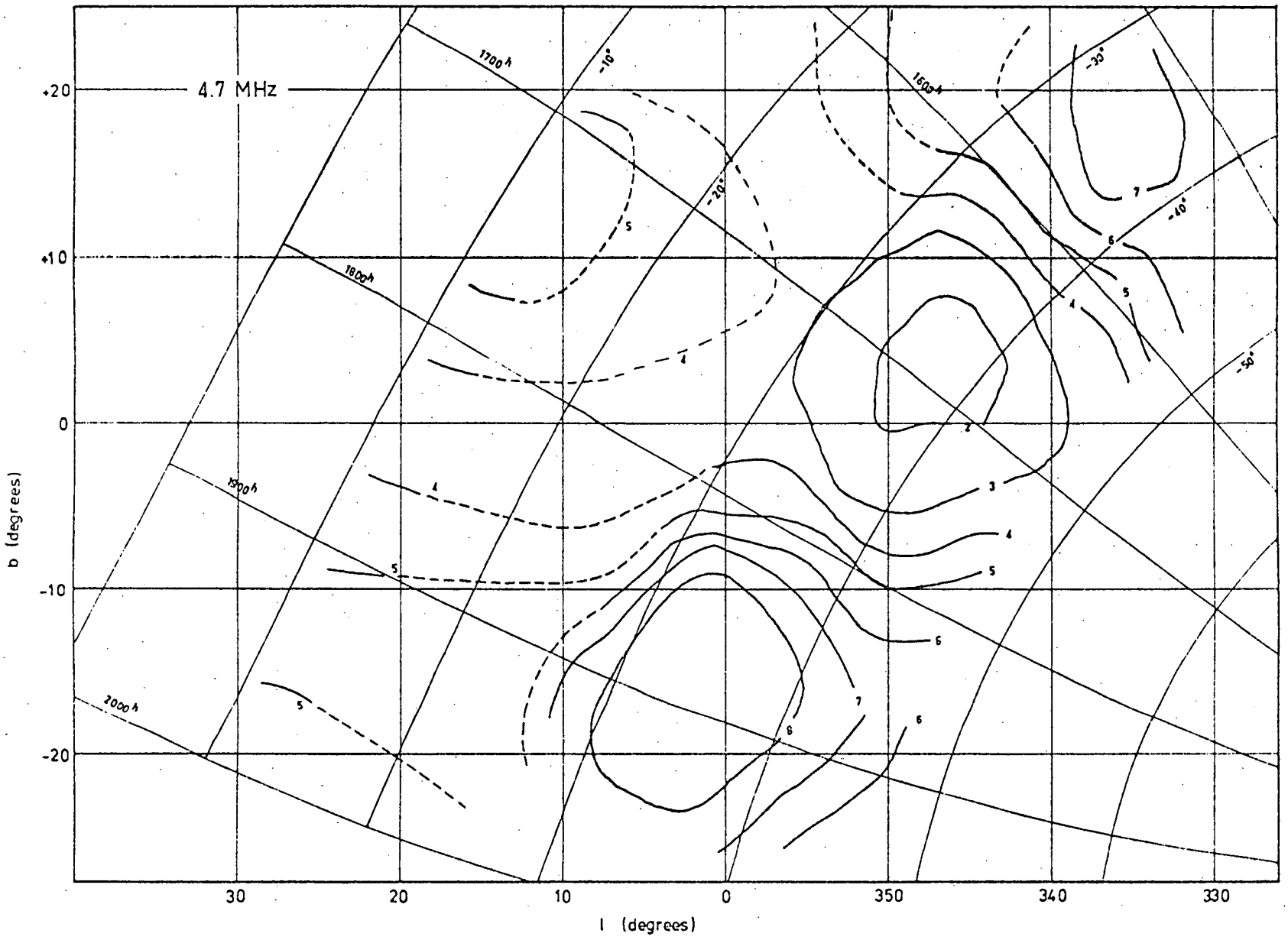
4.7 MHz
+20
+10
0
-10
-20
b (degrees)
30
20
10
0
350
340
330
l (degrees)
1700 h
1800 h
1900 h
2000 h
1600 h
-10°
-20°
-30°
-40°
-50°

FIGURE 6·14

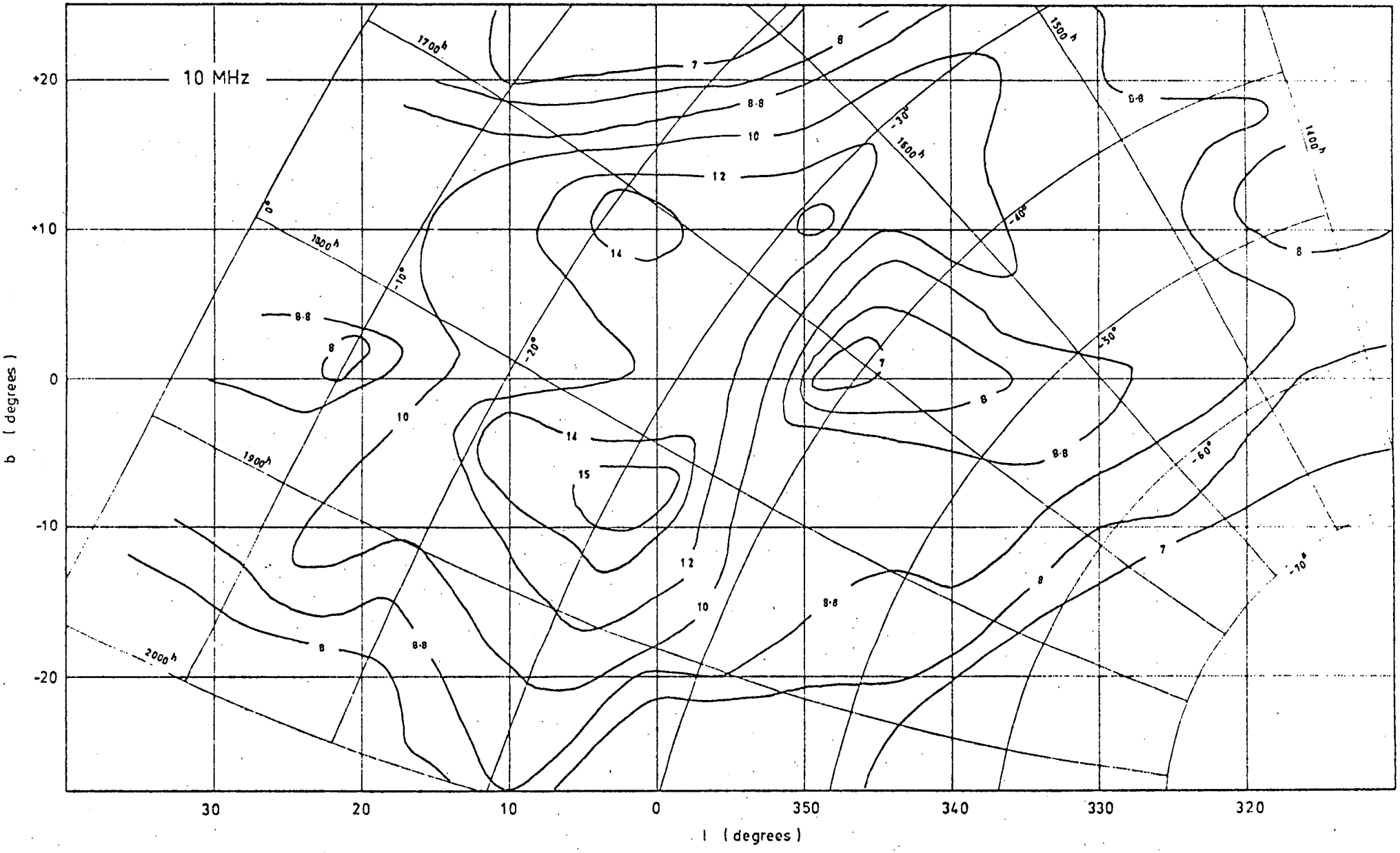
10 MHz
+20
+10
0
-10
-20
b (degrees)
30
20
10
0
350
340
330
320
l (degrees)
1700 h
1800 h
1900 h
2000 h
1500 h
1600 h
1400 h
0°
-10°
-20°
-30°
-40°
-50°
-60°
-70°
7
8
8·8
10
12
14
15

FIGURE 6·15

3.7 MHz survey (fig. 6.7)

This was prepared from a very limited number of good observations made in 1974 and is thus not very reliable. More useful information could be obtained by comparing the individual scans with the corresponding scans at other frequencies. The map is different from the surveys at the higher frequencies (i.e. 5-10 MHz) and appears more like the 2.1 MHz survey.

5.6 MHz (figs. 6.8 and 6.9)

Two 5.6 MHz maps were prepared as they illustrate the reproducibility of the data and because they cover slightly different longitude ranges. The first survey was obtained in 1974 using a 3^{o} sampling interval and the second in 1975 using a 2^{o} sampling interval. The maps resemble the new 4.7 MHz map.

8.3 MHz (fig. 6.10)

Most of the data for this survey was obtained in 1975 when many reasonable records were obtained. The main features of the map can be seen in the 10 MHz map.

13 MHz (fig. 6.11)

The best data obtained were undoubtedly at this frequency as it was a frequency little affected by transmitting station interference and sufficiently high not to be troubled by ionospheric absorption. Almost 24 hours of right ascension were covered and these data were used to prepare the 10 MHz composite map presented in Chapter 5.

16.5 MHz (Fig. 6.12)

This survey was made during 1974. It is the only survey made by the author which delineates the discrete absorption regions and as such provides a link between the low frequency surveys and the high resolution surveys at 19.7 MHz and 30 MHz.

Absolute Temperature Scale

The contour units of the nine low frequency surveys are shown in Table 6.1. As stated before, they have been chosen so that the region near the south galactic pole has that temperature determined by low resolution observations. The reference spectrum used was presented in Chapter 5.

Discrete Absorption Regions

Table 6.2 lists the discrete absorption regions observed at 29.9 MHz in the longitude range 320° to 30°. The regions have been identified with the nebulae listed in the RCW catalogue. (Rogers et al., 1960) and the dimensions quoted are included. Table 6.2 also gives the distances to the emission nebulae. The distances are photometric distances derived by Georgelin and Georgelin (1970) except for the distance to RCW 123 which is a kinematic distance derived by Wilson et al. (1970) from recombination line measurements.

Some of the discrete regions observed at 29.9 MHz are also visible on the 16.5 MHz map whereas others are not resolved. In Figure 6.16.I the 16.5 MHz contours are superimposed on the Hα survey of Sivan (1974). There is agreement between regions of depressed brightness and regions of Hα emission particularly in the range $330° \leq \ell \leq 355°$.

TABLE 6.2

DISCRETE ABSORPTION REGIONS AT 29.9 MHz

GALACTIC CO-ORDINATES ℓ	b	RCW No.	OPTICAL SIZE (min arc)	DISTANCE (kpc)
320.0	-1.8	89?		1.0
327.1	-0.3	97,98		3.4
333.2	-0.4	106	35 × 20	1.9
336.7	-1.3	108	210 × 120	1.3
342.1	+0.0	113	360 × 300	2.0
344.4	-0.4			
344.9	+1.6	119	180 × 145	1.6
349.1	-0.6	123	75 × 75	2.0 ± 1.5
353.2	+0.9	131	170 × 55	1.6
355.6	+0.0	132	110 × 80	1.4
359.6	+0.1	134,137?		
6.3	-1.4	146	120 × 90	1.6
7.8	+0.0			
12.4	-0.9	151,153?	100 × 35	2.6
18.4	+1.7	167	180 × 90	2.3
25.4	+0.0			

FIGURES 16.16.I and 16.16.II

16.5 MHz and 8.3 MHz contours superimposed on the
Hα emission survey of Sivan (1974)

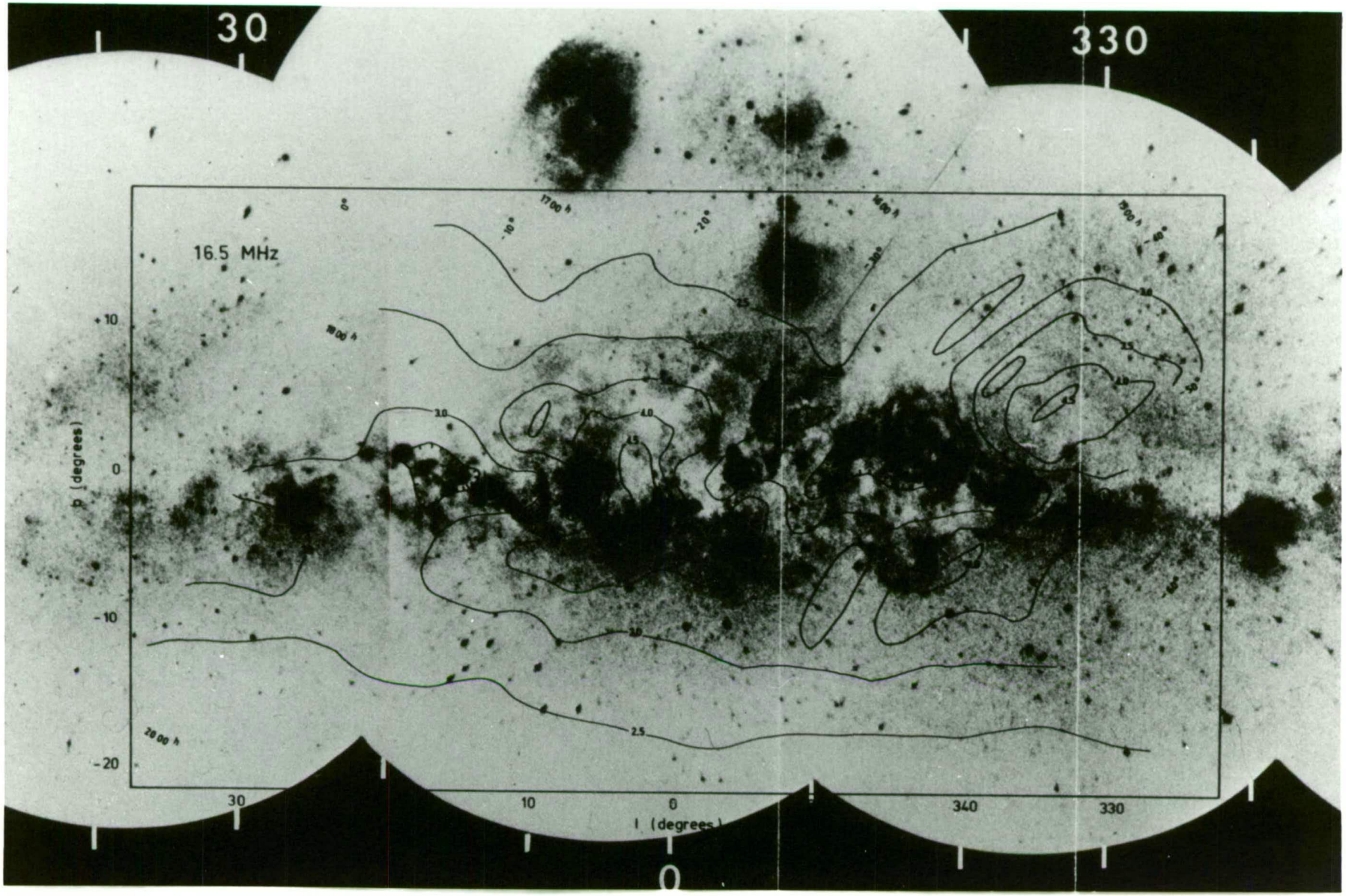
30
330
16.5 MHz
17.00 h
18.00 h
20.00 h
-10°
-20°
-30°
-40°
-50°
3.0
4.0
4.5
2.5
+10
0
-10
-20
b (degrees)
30
10
0
340
330
l (degrees)

76/12/68

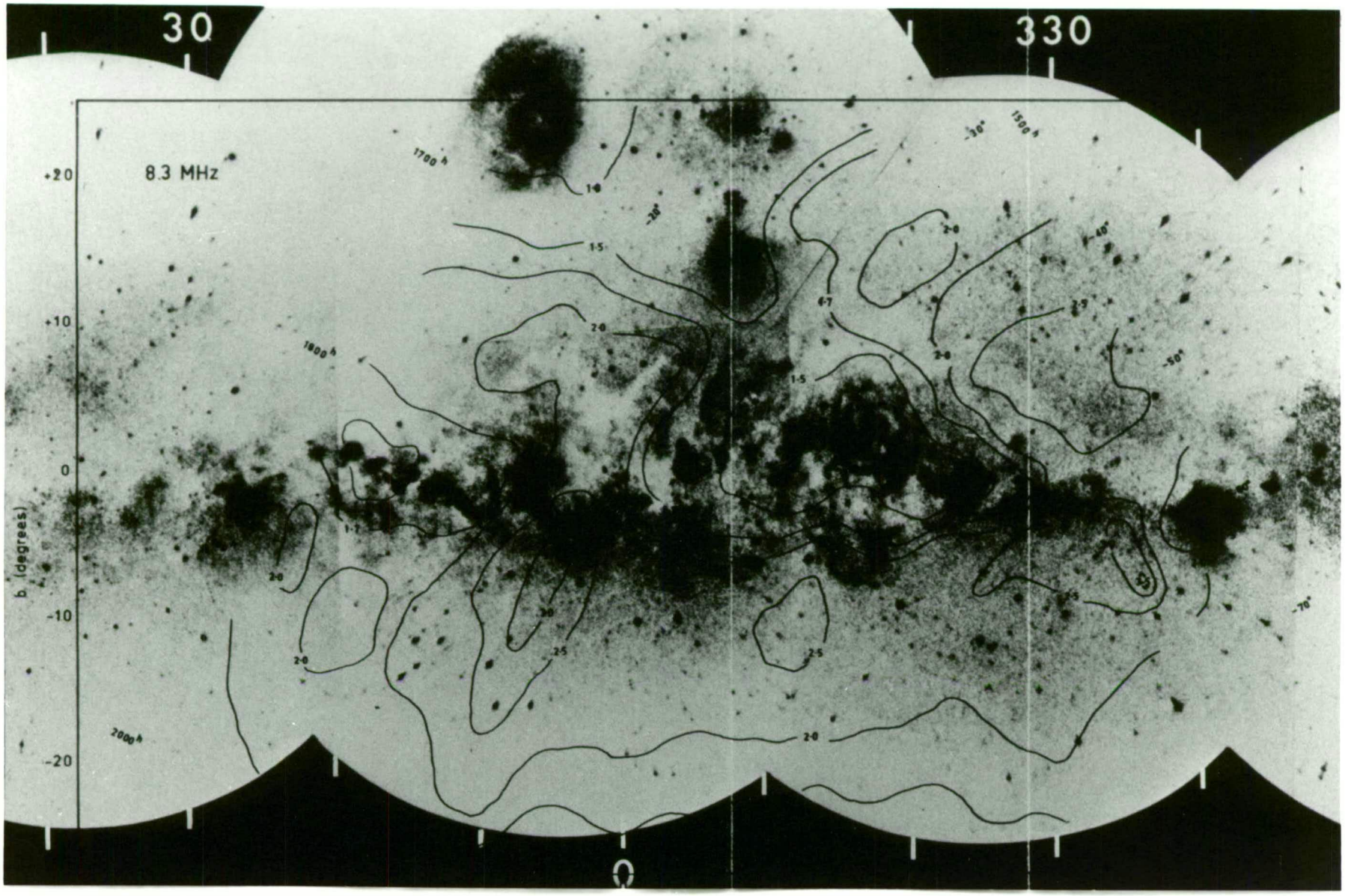
30
330
8.3 MHz
+20
+10
0
-10
-20
b (degrees)
0
1700 h
1500 h
1800 h
2000 h
-30°
-40°
-50°
-70°
1·0
1·5
2·0
2·5
1·7
2·7

76/12/69

Sivan's survey is more sensitive than the Rogers et al. (1960) survey and it is apparent that there is a diffuse emission between the discrete HII regions.

In figure 6.16.II the 8.3 MHz contours have been superimposed on the Hα emission. In this diagram the correlation between regions of depressed brightness and regions of strong Hα emission is also good although at this frequency there are no discrete regions of absorption.

The distances quoted indicate that the emission nebulae observed at low frequencies in directions towards the galactic centre do not lie in the local arm.

Galactic Background Spectra

Figures 6.17 - 6.20 present surveys at 19.7, 30, 85 and 153 MHz. The 19.7 MHz map is incomplete as the highest level contours are not included. However it was decided that this version of the map would suffice to show the correlation between the 19.7 and 30 MHz maps and the 19.7 and 16.5 maps. The original version was in old galactic co-ordinates and was multi-coloured.

The four high frequency surveys and the eight low frequency surveys were used to obtain galactic spectra in various directions. Table 6.3 gives details of all the twelve surveys.

The contour unit of the 30 MHz map is given as 1470 K. However, when line-of-sight spectra are plotted it is found that the 30 MHz points consistently fall above the line defined by the points at 153 MHz and 85 MHz. On the basis of the procedure outlined below a contour unit of 919 K has been used. With this contour unit smooth curves can be drawn through the spectral points.

Let $T(\nu,b)$ be the brightness temperature at frequency ν (in MHz) and for galactic latitude b. If we assume that the temperature spectral index is independent of frequency and latitude for b in the range -90° to -15° and ν in the range 30 - 153 MHz then

$$\frac{T(153,-15°)}{T(153,-90°)} = \frac{T(85,-15°)}{T(85,-90°)} = \frac{T(30,-15°)}{T(30,-90°)} = \gamma$$

and, $$T(30,-15°) = \gamma \times T(30,-90°).$$

γ can be calculated from the 85 and 153 MHz maps and $T(30,-90°)$ can be obtained from the south galactic pole spectrum. The calculated 30 MHz temperature at latitude -15° is a factor of approximately 1.6 lower than an average obtained from the 30 MHz map.

No allowance for differing beam size has been made and temperatures in a given direction have been taken straight from the

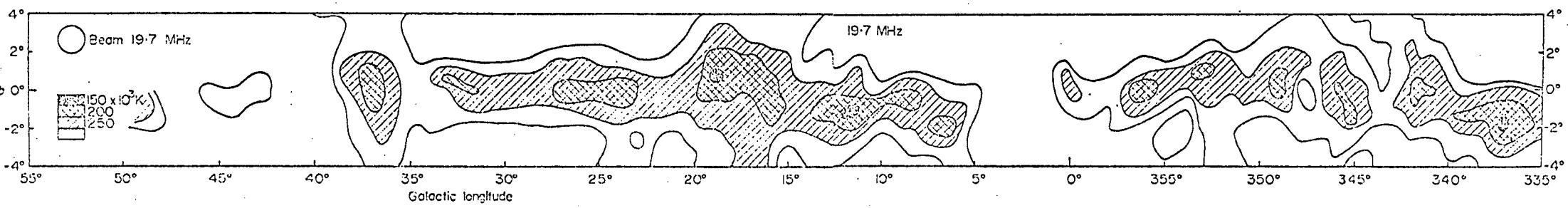

FIGURE 6.17

after Mathews et al. (1973)

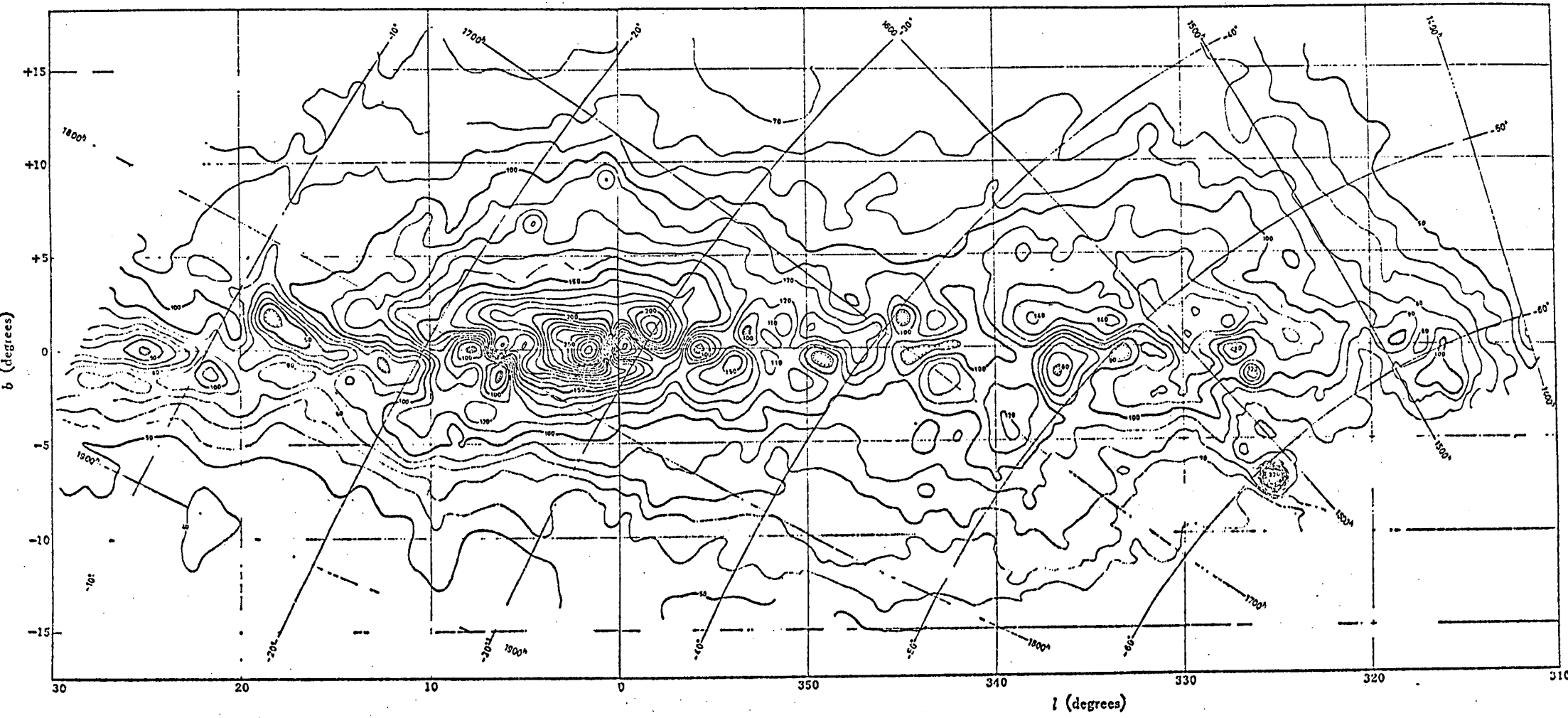

FIGURE 6·18 The 29.9 MHz Survey

after Jones and Finlay (1974)

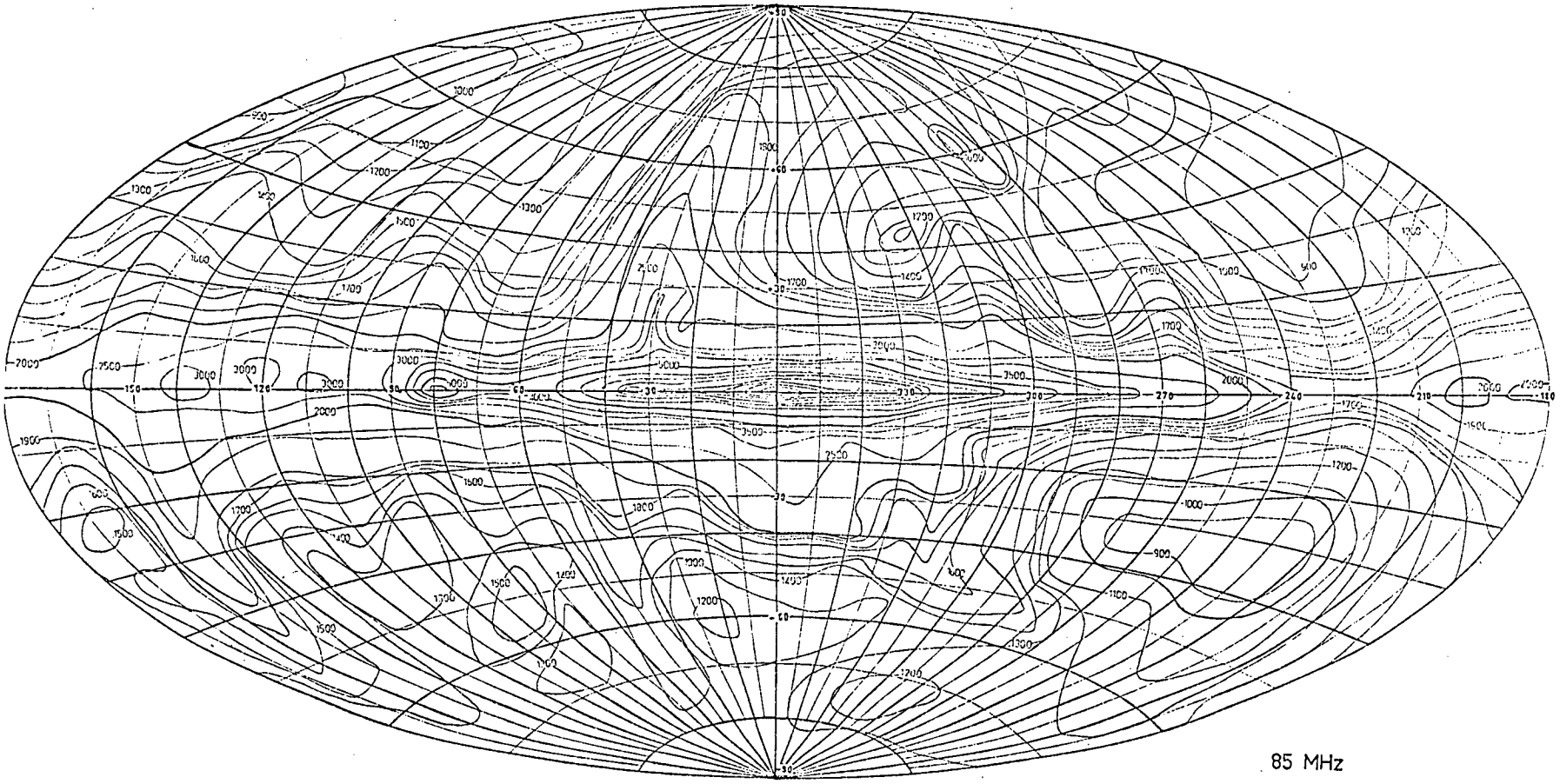

FIGURE 6.19

after Hamilton (1969)

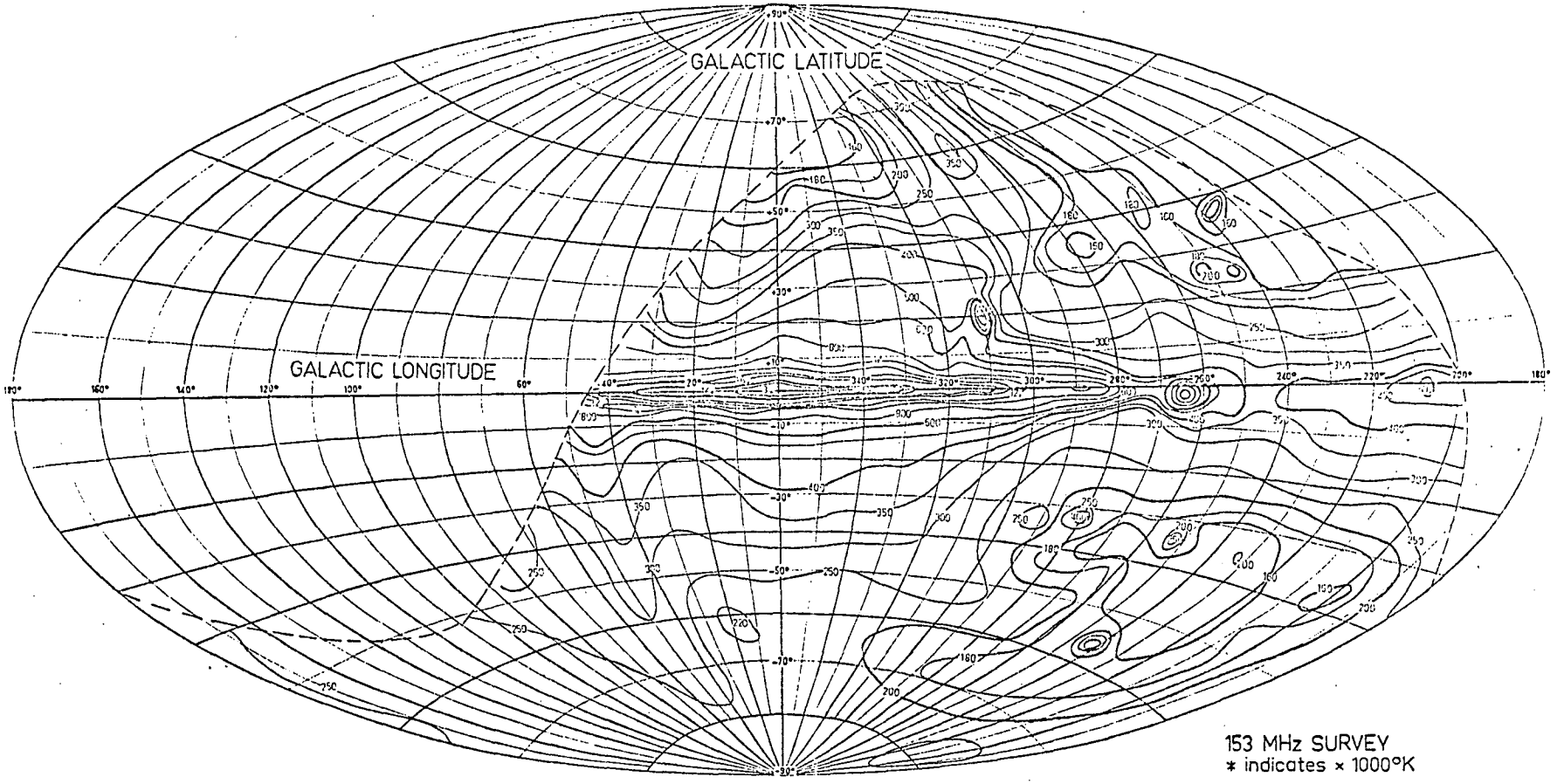

FIGURE 6.20

after Hamilton (1969)

TABLE 6.3

DETAILS OF SPECTRAL MEASUREMENTS

FREQUENCY (MHz)	RESOLUTION	ACCURACIES	OBSERVER
153	2^{o}	R $\pm$ 5%	Hamilton & Haynes (1969)
85	$3.5^{o} \times 3.8^{o}$	A $\pm$ 7%	Yates et al. (1967)
30	0.8^{o}	A $\pm$ 2%	Jones & Finlay (1974)
19.7	1.4^{o}	A 20%	Shain et al. (1961)
16.5	1.6^{o}	*	Cane (1975)
13.0	2.1^{o}	*	Cane
10.0	$4^{o} \times 5^{o}$	*	Hamilton & Haynes (1968)
8.3	3.2^{o}	*	Cane
5.6	4.8^{o}	*	Cane
4.7	$3^{o} \times 11^{o}$	*	Ellis & Hamilton (1966)
3.7	7.3^{o}	*	Cane
2.1	8^{o}	*	Reber (1968)

R = relative accuracy A = absolute accuracy

* Relative accuracy - about 20%
The absolute accuracy of the surveys at frequencies <20MHz is determined by the accuracy of the reference spectrum. The latter could be too high by up to 30% in the range 2.5 - 20 MHz.

after Cane (1976)

maps. However, when drawing a smooth spectrum care has been taken to ensure the observed relationship between intensities at one frequency but different latitudes has been retained.

Figures 6.21 - 6.23 show three sets of spectra for longitudes 330°, 10° and 20°. The most striking feature is the plateau in the $|b| \simeq 5°$ spectra for frequencies between approximately 6 and 15 MHz. This is seen in all sets of spectra for longitudes within 40° of the galactic centre. In figure 6.24 we show several spectra in the galactic plane. Unfortunately, there is little data in the region $30° \lesssim \ell \lesssim 100°$ as this is at the edge of the region accessible to both northern and southern observers. However Figure 6.24 shows that the effect observed (i.e. the plateau) is the result of additional emission and excess absorption taking place in directions towards the galactic centre in comparison to other directions.

Many other spectra have been compiled but are not illustrated. They all present the same basic features with minor variations. The most notable variation is that for longitudes in the approximate range 340° - 355° the galactic plane spectra are depressed further at low frequencies than for other longitudes.

The basic features of the spectra are outlined below:

(i) At frequencies greater than about 40 MHz the emission decreases with increasing latitude.

(ii) The b = 0° and b = 5° spectra turn over at approximately 30 MHz whereas the b = 10° and b = 20° spectra turn over at about 9 MHz and 6 MHz respectively.

(iii) There is a plateau in the spectra for latitudes less than 10° between 15 and 6 MHz.

(iv) As a consequence of (i) and (ii) the maximum intensity results at higher latitudes with decreasing frequency for frequencies less than 30 MHz.

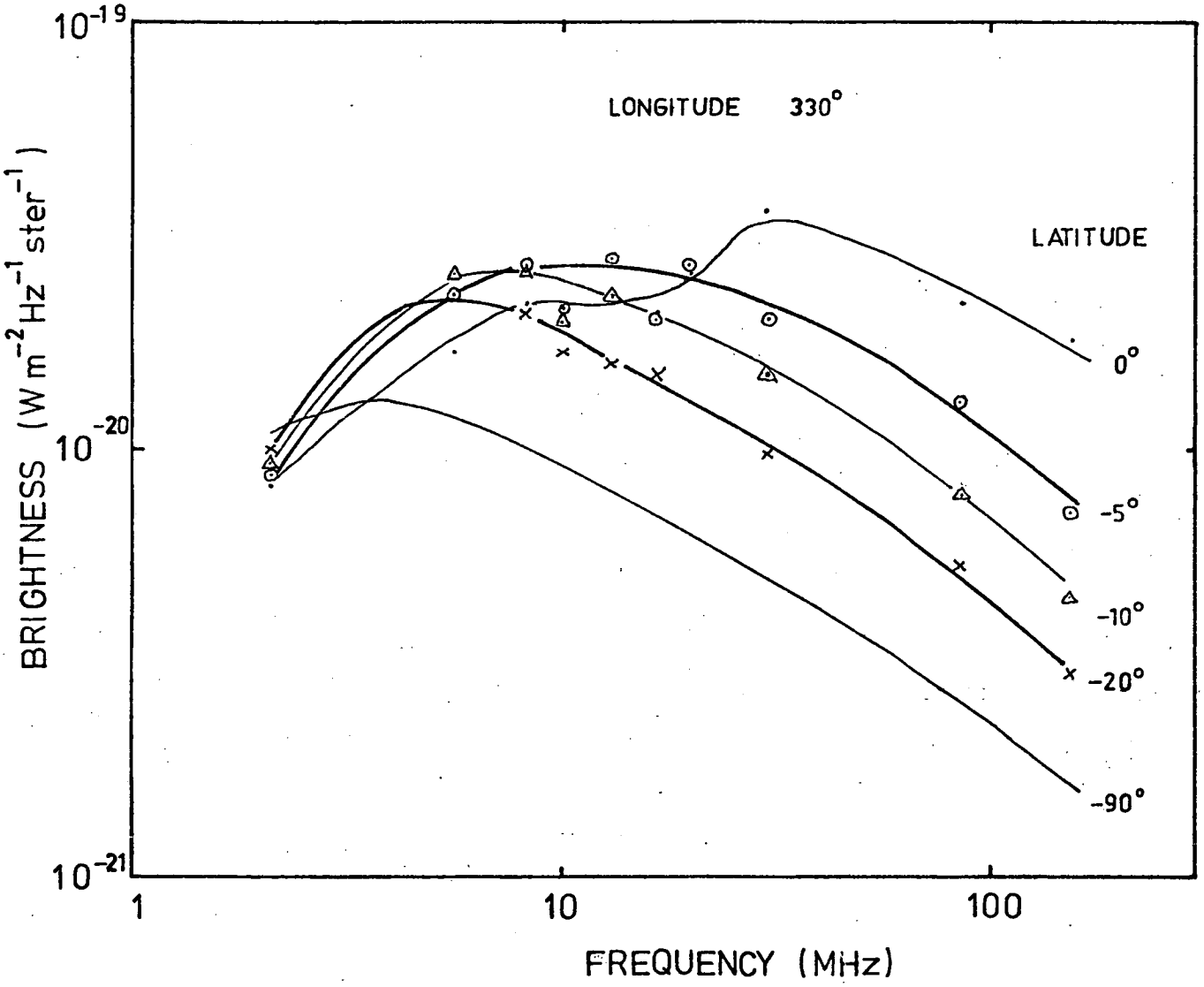
LONGITUDE 330°
LATITUDE
0°
-5°
-10°
-20°
-90°
BRIGHTNESS (W m⁻² Hz⁻¹ ster⁻¹)
10⁻¹⁹
10⁻²⁰
10⁻²¹
1
10
100
FREQUENCY (MHz)

FIGURE 6.21

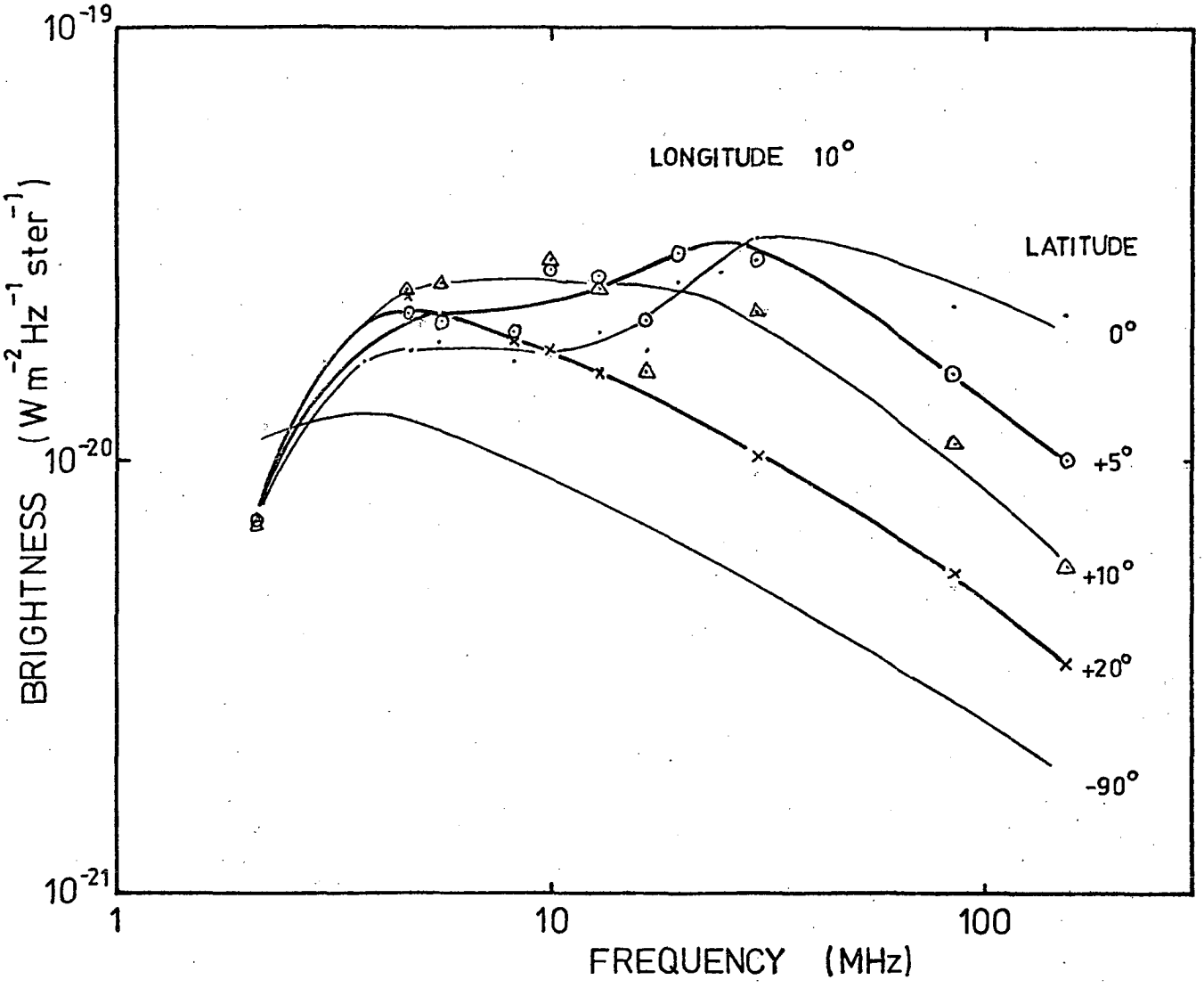
10^{-19}
10^{-20}
10^{-21}
BRIGHTNESS ($W m^{-2} Hz^{-1} ster^{-1}$)
LONGITUDE 10°
LATITUDE
0°
+5°
+10°
+20°
-90°
1
10
100
FREQUENCY (MHz)

FIGURE 6.22

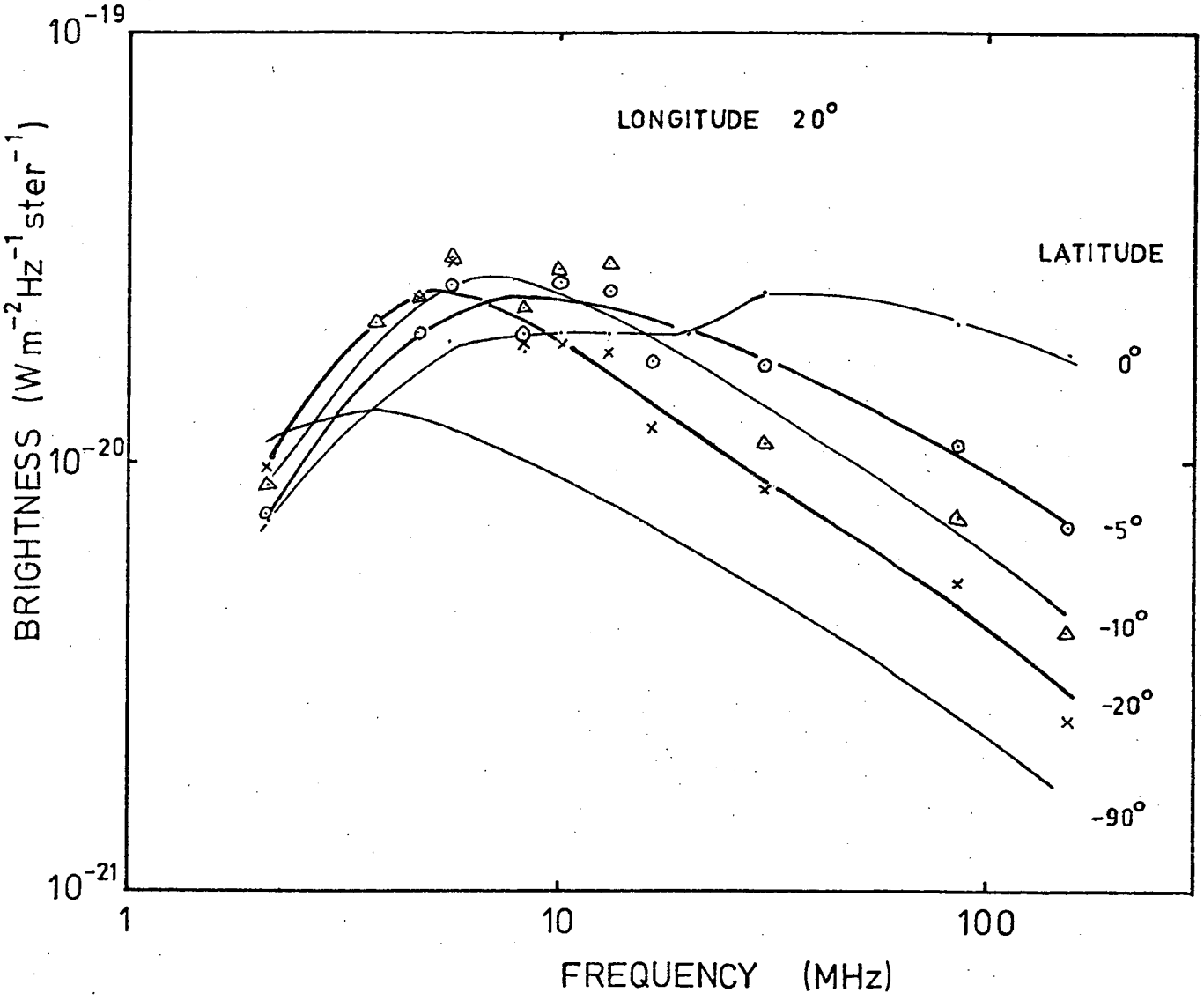
LONGITUDE 20°
LATITUDE
0°
-5°
-10°
-20°
-90°
BRIGHTNESS (W m^{-2} Hz^{-1} ster^{-1})
10^{-19}
10^{-20}
10^{-21}
1
10
100
FREQUENCY (MHz)

FIGURE 6.23

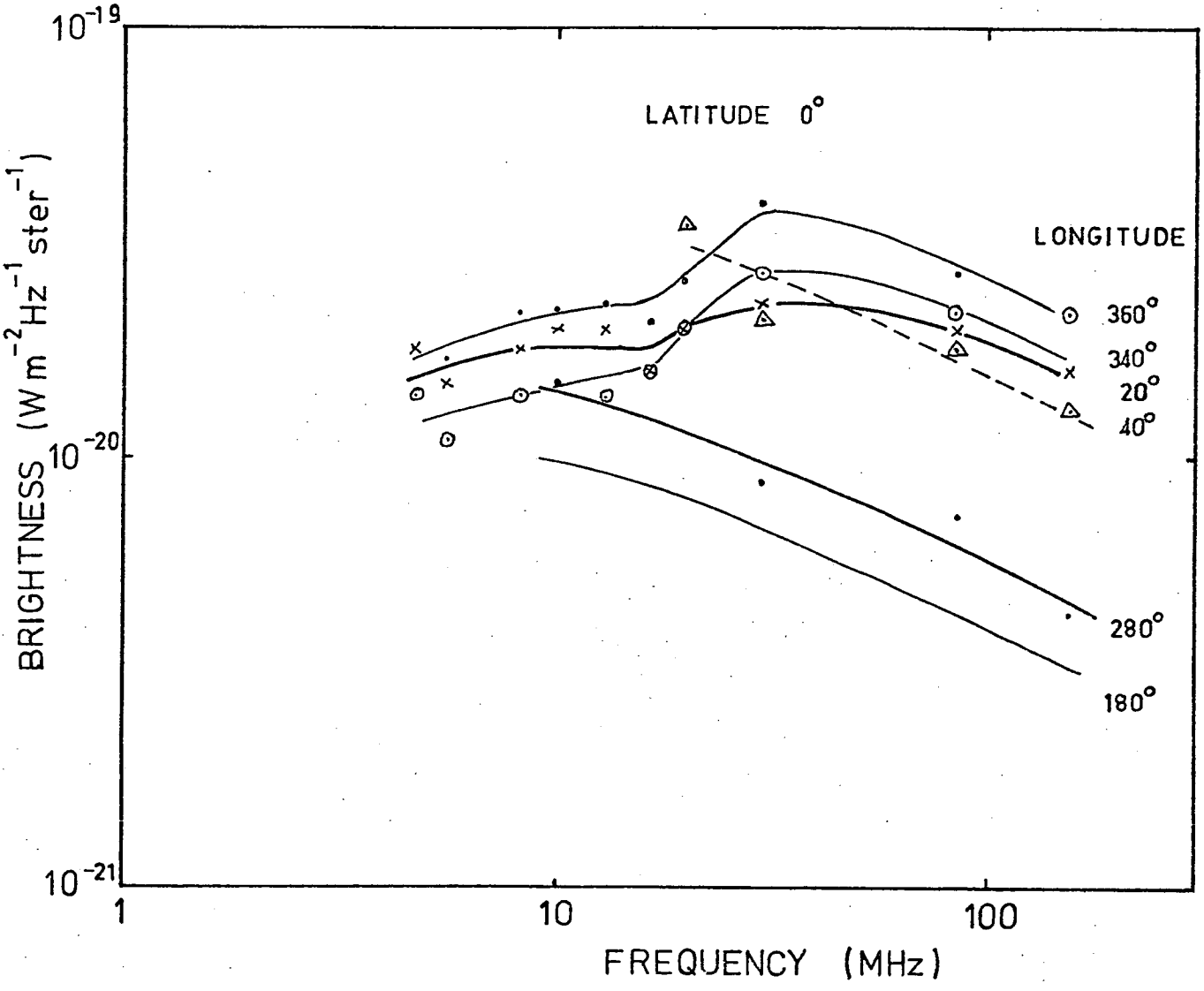
LATITUDE 0°
LONGITUDE
360°
340°
20°
40°
280°
180°
BRIGHTNESS (W m⁻² Hz⁻¹ ster⁻¹)
10⁻¹⁹
10⁻²⁰
10⁻²¹
1
10
100
FREQUENCY (MHz)

FIGURE 6.24

Discussion

The new data shows that the appearance of the sky does not change as rapidly with frequency as had been previously thought. With only the 19.7, 10, 4.7 and 2.1 MHz maps in existence in 1969 it is not surprising that Hamilton (1969) made the statement that "the changes are so great as to make comparisons of the maps difficult". To add to the confusion the contours of the 4.7 MHz map did not represent the data. The new map compiled by the author shows that the minimum along the galactic plane for the region of interest is centred at about 345° in accordance with the 5.6 and 8.3 MHz maps, whereas the map compiled by Ellis and Hamilton had the minimum centred at approximately 0°. It is interesting to note that an earlier version of the map presented by Ellis, Green and Hamilton (1963) did in fact present similar features to those seen in figure 6.14.

In the light of the discussion in Chapter 5 it is felt that the 10 MHz map of Hamilton and Haynes (1968) is in error in the region $270° \lesssim \ell \lesssim 355°$ and $0° \lesssim b \lesssim 60°$. Northern and southern sky surveys at 10 MHz could only be combined if the contours in this region were altered. This was achieved by incorporating 13 MHz data.

When the alterations to the 4.7 and 10 MHz maps have been taken into account it can be seen that there is a gradual trend from the 30 MHz map down to the 4.7 MHz map. Comparisons between the 30 MHz map and the two higher frequency maps are difficult, mainly because the 85 and 153 MHz maps are presented on a very small scale and because the resolution of the former map is not high enough. A comparison of the finer details in the galactic plane is better made with the 85 MHz pencil beam survey of Hill, Slee and Mills (1958).

The 3.7 and 2.1. MHz maps do not present the same features as the higher frequency maps. This is not really surprising as the optical depth changes by a factor of 5 between 4.7 MHz and 2.1 MHz. In the work that follows we shall consider the spectra as defined only to 5 MHz. We do this because the lower frequency data is less reliable due to ionospheric effects and it is apparent from figures 6.21 - 6.23 that the shapes of the spectra below approximately 5 MHz are determined by the 2.1 MHz data points.

REFERENCES FOR CHAPTER 6

CANE, H.V. 1975 Astron. Soc. Aust. 2 339.

CANE, H.V. 1976 Proc. Astron. Soc. Aust. 3 80.

CANE, H.V. & WHITHAM, P.S. 1977 Mon. Not. R. astr. Soc. 178 in press.

ELLIS, G.R.A., GREEN, R.J. and HAMILTON, P.A. 1963 Aust. J. Phys. 16 545.

ELLIS, G.R.A. and HAMILTON, P.A. 1966 Astrophys. J. 143 227.

GEORGELIN, Y.P. and GEORGELIN, Y.M. 1970 Astron. Astrophys. 6 349.

HAMILTON, P.A. 1969 Ph.D. Thesis (Uni. of Tas.).

HAMILTON, P.A. and HAYNES, R.F. 1968 Aust. J. Phys. 21 895.

HAMILTON, P.A. and HAYNES, R.F. 1969 Aust. J. Phys. 22 839.

HILL, E.R., SLEE, O.B. and MILLS, B.Y. 1958 Aust. J. Phys. 11 137.

JONES, B.B. and FINLAY, A.E. 1974 Aust. J. Phys. 27 687.

MATHEWS, H.E., PEDLAR, A. and DAVIES, R.D. Mon. Not. R. astr. Soc. 1973 165 149.

REBER, G. 1968 J. Franklin Inst. 285 1.

RODGERS, A.W., CAMPBELL, C.T. and WHITEOAK, J.B. 1960 Mon. Not. R. astr. Soc. 121 103.

SHAIN, C.A., KOMESAROFF, M.M. and HIGGINS, C.S. 1961 Aust. J. Phys. 14 508.

SIVAN, J.P. 1974 Astron. Astrophys. Suppl. 16 163.

WILSON, T.L., MEZGER, P.G., GARDNER, F.F. and MILNE, D.K. 1970 Astron. Astrophys. 6 364.

YATES, K.W., WIELEBINSKI, R. and LANDECKER, T.L. 1967 Aust. J. Phys. 20 595.

CHAPTER 7

THE LOW FREQUENCY ANALYSIS

Introduction

This chapter presents a specific model to explain the characteristics of the background spectra illustrated and discussed in Chapter 6.

Prior to the introduction of the model we will briefly review the previous low frequency observations of the Galaxy and their interpretation. In particular we are concerned with the information obtained about the distribution of ionized hydrogen.

We assume a basic model and then derive the main parameters from the data. The properties of the model will be discussed and also the limitations of the method used.

Previous Investigations

The first experimental evidence of free-free absorption processes occurring in the Galaxy was found by Shain (1951, 1954) and Shain and Higgins (1954). No discrete regions of absorption were observed (the beam was very broad) but it was found that the ratio of brightness temperature at 18.3 MHz to that at 100 MHz was lower in the direction of the galactic centre than in other directions.

The first observation of individual HII regions in absorption was made by Shain et al. (1961) using a pencil beam 1.4° wide at 19.7 MHz. Very good agreement was found between optically observed HII regions and "radio dark" areas. An extended minimum following the galactic plane out to longitudes ±35° from the centre was attributed to the integrated effect of many distant HII regions that were not individually resolved. There are two dark areas at $\ell = 319°$ and $\ell = 37°$ that do not correspond to the HII regions and

Komesaroff (1961) attributed these to a deficiency of emission, but Gould (1969) and Mills (1971) suggest that this is evidence for absorption taking place in the HI gas.

Observations of spectra of radio sources by Roman and Haddock (1956) showed low frequency cut-offs and led them to suggest the presence of a uniform absorbing layer of ionized hydrogen in the galactic plane. A similar model was adopted by Hoyle and Ellis (1963) to explain the turn over in galactic background spectra obtained by Ellis et al. (1962). They postulated that absorption was taking place in a layer of ionized hydrogen 600 pc thick. Assuming an electron temperature of 10^4 K, they obtained an electron density of $0.1\,cm^{-3}$. In directions away from the galactic plane it was assumed that all the radiation came from a large radio halo.

During the solar minimum 1960-1965 the southern surveys at 2.1 MHz (Reber, 1968) and 4.7 MHz (Ellis and Hamilton, 1966a) were made. Ellis and Hamilton (1966b) combined data from these surveys with new observations at 1.65 and 9.6 MHz and data from surveys at 19.7 MHz (Shain et al., 1961) and 18.3 MHz (Shain and Higgins, 1954). Again the simple model was used and it was found that the density of the absorbing gas was required to increase towards the galactic centre.

The above analysis was based on scans at a single declination but the method was extended to the whole southern sky by Hamilton (1969) and contour maps of the disk radiation, the extra-disk radiation and the absorption coefficent were obtained.

At about the same time the first RAE-1 results became available (Alexander et al., 1969). In the analyses that followed workers used the simple model and devoted their attentions to determining the properties of the absorbing gas. They chose to

neglect the presence of HII regions and to assume that the absorption was taking place in the HI clouds or the intercloud medium (e.g. Alexander et al., 1970; Stephens, 1971).

However, in more recent years observations have been made with instruments with higher resolution and the influence of HII regions has been made apparent; for examples see the discussion in Chapter 5 on the measurements of the local emissivity. Furthermore, the recent wide-field Hα survey by Sivan (1974) of the whole galactic plane delineates these regions and there is a good agreement between discrete absorption regions at low frequencies and optical nebulae (see Caswell, 1976 and Figure 6.16). As has been mentioned this agreement had been illustrated by Shain et al., (1961) using the less sensitive Hα survey of Rodgers et al., (1960).

The simple model used by previous workers consists of two components. These are the disk component, in which the regions of emission and absorption are uniformly mixed, and the extra-disk component. In this model the brightness at a frequency ν is, using formulae given in Chapter 2,

$$I(\nu) = \frac{\langle \eta L \rangle}{\tau} (1 - e^{-\tau}) + I_x e^{-\tau} \qquad (7.1)$$

where η is the volume emissivity of the non-thermal radiation, L is the path length over which the emission occurs, τ is the optical depth of the absorbing gas and I_x is the brightness of the extra-galactic radiation and the radiation from the galactic halo.

There is a major reason for departing from this simple model - to explain the observed reduction in brightness at low latitudes for low frequencies the model requires a very substantial radio halo. In fact, in such a model, all the radiation at latitudes greater than about 20° is produced outside the disk.

In Chapter 5 we have shown that the observations indicate that the extra-galactic radiation contributes at most one-third of the minimum brightness at 85 MHz and that there is little evidence for a radio halo.

The observed reduction in brightness can be obtained by the introduction of an ionized layer which does not extend as far from the galactic plane as the emission layer. Equation (7.1) would still apply, with I_x including disk emission from the layers above and below the galactic plane where no absorption occurs. However, the new spectra obtained by the author require a more complex model.

The Model

The model is illustrated in Figure 7.1 where we show a cross section through the Galaxy perpendicular to the galactic plane. The features of the model are as follows:

1. Synchrotron emission is confined to within 450 pc of the galactic plane. The volume emissivity is non-uniform, with the regions of higher emissivity identified with spiral arms.

2. Only the three spiral arms in the solar neighbourhood are considered; these are assumed to be 1 kpc wide and spaced 1 kpc apart. The local arm is called the S1 arm, the next the S2 arm and the third the S3 arm, in decreasing distance from the galactic centre.

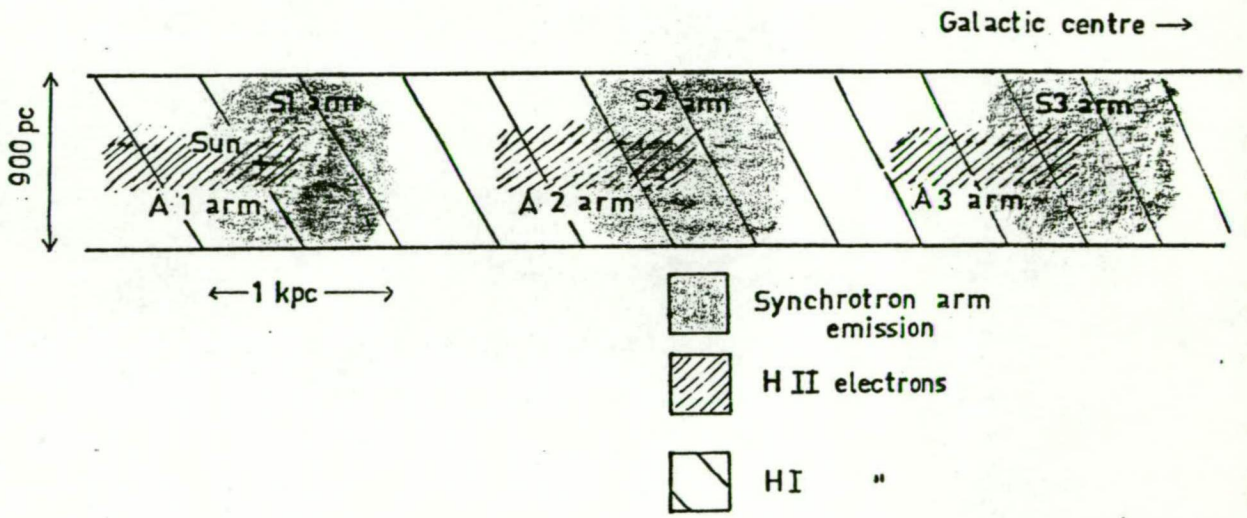

THE MODEL

FIGURE 7.1

3. The Sun is 700 pc from the inner edge of the S1 arm.

4. There is no radio halo but there is an isotropic extra-galactic contribution to the observed emission.

5. Free-free absorption takes place throughout the disk in a uniformly distributed gas which is identified with weak ionization of the HI distribution.

6. Absorption also takes place in HII regions and these are confined to spiral arms which are not coincident with the arms defined by synchrotron emission.

7. The arms defined by HII regions are called A arms and these are 1 kpc thick and are spaced 1 kpc apart. They extend 100-200 pc above and below the galactic plane.

8. The A arms are displaced 700 pc in the anti-centre direction relative to the S arms, as illustrated in Figure 7.1.

9. Absorption in the A1 arm is restricted to discrete HII regions. In the A2 and A3 arms absorption takes place in discrete HII regions and in a diffuse gas between the discrete HII regions. However, the absorption in the A2 and A3 arms is considered to take place uniformly along the path length contained in each arm.

Using the spectra presented in Chapter 6 certain parameters of the model can be evaluated. These are:-

(a) volume emissivities of the S1, S2 and S3 arms,

(b) the absorption coefficient at any frequency of the HI electron gas, and

(c) the absorption coefficients at any frequency of the A2 and A3 arms.

It will be shown that using the derived values the spectra predicted by the model are in agreement with the spectra presented in Chapter 6.

Before deriving the above properties of the model it is important to justify the use of the spectra since they have been obtained from surveys made with instruments of different angular resolution. The resolution of the lowest frequency survey being considered is 5° whereas the highest resolution is 0.8°.

For latitudes greater than about 5° the difference is not significant since there is no small scale structure. There is small scale (~1°) structure close to the galactic plane as may be seen in the 30 MHz survey (Figure 6.18). This is caused by local HII regions. In other directions the sky exhibits a more uniform distribution and it is the distribution of emission in these directions which is used to evaluate the model. The model has been developed to account for a feature which has not been previously reported, namely the plateau in the low latitude spectra for frequencies between approximately 6 and 15 MHz. At several longitudes the plateau extends to 19.7 MHz. The resolution of the instruments used at 19.7, 16.5 and 13 MHz are comparable, and thus the plateau has not been introduced by the combination of data obtained with instruments of different angular resolution. The main consequence of the observing telescopes

having finite resolution is the lessening of the effect of distant emission regions.

(a) Volume Emissivities of the S Arms

For lines of sight illustrated in Figure 7.2 path lengths in the various components can be determined. For example, the line of sight for b = 20° is composed of approximately 700 pc in the S1 arm and 550 pc in the inter-arm region. If values are assumed for (a) the ratio R of the emissivity of the S1 arm to the emissivity of the inter-arm regions and (b) the extra-galactic contribution T_{eg} then a value can be calculated for the emissivity η_1 of the S1 arm.

If the volume emissivity η of synchrotron emission is constant over a path length L then the brightness temperature T is given by,

$$T = \eta \times L$$

If T is in K and L is in pc then η is in K pc^{-1}.

Let $T_{20°}$ be the observed temperature at latitude 20° at some frequency ν. Then,

$$T_{20°} \simeq 700 \times \eta_1 + 500 \times \frac{\eta_1}{R} + T_{eg} \qquad (7.2)$$

where T_{eg} and η_1 have values corresponding to frequency ν.

Similarly the observed temperature at latitude 10° is given by,

$$T_{10°} \simeq T_{20°} + 450 \times \frac{\eta_1}{R} + 700 \times \eta_2$$

(where η_2 is the emissivity of the S2 arm) and the observed temperature at latitude 5° is given by,

$$T_{5°} \simeq T_{10°} + 200 \times \eta_2 + 1000 \times \frac{\eta_1}{R} + 900 \times \eta_3$$

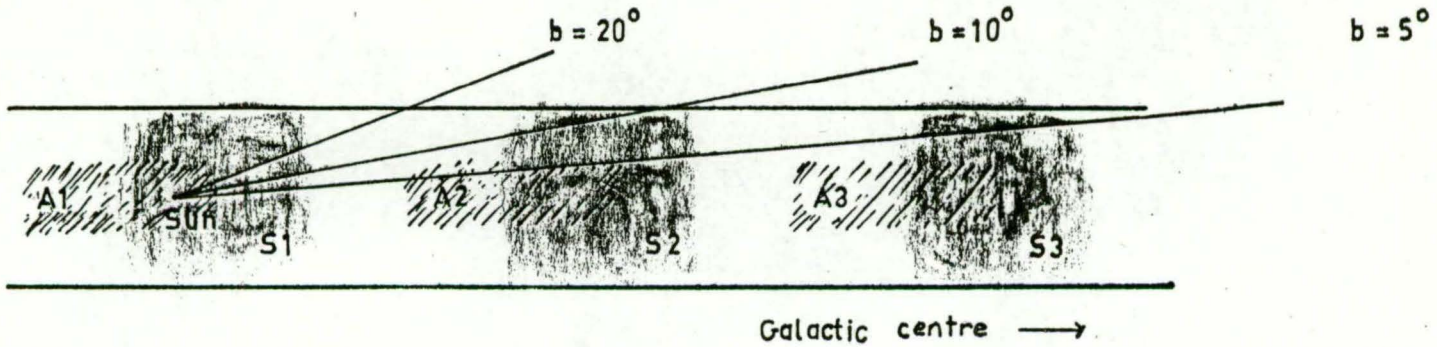

LINES OF SIGHT THROUGH THE GALAXY

FIGURE 7.2

From the spectra the average temperature for b = 20° at 85 MHz is 2200 K. Assume an extra galactic contribution of 280 K. From equation (7.2) we have

$$\eta_1 = \frac{(2200 - 280)}{700 + \frac{550}{R}}$$

R must be chosen so that η_1, the emissivity of the S1 arm has an acceptable value. Taking R = 8 gives η_1 = 2.5 K pc^{-1}, at 85 MHz. Assuming a temperature spectral index of 2.6 this is equivalent to a value of 6.5×10^{-40} watts $m^{-3}Hz^{1}ster^{-1}$at 10 MHz which is just below the upper limit obtained in Chapter 5.

Similarly, the values obtained for η_2 and η_3 are 2 K pc^{-1} and 1.5 K pc^{-1} at 85 MHz.

(b) Absorption Coefficients

To simplify the notation we introduce the absorption function F' defined by

$$F' = \frac{\tau \nu^{2.1}}{L} \propto n_e^2 T_e^{-1.35} \qquad (7.3)$$

where τ is the optical depth at frequency ν corresponding to a path length L.

Let F be the absorption function for the HI gas. F2 and F3 are the absorption functions for the A2 and A3 arms. Values for F, F2, F3 can be calculated from observed brightness temperatures. The calculation is similar to that used when calculating the emissivities of the S arms. However, temperatures need to be calculated as a function of frequency. We assume galactic and extra-galactic temperature spectral indices of 2.6 and 2.75.

The temperature at b = 20° is given by

$$T_{20°} = T_{S1} \frac{(1-e^{-\tau_1})}{\tau_1} + T_{IA} \frac{(1-e^{-\tau_2})e^{-\tau_1}}{\tau_2} + T_{eg}\, e^{-(\tau_1 + \tau_2)}$$

where T_{S1}, T_{IA} and T_{eg} are contributions to the emission from the S1 arm, the inter-arm region and from extra-galactic regions. τ_1 and τ_2 are optical depths due to the path lengths in the S1 arm and the inter-arm region. More specifically, at a frequency ν we have,

$$T_{20}(\nu) = 700 \times 2.5 \times \left(\frac{85}{\nu}\right)^{2.6} \left[\frac{1 - e^{-700\ F\ \nu^{-2.1}}}{700\ F\ \nu^{-2.1}}\right]$$

$$+ 550 \times 0.3 \times \left(\frac{85}{\nu}\right)^{2.6} \left[\frac{1 - e^{-550\ F\ \nu^{-2.1}}}{550\ F\ \nu^{-2.1}}\right] e^{-700\ F\ \nu^{-2.1}}$$

$$+ 280 \times \left(\frac{85}{\nu}\right)^{2.75} e^{-1250\ F\ \nu^{-2.1}} \qquad (7.3)$$

An initial estimate of F obtained from the shape of the b = 20° spectra can be refined by iterating with equation (7.3). The value obtained is

$$F \simeq 1.8 \times 10^{-2}$$

for L in pc, n_e in cm, ν in MHz and T in K.

This value can now be substituted in the equation for the temperature at b = 10° which is

$$T_{10}(\nu) = 700 \times 2.5 \times \left(\frac{85}{\nu}\right)^{2.6} \left[\frac{1 - e^{-700\ F\ \nu^{-2.1}}}{700\ F\ \nu^{-2.1}}\right]$$

$$+ 1000 \times 0.3 \times \left(\frac{85}{\nu}\right)^{2.6} \left[\frac{1 - e^{-1000\ F\ \nu^{-2.1}}}{1000\ F\ \nu^{-2.1}}\right] e^{-700\ F\ \nu^{-2.1}}$$

$$+ 700 \times 2.0 \times \left(\frac{85}{\nu}\right)^{2.6} \left[\frac{1 - e^{-700\ F\ \nu^{-2.1}}}{700\ F\ \nu^{-2.1}}\right] e^{-1700\ F\ \nu^{-2.1}}$$

$$+ 280 \times \left(\frac{85}{\nu}\right)^{2.75} e^{-2400\ F\ \nu^{-2.1}}$$

The calculated spectrum is a reasonable fit to the observations, as shown in Figure 7.3(a).

The b = 5° line of sight should just intersect the A2 arm. The method for evaluating F2 involves calculating the temperatures for b = 5° neglecting the absorption in the A2 arm and then comparing these with the observed temperatures.

Assuming that the height of the A2 arm is about 200 pc the temperature at b = 5° is given by

$$T_5(\nu) = 700 \times 2.5 \times \left(\frac{85}{\nu}\right)^{2.6} \left[\frac{1 - e^{-700\ F\ \nu^{-2.1}}}{700\ F\ \nu^{-2.1}}\right]$$

$$+ 1000 \times 0.3 \times \left(\frac{85}{\nu}\right)^{2.6} \left[\frac{1 - e^{-1000\ F\ \nu^{-2.1}}}{1000\ F\ \nu^{-2.1}}\right] e^{-700\ F\ \nu^{-2.1}}$$

$$+ e^{-900\ F2\ \nu^{-2.1}} \left\{ 900 \times 2.0 \times \left(\frac{85}{\nu}\right)^{2.6} \left[\frac{1 - e^{-900\ F\ \nu^{-2.1}}}{900\ F\ \nu^{-2.1}}\right] e^{-1700\ F\ \nu^{-2.1}} \right.$$

$$+ 1000 \times 0.3 \times \left(\frac{85}{\nu}\right)^{2.6} \left[\frac{1 - e^{-1000\ F\ \nu^{-2.1}}}{1000\ F\ \nu^{-2.1}}\right] e^{-2600\ F\ \nu^{-2.1}}$$

$$+ 900 \times 1.5 \times \left(\frac{85}{\nu}\right)^{2.6} \left[\frac{1 - e^{1000\ F\ \nu^{-2.1}}}{1000\ F\ \nu^{-2.1}}\right] e^{-3500\ F\ \nu^{-2.1}}$$

$$\left. + 280 \left(\frac{85}{\nu}\right)^{2.75} e^{-4400\ F\ \nu^{-2.1}} \right\} \qquad (7.4)$$

Equation (7.4) is of the form

$$T_5 = T_A + e^{-\tau}\ T_B$$

where T_A and T_B can be calculated. If $T_5(\nu)$ is calculated taking $\tau = 0$ and compared with the observed temperatures at latitude 5° then τ and hence F2 can be evaluated. The calculated value for F2 is approximately 0.15, where the same units apply as for F.

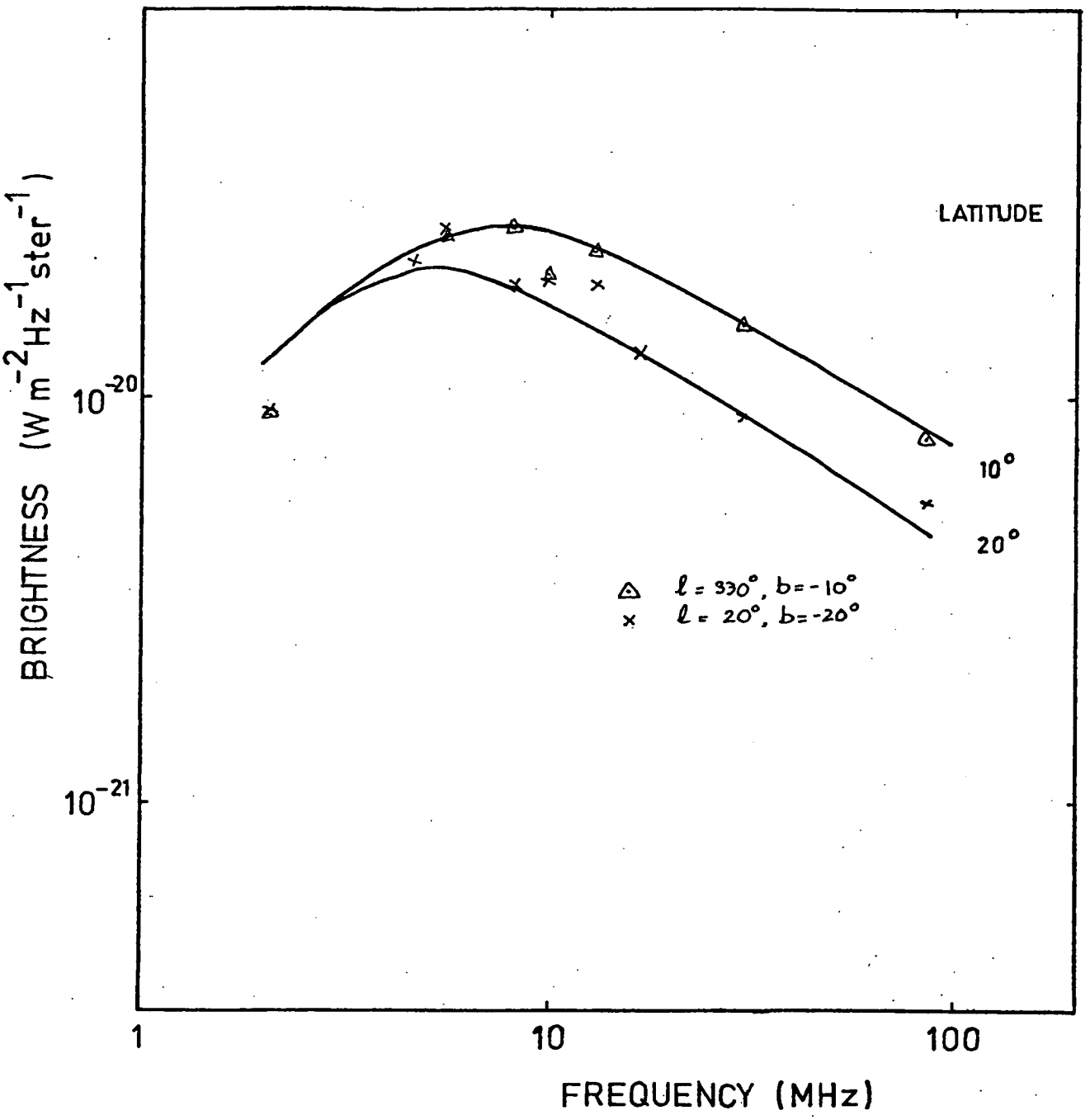

Spectra predicted by the model

FIGURE 7.3 (a)

The line of sight for b = 0° intersects the A3 arm and F3 can be determined, after allowance is made for emission coming from beyond the innermost arm. To reproduce the observed 85 MHz brightness at b = 0° an extra component of 6000 K is required. This component does not represent the total brightness of the galactic centre and the arms beyond the centre because the finite beam of the observing telescope tends to weight nearby emission regions more heavily. Hence we consider the galactic plane emission to be the emission which would be observed at b ≃ 0°.

To simplify the calculation we consider the HII gas to be situated between the arm and interarm regions and to have negligible width when determining path lengths in the emitting regions.

To simplify the calculation for the temperature at b ≃ 0° we introduce a function A_ν given by

$$A_\nu = 1000\ F\ \nu^{-2.1}$$

which is just the optical depth in 1000 pc of HI gas at a frequency ν.

The temperature at b ≃ 0° is given by

$$\begin{aligned}
T_{\simeq 0}(\nu) &= 700 \times 2.5 \times \left(\frac{85}{\nu}\right)^{2.6} \left[\frac{1 - e^{-700\ F\ \nu^{-2.1}}}{700\ F\ \nu^{-2.1}}\right] \\
&+ 1000 \times 0.3 \times \left(\frac{85}{\nu}\right)^{2.6} \left[\frac{1 - e^{-A_\nu}}{A_\nu}\right] e^{-700\ F\ \nu^{-2.1}} \\
&+ e^{-1000\ F2\ \nu^{-2.1}} \left\{ 1000 \times 2 \times \left(\frac{85}{\nu}\right)^{2.6} \left[\frac{1 - e^{-A_\nu}}{A_\nu}\right] e^{-1.7 \times A_\nu} \right. \\
&\left. + 1000 \times 0.3 \times \left(\frac{85}{\nu}\right)^{2.6} \left[\frac{1 - e^{-A_\nu}}{A_\nu}\right] e^{-2.7 \times A_\nu} \right\} \\
&+ e^{-(1000\ F2\ \nu^{-2.1} + 1000\ F3\ \nu^{-2.1})} \left\{ 1000 \times 1.5 \times \left(\frac{85}{\nu}\right)^{2.6} \left[\frac{1 - e^{-A_\nu}}{A_\nu}\right] e^{-3.7 \times A_\nu} \right. \\
&+ 280 \times \left(\frac{85}{\nu}\right)^{2.75} e^{-4.7 \times A_\nu} \\
&\left. + 6 \times 10^3 \left(\frac{85}{\nu}\right)^{2.6} e^{-4.7 \times A_\nu} \right\}
\end{aligned}$$

It is found that the best fit to the data is obtained when F3 = 0.75.

Finally we calculate the values of n_e and T_e appropriate to the values for F, F2 and F3. From equations (2.5) and (7.3) we have

$$F = 1.64 \times 10^5 \, n_e^2 \, T_e^{-1.35}$$

For the HI gas we have $F = 1.8 \times 10^{-2}$ which gives

$$n_e^2 \, T_e^{-1.35} = 1.1 \times 10^{-7} \text{ cm}^{-6} \text{ K}^{-1.35}$$

Taking $n_e = 0.03$ cm^{-3} we obtain $T_e \simeq 800$ K. These values are acceptable for the free electrons in the HI gas.

F2 and F3 are 0.15 and 0.75 giving $n_e^2 \, T_e^{-1.35} = 9 \times 10^{-7}$ and 4.5×10^{-6} cm^{-6} K$^{-1.35}$.

If we assume $T_e = 6000$ K we obtain $n_e^2 = 0.1$ and 0.6 cm^{-6}. These values are typical of mean square electron densities obtained from measurement of low density HII regions.

Results

In Figure 7.3(b) we show the polar spectrum predicted by the model together with the south galactic polar measurements. Although the predicted spectrum is a good fit to the observations a better fit at high frequencies is obtained if the path length in the local arm is slightly less than 400 pc, rather than 450 pc.

In Figure 7.3(c) we show the set of spectra fitted to the data when deriving the parameters of the model. It can be seen that the basic features as discussed in Chapter 6 are present. The agreement is best for the sets of spectra at longitudes 330°, 360° and 20°, the longitudes relatively free of discrete HII regions.

Most of the discrete HII regions lie in the next spiral arm and the model predicts that they should have no effect on the spectra at frequencies below about 10 MHz, since at these frequencies all the radiation is expected to come only from the local arm. The effect of

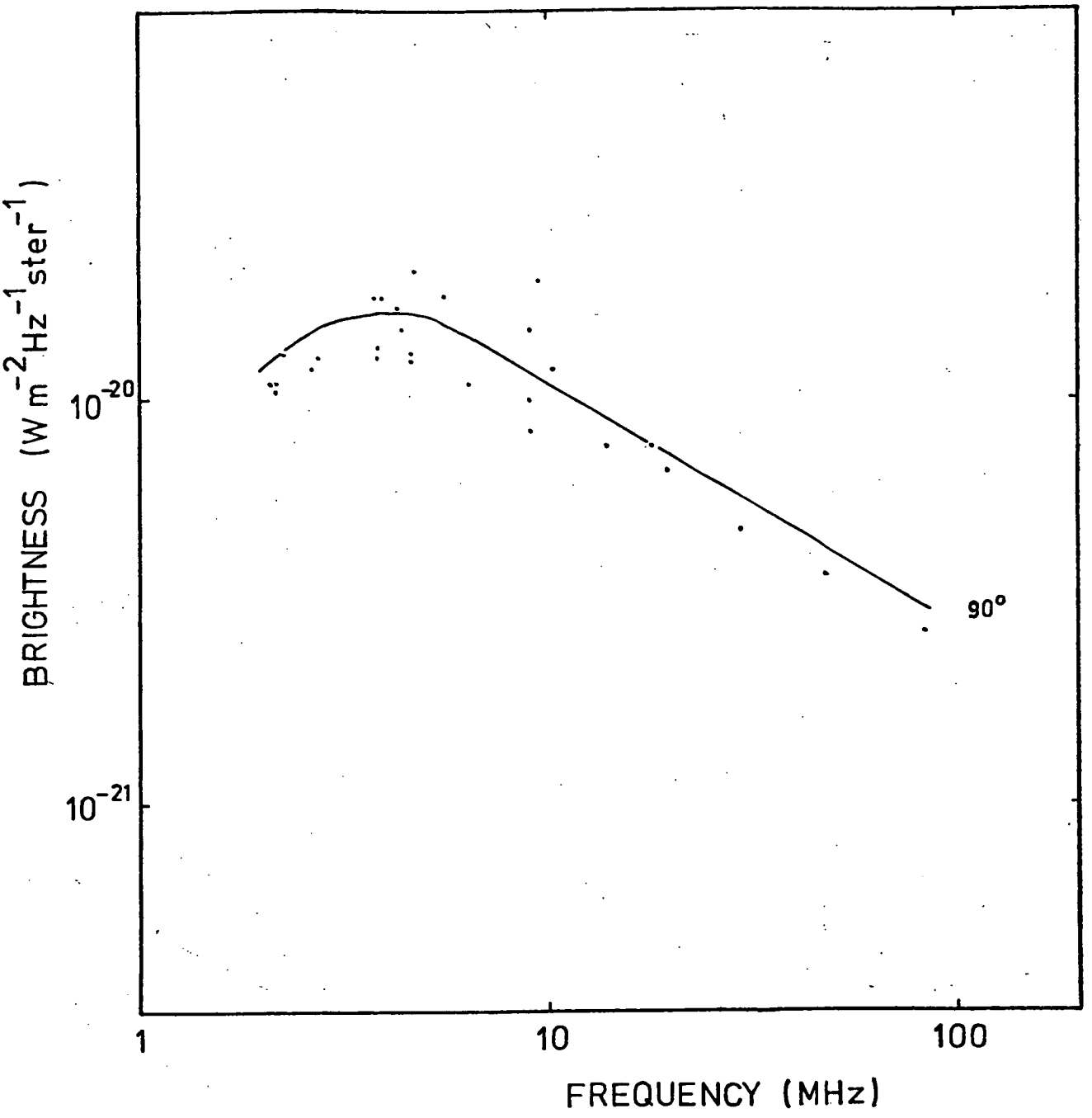

Spectra predicted by the model

FIGURE 7.3 (b)

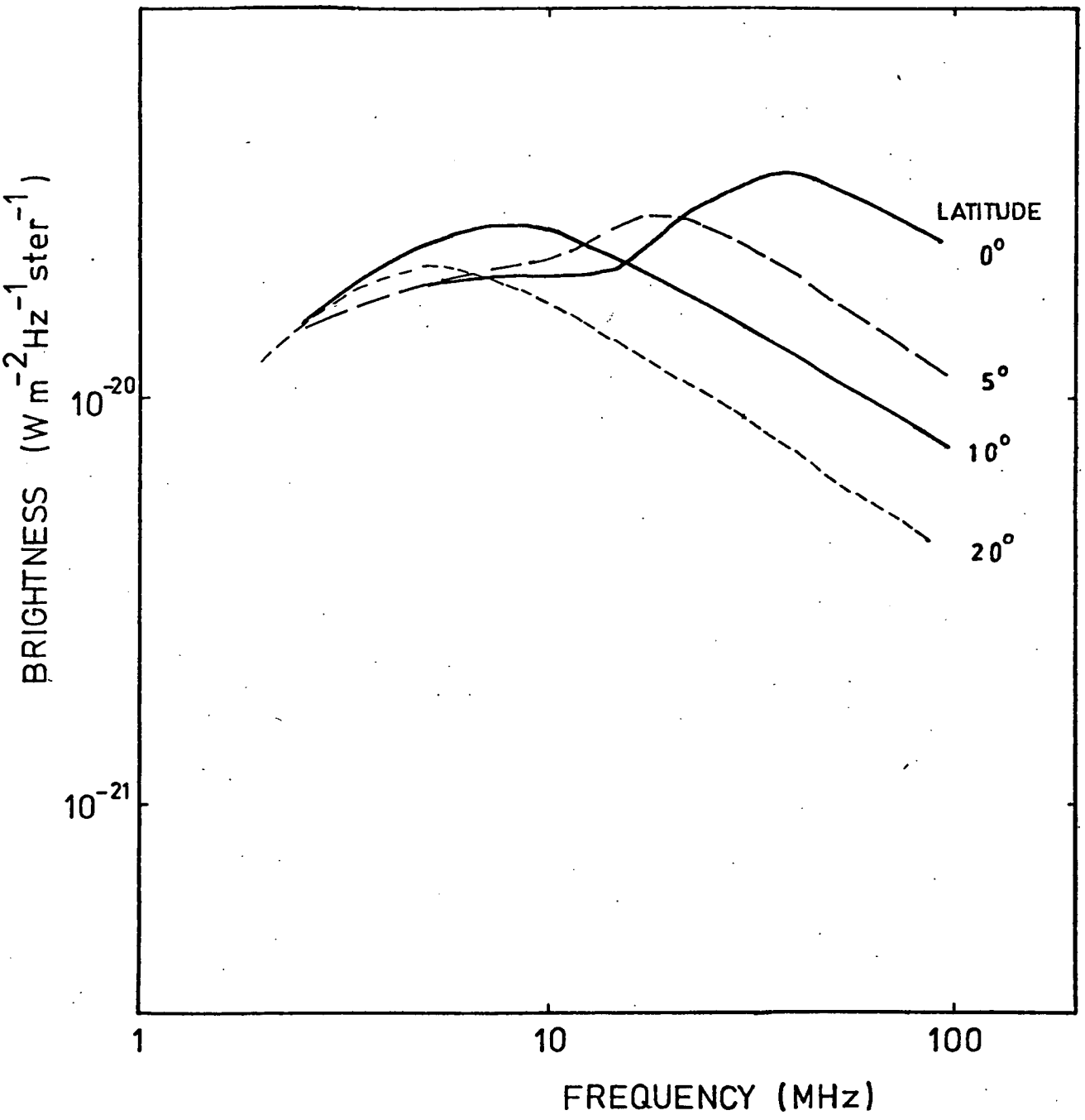

Spectra predicted by the model

FIGURE 7.3 (c)

the HII regions at higher frequencies would be to reduce the brightness near the galactic plane. In the limit when the optical depth in an HII region is greater than unity the brightness along the plane should be reduced to the level of the radiation at b = 20°.

The model predicts that the radiation at b = 0° can not be less than that at b = 20° and this means that it can not explain the galactic plane spectra for longitudes in the range 340° - 355° without modification. In general the model can not explain the variation of the emission along the galactic plane at frequencies below about 10 MHz. The variation could be caused by the HII regions in the A2 arm in which case the model would require major revision. This possibility appears likely because a smoothed version of the 16.5 MHz map to a resolution of 3° presents similar features to those seen in the lower frequency maps. However, it would mean that the b = 0° radiation would be generated over a longer path length than the b = 20° radiation and yet at low frequencies for longitudes in the range 340° - 355°, $T_{0°}$ is much less than $T_{20°}$. This situation could occur if we have under-estimated the extra-galactic and/or halo radiation.

Alternatively, the structure of the low frequency maps could arise from a variation of the synchrotron emissivity in the local arm or be caused by localized absorption in the local (A1) arm. The former is not contrary to observation as it was found in Chapter 5 that emissivity measurements in different directions do give different results. Also the presence of the spurs, which are local features, shows that the variations in emission can occur within a few hundred parsecs of the Sun. However, since this change in emissivity would only occur at low frequencies it would mean that the spectra in these directions would be curved. Although it seems likely that in many regions of the Galaxy curved emission spectra are more appropriate than straight spectra

it seems improbable that the electron energy spectrum could change over an area as small as that under discussion.

It seems likely that the structure of the low frequency maps is due to localized absorption in the local arm; this could perhaps be tested by other types of observation. For example the survey of OB-stars by Klare and Neckel (1970) shows that there are many early stars close to the Sun in the longitude range 340° - 350° and these would give rise to regions of ionized hydrogen. Similarly it can be seen in Figure 6.16 that there is diffuse Hα emission in this longitude range in addition to the obvious discrete regions. An estimate of the distance to this gas is required.

Another feature of the spectra which is not explained by the model is the variation of intensity with latitude seen in the low frequency data. It is found that as the observing frequency decreases, the latitude of maximum intensity increases, until at 2.1 MHz the maximum is almost at the south galactic pole. This implies that the optical depth in the gas decreases more rapidly with increasing latitude than does the emission. To accommodate this feature we would have to postulate that the absorption function is a function of latitude. In addition the minimum brightness at 2.1 MHz is near the galactic centre whereas at higher frequencies (i.e. 5 - 10 MHz) the minima occur at $\ell \simeq 345°$ and $\ell \simeq 18°$.

At very low frequencies it is expected that no radiation will be received from regions beyond a few hundred parsecs of the Sun. Thus structure seen at these frequencies must be caused by very local phenomena. If the two minima seen at frequencies in the range 5 - 10 MHz are due to localized absorption within several hundred parsecs of the Sun, then the single minimum seen at 2.1 MHz may be caused by an absorbing region even closer to the Sun. It is interesting to note that the Hα survey of Sivan shows emission near to the galactic centre

which is not seen in absorption and thus may be very close to the Sun.

Although the model has been derived to explain spectral variations with latitude for specific longitudes it is to be hoped that it will also predict longitude variations. However, without the introduction of the contribution of the spurs only moderate success can be achieved.

We adopt the spiral arm model of Georgelin and Georgelin (1976), who combined data from observations of HII regions, the high frequency radio continuum and neutral hydrogen. The spiral pattern has two symmetrical pairs of arms. In this model the Sun is not in a spiral arm but rather it is believed that the Sun lies in an inter-arm link. To create our model we have sketched in synchrotron arms on the inside of the arms proposed by Georgelin and Georgelin and placed the Sun within a branch of the S2 arm.

Since it is not possible to estimate the contribution of the arms beyond the galactic centre and because of the finite resolution of the observing instruments we will examine the longitude distribution for latitudes greater than approximately 5°.

In Figure 7.4 we show the distribution of the arms with galactic longitude and the circles where lines of sight at particular latitudes cut through the galactic disk. It can be seen that the emission should have steps at longitudes of approximately 325° and 25° where the line of sight is tangential to the S3 arm. Further steps should occur at 295° and 40°. These features were built into the model by Georgelin and Georgelin although the specific longitudes of the steps have been decreased slightly by placing the S arms on the inside of the A arms.

The model has been derived in such a way that the sudden drop in intensity of the $b \simeq 0°$ spectra is due to absorption in the A3 arm.

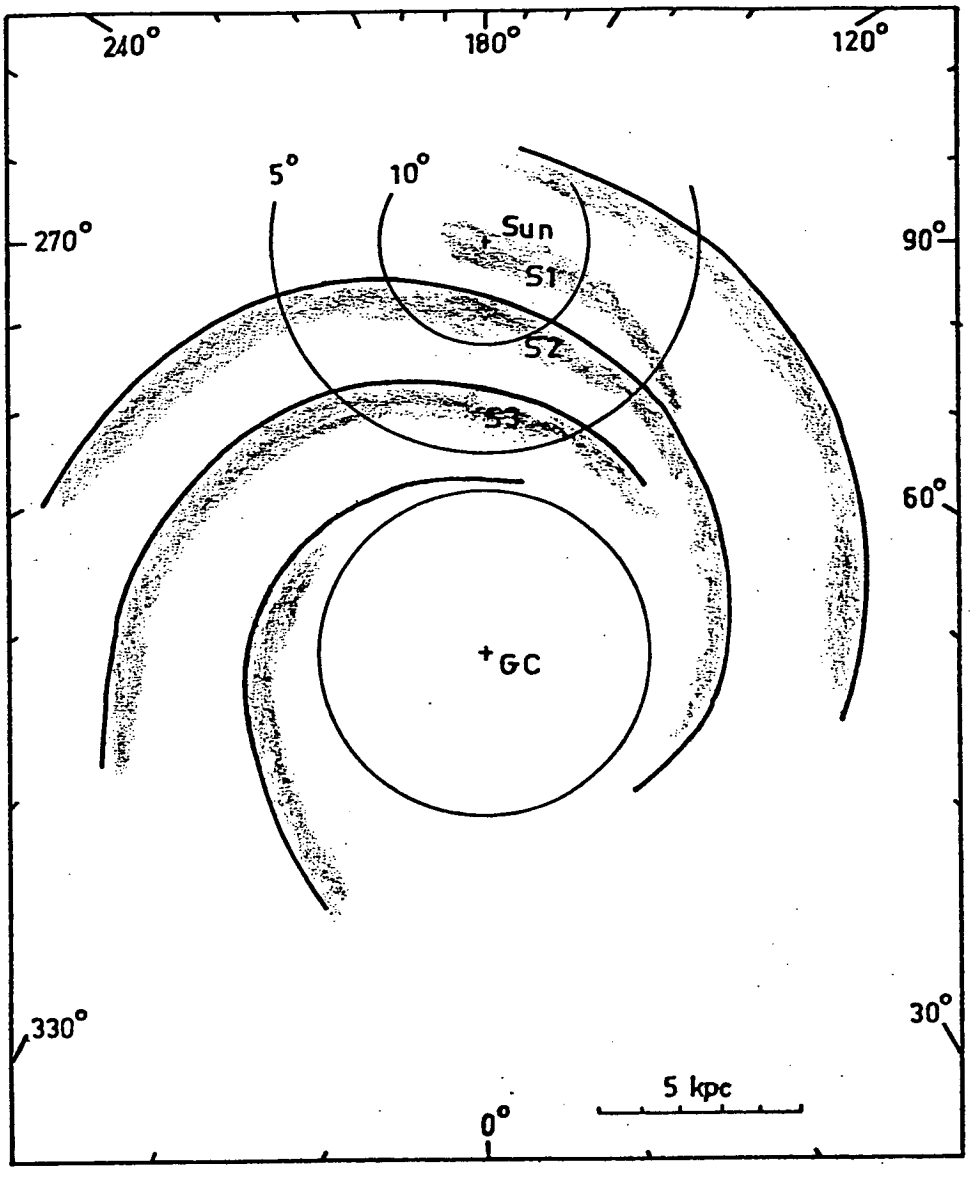

Spiral model of our Galaxy as proposed by Georgelin and Georgelin (1976). Synchrotron arms of the present model are sketched in. Arcs of circles centred on the Sun illustrate where lines of sight intersect the upper surface of the galactic disk.

FIGURE 7.4

Thus this feature should only occur for lines of sight which intersect the A3 arm, that is for longitudes within the range $325° \lesssim \ell \lesssim 35°$.

We now estimate the temperature at $b = 5°$ for longitudes $0°$, $315°$ and $290°$, at 85 MHz.

At longitude $0°$ the line of sight includes approximately 2500 pc of inter-arm gas, 1000 pc of S2 and S3 arm gas and 700 pc of S1 arm gas. Using the calculated emissivities this gives

$$T_{0,5}(85) = 2500 \times 0.3 + 1000(2 + 1.5) + 700 \times 2.5 \text{ K}$$

With an additional 280 K from extra-galactic sources this gives

$$T_{0,5}(85) = 6200 \text{ K}.$$

Similarly at $315°$ and $290°$

$$T_{315,5}(85) = 2500 \times 0.3 + 1000 \times 2 + 700 \quad 2.5 + 280 \text{ K}$$

$$= 4700 \text{ K}$$

and $$T_{290,5}(85) = 2000 \times 0.3 + 700 \times 2.5 + 280 \text{ K}$$

$$= 2600 \text{ K}.$$

The agreement with the 85 MHz map (Figure 5.3) is quite good. The observed temperatures are 6000 K, 3700 K and 2500 K for southern latitudes.

The temperatures for $b = 10°$ can be calculated in a similar manner. The calculated values are 4330 K, 3330 K and 2330 K whereas the observed values are 4000 K, 2500 K and 1700 K.

For longitudes in the range $230° \lesssim \ell \lesssim 130°$ the model predicts a

uniform temperature of about 2000 K for b = 20°. Outside this longitude range the model predicts, for this latitude, a temperature of 1000 K. It can be seen in Figure 6.19 that there is considerable variation with longitude of the temperatures at latitudes of 20° from the galactic plane. In the present model one must attribute this variation to the presence of the spurs. Moreover, the calculated temperatures assume a constant emissivity in the local arm whereas observations indicate that the emissivity of the local arm does vary.

A region of particular interest is the anti-centre region. In this direction the local emission arm contributes about 750 K at 85 MHz. Taking into account the extra-galactic contribution of 280 K the resulting temperature is 1030 K, which is about half the observed brightness temperature. This means that the emitting regions do not extend far beyond the local arm. Another inter-arm region and another arm of emissivity 0.7 K pc^{-1} would be sufficient to explain the observations. The shape of the low frequency end of the anti-centre spectrum is indeterminate due to a lack of data. If the spectrum turns over near 10 MHz then the absorption function of the A1 arm would need to be greater than 0.018 in the anti-centre direction.

Discussion

Emission Properties

The initial assumption is that the synchrotron emission is confined to spiral arms. This is consistent with the observed variations in emission with longitude. The width and spacing of the arms is probably the correct order of magnitude as observations of HII regions define this sort of distribution.

The position of the Sun in the local arm is not the same as in previous models of the Galaxy. Price (1974) found that his model provided a better fit to the data when he placed the Sun towards the inner edge of the local arm, whereas Yates (1968) found the best fit if the Sun was slightly displaced from the centre towards the outer edge. The model of Novaco and Vandenberg (1972) puts the Sun in a similar position to the Price model.

However certain observations, for example the results of the emissivity analysis in Chapter 5, are more readily explained if the Sun is situated towards the outer edge of the local arm. Certainly the Sun would need to be within the local arm to explain the high latitude brightness temperatures if we are not including a radio halo in our model.

The Sun is placed 200 pc on the anti-centre side from the centre of the local arm. This distance is nominal within limits but if the Sun is moved closer to the galactic centre the local arm emissivity must be increased, and also it becomes difficult to explain the latitude variation in emission for frequencies near 8 MHz where all the radiation is expected to come from the local arm.

The half-height of the synchrotron emission is difficult to determine. Even if an accurate value for the local emissivity was known it would not be possible to evaluate the half-height of the emission from polar brightness values because of the uncertainty about the amount of radiation coming from beyond the galactic disk. The fact that the model correctly predicts southern polar brightness temperatures while at the same time predicting an emissivity of the local arm compatible with direct estimates justifies our assumption that the synchrotron emission is confined to within 450 pc of the galactic plane. The condition that the line of sight for b = 10° intersects the S2 arm and the line of sight for b = 5° intersects the S3 arm puts a lower limit of 400 pc on the half-height of the emission. If a half-height smaller than 400 pc is chosen then the arms must be placed closer together.

The width of the arms does not affect the results qualitatively but choosing narrower arms will lead to higher emissivities.

The value derived for the emissivity of the local arm is within the limits determined in Chapter 5. The fact that the local arm has a higher emissivity than the inner arms is contrary to the usual assumption that the volume emissivity in the Galaxy decreases with distance from the galactic centre. However, the result is not inconsistent with information obtained from plots of brightness temperature T_b against cosec b where b is galactic latitude.

Consider the data presented by Baldwin (1967) (see Figure 7.5) where 400 MHz brightness temperatures are plotted against cosec b for galactic longitudes ℓ = 4° and ℓ = 70°. For ℓ = 4° the relation between T_b and cosec b is approximately represented by a straight line for

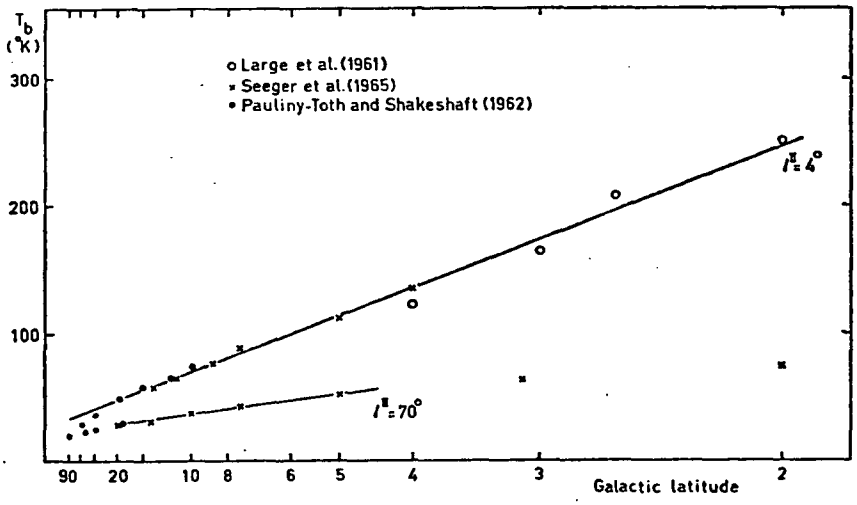

Brightness temperature T_b at 400 MHz as a function of latitude b (plotted as cosec b), for galactic longitudes $l^{II} = 4°$ and $l^{II} = 70°$.

FIGURE 7.5

after Baldwin (1967)

$20° \geq b \geq 2°$. If the straight line had held for latitudes up to 90° it would mean that the Galaxy could be represented as a flat disk of uniform emissivity since in this case,

$$T_b = \eta_1 L_0 \text{ cosec } b + C$$

where η_1 is the emissivity, L_0 is the half-height of the disk and C represents any isotropic contribution. However, for latitudes greater than 20°, where the observations are dominated by emission generated close to the Sun, the measured values of T_b fall below the line fitted to the low latitude data. This means that the emissivity must change near the Sun.

Assume the Sun is in a spherical region of radius L_0 and let the emissivity in this region be η_2. The resulting variation of brightness temperature with cosec b, ignoring any isotropic component, is given by

$$T_b = (\eta_1 L_0 \text{ cosec } b - \eta_1 L_0) + \eta_2 L_0$$

$$= \eta_1 L_0 \text{ cosec } b + (\eta_2 L_0 - \eta_1 L_0)$$

This is a straight line which is parallel to the line representing a disk of constant emissivity η_1, but is displaced up or down the temperature axis depending on whether $\eta_2 > \eta_1$ or $\eta_2 < \eta_1$. See Figure 7.6(b).

Now assume the Sun is in a region as illustrated in Figure 7.6(c). For lines of sight contained within this region the variation of brightness temperature with cosec b is given by

$$T_b = \eta_2 L_0 \text{ cosec } b.$$

For longer path lengths

$$T_b = (\eta_1 L_0 \text{ cosec } b - \eta_1 L_1) + \eta_2 L_1$$

$$= \eta_1 L_0 \text{ cosec } b + (\eta_2 - \eta_1) L_1$$

(a)

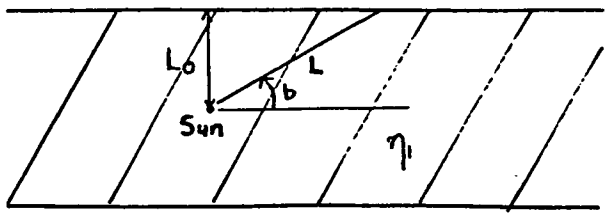

$$T_b = \eta_1 L$$
$$= \eta_1 L_0 \text{ cosec } b$$

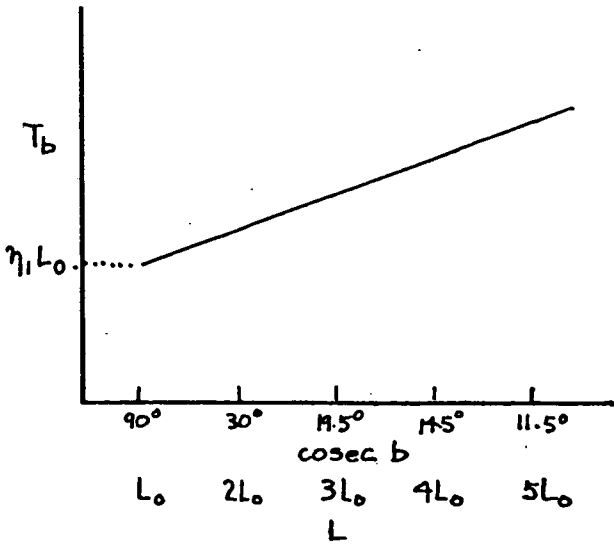

(b)

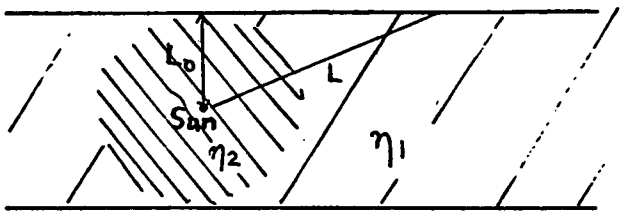

$$T_b = (\eta_1 L_0 \text{ cosec } b - \eta_1 L_0) + \eta_2 L_0$$
$$= \eta_1 L_0 \text{ cosec } b + (\eta_2 - \eta_1) L_0$$

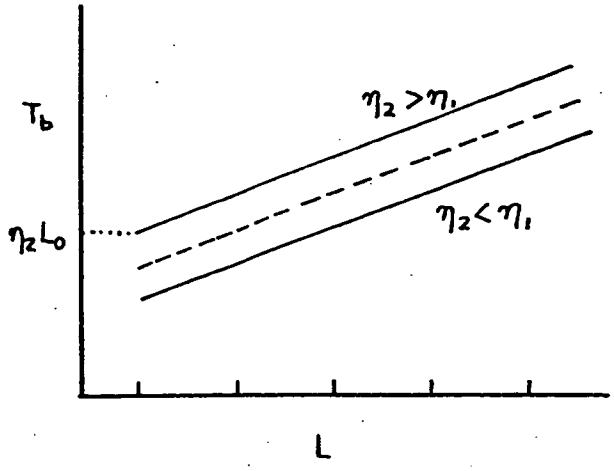

(c)

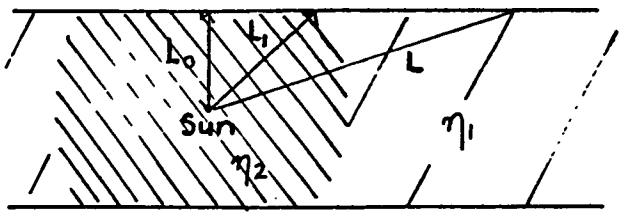

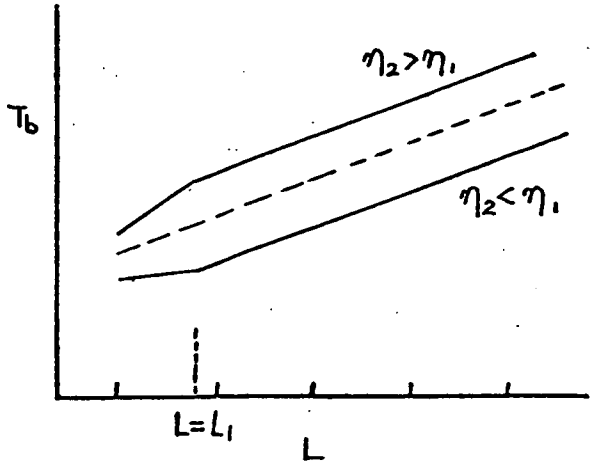

If $L \leq L_1$

$$T_b = \eta_2 L_0 \text{ cosec } b$$

If $L > L_1$

$$T_b = (\eta_1 L_0 \text{ cosec } b - \eta_1 L_1) + \eta_2 L_1$$
$$= \eta_1 L_0 \text{ cosec } b + (\eta_2 - \eta_1) L_1$$

FIGURE 7.6

Thus the variation with brightness temperature with cosec b for all path lengths is two straight line segments. The slopes of these lines are proportional to the emissivities of the two regions. It can be seen from Figure 7.6(c) that if the high latitude line is below the continuation of the low latitude line then η_2 must be greater than η_1.

Absorption Properties

The existence of a uniformly distributed electron gas with a half-height of about 450 pc is consistent with observations, principally those of pulsar signal dispersion as discussed in Chapter 4.

Although we expect HII regions to be confined to spiral arms where the young stars exist, the incorporation of HII arms increases the complexity of the model. However their existence is required by our interpretation of the data.

For frequencies below approximately 30 MHz the intensity decreases as the line of sight approaches the plane. The decrease in intensity for directions free of local HII regions implies the existence of a highly absorbing region with a narrow distribution perpendicular to the galactic plane. However this decrease only occurs for longitudes in the range $320° \lesssim \ell \lesssim 40°$ and suggests the presence of a ring or disk of ionized hydrogen. Assuming the Sun is 10 kpc from the galactic centre this distribution must be about 4 kpc from the Sun.

We have interpreted this distribution as a spiral arm composed of discrete HII regions and a diffuse gas due to low density HII regions.

The decrease in intensity is observed at latitudes up to about 5°. Unless the ionized gas ring or arm extends to 300 pc or more above the galactic plane it can have little effect at these latitudes. Since

HII regions are observed to be confined to within about 100 pc of the galactic plane, another absorbing arm closer to the Sun is required to explain the observations. To maintain uniformity and because observations indicate the presence of HII regions in the locality of the Sun, we introduced a third HII arm in the solar region.

The width and spacing of the A arms are in agreement with the features seen in Figure 4.1. The position of the Sun on the inside edge of the local HII arm is also established in this diagram. The displacement of the A arms relative to the S arms is necessary if the Sun is placed well within the local synchrotron emission arm. The possibility that the synchrotron emission arms are on the inside edge of the arms defined by HII regions was introduced in Chapter 4 when reconciling the results of observations of the galactic magnetic field.

Absorption in the A2 and A3 arms is assumed to take place uniformly along the path contained within these arms. This is a valid assumption since the arms are distant from the Sun and distant discrete HII regions are not resolved.

Absorption in the A1 arm is assumed to take place in discrete HII regions only. Since we consider lines of sight free of discrete regions absorption in the A1 arm is ignored when deriving parameters of the model. The assumption leading to the procedure used to derive absorption coefficients is equivalent to assuming F1 = F which means that the A1 arm has the same absorption function as the absorbing gas due to ionization of the HI distribution. This is consistent with the observation that electron densities in the local HII arm are less than those of inner arms (see Chapter 4).

The relative contributions of the A2 and A3 arms to the absorption close to the galactic plane is indeterminate in the model. Several types of observation indicate high electron densities within about 6 kpc of the galactic centre. The values of F2 and F3 were adjusted to incorporate

this feature.

If the line of sight for b = 5° is to intersect the A2 arm then the arm must have a half-height of about 100 pc. Using a value of 100 pc results in F 2 and F3 having the same value. Taking the half-height of the A2 arm to be 200 pc gives a value for F3 which is greater than F2. It is not necessary to establish the half-height of the A3 arm.

Summary

The galactic spectra discussed in Chapter 6 have been interpreted in terms of a model of the Galaxy in which synchrotron emission and absorption in HII regions predominate in spiral arms. It is proposed that the synchrotron arms are not coincident with the arms defined by HII regions and thus it is possible to explain the magnitude of the high latitude emission without including a galactic radio halo. It is not possible to predict the variation of brightness at high latitudes without a more detailed analysis involving an estimation of the contribution of the spurs and allowing for the variation of the emissivity in the local arm.

The model does not explain the variation of brightness along the galactic plane at low frequencies but it is suggested that the variation is due to absorption taking place in the local arm.

REFERENCES FOR CHAPTER 7

ALEXANDER,J.K., BROWN,L.W., CLARK,T.A. and STONE,R.G. 1970 Astron. Astrophys. 6 476.

BALDWIN,J.E. 1967 IAU Symposium 31 337.

CASWELL,J.L. 1976 Mon. Not. R.astr. Soc. 176 601.

ELLIS,G.R.A., WATERWORTH,M.D. and BESSELL,M.S. 1962 Nature 196 1079.

ELLIS,G.R.A. and HAMILTON,P.A. 1966a Astrophys. J. 143 227.

ELLIS,G.R.A. and HAMILTON,P.A. 1966b Astrophys. J. 146 78.

GEORGELIN,Y.M. and GEORGELIN,Y.P. 1976 Astron Astrophys. 49 57.

GOULD,R.J. 1969 Aust. J.Phys. 22 189.

HAMILTON,P.A. 1969 Ph.D Thesis (University of Tasmania).

HOYLE,F. and ELLIS,G.R.A. 1963 Aust. J.Phys. 16 1.

KLARE,G. and NECKEL,T. 1967 Z. Astrophys. 66 45.

KOMESAROFF,M.M. 1961 Aust. J.Phys. 14 515.

MILLS,B.Y. 1971 (Invited Paper) Proc. 12th. Int. Cosmic Ray Conf. (Hobart).

NOVACO,J.C. and VANDENBERG,N.R. 1972 GSFC Report X-693-72-8.

PRICE,R.M. 1974 IAU Symposium 60 637.

REBER,G. 1968 J. Franklin Inst. 285 1.

RODGERS,A.W., CAMPBELL,C.T., WHITEOAK,J.B., BAILEY,H.H. and HUNT,V.O. 1960 An Atlas of H-alpha Emission in the Southern Milky Way (Australian National University, Canberra).

ROMAN,N.G. and HADDOCK,F.T. 1956 Washington D.C., Naval Research Laboratory, NRL Rep. No. 4712.

SHAIN,C.A. 1951 Aust. J. Sci. Res. A4 258.

SHAIN,C.A. 1954 Aust. J. Phys. 7 150.

SHAIN,C.A. and HIGGINS,C.S. 1954 Aust. J.Phys. 7 138.

SHAIN,C.A., KOMESAROFF,M.M. and HIGGINS,C.S. 1961 Aust. J.Phys. 14 508.

SIVAN,J.P. 1974 Astron. Astrophys. Suppl. 16 163.

STEPHENS,S.A. 1971 Astron. Astrophys. 11 311.

YATES,K.W. 1968 Aust.J. Phys. 21 167.

CHAPTER 8

FUTURE OBSERVATIONS

In this chapter we will discuss the aspects of non-thermal galactic background radiation studies which present problems and the observations needed to clarify the uncertainties.

Many of the problems arise from the lack of low frequency data. There is very little data below 10 MHz (particularly in the northern hemisphere) and the data that does exist is of insufficient resolution to solve many of the problems. One problem which arises from the present work is whether the discrete absorption regions observed at frequencies greater than about 16 MHz in directions towards the galactic centre would be resolved at frequencies below about 10 MHz if observations could be made with an instrument of resolution less than 2^{o}. If they are not resolved then there must be insufficient background radiation to delineate the absorption regions. Whatever the result the measurement would allow a better determination of the path lengths over which the low frequency radiation is generated and hence lead to a better estimate of the local synchrotron emissivity.

From the spectra presented in Chapter 6 it can be seen that there is considerable latitude in drawing smooth curves through the data points. In particular, the low frequency end of the curves and the regions where the curves change shape are uncertain. The accuracy of the low frequency points is determined by the accuracy to which the galactic pole spectrum can be defined.

There are several problems arising from the results of measurements of the local synchrotron emissivity. A better estimate for the average emissivity is required. Estimates that have been made indicate that the local emissivity varies within the local arm. This aspect requires further investigation as does the relationship between

the synchrotron emissivity and the cosmic ray electron flux. Comparisons of the electron flux deduced from radio measurements and the observed flux at Earth are dependent on the assumed value of the galactic magnetic field. The investigations of the local magnetic field are found to contain conflict in interpretation and it appears that there could be variations of the field strength two to three times the average value.

Finally, there are many problems associated with the explanation of the variation of sky brightness especially at high latitudes. It is necessary to be able to assess the contributions of (a) the spurs (b) the extra-galactic radiation (c) any large scale spherical component around the Galaxy.

The observations required for the investigation of the above problems are not complicated and to a large extent consist of more observations of the type already being undertaken. In this latter category are for example; (a) measurements of the foreground emission in front of nearby HII regions, (b) measurements of the rotation measures of pulsars and other sources and (c) sky surveys.

More surveys are required particularly a northern survey at a frequency less than 10 MHz. At higher frequencies the shape of the background spectra would be improved if surveys could be made at 20, 45 and 60 MHz. A southern survey at about 22 MHz would complement the recent 22 MHz survey completed at Penticton, Canada.

To provide better definition of the galactic polar spectra more calibrated scaled array measurements must be made, particularly of the south pole region. The frequency regime of greatest uncertainty is near the turn over of both spectra so that measurements in the 2 - 10 MHz range are needed. For the determination of the differences

between the north and south polar spectra it would be preferable if new measurements could be made using the same equipment in both hemispheres.

The determination of the extra-galactic radiation presents many difficulties. The measurement on 30 Doradus by Shain should be repeated.

Observations of external galaxies should be encouraged, to determine the occurrence of haloes and the structure of spiral features.

Many of the above measurements could be made with existing instruments. For example the Llanherne array could be used to

(a) obtain more low frequency surveys, especially at frequencies less than 5 MHz;

(b) obtain a high resolution survey in the frequency range 16.5 - 20 MHz;

(c) observe nearby HII regions in order to obtain emissivity estimates;

(d) observe 30 Doradus and determine the extra-galactic component.

Similarly the "high" frequency array at Hobart could be used to obtain data in the frequency range 40 - 150 MHz.

To obtain a new northern survey at a frequency around 5 MHz a new array would need to be built. This would probably be the lowest frequency at which successful observations could be made but this would be sufficiently low to indicate the shape of the spectral turn-over in directions towards the anti-centre.

It is possible that during 1977-1978 the author will carry out observations of the two galactic polar regions. It is proposed that observations of the south galactic pole should be made at Hobart

using scaled arrays designed to operate at 5, 10, 15 and 20 MHz. Identical arrays would be built at Penticton (latitude $+49^{\circ}$) and measurements would subsequently be made of the north galactic pole using the same receiving equipment. Even without any absolute calibrations this experiment could give valuable information. At the same time it would be useful to compare signals from a single dipole and from a small array to gain some knowledge of the response of arrays.

A new array would need to be built to obtain a high resolution (less than 2°) southern survey at approximately 10 MHz. This is one of the most important measurements required if the model suggested in Chapter 7 is to be tested and extended.

In summary there is still much to be done in the field of galactic radio astronomy and many problems exist. However, although some measurements can not be made until the next solar minimum the measurements required to clarify the uncertainties are not difficult and many can be made with existing instruments.

APPENDIX I

THE GUM NEBULA

In 1971 a great interest was aroused in the Gum Nebula following the postulate by Brandt et al. (1971) that the nebula was a "fossil Strömgren sphere" produced by the Vela X supernova.

In 1973 the author compiled a 9 MHz map of the region. Under certain assumptions a value for the optical depth of the region of greatest absorption was obtained. One of the assumptions is now believed to be invalid and we wish to make further comments of the results of the observations.

In Figure I.1 we present the map, covering declinations -30° to -53° and Right Ascensions 0630 hrs to 1000 hrs. The contours give relative brightness with respect to a region of uniform brightness near R.A. 1230^{h}, Dec. -35°. From the new 10 MHz composite map we find that the region near the top of the map would be expected to have a brightness temperature of 3.7×10^{5} K so that the contour unit of the map is 1.9×10^{4} K.

In Cane (1973) it was assumed that all the absorption takes place in the nebula and that no radiation is generated in front of the nebula. This latter assumption was also made by Alexander et al. (1971), and Ellis (1972) but as pointed out by Beuermann (1973) it is invalid. In fact, at frequencies $\leq$ 10 MHz it is to be expected that all the radiation observed in the direction of the nebula would be generated in front of it, and measurements of the nebula at low frequencies may be used to derive the non-thermal emissivity in the solar neighbourhood.

At $\ell = 263^{\circ}$, $b = -10^{\circ}$ the brightness temperature at 9 MHz is

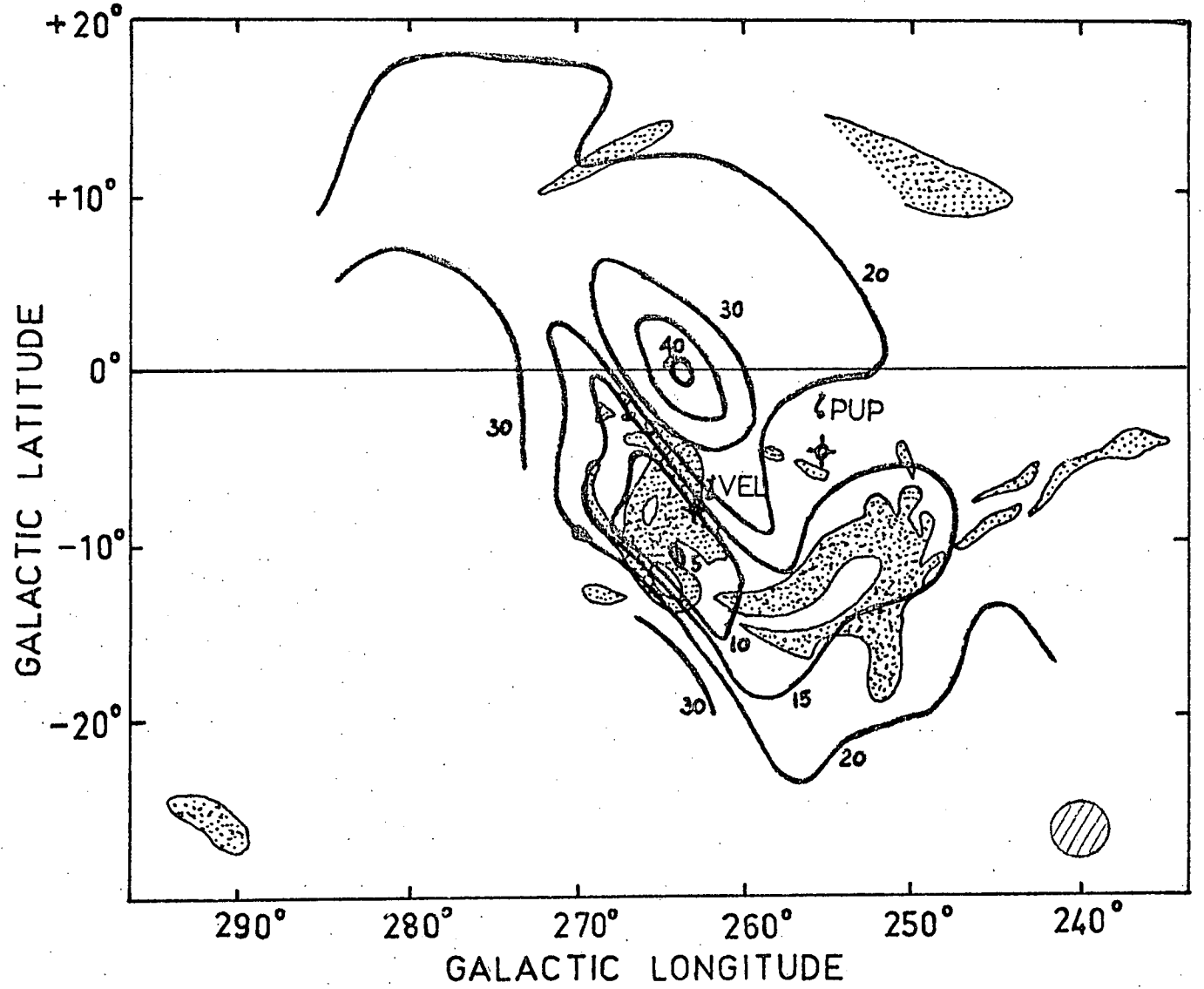

FIGURE I.1 Contours of relative brightness of the Gum Nebula at 9 MHz. The constituents, as sketched by Gum (1956), are indicated by shaded areas. The antenna resolution is shown as a hatched circle.

$\sim 10^5$ K and if we assume the distance to the front of the nebula is 300 pc, we obtain an emissivity of 3.3×10^{-40} watts m^{-3} Hz^{-1} $ster^{-1}$ if the radiation is only foreground emission. This value is below the upper bound for the local emissivity determined in Chapter 5 and so our assumption is probably correct. Thus the optical depth in this region must be at least unity. An upper limit on the electron temperature T_e of the nebula can be obtained if the emission measure is known.

The calculations of Alexander et al., Ellis and Cane used the emission measure obtained by Gum (1956), namely 600-900 cm^{-6} pc. However, a recent estimate by Reynolds (1976) puts the value at 260 ± 80 cm^{-6} pc.

Using this value and an optical depth of 1 in equation (2.5) gives an upper limit for T_e of 1.2×10^4 K. If we assume an optical depth of 2, then we obtain $T_e = 7400$ K.

Thus the temperature of the gas is probably $\lesssim 10^4$ K as found by Beuermann (1973) and so one of the main properties of a "fossil Strömgren sphere" (i.e. $T_e \geq 4 \times 10^4$ K) does not apply to the Gum Nebula. Additional evidence for this lower temperature comes from the observed intensities and line profiles of the Hα, [NII] λ6584 and [OIII] λ5007 emission lines by Reynolds (1976). These indicate a temperature of approximately 1.1×10^4 K.

The other main property of a "fossil Strömgren sphere" is a very large ionized region of angular extent of $\sim 90^\circ$. Reynolds (1976) finds that the Hα, [NII] and [OII] emission is confined to a region approximately 36° in diameter and concludes, as did Beuermann, that the angular diameter of the nebula is about 36°.

Now although the nebula is found to have the size and electron

temperature of a conventional HII region, it has another property which conventional HII regions do not have. This is an expanding shell structure. Beuermann has suggested that the nebula is an evolving HII region but Reynolds maintains that the expansion velocities are greater than those which could be produced by ζ Pup and γ^2 Vel and has suggested that the nebula could be an old supernova remnant which is being heated and ionized by the UV flux from ζ Pup and γ^2 Vel.

REFERENCES FOR APPENDIX I

ALEXANDER,J.K., BRANDT,J.C., MARAN,S.P. and STECHER,T.P., 1971 Astrophys.J. 167 487.

BEUERMANN,K.P., 1973 Astrophys. and Space Sci. 20 27.

CANE,H.V., 1973 Proc.Astron.Soc.Aust. 2 197.

ELLIS,G.R.A., 1972 Proc.Astron.Soc.Aust. 2 158.

BRANDT,J.C., STECHER,T.P., CRAWFORD,D.L. and MARAN,S.P., 1971 Astrophys.J. (Lett.) 163 L99.

GUM,C.S., 1956 Observatory 76 150.

REYNOLDS,R.J., 1976 Astrophys.J. 203 151.

APPENDIX II

INSTRUMENTATION

Introduction

Galactic surveys at five frequencies were made using the Llanherne low frequency array. This is situated near Hobart at latitude 42.9°S and longitude 147.5°E.

Observations were commenced in 1972 but because of poor observing conditions the final surveys were made from observations obtained after May 1974. In addition, by this date a PDP-8 computer had been installed and the sky observing program was operational. The computerized system enabled data to be collected at a much higher rate than before and facilitated corrections for receiver gain changes.

The Array

Figure II.1 shows an aerial photograph of the array. It is essentially a square array 630 m × 630 m and comprises 64 east-west rows of broadband dipoles. With these dimensions angular resolution in the range 12.4° to 1.4° is obtainable for the frequency range over which the array is useful, namely 2 - 18 MHz.

The design and dimensions of the broadband dipoles are illustrated in Figure II.2.

The feed is required to be well matched and achromatic and thus a Christmas-tree feed system is used. Each dipole is fed through the same length of transmission line to the centre of the array. The feeder network consists of 500 ohm open wire transmission line. When signals from two lines are combined 2:1 impedance transformers are used to restore impedance levels. The transmission lines form the ground screen for the array. The signal from each

FIGURE II.1

Aerial photograph of the Llanherne array.

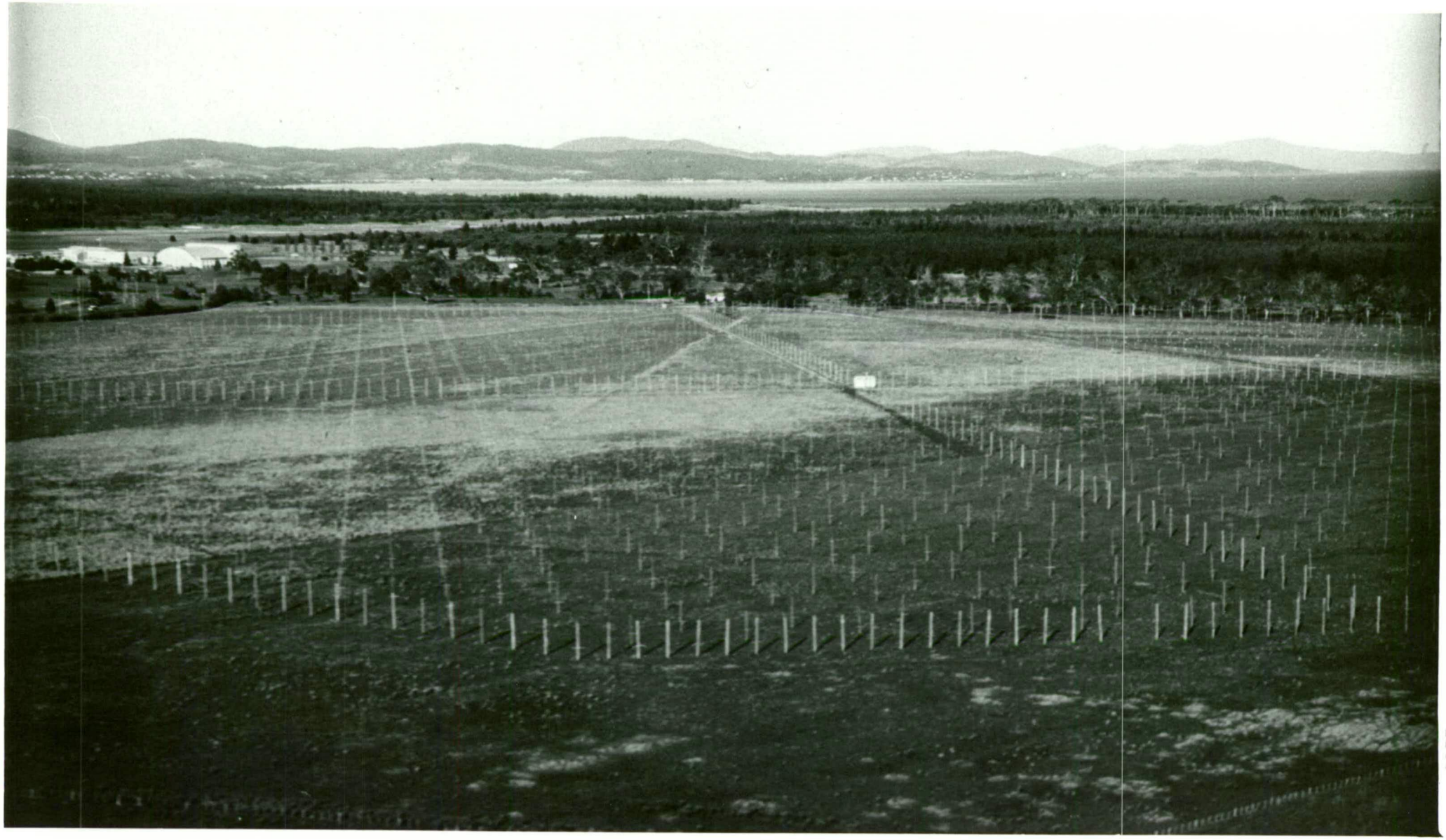

76/12/67

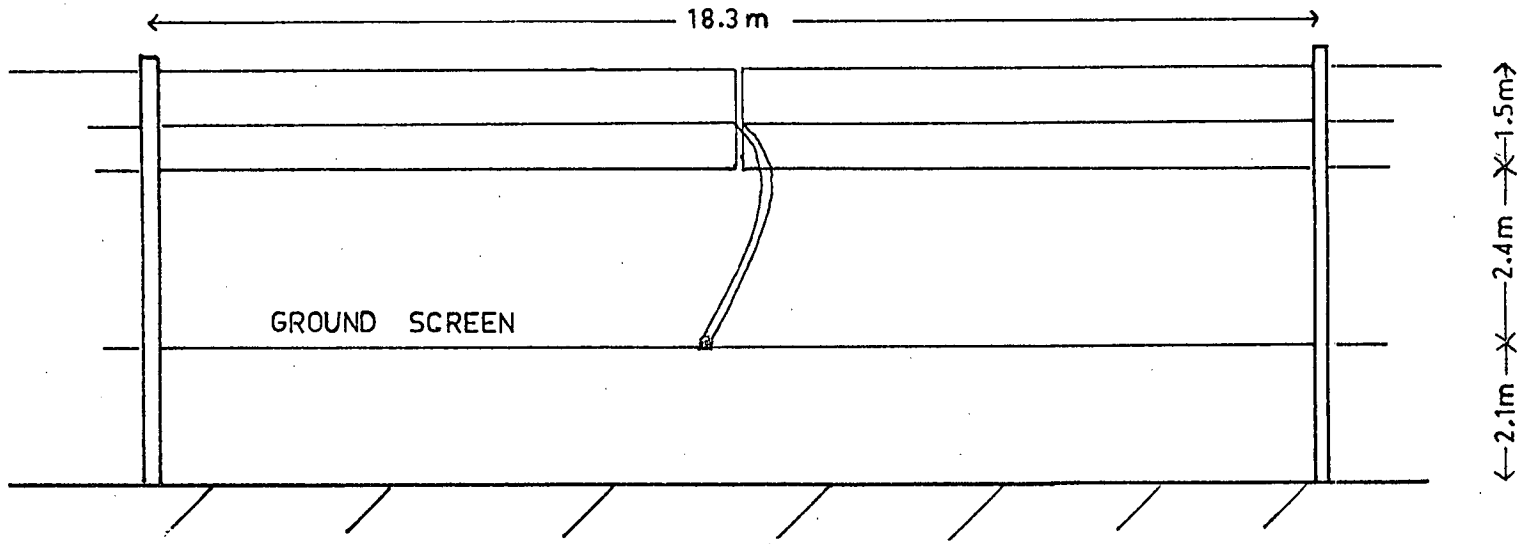

FIGURE II.2 Elevation of a single dipole

row is fed independently through the same length of line to the equipment hut.

The Phasing

Signals from the 64 rows are combined in different phase relationships to produce a beam at declinations in the range $+20^{\circ}$ to -90°. For frequencies less than approximately 16 MHz the beam can be steered to Dec. $+30^{\circ}$ without the introduction of significant sidelobes but above 16.5 MHz beam splitting occurs. To be more explicit, the first grating lobe comes above the horizon when the beam is steered sufficiently far off the zenith.

Figure II.3 is a schematic diagram of part of the phasing system. The basic design is a Christmas-tree system and it can be seen that with 64 ($= 2^6$) rows the system leads to 6 levels which are numbered in the diagram.

Pairs of cables are combined via a junction box and each junction box contains a number of cable delay loops which are introduced by the action of relays as they are required. The delay loops are switched into the appropriate side of the junction by a change-over relay; left side for steering south of the zenith and right side for steering north of the zenith. Figure II.4 illustrates a level 3 junction box.

At levels 1 and 2 there are 6 cable delay loops corresponding to 1°, 4°, 8°, 16°, and 32° phase shifts. At levels 3 to 6 cable delay loops less than 2 m long are omitted and a permanent compensatory delay loop is inserted. In eachcase this extra cable corresponds to half the maximum phase shift omitted. Figure II.3 shows which phase shifts are available at each level and the corresponding permanent shift inserted.

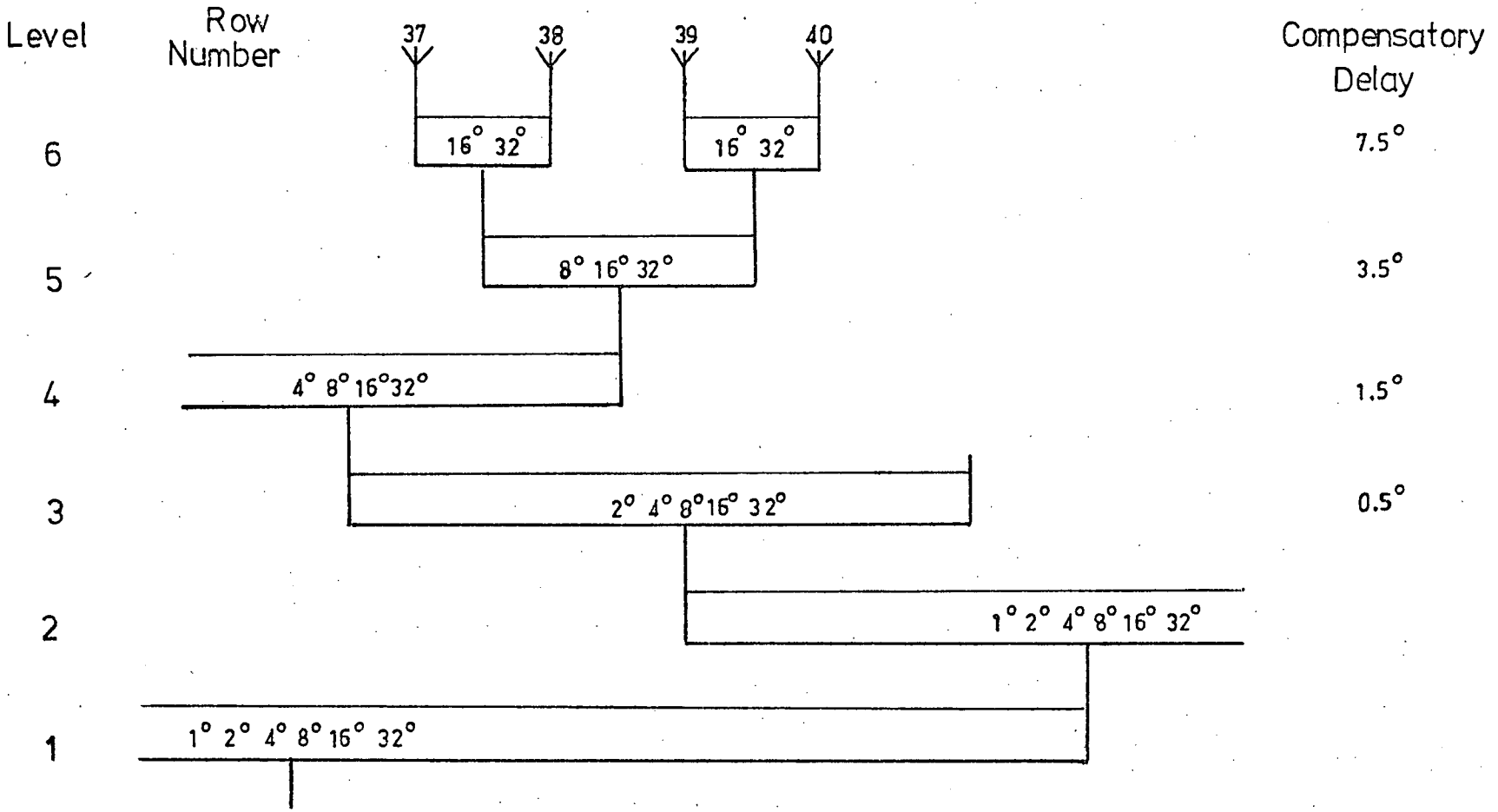

PHASING SYSTEM

FIGURE II.3

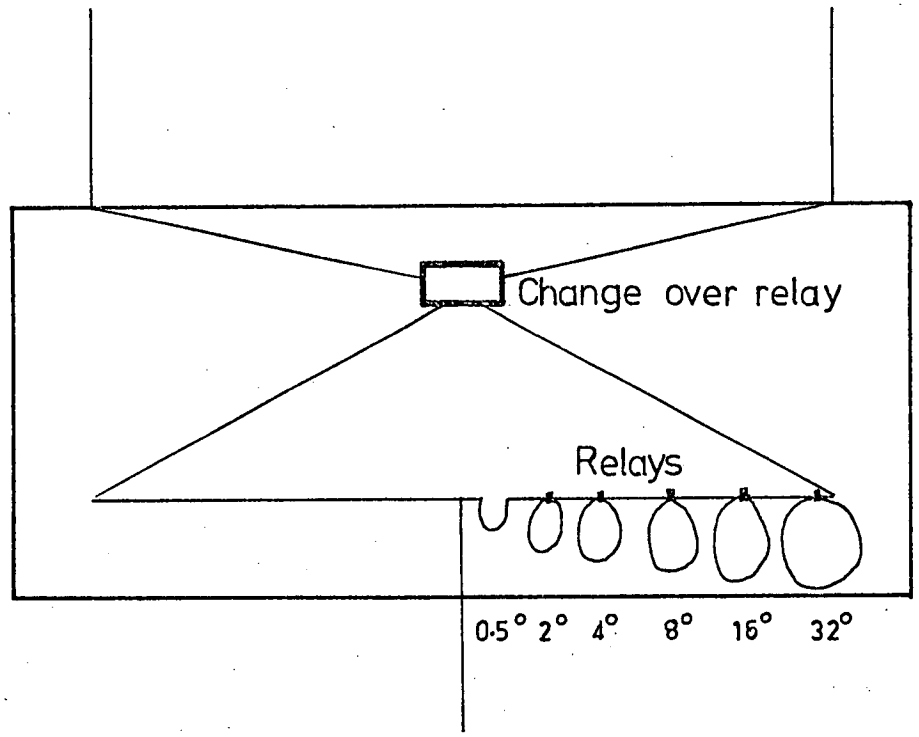

LEVEL 3 JUNCTION BOX

FIGURE II.4

As a consequence of the phasing system used the array is steered in so-called 'beam number' and not in integral values of declination. The beam number is the sum of the phase shifts added at level 1. For beam numbers less than 20, beam number and the angle of the beam from the zenith (in degrees) are the same but as the beam number increases beyond 20 the corresponding angle from the zenith increases slightly more rapidly. To calculate the position of the beam from the zenith (Z degrees) for any beam number (B) the following relationship should be used:

$$Z = \arcsin (B \times 0.01745)$$

Table II.1 shows the half-power beamwidth (HPBW) of the array when directed at zenith for the five frequencies at which surveys were made, namely 3.7, 5.6, 8.3, 13.0 and 16.5 MHz.

Receiving Equipment

The signal from the phasing box is fed through a passive band-pass filter of 2 - 30 MHz and then to a broadband pre-amplifier. The signal is then split into eight outputs and one of these fed to another pre-amplifier. The signal is then split five ways to feed five receivers. Each receiver has an output to a chart recorder and to an analogue to digital converter (ADC), the latter being interfaced to the on-line computer. A block diagram of the receiving system is shown in Figure II.5.

The receivers are of the superheterodyne type and can be tuned to frequencies in the range 2 - 21 MHz. A block diagram is shown in Figure II.6. System bandwidths of 2 kHz were used and the centre frequency was swept through approximately 20 kHz once every 1.5 secs. When this technique is employed the transmitting stations appear as impulses and can be rejected by the use of a minimum reading circuit.

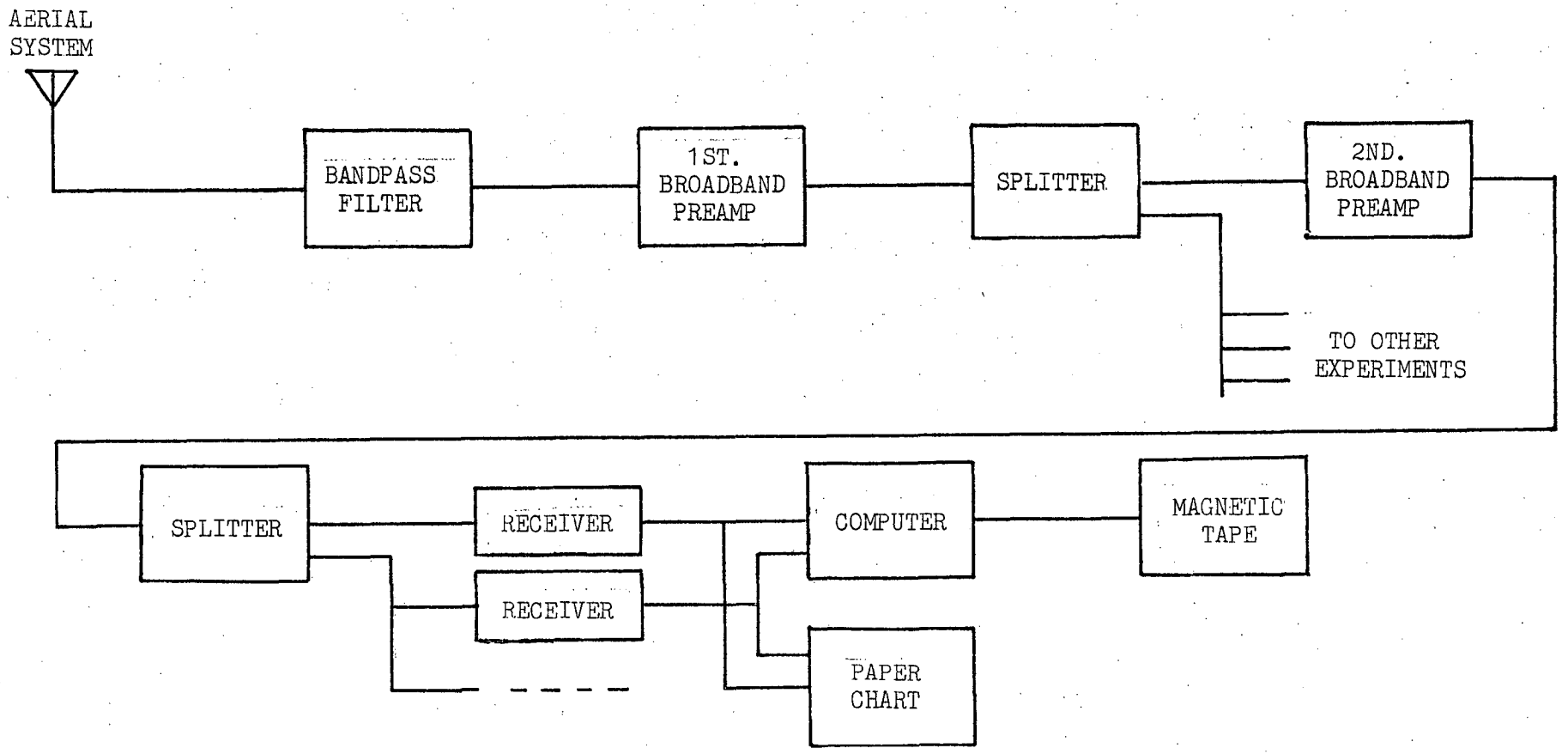

BLOCK DIAGRAM OF RECEIVING SYSTEM

FIGURE II.5

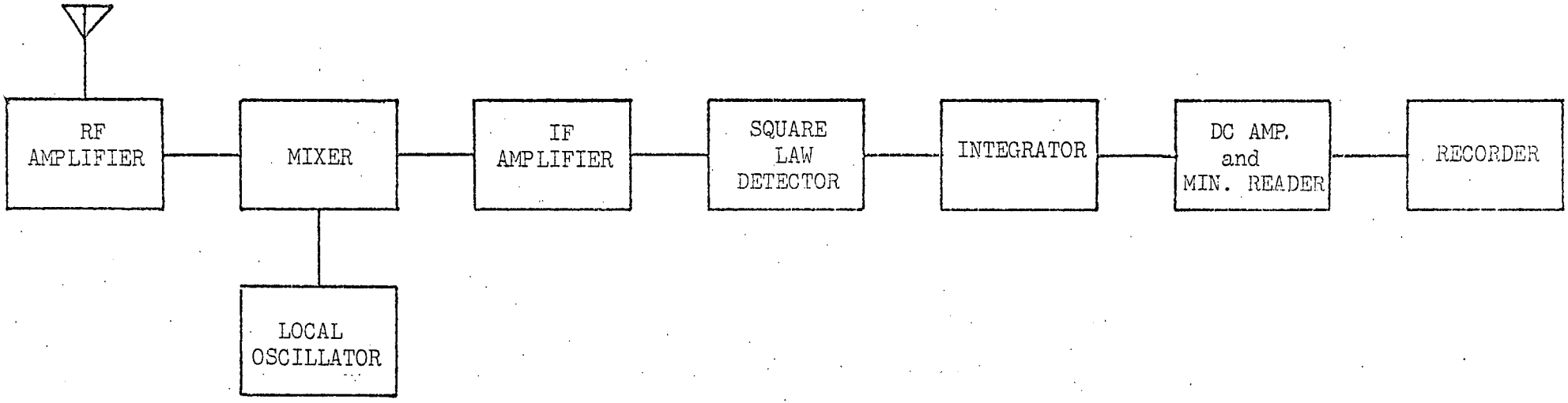

BLOCK DIAGRAM OF A RECEIVER

FIGURE II.6

TABLE II.1

BEAMWIDTH OF THE ARRAY

FREQUENCY (MHz)	HPBW (degrees)
16.5	1.5
13.0	1.9
8.3	3.0
5.6	4.5
3.7	6.8

Figure II.7 shows the post-detection stage of the receivers and the minimum reading circuit is enclosed by dotted lines. The outputs to the pen recorder and computer are indicated.

Observing Procedure

The interfacing between the PDP-8 and the old existing hardware i.e. phasing box, clocks etc. was designed and built by G.A. Gowland. The software for the computer was written by P.S. Whitham.

The computer was programmed to steer the beam cyclically over any range of declinations such that it stepped the same number of degrees each step and the beam remained at each position for a specified time. The total cycle time was chosen to be less than or equal to 5 mins. At a frequency of 13 MHz the sampling interval for a single declination to ensure no loss of information should be less than 4.5 mins. However, as one would not necessarily sample the same declination at the same time on successive days it was decided that the cycle time should be sufficiently short that one could interpolate between successive sample points without introducing significant errors. Hence a 5 min. cycle time was chosen for all frequencies.

After a specified 'settle time' the ADC commenced sampling each receiver every 1/10 sec. At the end of the dwell time for that declination a single average value for each receiver was stored. During the 58^{th} minute of each hour a constant noise level was supplied to all receivers and an average value stored. During the 59^{th} minute the aerial was disconnected and replaced by a dummy load at room temperature, thus giving a zero level. In addition, the 'house keeping' was performed and the values of the output levels for the hour were stored on magnetic tape.

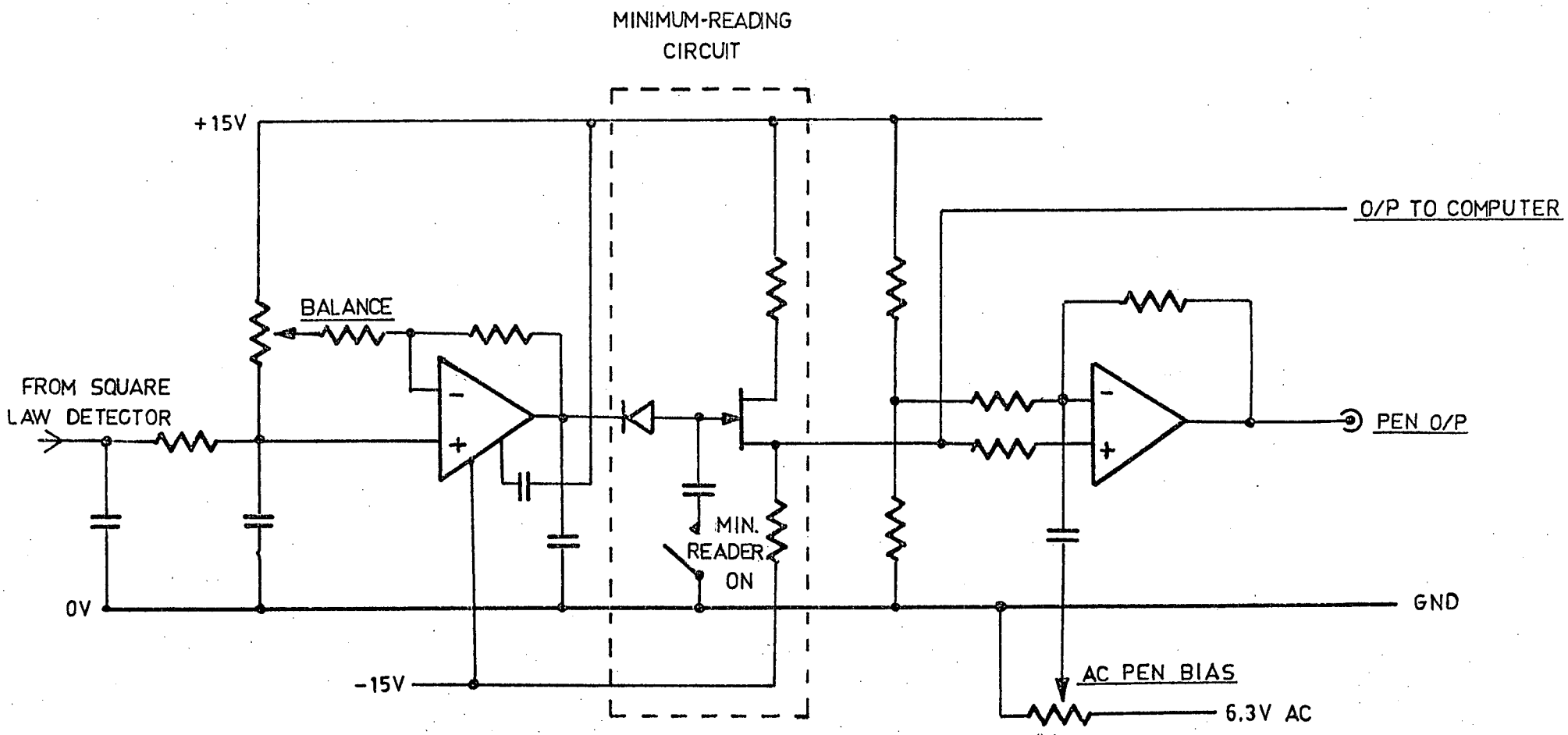

POST DETECTION STAGE OF RECEIVER

FIGURE II.7

Data Analysis

All the data was contained on the magnetic tapes but in a form not directly usable as successive sample points were from different receivers and the data from different declinations were interspersed. The tapes were read on the University Elliott 503 computer. Only the useful hours for each day at each frequency were analyzed and these were selected by examining the pen recorder charts. When the ionospheric f_oF_2 values became available (kindly supplied by G. Goldstone of I.P.S.O.) they were checked to ensure that for the hours selected ionospheric absorption was minimal for the appropriate frequencies. It was found that the hours selected were in fact those hours when the f_oF_2 values were low.

When the data were read from the magnetic tapes they were unscrambled and at the same time gain changes and zero divergences were taken into account. This was achieved by performing a straight line interpolation between hourly calibrations and zero levels and then each sample value was divided by the appropriate calibration value and the corresponding level was subtracted. The results were output on a plotter and consisted of separate declination scans for each frequency. The values at each frequency and declination were multiplied by appropriate scaling factors so that the plots were of a convenient size. The plotter pen was only lifted on the hour and not between sample points so that the plots were in the same form as pen recorder charts when the beam remains at a single declination. Figure II.8 shows an example of the plotter output.

The computer outputs could easily be compared by overlaying them on a light box. By comparing a number of records of the same scan and frequency it was immediately apparent which hours of a record were reduced by absorption or were high due to interference. It was

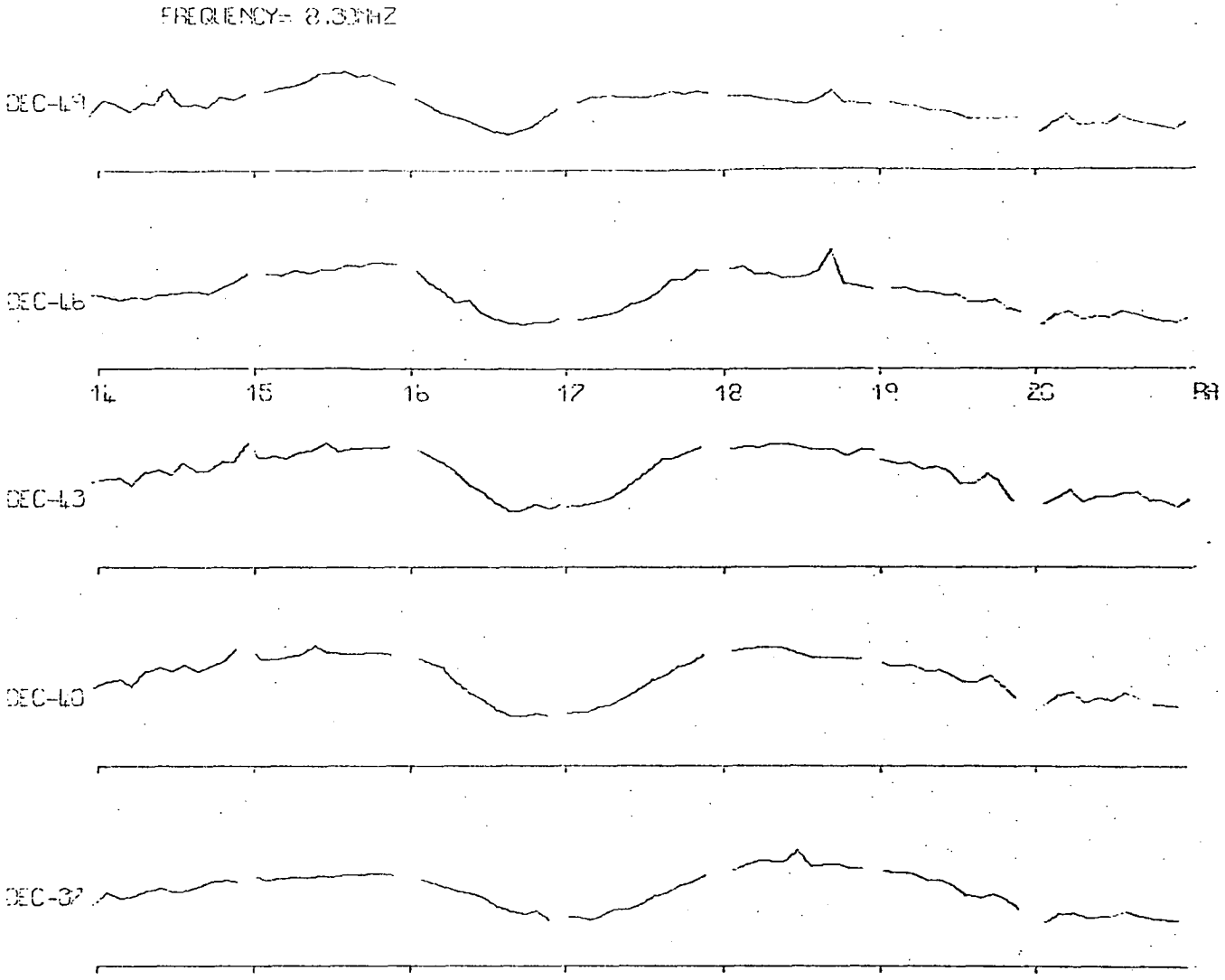

Computer output of declination scans after data read from magnetic tape and analyzed.

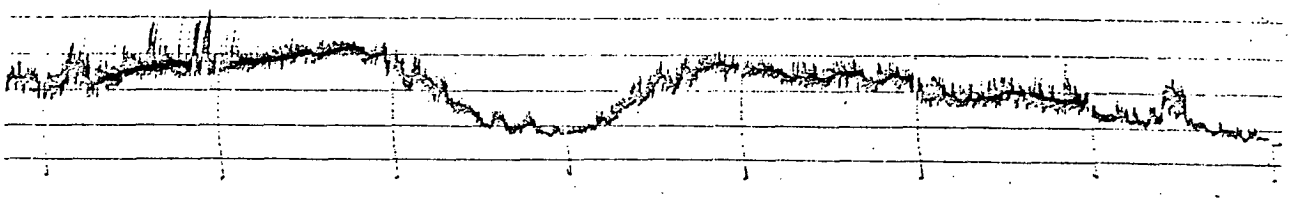

Pen recorder output for the same range of right ascension when no beam switching employed. The scan is Dec. - 45° at 8.3 MHz.

FIGURE II.8

evident the gain of the array could change. It was found that some records agreed in shape but not in amplitude under good ionospheric conditions (i.e. absorption could be excluded) and without noticeable interference. Since shape was the only interest this feature did not cause any problem.

For each declination and frequency the best records were selected for smoothness of trace, reproducibility and the absence of transmitting station interference. The good records were then overlaid on the light box and the profile which ran through the regions of greatest line density was constructed manually. The final set of scans was digitized manually and the values punched onto paper tape. To check for errors these data were then output on the Elliot plotter as a series of scans and compared with the original hand drawn scans. Copies of the computer scans are presented in Chapter 6. Finally, in Figure II.9 we present a flow chart illustrating the basic features of the data analysis.

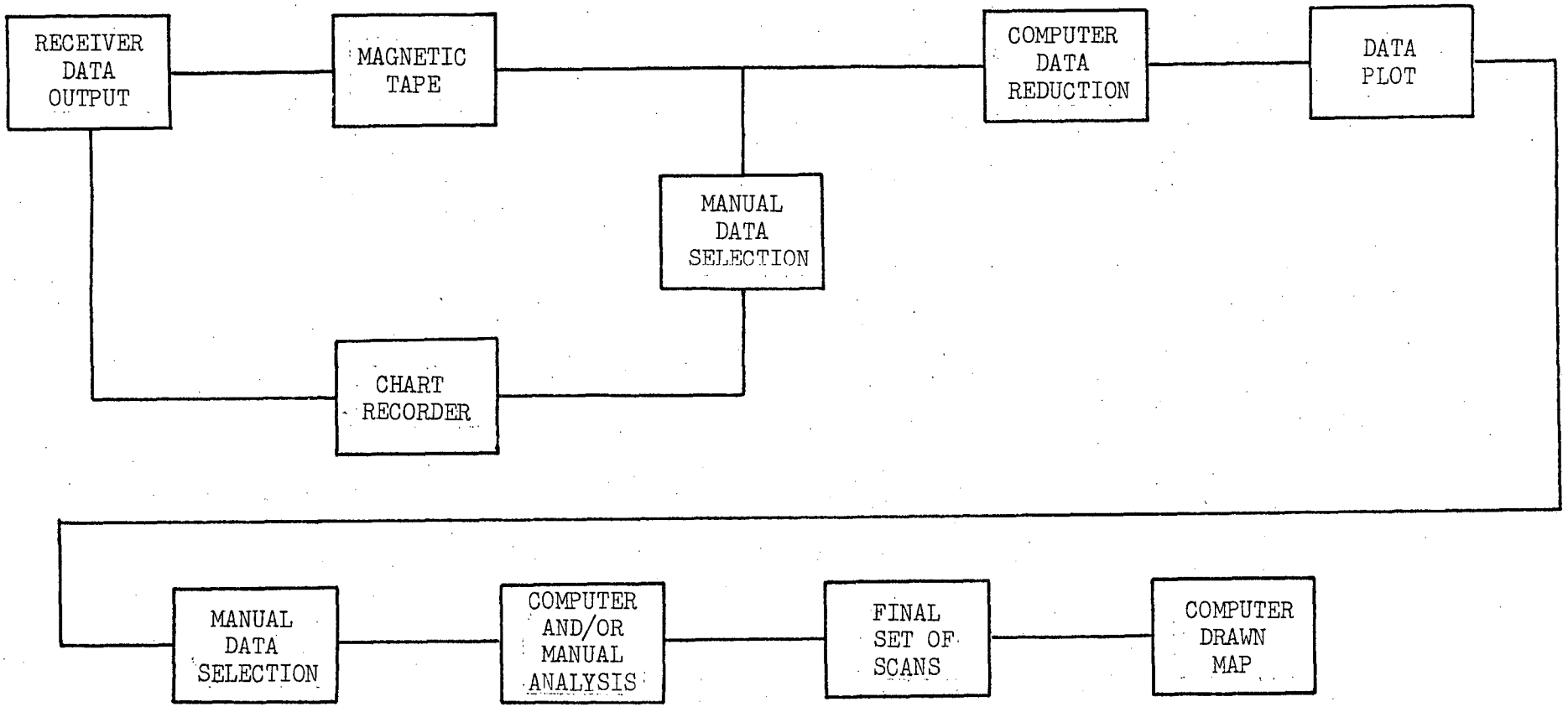

FLOW CHART OF FEATURES OF DATA ANALYSIS

FIGURE II.9